Synthetic Macromolecules for Cryopreservation and Cell Storage

By

Christopher David Stubbs

A thesis submitted to The University of Warwick

for the degree of

Doctor of Philosophy

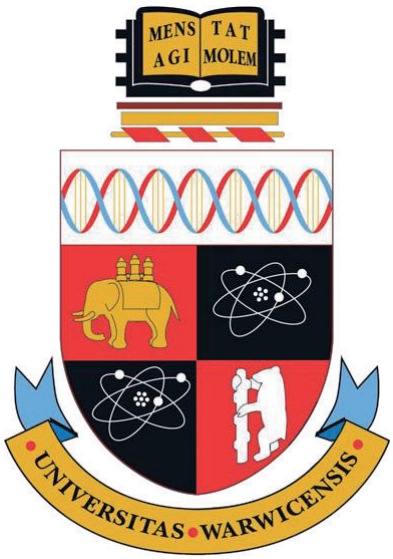

University of Warwick, Department of Chemistry

June 2019

Table of Contents

Chapter 1 - Introduction

Chapter 2 – Evaluating the IRI activity of Multivalent PVA Coated Nanoparticles

Chapter 3 - Synthesis and IRI Activity of Regioregular Poly(ampholytes)

Chapter 4 – Development of High Throughput Oxygen Tolerant Photoiniferter Polymerisation and Evaluation of Poly(ampholyte) Libraries

Chapter 5 - Evaluating the Effect of Hydrophobicity on Weakly IRI Active Materials *via* Photopolymerisation of *N*-vinylpyrrolidone

Chapter 6 – Conclusion

Chapter 7 – Publications

List of Figures

Chapter 1

Chapter 2

Chapter 3

Chapter 4

Chapter 5

Figure 5.06 Molecular weight distribution from SEC for the polymers described in Table 5.2 Polymers were produced at the same molecular weight with varying VAc incorporation. SEC was performed in DMF.

Figure 5.07 IRI activity of PVP-*co*-VAc polymers tested at 20 $mg.mL^{-1}$ and compared to a PVP_{62} homopolymer. MGS = mean grain size reported as an area. The dashed line indicates the activity of 20 $mg.mL^{-1}$ PEG. Error bars represent ± standard deviation from a minimum of 3 repeats.

Figure 5.08 **A** Impact of VAc content on IRI activity as a function of DP. MGS = mean grain size reported as an area. The dashed line indicates the activity of 20 $mg.mL^{-1}$ PEG. Error bars represent ± standard deviation from a minimum of 3 repeats; **B** Molecular weight distribution from SEC of polymers described in Table 5.03. SEC was performed in DMF.

Figure 5.09 Characterisation of PVP, PVP-*co*-VAc and PVP-*co*-VA. **A** Infrared spectra showing the introduction of the acetate group, and its subsequent removal after treatment with hydrazine. Vinyl acetate ester unit is highlighted; **B** ^{13}C NMR of Poly(N-vinylpyrrolidone), Poly(N-vinylpyrrolidone-co-vinyl acetate) and Poly(N-vinylpyrrolidone-co-vinyl alcohol). The additional methyl peak at 16 ppm and backbone carbon at 97 ppm indicate successful incorporation of the vinyl acetate monomer. The subsequent loss of these peaks after deprotection, and new peaks at 37 ppm and 47 ppm corresponding to the backbone carbons of the vinyl acetate unit demonstrate successful deprotection. NMRs were run in $CDCl_3$.

Figure 5.10 IRI activity of hydrophobically modified PVP copolymers. **A** IRI activity of all functionalised copolymers synthesised; **B** Mean grain

List of Schemes

Chapter 2

Chapter 3

Chapter 5

List of Tables

Chapter 1

Chapter 2

Chapter 3

Chapter 4

Chapter 5

List of Equations

Chapter 1

Equation 1.01 Blagdens Law allows the calculation of the expected freezing point depression on a colligative basis. ΔT_F is the change in freezing point of the solution, K_F is the cryoscopic constant of the solvent, in this case water, b is the molality (moles of solute per kg of solvent) and i is the van 't Hoff factor (number of ion particles per molecule of solute).

Equation 1.02 The Gibbs Thompson Effect allows the freezing point depression to be calculated. ΔT_F is the change in freezing point of the solution and is a function of γ, the interfacial energy of the ice/water interface; Ω, the molar volume of ice; T_m, the equilibrium melting temperature; ρ the radius of the surface curvature and ΔH, the heat of fusion of water.

List of Abbreviations

[CTA]	CTA concentration
[M]	Monomer concentration
%	Percent
°C	Degrees Celsius
°C.min^{-1}	Degrees Celsius per minute
ΔH	Heat of fusion of water
ΔT_F	Freezing point depression
±	Plus or minus
Å	Angstrom
ACVA	4,4'azobis(4-cynaovaleric acid)
AF(G)Ps	Antifreeze proteins and antifreeze glycoproteins
AFGP	Antifreeze glycoprotein
AFP	Antifreeze protein
AHD	Alkaline Haematin D-575
AIBN	2,2'-Azobis(2-methylpropionitrile)
atm	Atmospheres
ATRP	Atom Transfer Radical Polymerisation
b	Molality
BHT	Butylated hydroxytoluene
Boc	tert-Butyloxycarbonyl
BP	Boiling Point
chains.nm	Chains per nanometre squared
cm	Centimetre

CMB	Carboxymethyl Betaine
COOH-εPLL	Carboxylated poly(L-lysine)
CPDTC	2-Cyano-2-propyl dodecyl trithiocarbonate
CROP	Cationic Ring Opening Polymerisation
CRP	Controlled Radical Polymerisation
CSIRO	Commonwealth Scientific and Industrial Research Organisation
CTA	Chain Transfer Agent
CyMA	Cyclohexyl methacrylate
d	Diameter
Đ	Dispersity Index (mw/mn)
Da	Daltons
DCM	Dichloromethane
DIS	Dynamic Ice Shaping
DLS	Dynamic Light Scattering
DMAEMA	2-(Dimethylamino)ethyl methacrylate
DMF	Dimethylformamide
DMSO	Dimethyl sulfoxide
DP	Number average degree of polymerisation
DRI	Differential Refractive Index
eq	Equivalents
Et	Ethyl
eV	Electron volts
EXEP	Ethyl 2-((ethoxycarbonothioyl)thio)propanoate
$g.mol^{-1}$	Grams per mole
GOx	Glucose Oxidase

GPC	Gel Permeation Chromatography
GTP	Group Transfer Polymerisation
h	Hours
HEA	Hydroxyethylacrylamide
HEMA	2-Hydroxyethyl methacrylate
i	van 't Hoff factor
I_h	Hexagonal Ice
IPAc	Isopropenyl acetate
^{i}Pr	Isopropyl
FTIR	Fourier Transform Infrared spectroscopy
IRI	Ice Recrystallisation Inhibition
kDa	Kilodalton
K_F	Cryoscopic constant
KHI	Kinetic Hydrate Inhibitors
LAM	Less Activated Monomer
LED	Light Emitting Diode
LpAFP	Lolium perenne antifreeze protein
LS	Dual angle light scattering
m	Metre
M	Moles
M_0	Monomer at time 0
MA	Methyl acryate
MAA	Methacrylic Acid
macroCTA	Macro Chain Transfer Agent
MADIX	Macromolecular Design via the Interchange of Xanthates

MAM	More Activated Monomer
Me	Methyl
mg	Milligram
mg.mL^{-1}	Miligrams per mililitre
MGS	Mean Grain Size
MHz	Megahertz
mL	Millilitre
mm	Millimetre
MMA	Methyl methacrylaye
mmol	Millimole
M_n	Number average molecular weight
mol %	Mole %
M_p	Peak molecular weight
MpAFP	Marinomonas primoryensis antifreeze protein
M_r	Monomer molecular weight
M_t	Monomer at time t
mV	Millivolt
M_w	Weight average molecular weight
MW	Molecular Weight
MWCO	Molecular Weight Cut-Off
MXEP	Methyl 2-((ethoxycarbonothioyl)thio)propanoate
N/A	Not applicable
NCA	*N*-carboxyanhydrase
NIPAM	*N*-isopropylacrylamide
NIPMAM	*N*-isopropylmethacrylamide

nm	Nanometre
NMP	Nitroxide Mediated Polymerisation
NMR	Nuclear Magnetic Resonance
OH	Hydroxyl
PBS	Phosphate Buffered Saline
PEG	Poly(ethylene glycol)
PET	Photoelectron Transfer
PLL	Poly(L-Lysine)
ppm	Parts per million
PVA	Poly(vinyl alcohol)
PVAc	Poly(vinyl acetate)
PVP	Poly(*N*-vinyl pyrrolidone)
RAFT	Reversible Addition Fragmentation Chain Transfer
RBC	Red Blood Cell
RDRP	Reversible-Deactivation Radical Polymerisation
ROMP	Ring Opening Metathesis Polymerisation
ROP	Ring Opening Polymerisation
rpm	Revolutions per minute
SEC	Size Exclusion Chromatography
shsAFP	Shorthorn sculpin antifreeze protein
SPB	Sulfobetaine
SPR	Surface Plasmon Resonance
St	Styrene
TEA	Triethylamine
TEMPO	2,2,6,6-tetramethylpoperidinyl-1-oxyl

TEOA	Triethanolamine
TFA	Trifluoroacetic Acid
TGA	Thermogravimetric Analysis
TH	Thermal Hysteresis
Theo	Theoretical
THF	Tetrahydrofuran
T_m	Melting temperature
UV-Vis	Ultraviolet-Visible
VA	Vinyl Alcohol
VAc	Vinyl Acetate
VS	Viscometry
v/v	Volume by volume
wt %	Weight %
XPS	X-ray Photoelectron Spectroscopy
γ	Interfacial energy
μ	Micro (1x10-6)
ρ	Radius of surface curvature
Ω	Molar volume of ice

Acknowledgements

Firstly, thank you to my supervisor, Prof. Matthew Gibson for allowing me to undertake this work, as well as for his constant enthusiasm, guidance and encouragement. I would like to thank the European Research Council for their funding of this research project and the Materials Division of the Royal Society of Chemistry for a number of travel grants that allowed me to present this work at both APME and the ACS. I would like to thank my advisory panel, Prof. David Haddleton and Prof. Sebastien Perrier, for their insightful comments that have allowed me to develop as a researcher. I am grateful to the Polymer Characterisation RTP for funding a number of the SEC instruments used in this work, and particularly Dr. Dan Lester for spending a number of weeks to help me bring two old instruments back to life as the high throughput SEC used in **Chapter 4**. I'd like to thank Dr. James Lapworth, of Warwick Ventures, for answering all of my questions about patents, and for allowing me to help with the patent application process.

Within the Gibson group, I would like to thank the rest of Team Ice: Ben G, for his encyclopaedic knowledge of all things organic chemistry; Trisha, for allowing me to invade her pristine cell lab to cover it in blood, for answering all of my silly questions about cell biology and most importantly, for introducing me to Buddha Belly; Tom, for being an expert on all things PVA; Alice, for carrying out all of the groups ice shaping assays and for generally knowing a lot about ice, and Caroline, for ensuring the lab always ran smoothly. I would also like to thank Sarah-Jane, Collette, Ben M, Laura, Henry, Antonio, Kat, Marie, Muhammad, Ruben, Ioanna, Toru and Alex for sharing their knowledge, and for making the group such an interesting and exciting place to work.

Outside of Warwick, I would like to thank my family, Mum, Dad and Anna, for constant support and encouragement over the past 8 years at Warwick, and I would like to thank Barbara Wiseman for encouraging me to try and be the first Dr in the family. Finally, I would like to thank Jasmine, for her love and support, and for generally making this entire experience better than it would have been without her.

Declaration

This thesis is submitted to the University of Warwick in support of my application for the degree of Doctor of Philosophy. It has been composed by myself and has not been submitted in any previous form for any degree at any other University.

The work presented was carried out by the author except in the case of collaborative research, as outlined below:

- The synthesis and characterisation of the gold nanoparticles, and gold-PVA conjugates prepared in **Chapter 2** was carried out by Laura Wilkins at the University of Warwick. The synthesis of the PVAs, and all IRI testing were carried out by myself.
- Sucrose shaping assays discussed in **Chapter 2** were performed by Alice Fayter
- The Poly(allyl alcohol) tested in **Chapter 2** was provided by Prof. Marc Hillmyer of the Universty of Minnesota.
- The Poly(vinyl amine) splats in **Chapter 2** were carried out by Dr. Tom Congdon at the University of Warwick, and the images counted and data analysed by myself.
- The synthesis, characterisation and IRI activity testing of the non-regioregular poly(ampholyte) materials mentioned in **Chapter 3** was carried out by Julia Lipecki at the University of Warwick while working with myself as a Masters student.
- The catalytic cycle shown in **Chapter 4** was devised by myself and Dr. Tom Congdon at the University of Warwick.

- The high throughput SEC developed for use in **Chapter 4** was modified in collaboration with Dr. Daniel Lester at the University of Warwick.

Sections of this thesis have been accepted for publication as follows:

- **Chapter 1** – Biggs, C.I., Bailey, T.L., Graham, B., Stubbs, C., Fayter, AC., Gibson, M.I., *Nature Communications*, **2017,** 8, 1546., "*Polymer Mimics of Biomacromolecular Antifreezes"*
- **Chapter 2** - Stubbs, C., Wilkins, LE., Fayter, AC., Walker, M.,Gibson, M.I., *Langmuir,* **2018**, "*Multivalent Presentation of Ice Recrystallization Inhibiting Polymers on Nanoparticles Retains Activity"*
- **Chapter 3** - Stubbs, C., Lipecki, J., Gibson, M.I., *Biomacromolecules*, **2017**, 8, 295–302 "*Regio-Regular Alternating Polyampholytes have Enhanced Biomimetic Ice Recrystallization Activity Compared to Random Copolymers and the Role of Side Chain Verses Main Chain Hydrophobicity"*
- **Chapter 5** - Stubbs, C., Congdon, TR, Gibson, MI., European Polymer Journal, **2019,** 110, 330-336 "*Photo-Polymerisation and Study of the Ice Recrystallisation Inhibition of Hydrophobically Modified Poly(vinyl pyrrolidone) Co-polymers"*

Abstract

The transport and storage of mammalian cells is a significant technical challenge that is currently limiting the adoption of a range of cell-based technologies. Cryopreservation is an attractive method to enable the long-term storage of cells and tissues, however the necessary freezing and thawing processes cause extensive cell damage and therefore cryoprotectants are required to inhibit the mechanical and osmotic damage caused by ice growth (recrystallisation). Antifreeze proteins, used by plants, animals and bacteria to survive low temperature environments were initially considered to solve these problems, however their complex synthesis, and dynamic ice shaping limit their usefulness. As a result of these limitations, synthetic cryoprotectants are of great interest. The most potent synthetic ice recrystallisation inhibitor (IRI) currently known is poly(vinyl alcohol), and therefore **Chapter 2** details attempts to further understand its mechanism of action, by investigating the effect of a series of modifications on its IRI activity. **Chapter 3** explores the effect of regioregularity and hydrophobicity on poly(ampholyte) IRI activity, then uses the design rules observed to generate a highly active, scalable, cryoprotectant. **Chapter 4** details the development of a high throughput photoiniferter polymerisation, as well as the limitations of the technique. This process, paired with a high throughput cryopreservation assay, is then used to screen a library of 120 poly(ampholyte) terpolymers. **Chapter 5** investigates the effect of hydrophobic modification on an IRI inactive, fully flexible polymer, in order to determine whether IRI activity can be induced by simple polymer modification.

In summary, a number of polymeric materials are synthesised to probe the relationship between structure and function of a number of IRI active, and inactive, materials. The relationship between IRI activity and cryoprotectant activity is then investigated using a number of poly(ampholytes), observing that for some materials, IRI activity does not necessarily correlate with cryoprotectant activity.

Chapter 1

1.1 Introduction

Cryopreservation is an essential solution for the transportation and storage of biological materials, however significant damage is caused during the necessary freezing and thawing processes, limiting the current usability of this technique.[1] One method to potentially mitigate this damage is to examine the route by which nature has attempted to solve this problem. Polar fish, which are able to survive at temperatures below freezing have been shown to produce antifreeze(glyco) proteins (AF(G)Ps) which provide a non-colligative freezing point depression of their internal fluids preventing damage caused by freezing or thawing.[2–4] AF(G)Ps have been shown to have three main macroscopic effects; thermal hysteresis, depression of the freezing point below the melting point; ice recrystallisation inhibition, inhibition of the rate of growth of an ice crystal; and dynamic ice shaping, the influence of the AF(G)P on the morphology of the growing ice crystal.[5] These materials have been investigated as cryoprotectants, however their undesirable dynamic ice shaping properties,[6] as well as difficulties associated with large scale synthesis,[7,8] limit their widespread applicability. There is therefore a significant research effort based around the synthesis of bio-inspired polymeric[9,10] and small molecule[11] analogues of these materials.

1.1i Antifreeze Molecules

There are two main mechanisms which nature uses to allow organisms to survive, and flourish, in low temperature environments. These mechanisms are usually referred to as freeze tolerance and freeze avoidance,[12] with the employed mechanism usually dependent on the overall size of the organism, as well as the length of time which the organism spends in low temperature environments. Freeze avoidant organisms prevent the formation of any ice crystals *via* the formation of supercooled solutions through non-colligative depression of the freezing point, and the inhibition of ice nucleation.[13] This strategy works best for small volumes, and a series of insects have been reported to be able to prevent ice formation at temperatures as low as -40 °C.[14] On larger scales, however, freeze avoidance is almost impossible, and if temperatures are dropped below the depressed freezing point, explosive ice growth can cause significant damage to the organism.[15] Freeze tolerance prevents the formation of usually fatal intracellular ice through the use of a combination of small molecules and proteins both inside and outside the cell. Extracellular ice nucleating proteins ensure that any ice formed is outside of the cell, where the ice crystal morphologies can be controlled, and any damage caused by growing ice crystals can be mitigated. This extracellular ice formation causes a rise in the solute concentration, and thus the cell is slowly dehydrated as more water is expelled. This creates a greater solute concentration inside the cell, greatly reducing the freezing point and preventing intracellular ice formation.[16]

This ability to control extracellular ice morphology, and the temperature at which it nucleates, is due to the presence of ice structuring proteins in the extracellular matrix of the freeze tolerant organism. Ice structuring proteins have been observed in a

significant number of different species and are classified into two main categories; antifreeze proteins, or antifreeze glycoproteins.

Antifreeze glycoproteins were first discovered by Scholander in 1957, who observed that a variety of fish species were able to survive in water temperatures below the freezing point of their blood plasma. When fish were held in a tank of water at -3 °C (2.1 °C below their freezing point), the fish were able to survive as normal. However when ice was seeded next to the fish, seeding could propagate through the skin of the fish leading to almost immediate freezing and death.[17] This freezing point depression, or thermal hysteresis (TH), allows the species to survive in waters colder than the equilibrium freezing point of their blood serum, as long as the water temperature is above the hysteresis freezing point of the supercooled solution. It was later shown that this freezing point depression was too great to be a result of the colligative decrease caused by the osmolarity of the blood plasma alone, and that specific proteins, present in low concentrations were responsible for a significant proportion of the observed depression.[3]

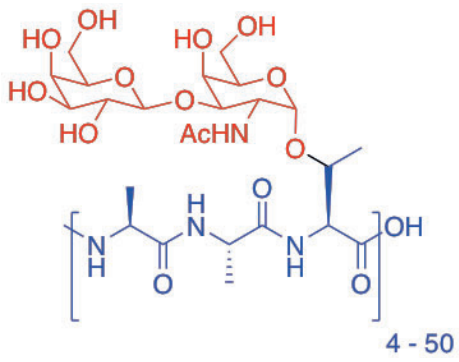

Figure 1.01: The structure of an AFGP. The protein backbone is highlighted in blue, and the disaccharide (β-D-galactosyl-(1→3)-α-*N*-acetyl-D-galactosamine) in red.

Antifreeze glycoproteins were found to consist of an alanine-alanine-threonine peptide repeat, with a disaccharide sugar attached to the threonine unit (Figure 1.01). AFGPs

are classified as AFGP 1-8 based on the molecular weight of the chain, varying from 33.7 kDa (AFGP 1) to 2.6 kDa (AFGP 8).[18] Small variations in amino acid sequence have also been observed, with some of AFGPs 6-8 containing a proline-alanine-threonine repeat unit in the chain.[19]

The molar mass of the AFGP chain has been shown to effect its thermal hysteresis activity, with longer chains generating a greater depression of the hysteresis freezing point, whilst demonstrating the expected colligative effect on the melting point of the solution, and hence creating a larger window during which ice growth is kinetically trapped.[20] These more active higher molecular weight fractions are found in lower concentrations, with as much as 90 % of the AFGP in a given plasma solution being AFGP 6-8.[21] Understanding the exact mechanism of action of these materials, however, is incredibly difficult, with almost all modification reducing the activity of the protein. Attempts to create more active materials by dimerising AFGP 6 did not show the expected activity increase commensurate to the increase in molecular weight, suggesting that there is a limit of activity for AFGPs which contain proline, whilst dimers of AFGP 8 actually showed decreased activity compared to the unmodified proteins.[22] Attempts have also been made to modify the sugar, however, due to the difficulty associated with total synthesis of AFGPs, these experiments were limited to chemical modification of the sugar whilst still attached to the protein backbone.[23] Complete removal of the sugar moiety removes all antifreeze activity, as does acetylation and complexation of the hydroxyl groups with borate. Oxidation of the primary alcohol groups was tolerated for the formation of aldehydes, however when fully oxidised to carboxylic acids all activity was again lost (Figure 1.02).

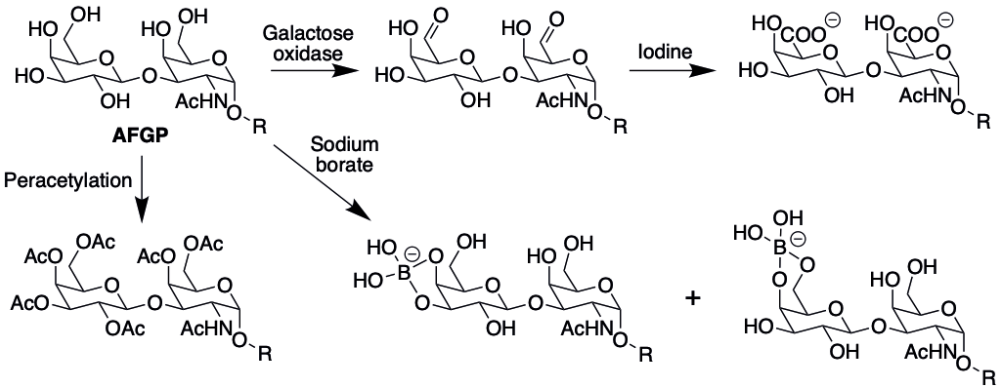

Figure 1.02: Modifications used to determine the effect of the sugar on AFGP activity. Adapted from Harding *et al.*[2]

More recently, Tachibana *et al.* conducted a systematic modification of the sugar moieties in AFGPs, demonstrating that the *N*-acetyl group at the C2 position, α configuration of the *O*-glyosidic linkage and the *γ*-methyl group of the threonine residue were all required for maximum antifreeze activity.[7] Investigations into the effect of the distance between the backbone and sugar have also been carried out, showing that shorter linkers are most effective, likely due to the conformation of the peptide backbone already being ideally suited for maximum ice binding efficiency.[24] While these materials in their natural form are incredibly active antifreezes (only TH activity was tested), they are very difficult to synthesise and are resistant to modification.

Table 1.01: Classification and representative structures of AFGPs and AFPs. Taken from Capicciotti *et al*.[25]

Characteristic	AFGP	Type I AFP	Type II AFP	Type III AFP	Type IV AFP
Mass (kDa)	2.6 - 33	3.3 – 4.5	11 – 24	6.5	12
Key Properties	AAT repeat; disaccharide	Alanine-rich α-helix	Disulfide bonded	β-sandwich	Alanine rich; helical bundle
Representative Structure	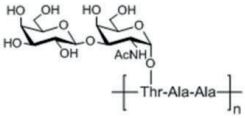				
Natural Source	Antarctic Notothenioids; northern cods	Right-eyed flounders; sculpins	Sea raven; smelt; herring	Ocean pout; wolfish; eel pout	Longhorn sculpin

In comparison to AFGPs, antifreeze proteins (AFPs), those lacking the sugar moiety, display significantly higher TH activity and lower ice recrystallisation inhibition (IRI) activity,[26] they are also significantly easier to synthesise and modify. The lack of post translational modification allows them to be expressed more easily, and therefore are much more widely researched. AFPs display much greater structural diversity and are characterised into four main types (Table 1.01). AFPs were first observed in Antarctic fish,[27] but have since been observed in a large variety of cold tolerant organisms.[28] One of the first AFPs to be widely studied was the Type I AFP from winter flounder, as with AFGPs, these proteins were shown to have high alanine content (~61 %), suggesting that mild hydrophobicity may be important for antifreeze activity.[29] As the structure of more AFPs has been elucidated, one consistent observation is the presence of both hydrophilic and hydrophobic domains in the secondary structure of the protein. AFPs have been shown to adopt α-helices, β-strands and polyproline type II coils.[30] Each of these structures allows for the presentation of an ordered ice binding face, which is held at an ideal orientation for optimal binding. These binding sites have been

determined through site directed mutagenesis, where substitution of amino acids directly involved in ice binding caused almost complete loss in activity. However substitutions on the non-binding face of the protein caused little reduction in activity (Figure 1.03).[31–33]

Once the binding site had been elucidated, the binding mechanism could be investigated, initial studies suggested that binding occurred due to precise spacing between the OH groups present in the protein, and the oxygen atoms on the surface of a growing ice face, ensuring a good pattern match for efficient hydrogen bonding.[34] More recently, however, studies using both molecular dynamics,[35] and solution state NMR spectroscopy[36] have suggested that the hydrophobic face of the AFP is most likely to be orientated towards the ice plane. It is widely believed that solution AFP will structure nearby water and cause it to form an ice like crystal structure, this structured water will freeze more readily than free water in solution, thus binding the AFP to the surface of the ice crystal.[37,38] These binding processes are however incredibly complex, and there is still some debate however as to whether this binding is reversible[39] or irreversible.[40]

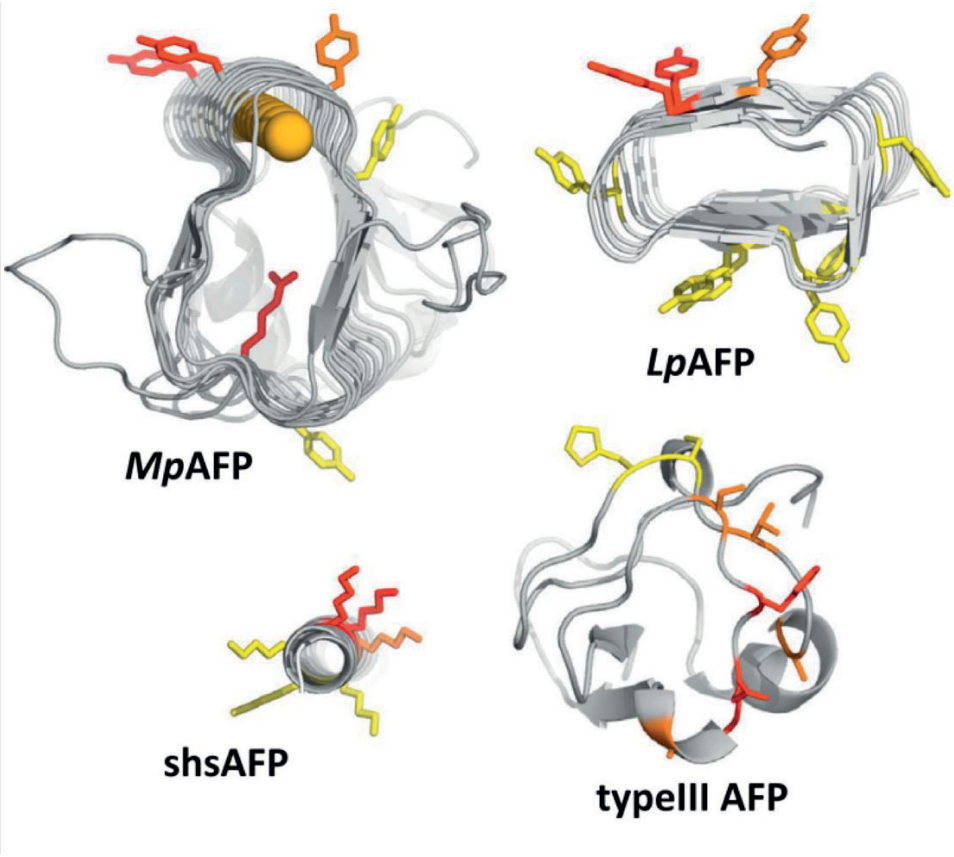

Figure 1.03: Protein mutants designed to help elucidate the ice binding site of some AFPs. Short chain amino acids were replaced with bulkier substituents and the side chain modifications coloured according to severity: yellow (0-20 % loss of activity), orange (20-90 % loss of activity), red (90-100 % loss of activity). Gold spheres represent calcium ions. Adapted from Davies.[30]

Whilst all materials discussed above are based on proteins, other biomaterials which display similar ice interactions have recently been observed. In 2009 a macromolecule was isolated from a freeze tolerant Alaskan beetle which contained little to no protein content whilst demonstrating antifreeze activity comparable to AFPs.[41] Antifreeze glycolipids displaying similar structures have since been observed in plants, insects and frogs.[42] In order to confirm the proposed structures, the total synthesis of these materials has also been reported[43,44] however little research has been carried out in this

area since, and the exact mechanism of interaction between these glycolipids and the growing ice surfaces have not been studied.

These antifreeze materials are thought to enhance low temperature survival *via* three main macroscopic effects. Each of these effects will be discussed further below.

1.1ii Thermal Hysteresis

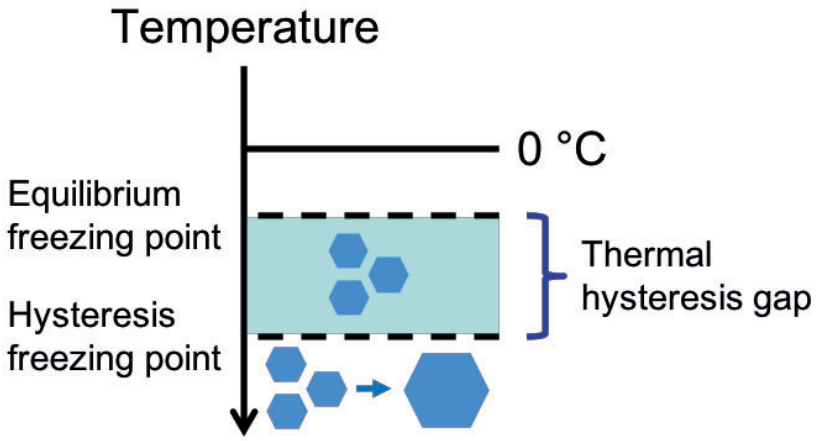

Figure 1.04: Cartoon demonstrating thermal hysteresis.

The main property of ice binding proteins which promotes survival at low temperatures is thermal hysteresis. This is a kinetic phenomenon which lowers the freezing point of a solution below the melting point, creating a temperature region within which ice crystals cannot grow, and no new nucleation occurs (Figure 1.04). This property has been widely observed in AFGPs[45] and AFPs[46] as well as supramolecular materials.[47] Whilst all dissolved solutes will cause some level of freezing point depression, the expected colligative depression can be calculated mathematically using Blagden's Law, Equation 1.01.

$$\Delta T_F = K_F \cdot b \cdot i$$

Equation 1.01: Blagdens Law allows the calculation of the expected freezing point depression on a colligative basis. ΔT_F is the change in freezing point of the solution, K_F is the cryoscopic constant of the solvent, in this case water, b is the molality (moles of solute per kg of solvent) and i is the van 't Hoff factor (number of ion particles per molecule of solute).

One remarkable feature of AFPs and AFGPs is that the depression is much greater than calculated based solely on the concentration of the solute, suggesting that a more complex interaction between these specific materials and the growing ice crystals is occurring. There have been many attempts to understand this mechanism, however the exact process has not yet been determined. It has been suggested that this freezing point depression is caused by an 'adsorption inhibition mechanism', in which AFGP irreversibly bound to the surface of the growing ice crystals causes convex ice growth between the adsorbed protein, Figure 1.05.[48]

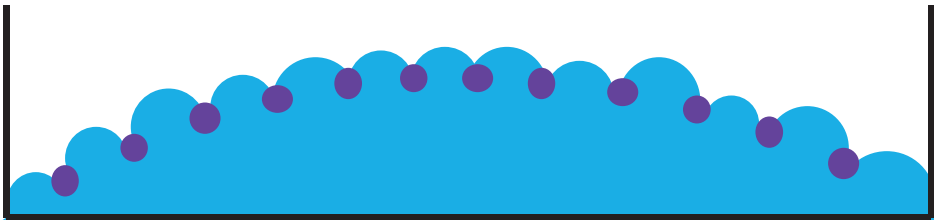

Figure 1.05: A cartoon to show the convex growth formed between bound AFGPs (Purple circles) within the thermal hysteresis gap. Purple circles are bound protein.

This adsorption is thought to inhibit macroscopic ice growth by increasing the curvature of the growth on the surface of the ice crystal. This convex curvature causes an increase in the vapour pressure of the ice, as this is inversely proportional to the radius of the growing surface. As the temperature decreases, the vapour pressure of

water molecules at the surface of the ice crystal increases at a rate greater than that of the water molecules present in the corresponding concave water surface. This results in local melting of the crystal, and therefore, a lower (more negative) temperature is required to balance the rate of addition of water to, and loss of water from, the ice face thus depressing the hysteresis freezing point.[49]

If the distance between the adsorbed protein is known, the level of freezing point depression can be calculated using Equation 1.02. According to this equation, the freezing point depression is a result of the local curvature of the convex surface, and therefore decreasing the distance between the bound AFP will decrease the radius of the convex surface (ρ) and therefore further depress the freezing point.[50]

$$\Delta T_F = \frac{2\gamma\Omega T_m}{\rho\Delta H}$$

Equation 1.02: The Gibbs Thompson Effect allows the freezing point depression to be calculated. ΔT_F is the change in freezing point of the solution and is a function of γ, the interfacial energy of the ice/water interface; Ω, the molar volume of ice; T_m, the equilibrium melting temperature; ρ the radius of the surface curvature and ΔH, the heat of fusion of water.

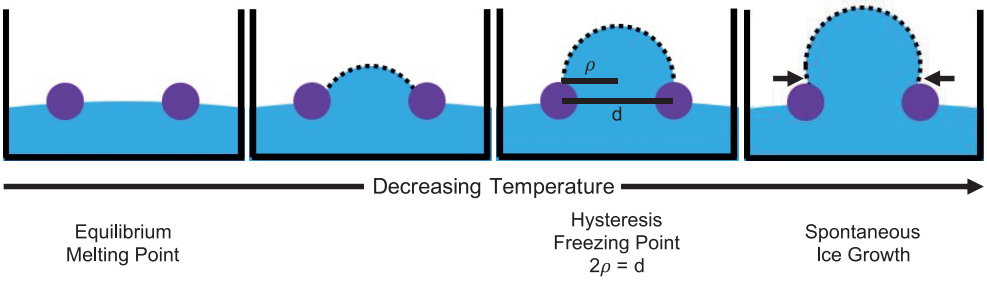

Figure 1.06: A schematic to show the increase in surface convexity as temperature decreases. The maximum depression is reached at the point at which $2\rho = d$. Further ice growth causes a reduction in the surface curvature (black arrows) and spontaneous growth.

From this equation, the maximum freezing point depression is observed when ρ is equal to half of the distance between adjacent proteins. Any further temperature decrease will lead to ice growth which causes a decrease in the convexity of the surface, and thus growth becomes energetically favourable. This causes surface nucleation and significant spontaneous ice growth as soon as the temperature is lowered past the hysteresis freezing point (Figure 1.06).[51] It has been shown that two main factors are responsible for the surface density, and hence activity, of a given antifreeze protein, exposure time and concentration.[52]

1.1iii Dynamic Ice Shaping

The crystal structure of ice depends on the conditions under which it was formed. While there are currently seventeen accepted polymorphs of ice,[53] water, upon cooling to 0 °C at 1 atm pressure will thermodynamically form ice with a hexagonal unit cell (but in practice homogeneous nucleation does not occur until -42 °C). This hexagonal ice is referred to as ice I_h and is the form in which all naturally formed ice and snow is observed. The hexagonal unit cell results in two main types of plane through which

ice can grow, the prism planes and the basal plane. All natural antifreeze proteins have been shown to bind to the prism plane of ice,[54,55] with some AFPs having also been shown to bind to the basal face, however this is rare.[56,57] Notably, AFP mutants which bind only the basal face do not demonstrate significant antifreeze activity.[58]

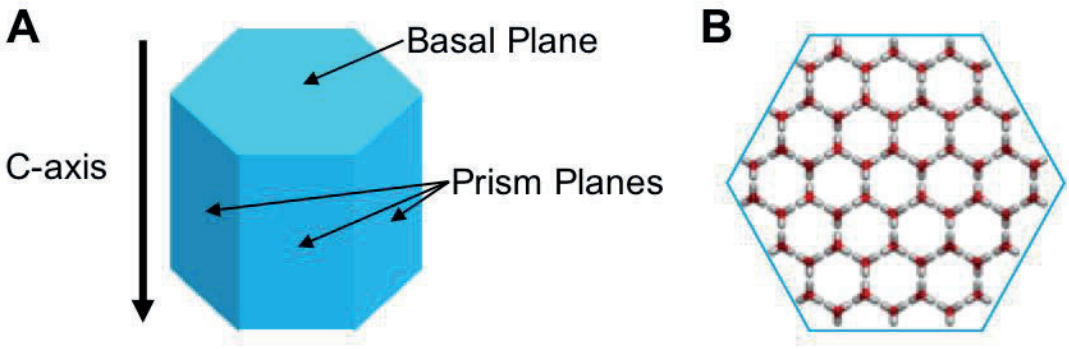

Figure 1.07: A The structure of Ice I_h with the basal plane and prism planes indicated; **B** A view of the atom arrangement in ice I_h perpendicular to the basal plane (looking down the c-axis). Red atoms are oxygen, white are hydrogen.

If ice growth from the prism plane is blocked, addition of water molecules can only occur at the basal plane. This will create new prism planes which can now be inhibited by free protein in solution. This growth and inhibition cycle will eventually lead to the formation of sphicular (needle like) ice crystals (Figure 1.08). The resulting crystal structures offer a macroscopic view of the ice face affinity of AFPs.

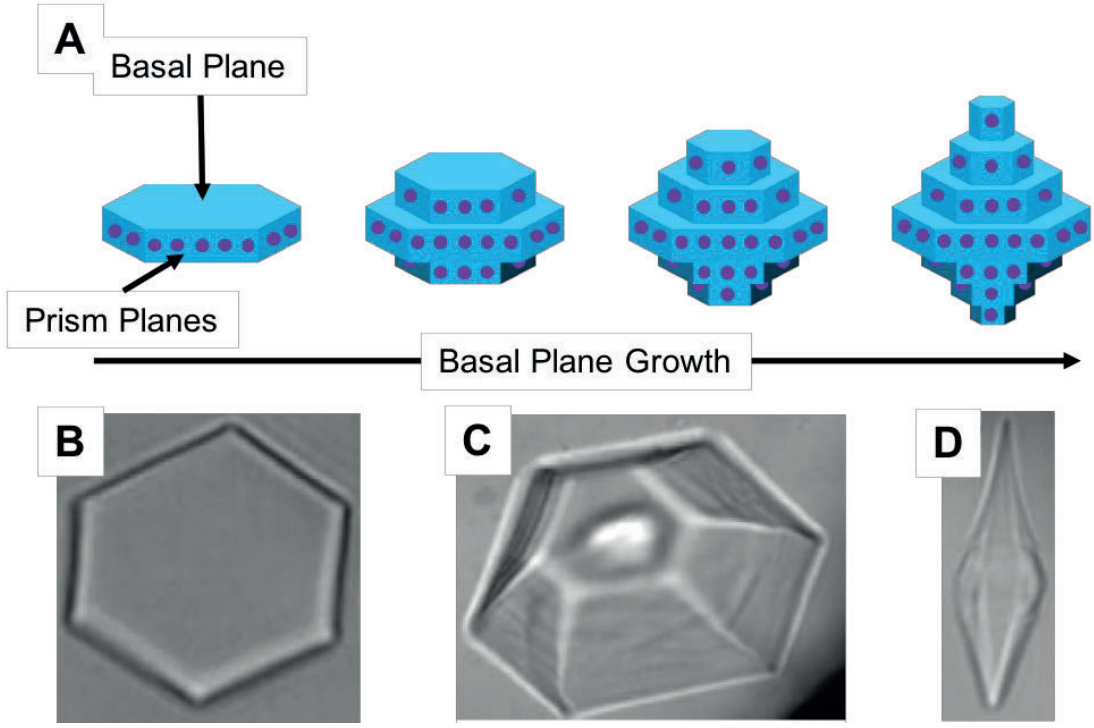

Figure 1.08: A A schematic to show how prism plane binding leads to dynamic ice shaping. Only the basal plane can grow due to the adsorption of protein (Purple circles) to the prism plane, this leads to sphicular ice growth and eventually cell damage. **B, C & D**; Ice crystal images of crystals grown in water (**B**), low concentration AFP solution (**C**) and high concentration AFP solution (**D**). Images **B**, **C** and **D** are adapted from Griffith *et al.*[54]

Dynamic ice shaping (DIS) and thermal hysteresis are intrinsically linked, with both requiring irreversible binding of the protein to the surface of the growing ice crystal for any effects to be observed. As a result of the similar mechanisms involved, all proteins which demonstrate TH activity will also to some extent engage in DIS.

1.1iv Ice Recrystallisation Inhibition

The final macroscopic mechanism by which AFPs may enable low temperature survival is ice recrystallisation inhibition (IRI). Ice recrystallisation is a thermodynamic process which encourages the growth of large ice crystals in a solution

at a temperature greater than the glass transition temperature. The ability of antifreeze proteins to non-colligatively inhibit ice recrystallisation was first observed by Knight in 1988.[59] In order to measure the effect of an AFP on ice recrystallisation the 'splat' assay was developed. In short, a solution of protein in saline was dropped from a height onto a plate cooled to -80 °C to form a polynucleated ice wafer. This ice wafer is then annealed for up to 18 hours at -8 °C, after which images of the wafers are recorded using a microscope (Figure 1.09). Both the annealing temperature and the concentration of salt in the solution are crucial for the assay to work. Careful consideration of these two factors are required to ensure the presence of liquid water between the grain boundaries at the annealing temperature. Without this water, no migration would be able to occur, and therefore no recrystallisation would be observed. As the ice crystals are formed, solute is forced out of the crystal, creating local regions of high salt concentration which cannot freeze at the annealing temperature.

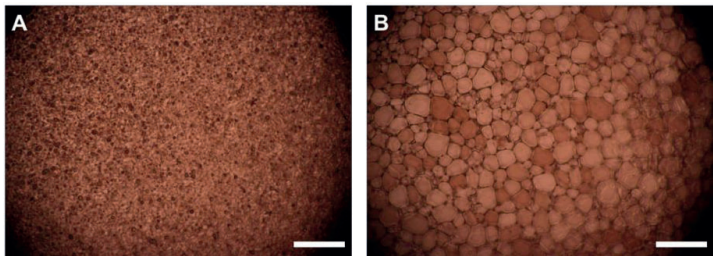

Figure 1.09: Images of polynucleated ice wafers of a PBS solution recorded in the splat assay, images are taken before (**A**) and after (**B**) 30 minutes annealing at -8 °C. Images are 20x magnification, scale bars are 200 μm.

Knight proposed that recrystallisation occurs as a result of grain boundary migration. Liquid channels trapped between the concave surface of a large ice crystal, and the more linear surface of a smaller one, will have different curvature, and therefore

different freezing points (see Equation 1.02 for the relationship between freezing point and curvature). This results in freezing of the concave surface, and local melting along the interface of the smaller crystal, resulting in migration of the grain boundary into the smaller crystal, and growth of the larger.[60]

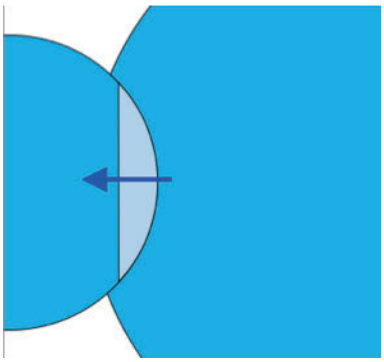

Figure 1.10: Grain Boundary Migration. Differing surface curvature causes a change in the melting point between the larger and smaller crystals, resulting in migration of the liquid inclusion (pale blue) into the smaller crystal, and growth of the larger crystal. The blue arrow indicates the direction of boundary migration.

More recently, computer simulations have proposed a two stage method for ice recrystallisation, with grain boundary migration dominating at later time points in the recrystallisation process, once a small number of large crystals have formed.[61] Ostwald ripening has been shown to dominate immediately after nucleation when the majority of crystals will be a very similar size, or in solutions with very high solute content, in which ice makes up a much smaller volume of the overall solution.[62] This process minimises the overall energy of the solution by reducing the surface area to volume ratio of the ice phase. As a result of the increased curvature and therefore lower melting point, the smallest crystals in solution will melt, releasing water into the solution, however as this is not constrained between adjacent ice grains, this can diffuse around the entire system. These free water molecules migrate to the larger

crystals where attaching to the surface becomes more energetically favourable, eventually resulting in an overall increase of crystal size and a reduction in crystal number. A variety of materials have been shown to be able to inhibit these recrystallisation processes, from AFGPs to synthetic polymers,[5] supramolecular structures[63] and even small molecules.[64] Classically, the rate of Ostwald ripening is determined by either the rate of diffusion of the small molecule,[65] or the rate at which species attach and detach from the surface of the crystal,[66] whichever is slower. This therefore suggests there are two likely possible mechanisms through which AFGPs inhibit the growth of ice. At low temperatures, some AFGPs have been observed to increase the solution viscosity to an extent much greater than predicted on a colligative basis.[67] This increase in viscosity would cause a decrease in the diffusion coefficient and therefore may contribute to the high IRI activity which these materials display. This is not a universal mechanism though, as some highly IRI active AFPs do not demonstrate this viscosity increase.[68] The other main theory as to how IRI active materials inhibit recrystallisation is by increasing the energetic cost of adding water to the ice surface, either through irreversible binding and blocking of potential growth sites (AFP/AFGPs) or for active non-binding materials through disruption of the semi-ordered water layer on the surface of the crystal.[64,69] At very short distances from the ice face, and in the absence of any external inhibitors, water has been shown to pre-arrange into a more ordered phase.[70] This semi-ordered layer reduces the energetic barrier to freezing, and promotes the growth of ice crystals. The water ordering ability of each face has been investigated, with different faces causing different levels of surface water ordering. The faster growing prism planes were shown to cause much more efficient structuring of the nearby water molecules, whilst also influencing the dynamics of the adjacent waters. Slower growing basal faces were shown to more

strongly influence the density of water at the interface, however these molecules displayed much more 'bulk water' like dynamics.[71] While there is a great deal of modelling investigating the effect of AFPs on growing ice crystals, there is little experimental evidence for these theories, and therefore the exact mechanisms which lead to a material displaying IRI activity are still unknown.

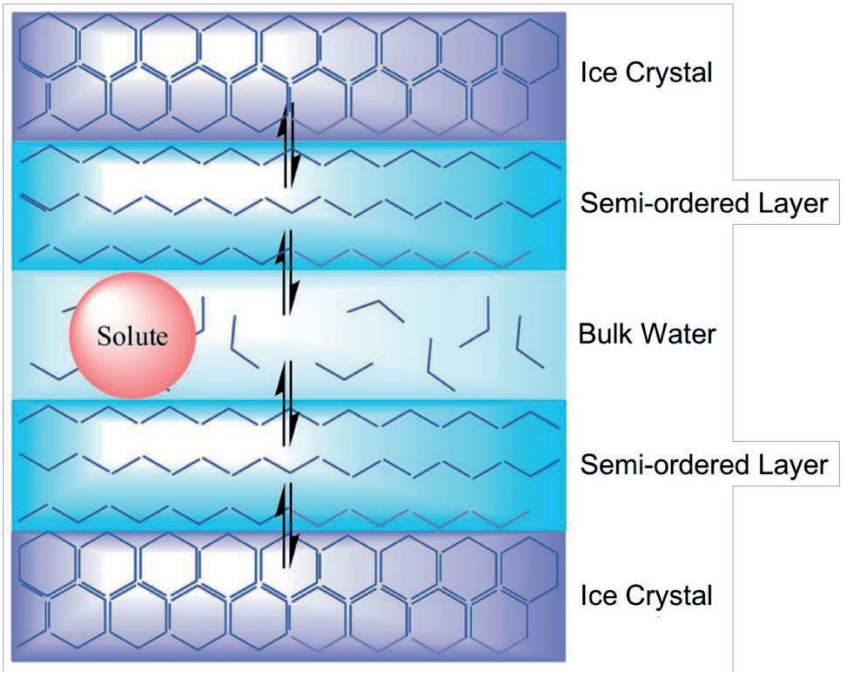

Figure 1.11: Illustration of the semi ordered layer and the mechanism proposed by Ben *et al.* for the inhibition of ice growth by solute molecules. The solute molecule will occupy a position at the interface of the semi-ordered layer and the bulk water, disrupting water ordering and raising the energetic barrier to recrystallisation. Image adapted from Ben *et al.*[64]

The ability to control the crystal size of ice is important in a number of commercial areas. Ice recrystallisation severely impairs the texture of ice cream, and therefore formulations which include ice recrystallisation inhibitors have been developed.[72,73] In the aerospace sector, the growth of ice on the surface of plane wings has to be carefully considered to ensure sufficient fuel is available to compensate for increased

weight and drag.[74] In order to enhance cryopreservation outcomes, understanding the effect of recrystallisation on biological materials is important. Recrystallisation affects cells in two main ways, mechanical damage caused by growing crystals rupturing cells, and the dehydration effect of ice growth increasing the solute concentration can cause osmotic shock. While storage at -80 °C will prevent most recrystallisation, significant cellular damage occurs during thawing, where temperature gradients will be formed across larger samples, encouraging recrystallisation.[75] Whilst AFPs and AF(G)Ps would appear to be ideal candidates for use as cryoprotectants, sphicular ice crystals which form as a result of dynamic ice shaping, cause a significant decrease in cell recovery at high concentrations.[76]

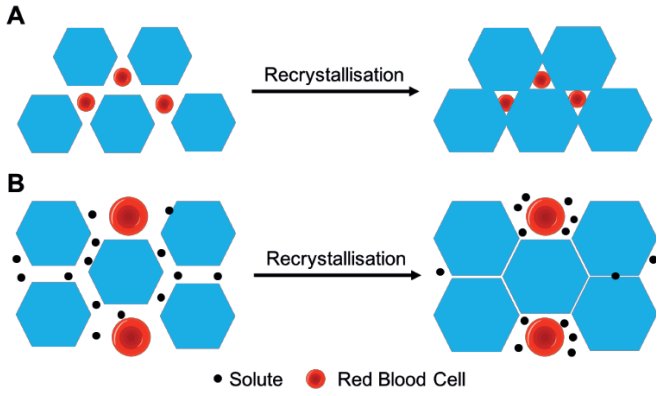

Figure 1.12: Illustration of the damage caused by ice recrystallisation. **A** Mechanical damage is caused by cells being crushed between growing ice crystals; **B** Osmotic damage caused by increased solute concentration around the cell causing dehydration.

In order to lessen the damage caused by recrystallisation a number of strategies have been investigated. Storing biological materials in the presence of AFPs within the TH gap of the protein reduces the mechanical and osmotic damage caused by ice growth. Rat hearts, stored in a solution of AFP I or AFP III at -1.3 °C were able to survive reperfusion and transplantation, compared to controls, where three out of four rats died

after reperfusion.[77] This non-freezing technique has also been demonstrated for the storage of other organs and over longer time scales.[78,79] Storage within the TH gap of an AFP however requires very precise control of the environment, as too much temperature variation can cause significant damage to the organ, and this technique has not been used for larger organs, whilst also being incredibly expensive. Another potential technique is to avoid ice formation altogether. Rapidly decreasing the temperature of a solution below the glass transition temperature will form amorphous ice, which has no crystals present to damage the frozen materials. Cryoprotectant free vitrification is however only useful for incredibly small volumes, as instantly freezing, and thawing, large volume samples without any temperature gradient across the sample is not currently possible.[80] For relatively small volume cell samples, vitrification in the presence of a high concentration of ethylene glycol or organic solvent (often dimethyl sulphoxide (DMSO)) is often used, this allows the formation of a glassy state, again in which no ice crystals are present to damage the cell. These solvents are however toxic,[81,82] and therefore significant purification is required after thawing to remove these additives as quickly as possible. The final potential solution is using standard slow freezing techniques paired with the incorporation of IRI active materials, which do not display TH or DIS. Inhibiting ice recrystallisation has been shown to correlate with enhanced cellular recovery in a variety of systems.[83–85] Fortunately, however, whilst TH and DIS are closely related, IRI appears to be an independent phenomenon, with a small number of AFPs which display incredibly weak TH and little ice shaping activity being incredibly IRI active.[86]

Polymeric and small molecule inhibitors are of significant interest, as very few synthetic materials have been shown to demonstrate TH/DIS. The goal of this effort is to identify low cost, biocompatible materials which have significant IRI activity.

1.2i Synthetic Mimics of Natural Proteins

The design of materials which are able to reproduce the function of proteins is of great scientific interest, with a variety of strategies having been investigated.[87,88] Solid phase peptide synthesis[89] allows precise control over the amino acid sequence, and therefore with careful design, the overall secondary structure of the material.[90–92] This route has been used for a wide variety of target molecules, to generate natural and non-natural peptide mimetics.[93,94] The main limitation of these materials is that they are expensive and time consuming to synthesise on large scales, especially if long peptides are required.[95] In situations where precise control of amino acid sequence is not necessary, the polymerisation of amino acid *N*-carboxyanhydrases (NCAs), allows the comparatively simple and large scale synthesis of homo-polypeptides *via* ring opening polymerisation (ROP) (Figure 1.13).[96] New, controlled methods for NCA polymerisation are still being investigated, demonstrating how important this route is to access linear and cyclic polypeptides.[97,98] Poly(amino acids) derived from NCA polymerisation are used in surfactants,[99] gene delivery[100] and drug delivery, as both micelles and vesicles.[101,102]

While these materials are much more synthetically accessible than those made through solid phase peptide synthesis, they are still much more complicated than the synthesis of vinyl derived polymers *via* standard free radical polymerisation. As a result of this, fully synthetic polymers which can recreate or enhance the functions of natural proteins, whilst being scalable and requiring little specialised equipment and experience, are of significant relevance.[103]

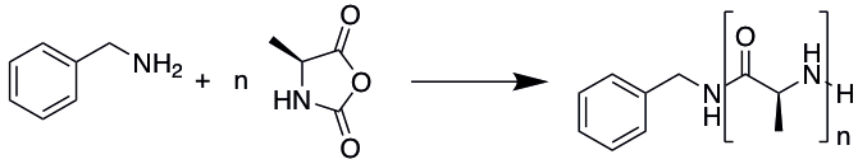

Figure 1.13: Reaction scheme for the NCA polymerisation of L-Alanine initiated by benzylamine.

Synthetic polymer networks have been widely investigated as mimics for the extracellular matrix, replacing the proteins and proteoglycans usually present with synthetic polymers such as poly(ethylene glycol) (PEG) or poly(hydroxyethyl methacrylate).[104] One significant advantage of these materials is the ability to fine tune the physical properties such as water content and stiffness. Poly(acrylamide) hydrogels have been shown to give control over the differentiation of stem cells, with harder materials producing more bone-like cells, whilst softer materials encourage brain-like cell development.[105] Hydrogels also benefit from the ability to incorporate chemical moieties which allow subsequent manipulation of the surface chemistry, PEG hydrogels containing cell-adhesive peptides protected with a photolabile caging group have been implanted, followed by exposure to transdermal light which encouraged accelerated vascularisation of the implant.[106] Bioinspired phospholipid polymers have also been used to prevent surface induced clotting on implanted artificial organs and biomedical devices, allowing for greater blood and tissue compatibility.[107]

Polymer mimics of antimicrobial proteins have also been investigated by Tew *et al.*, they observed that despite the wide variety of sources of antimicrobial peptides, they are often made up of facially amphiphilic proteins, with significant positive charges.[108] They were able to synthesise a variety of antimicrobial polymers based on these design rules, which are synthetically much easier to produce than the peptides on which they

are based.[109] These design rules were then used to aid in the synthesis of new antimicrobial polymers, *via* the ring opening metathesis polymerisation of a series of functionalised norbornenes, the products of which were significantly more selective for bacterial cells.[110]

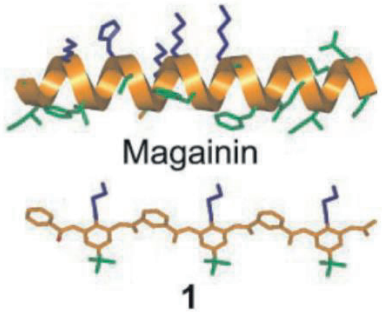

Figure 1.14: Structure of the antimicrobial peptide Magainin and the polymeric analogue (**1**) synthesised by Tew *et al.* Figure adapted from Ref 109.

While most of these materials are inspired by natural proteins, polymer chemists have significantly less control over the final structure of the material than those found in nature. Recent advances in controlled radical polymerisation however are slowly enabling much greater precision in the structures produced.

1.2ii Controlled Radical Polymerisation

Free radical polymerisation gives little ability to predict the molecular weight of the material produced without significant optimisation, as well as producing materials with a wide dispersity caused by the high rate of termination and number of possible side reactions. When these materials are compared to the precisely controlled structures of proteins, it is clear that greater control over the synthesis of these materials is required. The ability to generate materials with controlled architectures and predictable molecular weights is of great importance. Anionic[111,112] and

cationic[113,114] polymerisation techniques were the first to give fully 'living' polymer chains, which allowed accurate prediction of molecular weight based on conversion and monomer to initiator ratio, as well as the ability to easily perform chain extension experiments simply by the addition of more monomer. However these techniques are incredibly air sensitive, with limited monomer compatibility, and while they allow access to incredibly narrow molecular weight distributions,[115,116] and complex architectures,[117,118] these living techniques have widely been replaced by other more recent reversible-deactivation radical polymerisation (RDRP) techniques. These methods are based on the reversible deactivation of the growing polymer chain end, resulting in a lower rate of termination at any given time, and therefore allowing greater control over the length and molecular weight distribution of the resulting polymer (Figure 1.15). These techniques were pioneered by Otsu in the 1980's, with the development of iniferter polymerisation.[119] Iniferter polymerisation uses a single reagent which acts as an **ini**tiator, chain trans**fer** agent, and **ter**minating agent. More recently, iniferter polymerisation has attracted significant interest, due to its compatibility with air sensitive light mediated polymerisation.[120,121] The concept of a growing polymer chain which can be reversibly deactivated by exploiting a weak C-X bond laid the groundwork for later developments in more widely used RDRP polymerisation techniques. Currently, the most commonly applied RDRP methods are nitroxide mediated polymerisation (NMP),[122] atom transfer radical polymerisation (ATRP)[123] and reversible addition fragmentation chain transfer (RAFT)[124] polymerisation.

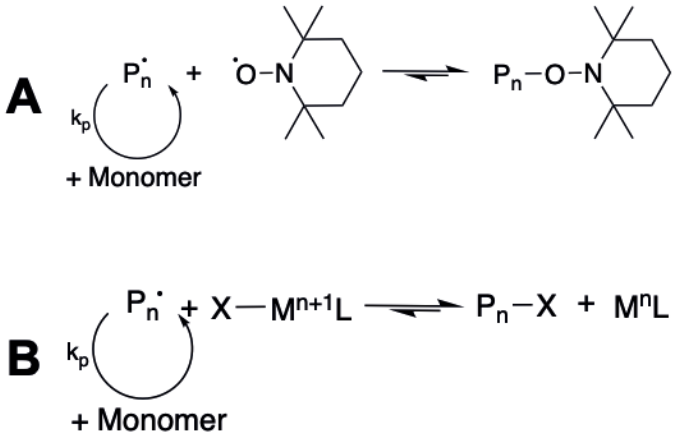

Figure 1.15: Generic reaction schemes for **A** NMP and **B** ATRP. In both processes, reversible deactivation of the growing polymer chain allows for reduced radical concentration and therefore greater control over the rate of propagation, ensuring all chains grow at an equal rate. P_n is the growing polymer chain, M is the transition metal, L the ligand and X is a halogen.

Nitroxide mediated polymerisation was developed in 1986 by Solomon *et al.* and uses a nitroxide species capable of forming a stable persistent radical[125] to reversibly terminate the radical end of the growing polymer chain. The rate of this bond formation and cleavage is determined by the structure of the nitroxide, growing polymer radical and the temperature of the reaction. Initially both a stable nitroxide e.g. 2,2,6,6-tetramethylpoperidinyl-1-oxyl (TEMPO) and a radical initiator were required,[126] however later developments removed this requirement, allowing alkylated TEMPO derivatives to act as both the initiating species and stable radical.[127] Whilst initially most polymerisations using NMP focussed on styrene and its derivatives,[128] almost all monomer classes have been shown to be compatible with NMP.[129] Despite these advantages, however, NMP is not as widely applied as ATRP or RAFT due to the high temperatures required for sufficiently fast polymerisation kinetics and the significant side reactions which occur when using methacrylic monomers.[130]

ATRP was developed independently by both Sawamoto[131] and Matyjaszewski[132] in 1995. ATRP is controlled by the equilibrium of the reaction between the deactivated polymer and the activated metal ligand complex, to form the propagating polymer chain, and the deactivated metal ligand species. A variety of factors can alter the position of this equilibrium, with the choice of monomer, metal, ligand, solvent and temperature all having a significant effect on the resulting rate of activation and deactivation. A higher constant of deactivation leads to polymers with a narrower molecular weight distribution, however if the rate of deactivation is too fast, the polymerisation will not proceed after the first deactivation step. As a result of this, the combination of initiator, ligand and solvent often need to be optimised for a given monomer in order to achieve a balance between rate of polymerisation and final molecular weight distribution, however some recent research has attempted to identify a set of universal conditions for most activated monomers.[133] ATRP has also recently been demonstrated to be able to carry out 'open air' polymerisation, in both aqueous media[134] and organic solvents,[135] as well as at ultra-low volumes.[136] ATRP also allows the synthesis of a number of complex polymer architectures.[137,138] Unfortunately, due to the position of this equilibrium, ATRP is not ideal for the polymerisation of less activated monomers, as well as there being issues with the removal of undesirable copper from the final polymer.

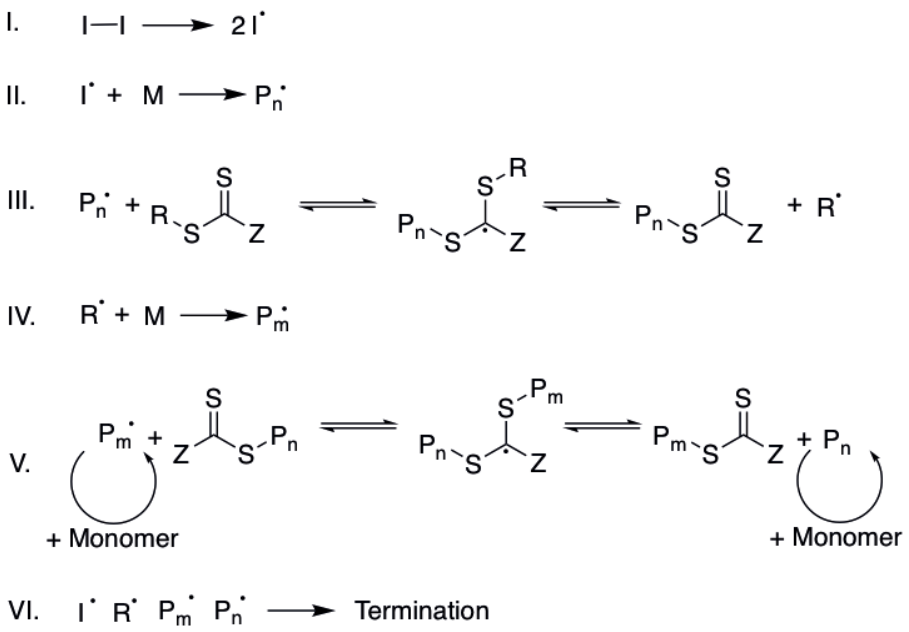

Figure 1.16: Proposed mechanism for RAFT polymerisation, with both the pre-equilibrium (**III**) and equilibrium (**V**) shown. Adapted from Perrier.[139]

RAFT polymerisation, developed in 1998 at CSIRO, involves the use of a dithioester or trithiocarbonate as a chain transfer agent (CTA) and a standard radical initiator. The initiator is activated as in a standard free radical polymerisation, and this will then react with the monomer present to form a polymer radical. This polymer radical will then undergo addition to the RAFT agent to form a macroCTA, releasing the R group of the RAFT agent to re-initiate the polymerisation (RAFT pre-equilibrium, Figure 1.16 III). This addition is reversible, and once all of the R groups have initiated polymerisations, the main equilibrium is reached between the active and dormant polymer chains. In order to ensure that all of the polymer chains are growing at the same rate, the rate of fragmentation must be much greater than the rate of propagation for the monomer used. This ensures that only one monomer addition happens in between each addition-fragmentation event, ensuring a linear increase of molecular weight with conversion. If the rate of fragmentation is sufficiently high, it also implies

that the number of chains which can undergo bimolecular termination is equal to the number of chains that were initially generated from the activation of the radical initiator.[139] This is advantageous when compared to other RDRP systems as it allows the living character of the polymer chains to be maintained at high conversion (97-100 %), allowing very efficient block copolymer synthesis.[140] In order to ensure the optimal equilibrium during the chain transfer reactions, the reactivity of the R and Z groups of the RAFT agent need to be carefully considered (Figure 1.17). When deciding on the Z group to be used, the reactivity of the C=S bond to radical addition must be greater than that of the C=C bond in the monomer, this governs the stability of the intermediate radical. Monomers are usually divided into two general classes, more activated monomers (MAMs), which contain electron donating groups which are able to stabilise the radical centre during a polymerisation, and less activated monomers (LAMs) which contain an electron withdrawing group adjacent to the radical centre causing destabilisation of the radical. If the macroCTA formed in the pre-equilibrium step is much less stable than the polymer radical, as is often found for more activated monomers, the addition reaction is disfavoured, and the polymerisation will proceed mostly *via* a free radical process.

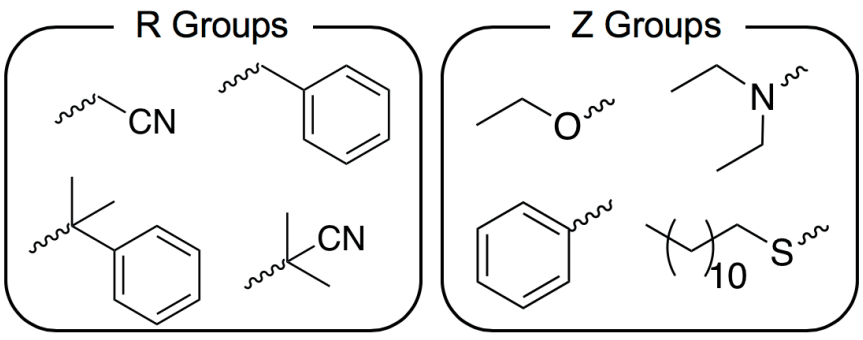

Figure 1.17: Examples of commonly used R and Z groups. Those on the top row are suited to LAMs, with those on the bottom row being more applicable for MAMs.

The polymerisation of MAMs is therefore often carried out using trithiocarbonates or dithiobenzoates. However, if the macroCTA formed is much more stable than the monomer radical, commonly observed for less activated monomers (LAMs), the initial addition of the polymer chain onto the RAFT agent will severely limit the polymerisation, and no further propagation will occur. LAMs therefore require the use of xanthates or dithiocarbamates, these species generate a less stable radical intermediate which favours fragmentation, and hence allows the polymerisation to proceed after the first monomer addition.[141] Examples of both 'more activated' and 'less activated' monomers are given in Figure 1.18.

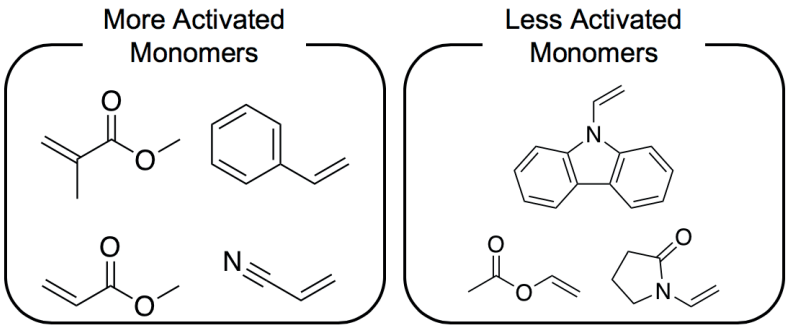

Figure 1.18: Examples of MAMs and LAMs commonly used in RAFT polymerisation.

The R group of the RAFT agent is involved in the initial radical addition of the growing polymer chain, as well as the subsequent reinitiation of the polymerisation. Therefore the same considerations with regard to C=S stability are required, whilst also needing to consider the ability of the R group radical to quickly reinitiate propagation of a new growing polymer chain. In order to ensure efficient reinitiation, the R group is usually similar in structure to those found in traditional radical initiators. Developments in RAFT agent design and synthesis allow simple access to a wide range of dithioesters and trithiocarbonate CTAs, with the one pot synthesis of a range

of RAFT agents demonstrated by O'Reilly in 2008.[142] For the polymerisation of less activated monomers, xanthate based CTAs with an ethanol Z group can be easily prepared from potassium ethyl xanthate,[143] if an alternate Z group is required, the reaction between a radical initiator and a bis(dithiocarbonate) can be exploited.[144] More recently, the synthesis of switchable RAFT agents has been reported for the formation of block copolymers of MAM and LAMs, these materials are based on dithiocarbamate RAFT agents, the protonation of which greatly affects the stability of the adjacent C=S bond, this therefore allows the monomer compatibility to be easily changed with the pH of the solution. This has been used for the formation of methyl methacrylate-*block*-vinyl acetate copolymers with narrow molecular weight distributions.[145]

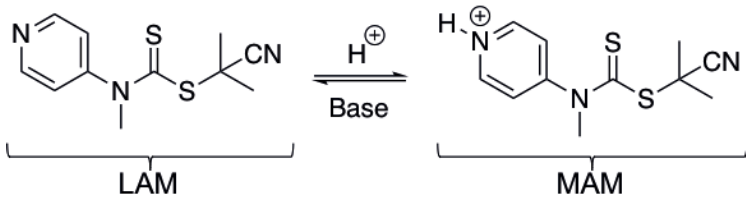

Figure 1.19: An example of a switchable RAFT agent. The deprotonated form is ideal for the polymerisation of less activated monomers, while the protonated form works equally well for more activated monomers. This allows the formation of block copolymers previously not possible through the use of RAFT.

As with other controlled polymerisation methods, RAFT also allows for the formation of complex macromolecular architectures, such as star,[146] branched,[147] hyperbranched[148] and surface grafted polymers.[149] As a result of the thiol group present on the end of the polymer chains formed during a RAFT polymerisation, these materials have also been widely exploited for the formation of multivalent gold

nanoparticles.[150,151] In some cases, however, this thiocarbonylthio end group is undesirable, and therefore a variety of mechanisms have also been developed for its removal.[152]

1.3 Polymer Mimics of Antifreeze Proteins

Recent advances in polymer chemistry, paired with the cost and toxicity issues associated with repurposing natural proteins, make synthetic macromolecular alternatives an attractive solution to preventing the damage caused by cryopreservation.[1] However, the structural diversity demonstrated by known AF(G)Ps, and the precise folding required to ensure the correct moieties are aligned perfectly with the growing crystallographic face, has made rational design of these materials incredibly challenging.[9] It has been demonstrated that IRI activity is important for successful cryopreservation, however at too high a concentration, dynamic ice shaping actively enhances cell damage,[6,75] therefore synthetic materials which display only IRI activity are thought to be ideal for these applications.[85] The first fully synthetic polymer reported to display significant IRI activity, poly(vinyl alcohol) (PVA) was observed by Knight in 1995.[60] PVA was also shown to display no thermal hysteresis, demonstrating that these three properties (TH, IRI, DIS) could be separated. More recently, poly(ampholytes) have also been discovered as another potential class of active cryoprotectants, with their discovery by Matsumura in 2009.[153] These two main classes of synthetic cryoprotectants will be discussed further below.

1.3i Synthesis of Poly(vinyl alcohol)

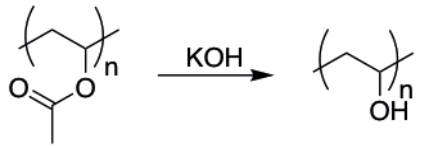

Figure 1.20: Deprotection of poly(vinyl acetate) using potassium hydroxide to form poly(vinyl alcohol).

Poly vinyl alcohol was first prepared in 1924 by Hermann and Haehnel, by treatment of the poly(vinyl acetate) precursor with potassium hydroxide (Figure 1.20).[154] Since its initial synthesis, poly(vinyl alcohol) has been used in a wide variety of areas, from as a surfactant for the emulsion polymerisation of vinyl acetate,[155] to wood glue.[156] Poly(vinyl alcohol) is also non-toxic[157] and therefore PVA based materials have been investigated for use in a variety of biomedical applications.[158,159] The ability to synthesise well defined polymers of vinyl acetate is therefore of significant commercial importance. The structure of vinyl esters however means that the propagating radical in a polymerisation reaction is not well stabilised. This leads to significant side reactions such as chain transfer to solvent,[160] head to head addition (which increases in frequency with increasing temperature),[161] and branching,[162] and hence broad molecular weight distributions in the final polymer. Selection of vinyl ester precursor is also important, with differently substituted esters leading to significant differences in the rate of hydrolysis. As an example, while vinyl pivalate is stable in a 0.2 wt % solution of KOH for over 4 hours, vinyl trifluoroacetate is fully deprotected in 1 hour at a 10x lower KOH concentration.[163] The tacticity of the resulting polymer can also be controlled through the use of differently substituted vinyl esters, with bulkier substituents promoting a greater syndiotactic content.[163,164]

In order to reduce the prevalence of these many side reactions, and produce more narrowly defined materials, as well as allow more complex polymer architectures to be investigated, controlled radical polymerisation has been explored. Whilst a variety of mechanisms for the controlled polymerisation of vinyl esters have been demonstrated using iron,[165] iodine[166] or cobalt[167] complexes, RAFT polymerisation is by far the most widely used method.

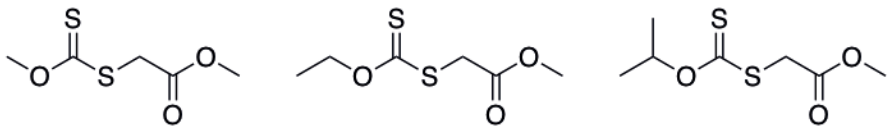

Figure 1.21: RAFT agents demonstrated by Stenzel *et al.* to be well suited for use in the polymerisation of vinyl acetate.

As with all RAFT polymerisations, the precise structure of the chain transfer agent must be considered. Vinyl acetate is considered to be a less activated monomer and therefore when xanthates or dithiocarbamates are employed, good control over the molecular weight distribution of the resulting poly(vinyl acetate) can be maintained. Stenzel *et al.* demonstrated that xanthates with methyl, ethyl and isopropyl alcohol substituents as the Z group gave excellent control over the polymerisation, allowing low dispersities to be achieved ($Đ < 1.3$), and with relatively simple synthesis of the chain transfer agent (Figure 1.21).[168] Selection of R group is arguably more important for vinyl esters than most activated monomer classes due to the low reactivity of the monomer towards radical addition. Stabilised R groups such as 2-cyanoisopropyl cause slow reinitiation and significant retardation of the polymerisation, however if unstable groups are used, such as 2-phenylethyl, fragmentation of the RAFT agent is inhibited, leading to low chain transfer constants and a free radical polymerisation mechanism dominates.[141]

As well as enabling greater control over the molecular weight, RAFT polymerisation also allows more complex architectures to be synthesised, with poly(vinyl acetate) block,[169] star,[146,170] comb[171] and bottlebrush[172] polymers having been reported.

1.3ii The IRI activity of PVA

In 1995, Knight observed that poly(vinyl alcohol) was a potent IRI but did not display significant thermal hysteresis.[60] This was one of the first instances of a synthetic polymer displaying such a property, and can be considered the birth of this field. Inada *et al.* evaluated the AF(G)P-like properties using commercial PVA samples.[173] They found that PVA displayed molecular–weight dependent IRI activity and that on a molar basis had activity comparable to the shortest AFGPs. A key point to note here is that due to the high molar mass of the polymers, they were actually 10 – 100 fold less active than AFGP on a mass basis, but still remain the most active synthetic polymers reported today. Due to the activity of PVA, a simple assumption would be that any poly(hydroxylated) polymer could show IRI, as AFGPs are also poly-ols to a first approximation. Gibson and co-workers have tested various polysaccharides and glycopolymers which were found to be weak IRIs; a poly-ol alone is not the minimum required feature of a synthetic IRI (Figure 1.22).[174,175] This suggests that the specific orientation of the hydroxyl groups in PVA is ideally suited for ice interaction and growth inhibition.

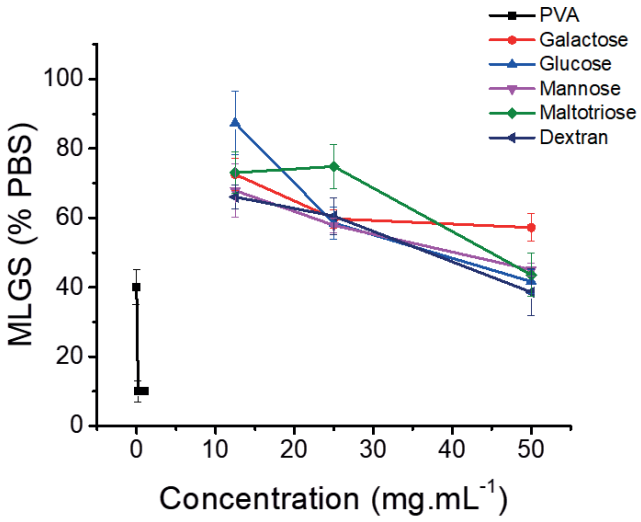

Figure 1.22: IRI activity of a series of poly-ols compared to PVA. MLGS = mean largest grain size reported as a length. Error bars represent ± standard deviation from a minimum of 3 repeats.

Budke *et al*. have postulated that the spacing between hydroxyls on PVA are a good match for the prism planes of a growing ice crystal and hence may explain its activity (Figure 1.23).[176] However, this does not take into account the observations with small-molecule IRIs about the role of amphiphilicity, and that an AFP's ice-binding face is actually the most hydrophobic, with the hydrophilic face directed into the unfrozen water layer; it is therefore possible that multiple molecular level mechanisms could give rise to the same macroscopic effects and this therefore warrants further investigation.

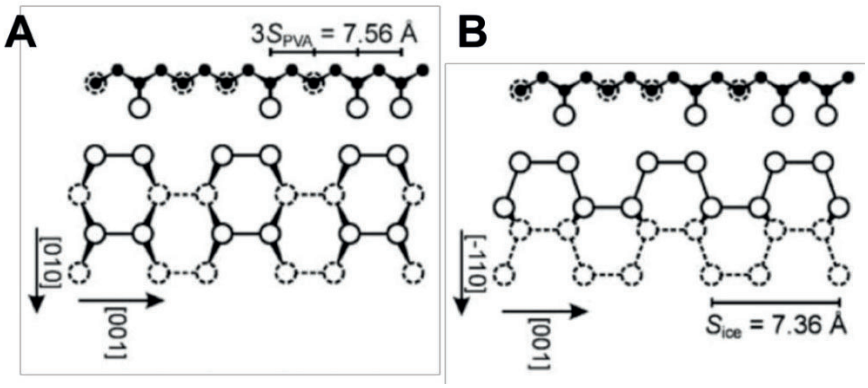

Figure 1.23: Proposed binding conformation for PVA to a growing ice face. The alignment between the primary (**A**) and secondary (**B**) prism faces are shown. Adapted from Budke *et al.*[176]

The above studies were all conducted using commercial PVA samples; these are characterised by broad molecular weight distributions ($M_w/M_n > 2$), low molecular weight contaminants (unless dialysed before use) and the presence of 0 – 20 mol % acetate groups remaining from its synthesis from poly(vinyl acetate). This inhomogeneity meant that drawing structure-activity relationships was challenging, if not impossible. To enable a more systematic approach, Congdon *et al*. employed controlled radical polymerisation (RAFT) to obtain well defined PVA of predictable chain length and narrow molecular weight dispersity.[177] By using hydrazine (rather than NaOH) to remove the acetate groups it was possible to obtain homogenous PVA. Selective re-acetylation, or copolymerisation with isopropenylacetate, revealed that incorporation of more than 20 mol % of any additional functionality lead to substantial reduction in the IRI activity. Crucially, this explains the inconsistent results from commercial PVAs due to their residual acetates, but also shows how sensitive the PVA structure is to structural modifications. Interestingly, similar effects are demonstrated by AFGP's which lose activity if >35 % of the hydroxyl groups are removed, but whether this is due to the loss of hydroxyl 'function' or a change in the folding of the

protein has not been resolved.[178] Conversely, block copolymerisation of PVA appeared to be tolerated, with no change in activity. Fusion proteins of AFPs with *N*-terminus maltose binding protein have been found to have identical activity to free proteins, supporting that large chain-end modifications are tolerated.[179]

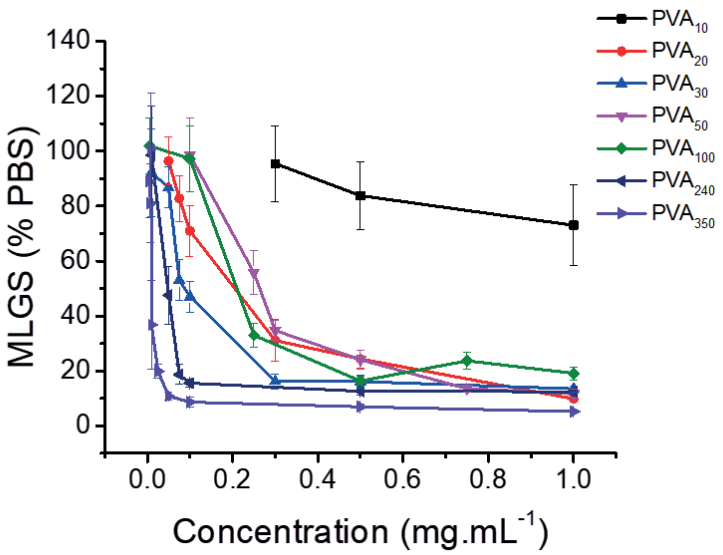

Figure 1.24: The IRI activity of PVA shows a significant molecular weight dependence, with longer PVA being more active. MLGS = mean largest grain size reported as a length. Error bars represent ± standard deviation from a minimum of 3 repeats.

Inada's original work had revealed a strong molecular weight dependence on activity (Figure 1.24).[173] Gibson and co-workers confirmed that even at relatively low molecular weights (< 10,000 g.mol^{-1}) there was significant IRI with an increase in chain length generally leading to an increase in IRI activity. The most startling increase was seen to be between DP 10 (~ 450 g.mol^{-1}) and DP 20 (~ 900 g.mol^{-1}) where the PVA essentially switched from being inactive to active. This was the first demonstration of the critical length of PVA required to activate IRI activity and is rather short when compared to AF(G)Ps.[177] This molecular weight dependence was

also exploited to generate the first example of an 'externally triggerable' IRI. Catechol end functional PVA was synthesised and upon addition of Fe^{3+} enabled formation of a supramolecular polymer with 3x molecular weight, and hence dramatically higher IRI.[180] A key advantage of using controlled radical polymerisation is the ability to modulate polymer architecture and topology.[181] 3-Armed, star branched PVA was found to have essentially identical activity to a 2–armed equivalent suggesting the third arm is redundant, and that total hydrodynamic volume rather than valency (number of hydroxyls) is a crucial parameter (Figure 1.25).

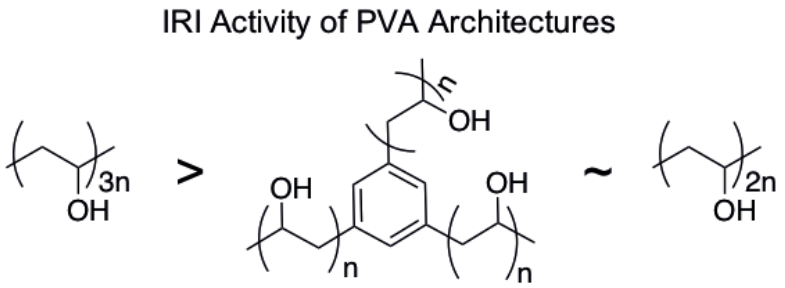

Figure 1.25: The effect of architecture on IRI activity. Linear PVA_{3n} is much more active than a star PVA of the same overall molecular weight. PVA_{2n} and the star PVA display similar activity as these materials have the same number of correctly orientated hydroxyl groups for binding.

Voets and co-workers synthesised bottlebrush PVAs and observed that the increased molecular weight did not correspond to an increase in activity, unlike with linear polymers, and hence determined that steric confinement limits activity.[172]

Whilst PVA has been the most studied polymeric IRI, findings from small molecule IRIs suggest that hydroxyl groups are not essential components and that a wide chemical space should be studied. Given the difficulties associated with the synthesis of PVA, as well as its resistance to modification, alternative polymeric materials are

of significant interest. Matsumura *et al.*, discovered that poly(ampholytes), polymers with mixed cationic and anionic groups, were remarkable cryopreservatives and seemed to have weak ice binding/affinity properties.[153] This novel class of cryoprotectant materials will be discussed further below.

1.3iii Synthesis and Cryoprotective Properties of Poly(ampholytes)

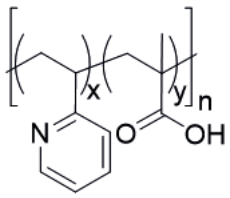

Figure 1.26: The first reported poly(ampholyte) was a copolymer of 2-vinylpyridine and methacrylic acid.

Polyampholytes, or mixed charge polymers, were first synthesised by Turner in 1950, as a 'synthetic alternative to proteins'. It was observed that a copolymer of 2-vinylpyridine and methacrylic acid demonstrates similar solubility and electrophoretic mobility to proteins (Figure 1.26).[182] Further research into these materials demonstrated that they are able to behave as poly(anions) in alkaline solutions, and poly(cations) in acidic solutions, whilst also demonstrating no charge near their isoelectric point.[183] Thus, these materials are interesting synthetic alternatives to proteins, and have been investigated for use in a wide range of applications such as drag reducers and bioadhesives.[184,185]

There are a variety of synthetic strategies which can be used to access poly(ampholytes), initially, most examples were synthesised through the free radical

copolymerisation of oppositely charged monomers generating statistical polymerisations, for example methacrylic acid (MAA) and either 2-vinyl pyridine[183] or dimethylaminoethyl methacrylate (DMAEMA)[186] (Figure 1.27 A). Later developments in living polymerisation techniques enabled the synthesis of the first polyampholyte blocks in the early 1970's by Stille.[187] 2-vinyl pyridine was copolymerised with a variety of methacrylate monomers, followed by deprotection of the methacrylate into the corresponding acid. Anionic polymerisation, however, is practically very challenging and this limited the synthesis of these materials to groups specifically designed to carry out these complex procedures. Since then, a variety of controlled radical techniques have been used to access poly(ampholytes), for example group transfer polymerisation (GTP),[188] nitroxide mediated polymerisation[189] and reversible activation-fragmentation chain transfer polymerisation.[190] More recently, the ring opening polymerisation of an *N*-maleamic acid functionalised homocysteine thiolactone monomer has also been exploited by Du Prez and co-workers to synthesise purely alternating polyampholytes with no compositional drift.[191] In some cases, the desired ampholytic units cannot be directly polymerised, and therefore a precursor material may be synthesised, followed by post polymerisation modification. This technique has been used for the synthesis of poly(ampholytes) from poly(amino acids) (Fig. 1.27 B)[153] and purely alternating maleic anhydride copolymers (Fig. 1.27 C).[192]

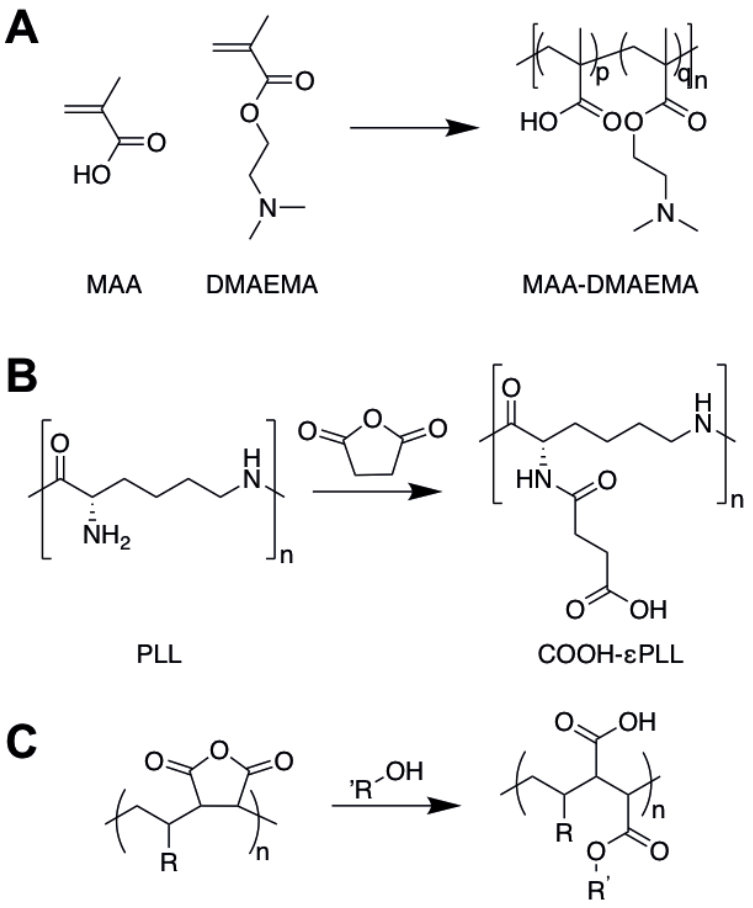

Figure 1.27: Common synthetic strategies used to access poly(ampholytes). **A** Copolymerisation of methacrylic acid and dimethylaminoethyl methacrylate; **B** Post-polymerisation modification of poly(L-lysine) using succinic anhydride; **C** Copolymerisation of maleic anhydride followed by post polymerisation modification using an alcohol.

Poly(ampholytes) were first investigated as cryoprotectants by Matsumura, finding that ε-poly lysine, when reacted with succinic anhydride, acts as a low-toxic cryoprotectant for the DMSO free storage of stem cells. It was observed that varying the ratio of cationic and anionic groups altered the recovery of the cells, indicating that a precise balance between the charges is required for maximum cryoprotective activity.[153] This necessary ratio was further investigated by Gibson, polymers of aminoethyl methacrylate were functionalised with varying amounts of succinic acid

to generate materials with a range of positive to negative charge ratios. It was found that IRI activity, thought to be related to cryoprotective ability, is greatest when a 1:1 ratio of charges is observed, with activity being lost as one charge starts to dominate. The nature of the charge was also shown to be important, with zwitterionic monomers containing both charges shown to have no activity.[193] Further investigations again demonstrated the importance of this charge balance, Matsumura synthesised copolymers of 2-dimethylaminoethyl methacrylate and methacrylic acid at varying compositions, again demonstrating the requirement for a 1:1 ratio of charges for optimal cryoprotective activity. Interestingly, it was also shown that increasing the hydrophobicity of the polymer *via* the incorporation of octyl or butyl methacrylate further increased both IRI activity and cellular recovery after thawing.[194] The effect of hydrophobicity increase on cryoprotectant activity was then investigated further, with hydrophobically modified p(DMAEMA-MAA) compared to poly(carboxymethyl betaine) (poly(CMB)) and poly(sulfobetaine) (poly(SPB)), and their hydrophobically modified counterparts. Incorporation of either butyl or octyl methacrylate into poly(DMAEMA-MAA) enhanced activity from ~60 % to 90 % recovery. Interestingly, poly(CMB) which has a remarkably similar structure to poly(DMAEMA-MAA) was shown to demonstrate no cryoprotective ability and very weak IRI activity, hydrophobic modification resulted in a significant increase in IRI activity, however had no effect on cellular recovery. Poly(SPB) showed a small change in IRI activity and no change in cell recovery after hydrophobic modification, suggesting that this is not a guaranteed method by which to enhance cryoprotectant activity in moderately active IRI materials, and that the activity of these materials may not be related to their IRI, but instead are interacting with the cell membrane.[195]

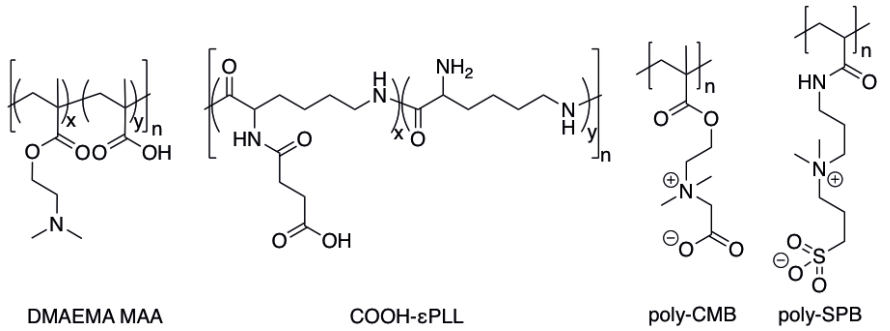

Figure 1.28: Poly(ampholyte) structures tested by Matsumura.

Other investigations into fully synthetic poly(ampholytes) have demonstrated that a copolymer of dimethylaminopropyl methacrylamide and acrylic acid are efficient cryoprotectants for the DMSO free cryopreservation of 3T3 cells. It was observed that with the inclusion of 9 % hydrophobic *N*-tert-butyl acrylamide, 90 % recovery (relative to 10 % DMSO) was observed immediately post thaw, however long term viability was poor. The addition of 2 % DMSO helped to reduce this loss, with results comparable to 10 % DMSO alone.[196] Matsumura has also developed poly(ampholyte) based hydrogel cryoprotectants, which form *in situ, via* a biocompatible copper free click reaction. These hydrogels were then used to demonstrate the DMSO free cryopreservation of mammalian cells.[197] Given the successes observed using poly(ampholytes) to aid in suspension freezing, Matsumura also investigated the applicability of these materials for the cryopreservation of cellular monolayers.[198] Monolayers are significantly more difficult to freeze[199] whilst also acting as a more realistic substitute for organs and tissues.[200] It was observed that DMSO can be omitted during slow vitrification by using a cryoprotectant solution of ethylene glycol, COOH-εPLL and sucrose. Freezing rates as low as 4.9 °C/minute were used, with good recovery of the cells immediately after thawing and after 1 day of cell culture. COOH- εPLL has since been shown to be effective for the cryopreservation of a wide variety of other cell types, for example chondrocyte cell sheets,[201] mouse oocytes,[202]

pig[203] and mouse[204] embryos and long term studies on human mesenchymal stem cells.[205]

Using the findings of Matsumura and others, Mitchell *et al*. reported one of the first rationally designed cryoprotectants, using the commercially available ampholyte precursor poly(methyl vinyl ether-*alt*-maleic anhydride). This material was functionalised with a Boc-protected aminoethanol, followed by deprotection to generate a poly(ampholyte) with exact 1:1 charge ratios, and then applied to the cryopreservation of blood cells using a slow thawing technique that gave excellent recovery when paired with HES as a co-cryoprotectant.[206] Given the activity of these materials, the potential of maleic anhydride copolymers as ampholyte precursors was determined to be of interest. Poly(methyl vinyl ether-*alt*-maleic anhydride) is produced using a standard free radical polymerisation, which while efficient and low cost, leads to little control over the molecular weight, dispersity, and monomer incorporation of the polymer.

In an attempt to understand the mechanism by which polyampholytes provide efficient protection, Matsumura investigated the effect of three different cryoprotective polymers on the integrity of the cell membrane. Samples which gave greater cellular recovery post-thaw were shown to cause a greater depression in the membrane phase-transition temperature. Leakage experiments also suggest that the polymers interact with membranes, with improved cryoprotective activity also corresponding to less post-thaw leakage from a cryopreserved liposome.[207] This membrane interaction has been exploited by Matsumura for the introduction of lysozyme proteins into cells through a freeze-thaw mechanism, which enables a 4-fold increase in uptake when compared to non-frozen cells.[208] It was then demonstrated that these poly(ampholyte) based nanocarrier complexes allow more protein internalisation when compared to 10

% DMSO, which is known to enhance membrane permeability.[209] Taken together, these results suggest that whilst also providing superior cell viability post thaw, poly(ampholytes) interact with the membrane during the freezing process to allow greater payload uptake when incorporated into a protein-nanocarrier complex. Even more recently, Matsumura has used hydrophobic poly(ampholytes) to enable the internalisation of gold nanoparticles into a cell sized liposome. The poly(ampholytes) were shown to localise in the disordered phase of the membrane and allow greater internalisation of particles at low temperatures.[210]

1.5 Summary

Antifreeze(glyco) proteins are incredibly potent inhibitors of ice growth, however due to their incredibly efficient ice binding, they also display unfavourable freezing point depression and dynamic ice shaping. Studies showing that these effects can be separated or minimised have inspired the development of materials which display only IRI activity for use as cryoprotectants. Of the materials which display only IRI activity, PVA is one of the most widely studied yet its exact mechanism of action is still unknown, attempts to identify its essential structural features may help to elucidate design rules to aid in the development of novel synthetic cryoprotectants. More recently, poly(ampholytes) have been identified as effective cryoprotectants, despite even the most active materials displaying relatively weak IRI activity. The mechanism of action is again not well understood, and therefore this provides another interesting route for the identification and development of new cryoprotectant materials.

1.6 Project Aims and Objectives

The aim of this work is to develop a better understanding of the necessary features of two main classes of cryoprotectant material; poly(ampholytes), and uncharged vinyl polymers, as well as identifying more active materials in the process. RAFT polymerisation, photoiniferter polymerisation and post-polymerisation modification have been exploited to systematically investigate structure activity relationships between active and inactive materials. By understanding these materials, and their necessary features, it is hoped that better cryoprotectant materials can be developed, and the goal of long-term cell storage using non-toxic materials and to achieve quantitative recoveries can be realised.

1.7 Thesis Summary

Chapter 2 studies the IRI activity of a multivalent PVA nanoparticle, as well as comparing the activity of a PVA homopolymer to a number of structural analogues in an attempt to identify the necessary structural features responsible for its activity. Chapter 3 investigates the effect of hydrophobicity and regioregularity on the IRI activity of a series of alternating poly(ampholytes), followed by the synthesis of a novel cryoprotectant based on a commercially available precursor, and its activity as a cryoprotectant for red blood cells. Chapter 4 details the optimisation of a high throughput screening process for the synthesis of libraries of DMSO free polymers without degassing, and its application for the synthesis of a library of poly(ampholytes), followed by the high throughput testing of these materials. Chapter 5 demonstrates the synthesis of a number of IRI inactive vinyl pyrrolidone copolymers, and the effect of hydrophobic modification on the observed IRI activity.

1.8 References

(1) Koshimoto, C.; Mazur, P. Effects of Warming Rate, Temperature, and Antifreeze Proteins on the Survival of Mouse Spermatozoa Frozen at an Optimal Rate. *Cryobiology* **2002**, *45* (1), 49–59.

(2) Harding, M. M.; Anderberg, P. I.; Haymet, A. D. J. "Antifreeze" Glycoproteins from Polar Fish. *Eur. J. Biochem.* **2003**, *270* (7), 1381–1392.

(3) DeVries, A. L.; Wohlschlag, D. E. Freezing Resistance in Some Antarctic Fishes. *Science* **1969**, *163* (3871), 1073–1075.

(4) Devries, A. L. Glycoproteins as Biological Antifreeze Agents in Antarctic Fishes. *Science* **1971**, *172* (3988), 1152–1155.

(5) Gibson, M. I. Slowing the Growth of Ice with Synthetic Macromolecules: Beyond Antifreeze(Glyco) Proteins. *Polym. Chem.* **2010**, *1* (8), 1141.

(6) Chao, H.; Davies, P. L.; Carpenter, J. F. Effects of Antifreeze Proteins on Red Blood Cell Survival during Cryopreservation. *J. Exp. Biol.* **1996**, *199* (Pt 9), 2071–2076.

(7) Tachibana, Y.; Fletcher, G. L.; Fujitani, N.; Tsuda, S.; Monde, K.; Nishimura, S.-I. Antifreeze Glycoproteins: Elucidation of the Structural Motifs That Are Essential for Antifreeze Activity. *Angew. Chemie Int. Ed.* **2004**, *43* (7), 856–862.

(8) Tsuda, T.; Nishimura, S. I. Synthesis of an Antifreeze Glycoprotein Analogue: Efficient Preparation of Sequential Glycopeptide Polymers. *Chem. Commun.* **1996**, *2* (24), 2779–2780.

(9) Biggs, C. I.; Bailey, T. L.; Graham, B.; Stubbs, C.; Fayter, A.; Gibson, M. I. Polymer Mimics of Biomacromolecular Antifreezes. *Nat. Commun.* **2017**, *8* (1), 1546.

(10) Voets, I. K. From Ice-Binding Proteins to Bio-Inspired Antifreeze Materials. *Soft Matter* **2017**, *13* (28), 4808–4823.

(11) Balcerzak, A. K.; Febbraro, M.; Ben, R. N. The Importance of Hydrophobic Moieties in Ice Recrystallization Inhibitors. *RSC Adv.* **2013**, *9*, 3232–3236.

(12) Duman, J. G. Antifreeze and Ice Nucleator Proteins in Terrestrial Arthropods. *Annu. Rev. Physiol.* **2001**, *63* (1), 327–357.

(13) Storey, K. B.; Storey, J. M. Freeze Tolerance in Animals. *Physiol. Rev.* **1988**, *68* (1), 27–84.

(14) Sømme, L. Supercooling and Winter Survival in Terrestrial Arthropods. *Comp. Biochem. Physiol. Part A Physiol.* **1982**, *73* (4), 519–543.

(15) Harrison, K.; Hallett, J.; Burcham, T. S.; Feeney, R. E.; Kerr, W. L.; Yeh, Y. Ice Growth in Supercooled Solutions of Antifreeze Glycoprotein. *Nature* **1987**, *328* (6127), 241–243.

(16) Zachariassen, K. E.; Hammel, H. T. Nucleating Agents in the Haemolymph of Insects Tolerant to Freezing. *Nature* **1976**, *262* (5566), 285–287.

(17) Scholander, P. F.; Kanwisker, J. W.; Hammel, H. T.; Gordon, M. S. Supercooling and Osmoregulation in Arctic Fish. *J. Cell. Comp. Physiol.* **1957**, *49* (891), 5–24.

(18) Feeney, E.; Devries, L.; Komatsu, K. Chemical and Physical Properties of Freezing Glycoproteins from Antarctic Fishes. *J. Biol. Chem.* **1970**, *245* (11), 2901–2908.

(19) Lin, Y.; Duman, J. G.; DeVries, A. L. Studies on the Structure and Activity of Low Molecular Weight Glycoproteins from an Antarctic Fish. *Biochem. Biophys. Res. Commun.* **1972**, *46* (1), 87–92.

(20) Knight, C. A.; DeVries, A. L.; Oolman, L. D. Fish Antifreeze Protein and the

Freezing and Recrystallization of Ice. *Nature* **1984**, *308* (5956), 295–296.

(21) Burcham, T. S.; Osuga, D. T.; Chino, H.; Feeney, R. E. Analysis of Antifreeze Glycoproteins in Fish Serum. *Anal. Biochem.* **1984**, *139* (1), 197–204.

(22) Burcham, T. S.; Knauf, M. J.; Osuga, D. T.; Feeney, R. E.; Yeh, Y. Antifreeze Glycoproteins: Influence of Polymer Length and Ice Crystal Habit on Activity. *Biopolymers* **1984**, *23* (7), 1379–1395.

(23) Ahmed, A. I.; Osuga, D. T.; Feeney, R. E. Antifreeze Glycoprotein from an Antarctic Fish. Effects of Chemical Modifications of Carbohydrate Residues on Antifreeze and Antilectin Activities. *J. Biol. Chem.* **1973**, *248* (24), 8524–8527.

(24) Liu, S.; Ben, R. N. C-Linked Galactosyl Serine AFGP Analogues as Potent Recrystallization Inhibitors. *Org. Lett.* **2005**, *7* (12), 2385–2388.

(25) Capicciotti, C. J.; Malay, D.; Ben, R. N. Ice Recrystallization Inhibitors: From Biological Antifreezes to Small Molecules. In *Recent Developments in the Study of Recrystallization*; Wilson, P., Ed.; InTech, 2013; Vol. 2, pp 177–224.

(26) Budke, C.; Dreyer, A.; Jaeger, J.; Gimpel, K.; Berkemeier, T.; Bonin, A. S.; Nagel, L.; Plattner, C.; Devries, A. L.; Sewald, N.; Koop, T. Quantitative Efficacy Classification of Ice Recrystallization Inhibition Agents. *Cryst. Growth Des.* **2014**, *14* (9), 4285–4294.

(27) Duman, J. G.; Devries, A. L. Freezing Resistance in Winter Flounder Pseudopleuronectes Americanus. *Nature* **1974**, *247* (5438), 237–238.

(28) Davies, P. L.; Sykes, B. D. Antifreeze Proteins. *Curr. Opin. Struct. Biol.* **1997**, *7* (6), 828–834.

(29) Duman, J. G.; DeVries, A. L. Isolation, Characterization, and Physical Properties of Protein Antifreezes from the Winter Flounder,

Pseudopleuronectes Americanus. *Comp. Biochem. Physiol. Part B Comp. Biochem.* **1976**, *54* (3), 375–380.

(30) Davies, P. L. Ice-Binding Proteins: A Remarkable Diversity of Structures for Stopping and Starting Ice Growth. *Trends Biochem. Sci.* **2014**, *39* (11), 548–555.

(31) Garnham, C. P.; Gilbert, J. A.; Hartman, C. P.; Campbell, R. L.; Laybourn-Parry, J.; Davies, P. L. A Ca 2+ -Dependent Bacterial Antifreeze Protein Domain Has a Novel β-Helical Ice-Binding Fold . *Biochem. J.* **2008**, *411* (1), 171–180.

(32) Middleton, A. J.; Brown, A. M.; Davies, P. L.; Walker, V. K. Identification of the Ice-Binding Face of a Plant Antifreeze Protein. *FEBS Lett.* **2009**, *583* (4), 815–819.

(33) Baardsnes, J.; Jelokhani-Niaraki, M.; Kondejewski, L. H.; Kuiper, M. J.; Kay, C. M.; Hodges, R. S.; Davies, P. L. Antifreeze Protein from Shorthorn Sculpin: Identification of the Ice-Binding Surface. *Protein Sci.* **2002**, *10* (12), 2566–2576.

(34) Knight, C. A.; Driggers, E.; DeVries, A. L. Adsorption to Ice of Fish Antifreeze Glycopeptides 7 and 8. *Biophys. J.* **1993**, *64* (1), 252–259.

(35) Wierzbicki, A.; Dalal, P.; Cheatham, T. E.; Knickelbein, J. E.; Haymet, A. D. J.; Madura, J. D. Antifreeze Proteins at the Ice/Water Interface: Three Calculated Discriminating Properties for Orientation of Type I Proteins. *Biophys. J.* **2007**, *93* (5), 1442–1451.

(36) Chao, H.; Houston, M. E.; Hodges, R. S.; Kay, C. M.; Sykes, B. D.; Loewen, M. C.; Davies, P. L.; Sönnichsen, F. D. A Diminished Role for Hydrogen Bonds in Antifreeze Protein Binding to Ice. *Biochemistry* **1997**, *36* (48), 14652–14660.

(37) Garnham, C. P.; Campbell, R. L.; Davies, P. L. Anchored Clathrate Waters Bind Antifreeze Proteins to Ice. *Proc. Natl. Acad. Sci.* **2011**, *108* (18), 7363–7367.

(38) Liou Y; Tocilj A; Davies P. L; Jia Z. Mimicry of Ice Structure by Surface Hydroxyls and Water of a Beta-Helix AFP. **2000**, *406* (July), 1998–2000.

(39) Mochizuki, K.; Molinero, V. Antifreeze Glycoproteins Bind Reversibly to Ice via Hydrophobic Groups. *J. Am. Chem. Soc.* **2018**, *140* (14), 4803–4811.

(40) Meister, K.; DeVries, A. L.; Bakker, H. J.; Drori, R. Antifreeze Glycoproteins Bind Irreversibly to Ice. *J. Am. Chem. Soc.* **2018**, *140* (30), 9365–9368.

(41) Walters, K. R.; Serianni, A. S.; Sformo, T.; Barnes, B. M.; Duman, J. G. A Nonprotein Thermal Hysteresis-Producing Xylomannan Antifreeze in the Freeze-Tolerant Alaskan Beetle Upis Ceramboides. *Proc. Natl. Acad. Sci.* **2009**, *106* (48), 20210–20215.

(42) Walters, K. R.; Serianni, A. S.; Voituron, Y.; Sformo, T.; Barnes, B. M.; Duman, J. G. A Thermal Hysteresis-Producing Xylomannan Glycolipid Antifreeze Associated with Cold Tolerance Is Found in Diverse Taxa. *J. Comp. Physiol. B Biochem. Syst. Environ. Physiol.* **2011**, *181* (5), 631–640.

(43) Crich, D.; Rahaman, M. Y. Synthesis and Structural Verification of the Xylomannan Antifreeze Substance from the Freeze-Tolerant Alaskan Beetle Upis Ceramboides. *J. Org. Chem.* **2011**, *76* (21), 8611–8620.

(44) Ishiwata, A.; Sakurai, A.; Nishimiya, Y.; Tsuda, S.; Ito, Y. Synthetic Study and Structural Analysis of the Antifreeze Agent Xylomannan from Upis Ceramboides. *J. Am. Chem. Soc.* **2011**, *133* (48), 19524–19535.

(45) Wu, Y.; Banoub, J.; Goddard, S. V.; Kao, M. H.; Fletcher, G. L. Antifreeze Glycoproteins: Relationship between Molecular Weight, Thermal Hysteresis

and the Inhibition of Leakage from Liposomes during Thermotropic Phase Transition. *Comp. Biochem. Physiol. Part B Biochem. Mol. Biol.* **2001**, *128* (2), 265–273.

(46) Tyshenko, M. G.; Doucet, D.; Davies, P. L.; Walker, V. K. The Antifreeze Potential of the Spruce Budworm Thermal Hysteresis Protein. *Nat. Biotechnol.* **1997**, *15* (9), 887–890.

(47) Drori, R.; Li, C.; Hu, C.; Raiteri, P.; Rohl, A. L.; Ward, M. D.; Kahr, B. A Supramolecular Ice Growth Inhibitor. *J. Am. Chem. Soc.* **2016**, *138* (40), 13396–13401.

(48) Raymond, J. A.; Devriesf, A. L.; DeVries, A. L. Adsorption Inhibition as a Mechanism of Freezing Resistance in Polar Fishes. *Proc. Natl. Acad. Sci. USA* **1977**, *74* (6), 2589–2593.

(49) Mazur, P. A Biologist's View of the Relevance of Thermodynamics and Physical Chemistry to Cryobiology. *Cryobiology* **2010**, *60* (1), 4–10.

(50) Drori, R.; Davies, P. L.; Braslavsky, I. Experimental Correlation between Thermal Hysteresis Activity and the Distance between Antifreeze Proteins on an Ice Surface. *RSC Adv.* **2015**, *5* (11), 7848–7853.

(51) Kristiansen, E.; Zachariassen, K. E. The Mechanism by Which Fish Antifreeze Proteins Cause Thermal Hysteresis. *Cryobiology* **2005**, *51* (3), 262–280.

(52) Drori, R.; Celik, Y.; Davies, P. L.; Braslavsky, I. Ice-Binding Proteins That Accumulate on Different Ice Crystal Planes Produce Distinct Thermal Hysteresis Dynamics. *J. R. Soc. Interface* **2014**, *11* (98).

(53) Matsui, T.; Hirata, M.; Yagasaki, T.; Matsumoto, M.; Tanaka, H. Communication: Hypothetical Ultralow-Density Ice Polymorphs. *J. Chem. Phys.* **2017**, *147* (9), 091101.

(54) Griffith, M.; Yaish, M. W. F. Antifreeze Proteins in Overwintering Plants: A Tale of Two Activities. *Trends Plant Sci.* **2004**, *9* (8), 399–405.

(55) Raymond, J. A.; Wilson, P.; DeVries, A. L. Inhibition of Growth of Nonbasal Planes in Ice by Fish Antifreezes. *Proc. Natl. Acad. Sci.* **1989**, *86* (3), 881–885.

(56) Graether, S. P.; Kuiper, M. J.; Walker, V. K.; Jia, Z.; Sykes, B. D.; Davies, P. L.; Gagné, S. M.; Walker, V. K.; Jia, Z.; Sykes, B. D.; Davies, P. L.; Gagné, S. M.; Walker, V. K.; Jia, Z.; Sykes, B. D.; Davies, P. L. β-Helix Structure and Ice-Binding Properties of a Hyperactive Antifreeze Protein from an Insect. *Nature* **2000**, *406* (6793), 325–328.

(57) Bayer-Giraldi, M.; Sazaki, G.; Nagashima, K.; Kipfstuhl, S.; Vorontsov, D. A.; Furukawa, Y. Growth Suppression of Ice Crystal Basal Face in the Presence of a Moderate Ice-Binding Protein Does Not Confer Hyperactivity. *Proc. Natl. Acad. Sci.* **2018**, *115* (29), 7479–7484.

(58) Rahman, A. T.; Arai, T.; Yamauchi, A.; Miura, A.; Kondo, H.; Ohyama, Y.; Tsuda, S. Ice Recrystallization Is Strongly Inhibited When Antifreeze Proteins Bind to Multiple Ice Planes. *Sci. Rep.* **2019**, *9* (1), 2212.

(59) Knight, C. A.; Hallett, J.; DeVries, A. L. Solute Effects on Ice Recrystallization: An Assessment Technique. *Cryobiology* **1988**, *25* (1), 55–60.

(60) Knight, C. A.; Wen, D.; Laursen, R. A. Nonequilibrium Antifreeze Peptides and the Recrystallization of Ice. *Cryobiology* **1995**, *32* (1), 23–34.

(61) Chan, H.; Cherukara, M. J.; Narayanan, B.; Benmore, C. J.; Gray, S.; KRS Sankaranarayanan, S. Ice Grains Grow by Dissolution, Ripening and Grain Boundary Migration. *arXiv e-prints* **2016**, arXiv:1612.00363.

(62) Olijve, L. L. C.; Oude Vrielink, A. S.; Voets, I. K. A Simple and Quantitative Method to Evaluate Ice Recrystallization Kinetics Using the Circle Hough

Transform Algorithm. *Cryst. Growth Des.* **2016**, *16* (8), 4190–4195.

(63) Mizrahy, O.; Bar-Dolev, M.; Guy, S.; Braslavsky, I. Inhibition of Ice Growth and Recrystallization by Zirconium Acetate and Zirconium Acetate Hydroxide. *PLoS One* **2013**, *8* (3), e59540.

(64) Balcerzak, A. K.; Capicciotti, C. J.; Briard, J. G.; Ben, R. N. Designing Ice Recrystallization Inhibitors: From Antifreeze (Glyco)Proteins to Small Molecules. *RSC Adv.* **2014**, *4* (80), 42682–42696.

(65) Lifshitz, I. M.; Slyozov, V. V. The Kinetics of Precipitation from Supersaturated Solid Solutions. *J. Phys. Chem. Solids* **1961**, *19* (1–2), 35–50.

(66) Kahlweit, M. Ostwald Ripening of Precipitates. *Adv. Colloid Interface Sci.* **1975**, *5* (1), 1–35.

(67) Eto, T. K.; Rubinsky, B. Antifreeze Glycoproteins Increase Solution Viscosity. *Biochem. Biophys. Res. Commun.* **1993**, *197* (2), 927–931.

(68) Graether, S. P.; Slupsky, C. M.; Davies, P. L.; Sykes, B. D. Structure of Type I Antifreeze Protein and Mutants in Supercooled Water. *Biophys. J.* **2001**, *81* (3), 1677–1683.

(69) Tam, R. Y.; Ferreira, S. S.; Czechura, P.; Ben, R. N.; Chaytor, J. L. Hydration Index-a Better Parameter for Explaining Small Molecule Hydration in Inhibition of Ice Recrystallization. *J. Am. Chem. Soc.* **2008**, *130* (51), 17494–17501.

(70) Fletcher, N. H. Surface Structure of Water and Ice. *Philos. Mag.* **1962**, *7* (74), 255–269.

(71) Hayward, J. A.; Haymet, A. D. J. Ice/Water Interface: Molecular Dynamics Simulations of the Basal, Prism, {20$\bar{2}$1}, and {21$\bar{1}$0} Interfaces of Ice Ih. *J. Chem. Phys.* **2001**, *114* (8), 3713–3726.

(72) Meldolesi, A. GM Fish Ice Cream. *Nat. Biotechnol.* **2009**, *27* (8), 682–682.

(73) Li, B.; Sun, D.-W. Novel Methods for Rapid Freezing and Thawing of Foods – a Review. *J. Food Eng.* **2002**, *54* (3), 175–182.

(74) Valarezo, W. O.; Lynch, F. T.; McGhee, R. J. Aerodynamic Performance Effects Due to Small Leading-Edge Ice (Roughness) on Wings and Tails. *J. Aircr.* **1993**, *30* (6), 807–812.

(75) Carpenter, J. F.; Hansen, T. N. Antifreeze Protein Modulates Cell Survival during Cryopreservation: Mediation through Influence on Ice Crystal Growth. *Proc. Natl. Acad. Sci.* **2000**, *89* (19), 8953–8957.

(76) Matsumoto, S.; Matsusita, M.; Morita, T.; Kamachi, H.; Tsukiyama, S.; Furukawa, Y.; Koshida, S.; Tachibana, Y.; Nishimura, S.-I.; Todo, S. Effects of Synthetic Antifreeze Glycoprotein Analogue on Islet Cell Survival and Function during Cryopreservation. *Cryobiology* **2006**, *52* (1), 90–98.

(77) Amir, G.; Rubinsky, B.; Kassif, Y.; Horowitz, L.; Smolinsky, A. K.; Lavee, J. Preservation of Myocyte Structure and Mitochondrial Integrity in Subzero Cryopreservation of Mammalian Hearts for Transplantation Using Antifreeze Proteins - An Electron Microscopy Study. *Eur. J. Cardio-thoracic Surg.* **2003**, *24* (2), 292–297.

(78) Soltys, K. A.; Batta, A. K.; Koneru, B. Successful Nonfreezing, Subzero Preservation of Rat Liver with 2,3-Butanediol and Type I Antifreeze Protein. *J. Surg. Res.* **2001**, *96* (1), 30–34.

(79) Amir, G.; Horowitz, L.; Rubinsky, B.; Yousif, B. S.; Lavee, J.; Smolinsky, A. K. Subzero Nonfreezing Cryopresevation of Rat Hearts Using Antifreeze Protein I and Antifreeze Protein III. *Cryobiology* **2004**, *48* (3), 273–282.

(80) Akiyama, Y.; Shinose, M.; Watanabe, H.; Yamada, S.; Kanda, Y.

Cryoprotectant-Free Cryopreservation of Mammalian Cells by Superflash Freezing. *Proc. Natl. Acad. Sci.* **2019**, *116* (16), 7738–7743.

(81) Iwatani, M.; Ikegami, K.; Kremenska, Y.; Hattori, N.; Tanaka, S.; Yagi, S.; Shiota, K. Dimethyl Sulfoxide Has an Impact on Epigenetic Profile in Mouse Embryoid Body. *Stem Cells* **2006**, *24* (11), 2549–2556.

(82) Shu, Z.; Heimfeld, S.; Gao, D. Hematopoietic SCT with Cryopreserved Grafts: Adverse Reactions after Transplantation and Cryoprotectant Removal before Infusion. *Bone Marrow Transplant.* **2014**, *49* (4), 469–476.

(83) Wu, L. K.; Tokarew, J. M.; Chaytor, J. L.; Von Moos, E.; Li, Y.; Palii, C.; Ben, R. N.; Allan, D. S. Carbohydrate-Mediated Inhibition of Ice Recrystallization in Cryopreserved Human Umbilical Cord Blood. *Carbohydr. Res.* **2011**, *346* (1), 86–93.

(84) Briard, J. G.; Jahan, S.; Chandran, P.; Allan, D.; Pineault, N.; Ben, R. N. Small-Molecule Ice Recrystallization Inhibitors Improve the Post-Thaw Function of Hematopoietic Stem and Progenitor Cells. *ACS Omega* **2016**, *1* (5), 1010–1018.

(85) Briard, J. G.; Poisson, J. S.; Turner, T. R.; Capicciotti, C. J.; Acker, J. P.; Ben, R. N. Small Molecule Ice Recrystallization Inhibitors Mitigate Red Blood Cell Lysis during Freezing, Transient Warming and Thawing. *Sci. Rep.* **2016**, *6* (1), 23619.

(86) Lauersen, K. J.; Brown, A.; Middleton, A.; Davies, P. L.; Walker, V. K. Expression and Characterization of an Antifreeze Protein from the Perennial Rye Grass, Lolium Perenne. *Cryobiology* **2011**, *62* (3), 194–201.

(87) Moser, R.; Klauser, S.; Leist, T.; Langen, H.; Epprecht, T.; Gutte, B. Applications of Synthetic Peptides. *Angew. Chemie Int. Ed. English* **1985**, *24* (9), 719–727.

(88) Groß, A.; Hashimoto, C.; Sticht, H.; Eichler, J. Synthetic Peptides as Protein Mimics. *Front. Bioeng. Biotechnol.* **2016**, *3* (January).

(89) Merrifield, R. B. Solid Phase Peptide Synthesis. I. The Synthesis of a Tetrapeptide. *J. Am. Chem. Soc.* **1963**, *85* (14), 2149–2154.

(90) Kumita, J. R.; Smart, O. S.; Woolley, G. A. Photo-Control of Helix Content in a Short Peptide. *Proc. Natl. Acad. Sci.* **2000**, *97* (8), 3803–3808.

(91) Chapman, R.; Danial, M.; Koh, M. L.; Jolliffe, K. A.; Perrier, S. Design and Properties of Functional Nanotubes from the Self-Assembly of Cyclic Peptide Templates. *Chem. Soc. Rev.* **2012**, *41* (18), 6023–6041.

(92) Yu, M.; Nowak, A. P.; Deming, T. J.; Pochan, D. J. Methylated Mono- and Diethyleneglycol Functionalized Polylysines: Nonionic, α-Helical, Water-Soluble Polypeptides [14]. *J. Am. Chem. Soc.* **1999**, *121* (51), 12210–12211.

(93) Palomo, J. M. Solid-Phase Peptide Synthesis: An Overview Focused on the Preparation of Biologically Relevant Peptides. *RSC Adv.* **2014**, *4* (62), 32658–32672.

(94) Sears, P. Toward Automated Synthesis of Oligosaccharides and Glycoproteins. *Science* **2002**, *291* (5512), 2344–2350.

(95) Deng, C.; Wu, J.; Cheng, R.; Meng, F.; Klok, H. A.; Zhong, Z. Functional Polypeptide and Hybrid Materials: Precision Synthesis via α-Amino Acid N-Carboxyanhydride Polymerization and Emerging Biomedical Applications. *Prog. Polym. Sci.* **2014**, *39* (2), 330–364.

(96) Kricheldorf, H. R. Polypeptides and 100 Years of Chemistry of α-Amino Acid N-Carboxyanhydrides. *Angew. Chemie Int. Ed.* **2006**, *45* (35), 5752–5784.

(97) Habraken, G. J. M.; Wilsens, K. H. R. M.; Koning, C. E.; Heise, A. Optimization of N-Carboxyanhydride (NCA) Polymerization by Variation of

Reaction Temperature and Pressure. *Polym. Chem.* **2011**, *2* (6), 1322–1330.

(98) Kim, I.; Zhang, Y.; Augustine, R.; Song, W.; Liu, R.; Jin, H. Straightforward Access to Linear and Cyclic Polypeptides. *Commun. Chem.* **2018**, *1* (1), 1–7.

(99) Hanson, J. A.; Chang, C. B.; Graves, S. M.; Li, Z.; Mason, T. G.; Deming, T. J. Nanoscale Double Emulsions Stabilized by Single-Component Block Copolypeptides. *Nature* **2008**, *455* (7209), 85–88.

(100) Gabrielson, N. P.; Lu, H.; Yin, L.; Li, D.; Wang, F.; Cheng, J. Reactive and Bioactive Cationic α-Helical Polypeptide Template for Nonviral Gene Delivery. *Angew. Chemie Int. Ed.* **2012**, *51* (5), 1143–1147.

(101) Schätzlein, A. G.; Le, T. B. H.; Uchegbu, I. F.; Mazza, M.; Lalatsa, A. Amphiphilic Poly(l-Amino Acids) — New Materials for Drug Delivery. *J. Control. Release* **2012**, *161* (2), 523–536.

(102) Cabral, H.; Kataoka, K. Progress of Drug-Loaded Polymeric Micelles into Clinical Studies. *J. Control. Release* **2014**, *190*, 465–476.

(103) Deming, T. J.; Klok, H.-A.; Armes, S. P.; Becker, M. L.; Champion, J. A.; Chen, E. Y.-X.; Heilshorn, S. C.; van Hest, J. C. M.; Irvine, D. J.; Johnson, J. A.; Kiessling, L. L.; Maynard, H. D.; de la Cruz, M. O.; Sullivan, M. O.; Tirrell, M. V.; Anseth, K. S.; Lecommandoux, S.; Percec, S.; Zhong, Z.; Albertsson, A.-C. Polymers at the Interface with Biology. *Biomacromolecules* **2018**, *19* (8), 3151–3162.

(104) Rosales, A. M.; Anseth, K. S. The Design of Reversible Hydrogels to Capture Extracellular Matrix Dynamics. *Nat. Rev. Mater.* **2016**, *1* (2), 1–15.

(105) Engler, A. J.; Sen, S.; Sweeney, H. L.; Discher, D. E. Matrix Elasticity Directs Stem Cell Lineage Specification. *Cell* **2006**, *126* (4), 677–689.

(106) Lee, T. T.; García, J. R.; Paez, J. I.; Singh, A.; Phelps, E. A.; Weis, S.; Shafiq,

Z.; Shekaran, A.; Del Campo, A.; García, A. J. Light-Triggered in Vivo Activation of Adhesive Peptides Regulates Cell Adhesion, Inflammation and Vascularization of Biomaterials. *Nat. Mater.* **2015**, *14* (3), 352–360.

(107) Ishihara, K. Bioinspired Phospholipid Polymer Biomaterials for Making High Performance Artificial Organs. *Sci. Technol. Adv. Mater.* **2000**, *1* (3), 131–138.

(108) Som, A.; Vemparala, S.; Ivanov, I.; Tew, G. N. Synthetic Mimics of Antimicrobial Peptides. *Biopolym. - Pept. Sci. Sect.* **2008**, *90* (2), 83–93.

(109) Tew, G. N.; Liu, D.; Chen, B.; Doerksen, R. J.; Kaplan, J.; Carroll, P. J.; Klein, M. L.; DeGrado, W. F. De Novo Design of Biomimetic Antimicrobial Polymers. *Proc. Natl. Acad. Sci.* **2002**, *99* (8), 5110–5114.

(110) Lienkamp, K.; Madkour, A. E.; Musante, A.; Nelson, C. F.; Nüsslein, K.; Tew, G. N. Antimicrobial Polymers Prepared by ROMP with Unprecedented Selectivity: A Molecular Construction Kit Approach. *J. Am. Chem. Soc.* **2008**, *130* (30), 9836–9843.

(111) Baskaran, D.; Müller, A. H. E. Anionic Vinyl Polymerization-50 Years after Michael Szwarc. *Prog. Polym. Sci.* **2007**, *32* (2), 173–219.

(112) Szwarc, M. 'Living' Polymers. *Nature* **1956**, *178* (4543), 1168–1169.

(113) Aoshima, S.; Kanaoka, S. A Renaissance in Living Cationic Polymerization. *Chem. Rev.* **2009**, *109* (11), 5245–5287.

(114) Kennedy, J. P. Living Cationic Polymerization of Olefins . How Did The. *J. Polym. Sci. Part A Polym. Chem.* **1999**, *37*, 2285–2293.

(115) Seno, K.-I.; Kanaoka, S.; Aoshima, S. Thermosensitive Diblock Copolymers with Designed Molecular Weight Distribution: Synthesis by Continuous Living Cationic Polymerization and Micellization Behavior. *J. Polym. Sci. Part A Polym. Chem.* **2008**, *46* (6), 2212–2221.

(116) Freyss, D.; Rempp, P.; Benoît, H. Polydispersity of Anionically Prepared Block Copolymers. *J. Polym. Sci. Part B Polym. Lett.* **2003**, *2* (2), 217–222.

(117) Shibata, T.; Kanaoka, S.; Aoshima, S. Quantitative Synthesis of Star-Shaped Poly(Vinyl Ether)s with a Narrow Molecular Weight Distribution by Living Cationic Polymerization. *J. Am. Chem. Soc.* **2006**, *128* (23), 7497–7504.

(118) Hadjichristidis, N.; Pitsikalis, M.; Pispas, S.; Iatrou, H. Polymers with Complex Architecture by Living Anionic Polymerization. *Chem. Rev.* **2001**, *101* (12), 3747–3792.

(119) Yoshida, M.; Tazaki, T.; Otsu, T.; Yoshida, M.; Tazaki, T. A Model for Living Radical Polymerization. *Die Makromol. Chemie, Rapid Commun.* **1982**, *3* (2), 133–140.

(120) Lamb, J.; Qin, K. P.; Johnson, J. A. Visible-Light Mediated, Additive-Free, and Open-to-Air Controlled Radical Polymerization of Acrylates and Acrylamides. *Polym. Chem.* **2019**, *00*, 1–3.

(121) Chen, M.; Zhong, M.; Johnson, J. A. Light-Controlled Radical Polymerization: Mechanisms, Methods, and Applications. *Chem. Rev.* **2016**, *116* (17), 10167–10211.

(122) Solomon, D. H. Genesis of the CSIRO Polymer Group and the Discovery and Significance of Nitroxide-Mediated Living Radical Polymerization. *J. Polym. Sci. Part A Polym. Chem.* **2005**, *43* (23), 5748–5764.

(123) Matyjaszewski, K. Atom Transfer Radical Polymerization (ATRP): Current Status and Future Perspectives. *Macromolecules* **2012**, *45* (10), 4015–4039.

(124) Chiefari, J.; Chong, Y. K. B.; Ercole, F.; Krstina, J.; Jeffery, J.; Le, T. P. T.; Mayadunne, R. T. A.; Meijs, G. F.; Moad, C. L.; Moad, G.; Rizzardo, E.; Thang, S. H.; South, C. Living Free-Radical Polymerization by Reversible

Addition - Fragmentation Chain Transfer : The RAFT Process. *Macromolecules* **1998**, *9297* (98), 5559–5562.

(125) Fischer, H. The Persistent Radical Effect: A Principle for Selective Radical Reactions and Living Radical Polymerizations. *Chem. Rev.* **2001**, *101* (12), 3581–3610.

(126) Georges, M. K.; Veregin, R. P. N.; Kazmaier, P. M.; Hamer, G. K. Narrow Molecular Weight Resins by a Free-Radical Polymerization Process. *Macromolecules* **1993**, *26* (11), 2987–2988.

(127) Hawker, C. J.; Barclay, G. G.; Orellana, A.; Dao, J.; Devonport, W. Initiating Systems for Nitroxide-Mediated "living" Free Radical Polymerizations: Synthesis and Evaluation. *Macromolecules* **1996**, *29* (16), 5245–5254.

(128) Butz, S.; Hillermann, J.; Schmidt-Naake, G.; Kressler, J.; Thomann, R.; Heck, B.; Stühn, B. Synthesis and Microphase Separation of Diblock Copolymers of Styrene and P-Chlorostyrene Prepared by Using N-Oxyl Capped Macroinitiators. *Acta Polym.* **2002**, *49* (12), 693–699.

(129) Nicolas, J.; Guillaneuf, Y.; Lefay, C.; Bertin, D.; Gigmes, D.; Charleux, B. Nitroxide-Mediated Polymerization. *Prog. Polym. Sci.* **2013**, *38* (1), 63–235.

(130) Grubbs, R. B. Nitroxide-Mediated Radical Polymerization: Limitations and Versatility. *Polym. Rev.* **2011**, *51* (2), 104–137.

(131) Kato, M.; Kamigaito, M.; Sawamoto, M.; Higashimura, T. Polymerization of Methyl Methacrylate with the Carbon Tetrachloride/Dichlorotris-(Triphenylphosphine)Ruthenium(II)/ Methylaluminum Bis(2,6-Di-Tert-Butylphenoxide) Initiating System: Possibility of Living Radical Polymerization. *Macromolecules* **1995**, *28* (5), 1721–1723.

(132) Matyjaszewski, K. Controlled/"Living" Radical Polymerization. Halogen Atom

Transfer Radical Polymerization Promoted by a Cu(I)/Cu(11) Redox Process. *Macromolecules* **1995**, No. I, 7901–7910.

(133) Whitfield, R.; Anastasaki, A.; Nikolaou, V.; Jones, G. R.; Engelis, N. G.; Discekici, E. H.; Fleischmann, C.; Willenbacher, J.; Hawker, C. J.; Haddleton, D. M. Universal Conditions for the Controlled Polymerization of Acrylates, Methacrylates, and Styrene via Cu(0)-RDRP. *J. Am. Chem. Soc.* **2017**, *139* (2), 1003–1010.

(134) Enciso, A. E.; Fu, L.; Russell, A. J.; Matyjaszewski, K. A Breathing Atom-Transfer Radical Polymerization: Fully Oxygen-Tolerant Polymerization Inspired by Aerobic Respiration of Cells. *Angew. Chemie Int. Ed.* **2018**, *57* (4), 933–936.

(135) Liarou, E.; Whitfield, R.; Anastasaki, A.; Engelis, N. G.; Jones, G. R.; Velonia, K.; Haddleton, D. M. Copper-Mediated Polymerization without External Deoxygenation or Oxygen Scavengers. *Angew. Chemie Int. Ed.* **2018**, *57* (29), 8998–9002.

(136) Engelis, N. G.; Marathianos, A.; Patias, G.; Jones, G. R.; Haddleton, D. M.; Whitfield, R.; Iacono, C. E.; Anastasaki, A.; Liarou, E. Ultra-Low Volume Oxygen Tolerant Photoinduced Cu-RDRP. *Polym. Chem.* **2019**, 963–971.

(137) Sumerlin, B. S.; Tsarevsky, N. V.; Louche, G.; Lee, R. Y.; Matyjaszewski, K. Highly Efficient “Click” Functionalization of Poly(3-Azidopropyl Methacrylate) Prepared by ATRP. *Macromolecules* **2005**, *38* (18), 7540–7545.

(138) Li, W.; Matyjaszewski, K. Star Polymers via Cross-Linking Amphiphilic Macroinitiators by AGET ATRP in Aqueous Media. *J. Am. Chem. Soc.* **2009**, *131* (30), 10378–10379.

(139) Perrier, S. 50th Anniversary Perspective: RAFT Polymerization - A User

Guide. *Macromolecules* **2017**, *50* (19), 7433–7447.

(140) Gody, G.; Maschmeyer, T.; Zetterlund, P. B.; Perrier, S. Rapid and Quantitative One-Pot Synthesis of Sequence-Controlled Polymers by Radical Polymerization. *Nat. Commun.* **2013**, *4*, 1–9.

(141) Harrisson, S.; Liu, X.; Ollagnier, J.-N.; Coutelier, O.; Marty, J.-D.; Destarac, M. RAFT Polymerization of Vinyl Esters: Synthesis and Applications. *Polymers* **2014**, *6* (5), 1437–1488.

(142) Skey, J.; O'Reilly, R. K. Facile One Pot Synthesis of a Range of Reversible Addition-Fragmentation Chain Transfer (RAFT) Agents. *Chem. Commun.* **2008**, No. 35, 4183–4185.

(143) Destarac, M.; Brochon, C.; Catala, J. M.; Wilczewska, A.; Zard, S. Z. Macromolecular Design via the Interchange of Xanthates (MADIX): Polymerization of Styrene with O-Ethyl Xanthates as Controlling Agents. *Macromol. Chem. Phys.* **2002**, *203* (16), 2281–2289.

(144) Bouhadir, G.; Legrand, N.; Quiclet-Sire, B.; Zard, S. Z. A New Practical Synthesis of Tertiary S-Alkyl Dithiocarbonates and Related Derivatives. *Tetrahedron Lett.* **1999**, *40* (2), 277–280.

(145) Rizzardo, E.; Moad, G.; Benaglia, M.; Chong, Y. K.; Thang, S. H.; Chiefari, J. Universal (Switchable) RAFT Agents. *J. Am. Chem. Soc.* **2009**, *131* (20), 6914–6915.

(146) Congdon, T. R.; Notman, R.; Gibson, M. I. Synthesis of Star-Branched Poly(Vinyl Alcohol) and Ice Recrystallization Inhibition Activity. *Eur. Polym. J.* **2017**, *88*, 320–327.

(147) Wang, Z.; He, J.; Tao, Y.; Yang, L.; Jiang, H.; Yang, Y. Controlled Chain Branching by RAFT-Based Radical Polymerization. *Macromolecules* **2003**, *36*

(20), 7446–7452.

(148) Moad, G. RAFT (Reversible Addition-Fragmentation Chain Transfer) Crosslinking (Co)Polymerization of Multi-Olefinic Monomers to Form Polymer Networks. *Polym. Int.* **2015**, *64* (1), 15–24.

(149) Grande, C. D.; Tria, M. C.; Jiang, G.; Ponnapati, R.; Advincula, R. Surface-Grafted Polymers from Electropolymerized Polythiophene RAFT Agent. *Macromolecules* **2011**, *44* (4), 966–975.

(150) Richards, S. J.; Isufi, K.; Wilkins, L. E.; Lipecki, J.; Fullam, E.; Gibson, M. I. Multivalent Antimicrobial Polymer Nanoparticles Target Mycobacteria and Gram-Negative Bacteria by Distinct Mechanisms. *Biomacromolecules* **2018**, *19* (1), 256–264.

(151) Spain, S. G.; Albertin, L.; Cameron, N. R. Facile in Situ Preparation of Biologically Active Multivalent Glyconanoparticles. *Chem. Commun.* **2006**, No. 40, 4198–4200.

(152) Willcock, H.; O'Reilly, R. K. End Group Removal and Modification of RAFT Polymers. *Polym. Chem.* **2010**, *1* (2), 149–157.

(153) Matsumura, K.; Hyon, S.-H. H. Polyampholytes as Low Toxic Efficient Cryoprotective Agents with Antifreeze Protein Properties. *Biomaterials* **2009**, *30* (27), 4842–4849.

(154) Hermann, W. O.; Haehnel, W. Process for the Preparation of Polymerized Vinyl Alcohol and Its Derivatives. 1672156A, 1924.

(155) Yuki, K.; Sato, T.; Maruyama, H.; Yamauchi, J.; Okaya, T. The Role of Polyvinyl Alcohol in Emulsion Polymerization. *Polym. Int.* **1993**, *30* (4), 513–517.

(156) Qiao, L.; Coveny, P. K.; Easteal, A. J. Modifications of Poly(Vinyl Alcohol)

for Use in Poly(Vinyl Acetate) Emulsion Wood Adhesives. *Pigment Resin Technol.* **2002**, *31* (2), 88–95.

(157) DeMerlis, C. .; Schoneker, D. . Review of the Oral Toxicity of Polyvinyl Alcohol (PVA). *Food Chem. Toxicol.* **2003**, *41* (3), 319–326.

(158) Chong, S. F.; Smith, A. A. A.; Zelikin, A. N. Microstructured, Functional PVA Hydrogels through Bioconjugation with Oligopeptides under Physiological Conditions. *Small* **2013**, *9* (6), 942–950.

(159) Schmedlen, R. H.; Masters, K. S.; West, J. L. Photocrosslinkable Polyvinyl Alcohol Hydrogels. *Biomaterials* **2002**, *23*, 4325–4332.

(160) Clarke, J. T.; Howard, R. O.; Stockmayer, W. H.; Stockmayex, H.; Howard, R. O. Chain Transfer in Vinyl Acetate Polymerization. *Die Makromol. Chemie* **1961**, *44* (1), 427–447.

(161) Flory, P. J.; Leutner, F. S. Occurrence of Head-to-Head Arrangements of Structural Units in Polyvinyl Alcohol. *J. Polym. Sci.* **1948**, *3* (6), 880–890.

(162) Ahmad, N. M.; Heatley, F.; Lovell, P. A. Chain Transfer to Polymer in Free-Radical Solution Polymerization of n -Butyl Acrylate Studied by NMR Spectroscopy . *Macromolecules* **2002**, *31* (9), 2822–2827.

(163) Yamada, K.; Nakano, T.; Okamoto, Y. Synthesis of Syndiotactic Poly(Vinyl Alcohol) from Fluorine-Containing Vinyl Esters. *Polymer Journal*. 2005, pp 641–645.

(164) Lyoo, W. S.; Han, S. S.; Kim, J. H.; Yoon, W. S.; Lee, C. J.; Kwon, I. C.; Lee, J.; Ji, B. C.; Han, M. H. Bulk Polymerization of Vinyl Pivalate Using Low-Temperature Azoinitiator and Saponification for the Preparation of Poly(Vinyl Alcohol) Microfibrils. *Angew. Makromol. Chemie* **1999**, *271* (4706), 46–52.

(165) Wakioka, M.; Baek, K. Y.; Ando, T.; Kamigaito, M.; Sawamoto, M. Possibility

of Living Radical Polymerization of Vinyl Acetate Catalyzed by Iron(i) Complex. *Macromolecules* **2002**, *35* (2), 330–333.

(166) Iovu, M. C.; Matyjaszewski, K. Controlled/Living Radical Polymerization of Vinyl Acetate by Degenerative Transfer with Alkyl Iodides. *Macromolecules* **2003**, *36* (25), 9346–9354.

(167) Debuigne, A.; Caille, J. R.; Jerome, R. Highly Efficient Cobalt-Mediated Radical Polymerization of Vinyl Acetate. *Angew. Chemie Int. Ed.* **2005**, *44* (7), 1101–1104.

(168) Stenzel, M. H.; Cummins, L.; Roberts, G. E.; Davis, T. P.; Vana, P.; Barner-Kowollik, C. Xanthate Mediated Living Polymerization of Vinyl Acetate: A Systematic Variation in MADIX/RAFT Agent Structure. *Macromol. Chem. Phys.* **2003**, *204* (9), 1160–1168.

(169) Congdon, T. R.; Notman, R.; Gibson, M. I. Influence of Block Copolymerization on the Antifreeze Protein Mimetic Ice Recrystallization Inhibition Activity of Poly(Vinyl Alcohol). *Biomacromolecules* **2016**, *17* (9), 3033–3039.

(170) Stenzel, M. H.; Davis, T. P.; Barner-Kowollik, C. Poly(Vinyl Alcohol) Star Polymers Prepared via MADIX/RAFT Polymerisation. *Chem. Commun.* **2004**, No. 13, 1546.

(171) Bernard, J.; Favier, A.; Davis, T. P.; Barner-Kowollik, C.; Stenzel, M. H. Synthesis of Poly(Vinyl Alcohol) Combs via MADIX/RAFT Polymerization. *Polymer (Guildf).* **2006**, *47* (4), 1073–1080.

(172) Olijve, L. C.; Hendrix, M. R.; Voets, I. K. Influence of Polymer Chain Architecture of Poly(Vinyl Alcohol) on the Inhibition of Ice Recrystallization. *Macromol. Chem. Phys.* **2016**, *217* (8), 951–958.

(173) Inada, T.; Lu, S.-S. Inhibition of Recrystallization of Ice Grains by Adsorption of Poly(Vinyl Alcohol) onto Ice Surfaces. *Cryst. Growth Des.* **2003**, *3* (5), 747–752.

(174) Gibson, M. I.; Barker, C. A.; Spain, S. G.; Albertin, L.; Cameron, N. R. Inhibition of Ice Crystal Growth by Synthetic Glycopolymers: Implications for the Rational Design of Antifreeze Glycoprotein Mimics. *Biomacromolecules* **2009**, *10* (2), 328–333.

(175) Deller, R. C.; Congdon, T.; Sahid, M. A.; Morgan, M.; Vatish, M.; Mitchell, D. A.; Notman, R.; Gibson, M. I. Ice Recrystallisation Inhibition by Polyols: Comparison of Molecular and Macromolecular Inhibitors and Role of Hydrophobic Units. *Biomater. Sci.* **2013**, *1* (5), 478.

(176) Budke, C.; Koop, T. Ice Recrystallization Inhibition and Molecular Recognition of Ice Faces by Poly(Vinyl Alcohol). *ChemPhysChem* **2006**, *7* (12), 2601–2606.

(177) Congdon, T.; Notman, R.; Gibson, M. I. Antifreeze (Glyco)Protein Mimetic Behavior of Poly(Vinyl Alcohol): Detailed Structure Ice Recrystallization Inhibition Activity Study. *Biomacromolecules* **2013**, *14* (5), 1578–1586.

(178) Devries, A. L.; Komatsu, S. K.; Feeney, R. E. Chemical and Physical Properties of Freezing Point-Depressing Glycoproteins from Antartic Fishes. *J. Biol. Chem.* **1970**, *245* (11), 2901–2908.

(179) DeLuca, C. I.; Comley, R.; Davies, P. L. Antifreeze Proteins Bind Independently to Ice. *Biophys. J.* **1998**, *74* (3), 1502–1508.

(180) Phillips, D. J.; Congdon, T. R.; Gibson, M. I. Activation of Ice Recrystallization Inhibition Activity of Poly(Vinyl Alcohol) Using a Supramolecular Trigger. *Polym. Chem.* **2016**, *7* (9), 1701.

(181) Hawker, C. J.; Wooley, K. L. The Convergence of Synthetic Organic and Polymer Chemistries. *Science* **2005**, *309* (5738), 1200–1205.

(182) Alfrey, T.; Morawetz, H.; Fitzgerald, E. B.; Fuoss, R. M. Synthetic Electrical Analog of Proteins. *J. Am. Chem. Soc.* **1950**, *72* (4), 1864.

(183) Alfrey, T.; Morawetz, H. Amphoteric Polyelectrolytes. I. 2-Vinylpyridine-Methacrylic Acid Copolymers. *J. Am. Chem. Soc.* **1952**, *74* (2), 436–438.

(184) Mumick, P. S.; Welch, P. M.; Salazar, L. C.; McCormick, C. L. Water-Soluble Copolymers. 56. Structure and Solvation Effects of Polyampholytes in Drag Reduction. *Macromolecules* **1994**, *27* (2), 323–331.

(185) Li, G.; Xue, H.; Gao, C.; Zhang, F.; Jiang, S. Nonfouling Polyampholytes from an Ion-Pair Comonomer with Biomimetic Adhesive Groups. *Macromolecules* **2010**, *43* (1), 14–16.

(186) Ehrlich, G.; Doty, P. Macro-Ions. III. The Solution Behavior of a Polymeric Ampholyte 1. *J. Am. Chem. Soc.* **1954**, *76* (14), 3764–3777.

(187) Kamachi, M.; Kurihara, M.; Stille, J. K. Synthesis of Block Polymers for Desalination Membranes. Preparation of Block Copolymers of 2-Vinylpyridine and Methacrylic Acid or Acrylic Acid. *Macromolecules* **1972**, *5* (2), 161–167.

(188) Patrickios, C. S.; Hertler, W. R.; Abbott, N. L.; Hatton, T. A. Diblock, ABC Triblock, and Random Methacrylic Polyampholytes: Synthesis by Group Transfer Polymerization and Solution Behavior. *Macromolecules* **1994**, *27* (4), 930–937.

(189) Gabaston, L. .; Furlong, S. .; Jackson, R. .; Armes, S. . Direct Synthesis of Novel Acidic and Zwitterionic Block Copolymers via TEMPO-Mediated Living Free-Radical Polymerization. *Polymer (Guildf).* **1999**, *40* (16), 4505–4514.

(190) Colby, R. H.; Ford, W. T.; Kaur, B.; Slater, L. A.; Liang, S.; Mourey, T. H.;

D'Souza, L. Model Random Polyampholytes from Nonpolar Methacrylic Esters. *Macromolecules* **2011**, *44* (10), 3810–3816.

(191) Du Prez, F.; Kaya, N. U.; Badi, N.; Frank, D.; Resetco, C. Precisely Alternating Functionalized Polyampholytes Prepared in a Single Pot from Sustainable Thiolactone Building Blocks. *ACS Macro Lett.* **2017**, *6* (3), 277–280.

(192) Stubbs, C.; Lipecki, J.; Gibson, M. I. Regioregular Alternating Polyampholytes Have Enhanced Biomimetic Ice Recrystallization Activity Compared to Random Copolymers and the Role of Side Chain versus Main Chain Hydrophobicity. *Biomacromolecules* **2017**, *18* (1), 295–302.

(193) Mitchell, D. E.; Lilliman, M.; Spain, S. G.; Gibson, M. I. Quantitative Study on the Antifreeze Protein Mimetic Ice Growth Inhibition Properties of Poly(Ampholytes) Derived from Vinyl-Based Polymers. *Biomater. Sci.* **2014**, *2* (12), 1787–1795.

(194) Rajan, R.; Jain, M.; Matsumura, K. Cryoprotective Properties of Completely Synthetic Polyampholytes via Reversible Addition-Fragmentation Chain Transfer (RAFT) Polymerization and the Effects of Hydrophobicity. *J. Biomater. Sci. Polym. Ed.* **2013**, *24* (August 2015), 1767–1780.

(195) Rajan, R.; Kazuaki, M. Preparation of Novel Synthetic Cryoprotectants. *Cryobiol. cryotechnology* **2014**, *60* (2), 99–103.

(196) Zhao, J.; Johnson, M. A.; Fisher, R.; Burke, N. A. D.; Stöver, H. D. H. Synthetic Polyampholytes as Macromolecular Cryoprotective Agents. *Langmuir* **2018**, acs.langmuir.8b01602.

(197) Jain, M.; Rajan, R.; Hyon, S.-H. H.; Matsumura, K. Hydrogelation of Dextran-Based Polyampholytes with Cryoprotective Properties via Click Chemistry. *Biomater. Sci.* **2014**, *2* (3), 308–317.

(198) Matsumura, K.; Kawamoto, K.; Takeuchi, M.; Yoshimura, S.; Tanaka, D.; Hyon, S.-H. H. Cryopreservation of a Two-Dimensional Monolayer Using a Slow Vitrification Method with Polyampholyte to Inhibit Ice Crystal Formation. *ACS Biomater. Sci. Eng.* **2016**, *2* (6), 1023–1029.

(199) Armitage, W. J.; Juss, B. K. The Influence of Cooling Rate on Survival of Frozen Cells Differs in Monolayers and in Suspensions. *Cryo-Letters* **1996**, *17*, 213–218.

(200) Pasch, J.; Schiefer, A.; Heschel, I.; Rau, G. Cryopreservation of Keratinocytes in a Monolayer. *Cryobiology* **1999**, *39* (2), 158–168.

(201) Maehara, M.; Sato, M.; Watanabe, M.; Matsunari, H.; Kokubo, M.; Kanai, T.; Sato, M.; Matsumura, K.; Hyon, S. H.; Yokoyama, M.; Mochida, J.; Nagashima, H. Development of a Novel Vitrification Method for Chondrocyte Sheets. *BMC Biotechnol.* **2013**, *13* (1), 1.

(202) Watanabe, H.; Kohaya, N.; Kamoshita, M.; Fujiwara, K.; Matsumura, K.; Hyon, S. H.; Ito, J.; Kashiwazaki, N. Efficient Production of Live Offspring from Mouse Oocytes Vitrified with a Novel Cryoprotective Agent, Carboxylated ε-Poly-L-Lysine. *PLoS One* **2013**, *8* (12), 10–14.

(203) Kamoshita, M.; Kato, T.; Fujiwara, K.; Namiki, T.; Matsumura, K.; Hyon, S. H.; Ito, J.; Kashiwazaki, N. Successful Vitrification of Pronuclear-Stage Pig Embryos with a Novel Cryoprotective Agent, Carboxylated ϵ-Poly-L-Lysine. *PLoS One* **2017**, *12* (4), 1–12.

(204) Shibao, Y.; Fujiwara, K.; Kawasaki, Y.; Matsumura, K.; Hyon, S.-H.; Ito, J.; Kashiwazaki, N. The Effect of a Novel Cryoprotective Agent, Carboxylated ε-Poly-l-Lysine, on the Developmental Ability of Re-Vitrified Mouse Embryos at the Pronuclear Stage. *Cryobiology* **2014**, *68* (2), 200–204.

(205) Matsumura, K.; Hayashi, F.; Nagashima, T.; Hyon, S. H. Long-Term Cryopreservation of Human Mesenchymal Stem Cells Using Carboxylated Poly-l-Lysine without the Addition of Proteins or Dimethyl Sulfoxide. *J. Biomater. Sci. Polym. Ed.* **2013**, *24* (12), 1484–1497.

(206) Mitchell, D. E.; Cameron, N. R.; Gibson, M. I. Rational, yet Simple, Design and Synthesis of an Antifreeze-Protein Inspired Polymer for Cellular Cryopreservation. *Chem. Commun.* **2015**, *51* (65), 12977–12980.

(207) Rajan, R.; Hayashi, F.; Nagashima, T.; Matsumura, K. Toward a Molecular Understanding of the Mechanism of Cryopreservation by Polyampholytes: Cell Membrane Interactions and Hydrophobicity. *Biomacromolecules* **2016**, *17* (5), 1882–1893.

(208) Ahmed, S.; Fujita, S.; Matsumura, K. Enhanced Protein Internalization and Efficient Endosomal Escape Using Polyampholyte-Modified Liposomes and Freeze Concentration. *Nanoscale* **2016**, *8* (35), 15888–15901.

(209) Ahmed, S.; Miyawaki, O.; Matsumura, K. Enhanced Adsorption of a Protein-Nanocarrier Complex onto Cell Membranes through a High Freeze Concentration by a Polyampholyte Cryoprotectant. *Langmuir* **2018**, *34* (6), 2352–2362.

(210) Ahmed, S.; Matsumura, K.; Hamada, T. Hydrophobic Polyampholytes and Nonfreezing Cold Temperature Stimulate Internalization of Au Nanoparticles to Zwitterionic Liposomes. *Langmuir* **2019**, *35* (5), 1740–1748.

Chapter 2

Evaluating the IRI activity of Multivalent PVA Coated Nanoparticles

2.1 Abstract

Poly(vinyl alcohol) (PVA) has emerged as the most potent mimic of antifreeze (glyco) proteins' ice recrystallization inhibition (IRI) activity, despite its lack of structural similarities and flexible, rather than rigid, backbone. The precise spacing of hydroxyl groups is hypothesized to enable PVA to recognise the prism planes of ice but not the basal plane, due to hydroxyl pattern matching of the ice surface giving rise to the macroscopic activity. Firstly, we present well-defined PVA derived from reversible addition fragmentation chain transfer (RAFT) polymerisation immobilised onto gold nanoparticles to enable the impact of nanoscale assembly and confinement on the observed IRI activity. Unlike previous reports using star branched or bottle-brush PVAs, the nanoparticle-PVAs retain all IRI activity compared to polymers in solution. Evidence is presented to show that this is due to the low grafting densities on the particle surface meaning the chains are free to explore the ice faces, rather than being constrained as in star-branched polymers. These results demonstrate a route to develop more functional IRI's with the inclusion of metallic particle cores for imaging and associated applications in cryobiology. We have also investigated how the specific structure of PVA is necessary for optimal ice binding, we have sequentially modified PVA to investigate the importance of the hydrogen bonding pattern.

2.2 Disclaimer

- The nanoparticle sections of work (2.4i and 2.4ii) were done in collaboration with Laura Wilkins who carried out all nanoparticle synthesis and characterisation, as well as the washing of the samples. (DLS, UV-VIS, TEM, TGA and XRD).
- Sucrose shaping assays were carried out by Alice Fayter (2.4ii).
- Poly(allyl alcohol) was provided by Marc Hillmyer (2.4iii).
- Poly(vinyl amine) IRI assays were carried out by Thomas Congdon, and the images analysed by myself (2.4iii).

2.3 Introduction

Nature has evolved a diverse range of biological macromolecules which can modulate the formation and growth of ice to enable extremophiles to survive at sub-zero temperatures.[1,2] The range of macromolecules known to have this function includes antifreeze proteins (AFPs),[1] antifreeze glycoproteins (AFGP),[3] lipopolysaccharides[4] and polysaccharides.[5] The exact mechanism of action, and the extent of actual ice binding is not clear[6] with different proteins targeting different crystallographic faces of ice. Despite the challenges of studying ice/water interfacial processes and the current knowledge gaps, it has emerged that synthetic polymers can be designed to reproduce AF(G)P properties even without any structural similarities to native antifreeze proteins.[7–9] In particular, ice recrystallisation inhibition (IRI; slowing ice growth rates) activity can be selectively retained, in favour of thermal hysteresis/dynamic ice shaping, implying multiple mechanisms of action.[10] IRI activity is particularly desirable as ice crystal growth during thawing is a major cause of cell death during the cryopreservation of donor cells/tissues. Carpenter *et al.* first demonstrated that modulation of ice growth during thawing could improve the cryopreservation of red blood cells[11] but that excessive dynamic ice shaping (a secondary property of AF(G)Ps) limited the concentration which could be applied due to formation of sphicular ice morphologies which damage cell membranes.[12,13] Gibson and coworkers have demonstrated that polymeric IRIs can be used to significantly improve the cryopreservation of blood cells,[14,15] nucleated cells[16] and even cell monolayers.[17]

Despite this diverse range of materials shown to have IRI activity, there is an outstanding question of how the different natural and synthetic antifreeze

macromolecules interact with ice. We do not know the roles of bound and un-bound components,[6] if all ice binding proteins have the same mechanism or even if multiple molecular level mechanisms can give rise to similar macroscopic effects. For example, AFPs are rigid and have an identifiable ice-binding face. AFGPs, however, are more flexible[18] and may bind *via* their peptide backbone,[19] with the hydrophilic carbohydrate hydroxyl groups pointing away. This is in contrast to PVA, which is hypothesised to hydrogen bond *via* its hydroxyls to the ice surface (Figure 2.01).[20,21]

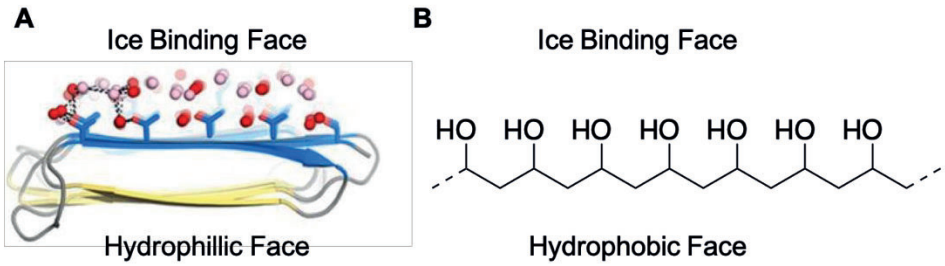

Figure 2.01: Ice binding faces of an AFP from longhorn beetle (**A**) and poly(vinyl alcohol) (**B**) showing the difference in binding face hydrophobicities. Adapted from Ref. 22.

To further complicate the picture, synthetic materials with significant amphipathic character (opposing hydrophilic/hydrophobic face)[23] but no obvious ice-binding sites, such as graphene oxide[24] and metallohelices,[25] also inhibit ice growth, supporting a mechanism where they sit at the semi-ordered layer and slow the rate of water transfer.[26]

An advantage of synthetic over natural polymers is the ability to tune their architecture[27,28] (e.g. stars, brushes, cycles) to modulate function. Vail *et al.* used RAFT polymerisation and column chromatography to obtain ultra-low dispersity PVA, showing that IRI activity activates above 10 repeat units in length[29,30] and that

block copolymerisation,[31] but not statistical co-polymerisation, is a tolerated modification supporting the hydroxyl hydrogen-bonding to ice model of Koop.[20] Voets *et al.* found that bottle-brush PVA had no molecular-weight enhancement effects suggesting confinement of the PVA chains limits prism-face binding,[32] and Congdon *et al.* showed that 3-arm star polymers have equal activity to 2-arms, despite having higher molecular weight.[33] Interestingly, Type I AFPs are known to oligomerize to produce hyperactive variants, which can be considered to be the protein equivalent of varying polymer architecture to enhance activity.[34] There is clearly a complex relationship between macromolecular architecture and IRI, and the design of more complex materials with multifunctional properties, such as imaging modalities, require more detailed studies to both help translation but to also understand the mechanism of action.

Considering the above, we have identified two potential avenues for further investigation of the IRI activity of PVA. Firstly, we designed and synthesised metal-core nanoparticles bearing multiple copies of poly(vinyl alcohol) on their surface, using RAFT polymerisation to enable control over molecular weight and to install a thiol-anchoring group. We identified polymers which led to colloidally stable gold particle dispersions to enable the ice recrystallisation activity and ice shaping activity of the hybrids to be quantified and compared to free polymers in solution. Secondly, we attempted to identify the specific structural features that give PVA its significant IRI activity, we achieved this by comparing the IRI activity of PVA and a series of structural analogues, PVA was compared to poly(vinyl ketone), poly(vinyl amine), poly(allyl alcohol), poly(acrylic acid), and poly(methylol).

2.4 Results and Discussion

2.4i Synthesis and Characterisation of PVA Coated Gold Nanoparticles

To obtain multivalent polymer-coated nanoparticles, RAFT/MADIX polymerisation was exploited to install a protected thiol at ω-chain ends *via* a xanthate chain-transfer agent,[30,33,35] essential for a controlled polymerisation of vinyl acetate, Scheme 2.01. Vinyl acetate was polymerised using various ratios of *S*-benzyl *O*-ethyl carbondithioate to give a panel of poly(vinyl acetates)'s (PVAc), which were characterised by SEC (size exclusion chromatography) and IR (infrared) spectroscopy. Dispersity and M_n values were rather broad, as expected for lesser activated monomers and were in reasonable agreement to the theoretical values (Figure 2.02). These polymers were subsequently hydrolysed by addition of hydrazine, to remove the acetate protecting groups, which was confirmed by the absence of acetate methyl groups in ^{1}H NMR as well as complete removal of carbonyl stretches (1729 cm^{-1}) and appearance of hydroxyl groups (~3300 cm^{-1}) in the infrared (Figure 2.03).

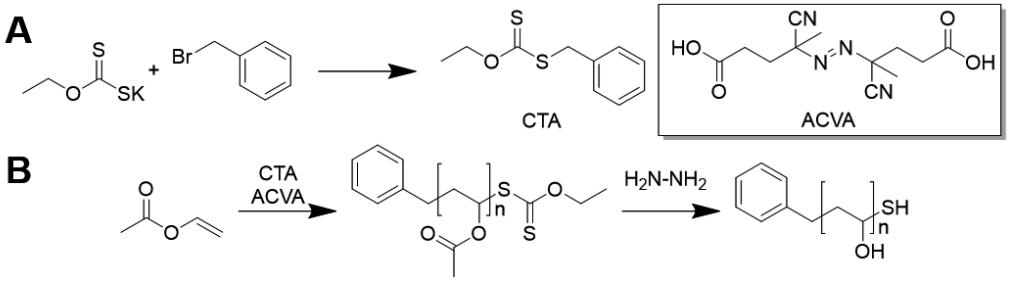

Scheme 2.01: A Synthesis of S-benzyl O-ethyl carbondithioate and structure of ACVA (half life at 69°C is 10h); **B** Synthetic strategy used for generating a thiol terminated PVA using MADIX polymerisation.

Table 2.01: Poly(vinyl acetate) synthesised in this study.

Polymer[(a)]	[M]/[CTA] (-)[(b)]	Conversion (%)[(c)]	M_n (Theo) (g.mol^{-1})[(d)]	M_n (SEC) (g.mol^{-1})[(e)]	*Đ* (-)[(f)]
PVAc$_6$	10	72	600	500	1.41
PVAc$_{18}$	40	59	2,000	1,600	1.24
PVAc$_{42}$	60	68	3,500	3,600	1.38
PVAc$_{98}$	100	45	3,900	8,500	1.37
PVAc$_{140}$	250	56	12,000	12,000	1.53

(a) Sample names are determined according to the number average degree of polymerisation determined by SEC; **(b)** Monomer to RAFT agent molar ratio; **(c)** Determined by ^{1}H NMR using mesitylene as an internal standard; **(d)** Determined from feed ratio and conversion; **(e)** Determined by SEC; **(f)** Đ is M_w/M_n from SEC.

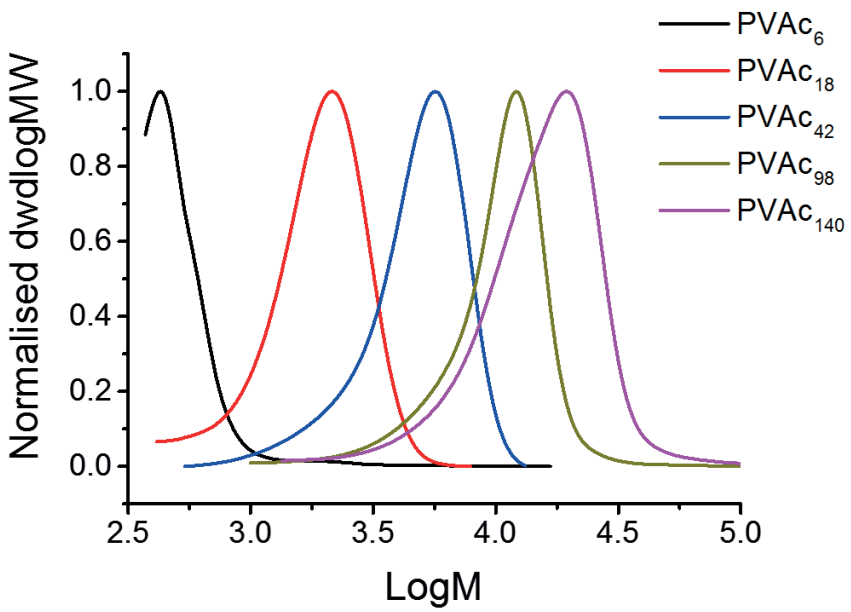

Figure 2.02: Molecular weight distribution from SEC for the PVAc samples synthesised in this work. SEC was carried out in THF.

It must be noted that the dispersity of PVA$_6$ is likely to be greater than reported by SEC due to overlap between the polymer and solvent peak.

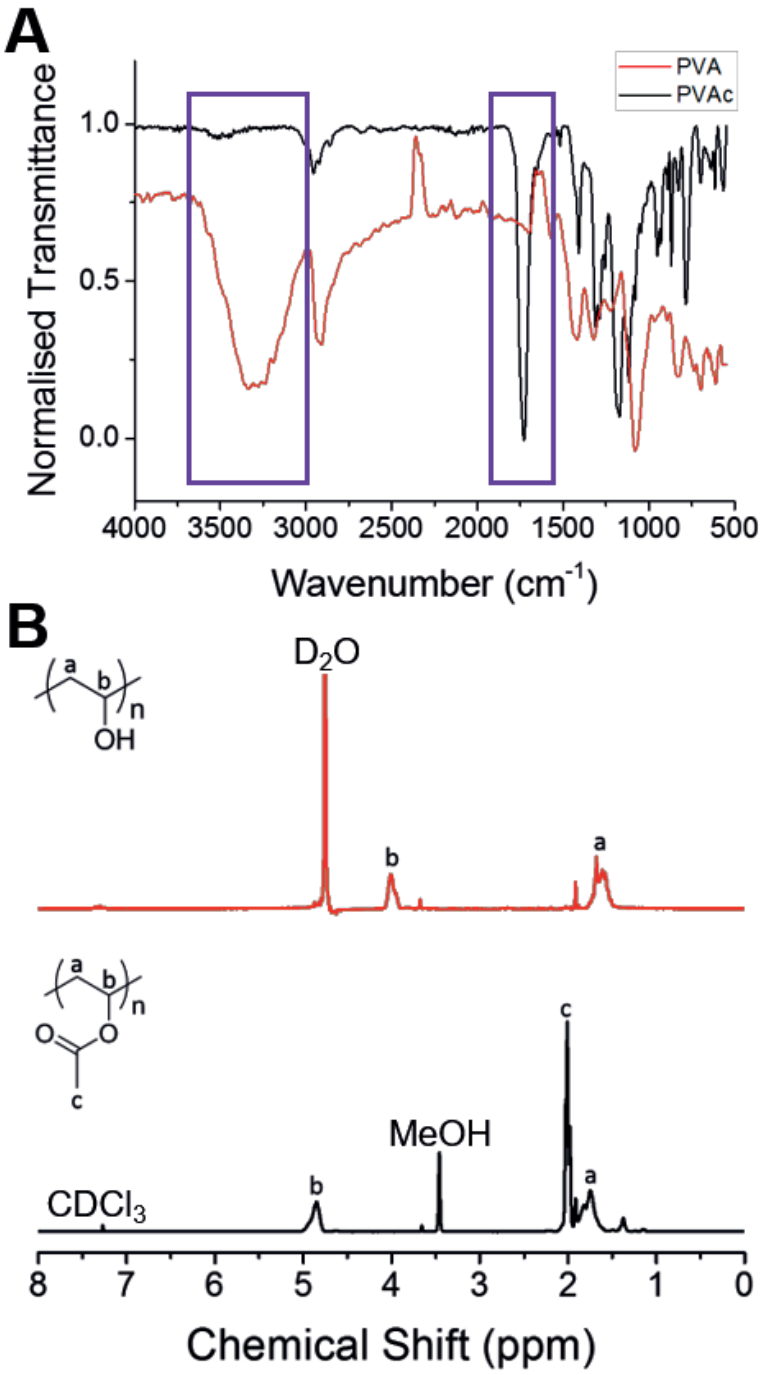

Figure 2.03: Characterisation data for the deprotection of PVAc to PVA using hydrazine. Deprotection was confirmed by FTIR (**A**) and ^{1}H NMR (**B**). The carbonyl and hydroxyl regions have been highlighted on the FTIR (purple box). PVAc NMR was carried out in $CDCl_3$, and PVA in D_2O. Solvent peaks are indicated as appropriate.

4 nm Diameter gold nanoparticles were synthesised by reducing a solution of gold(III) chloride and trisodium citrate with sodium borohydride.[36] PVAs were immobilised by simple mixing and excess polymer was removed by repeated centrifugation and resuspension cycles. The resulting hybrid nanoparticles were fully characterised by TEM (transmission electron microscopy), DLS (dynamic light scattering), XPS (X-ray photoelectron spectroscopy), UV-Visible spectroscopy and TGA (thermogravimetric analysis).

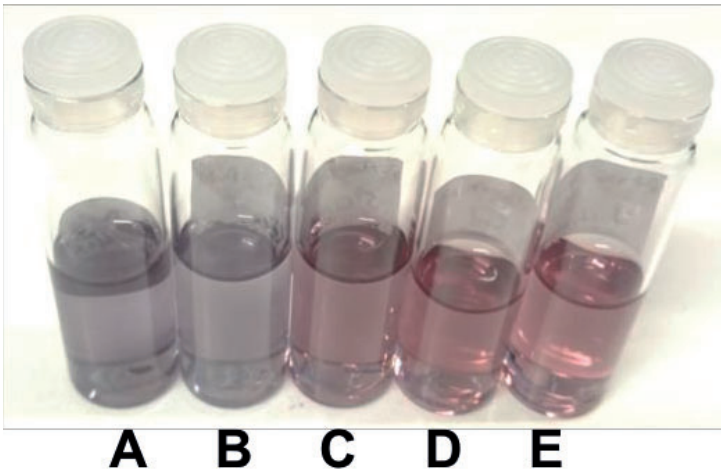

Figure 2.04: Photograph of the PVA@Au_4 samples in water. **A** PVA_6@Au_4; **B** PVA_{18}@Au_4; **C** PVA_{42}@Au_4; **D** PVA_{98}@Au_4; **E** PVA_{140}@Au_4.

From visual analysis (Figure 2.04) it was clear that PVA_6, PVA_{18} and PVA_{42} did not lead to stable AuNP dispersions, with the coloration of the solutions becoming purple/blue, indicative of surface plasmon resonance (SPR) bands of the gold coupling due to aggregation of the nanoparticles.[37] These were therefore excluded from further study. For the other polymers, surface functionalisation was confirmed by an increase

in hydrodynamic diameter from 4 to ~10 nm, and a small red-shift in the SPR_{max}. TEM analysis confirmed that the particle size and distribution did not change after polymer functionalisation (Figure 2.05).

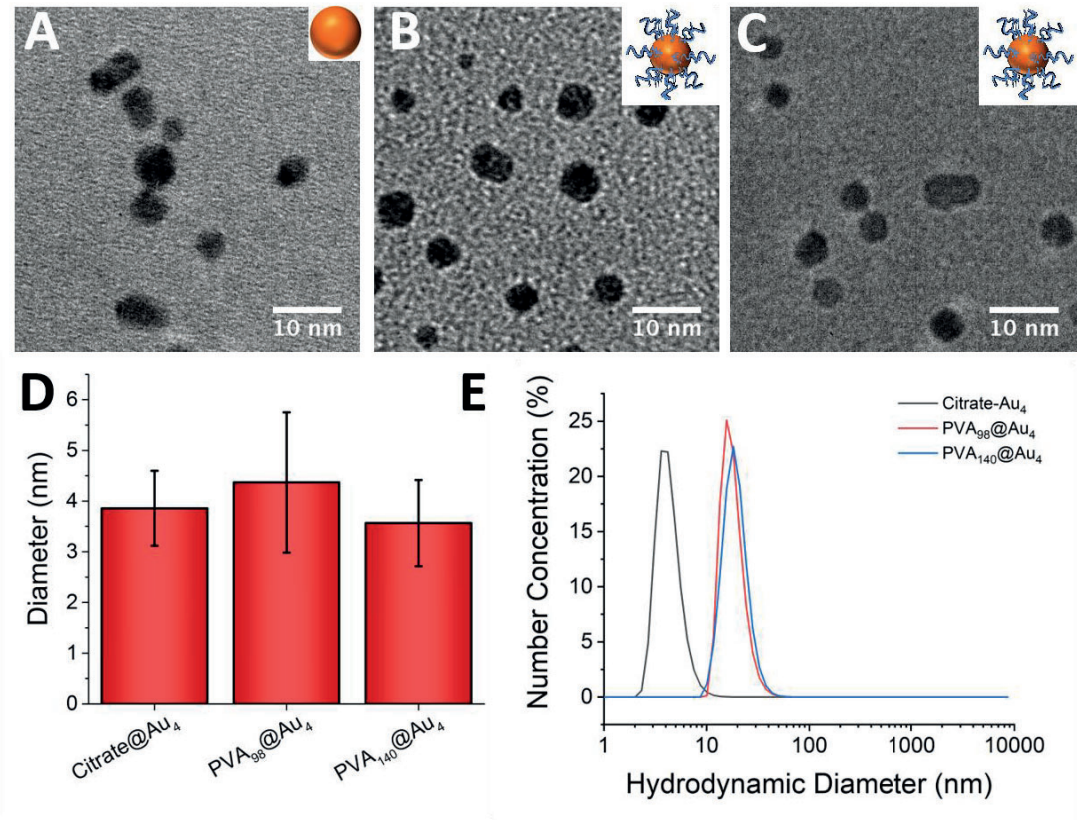

Figure 2.05: Gold nanoparticle characterisation. **A** TEM of citrate stabilised Au_4 nanoparticles; **B** TEM of $PVA_{98}@Au_4$; **C** TEM of $PVA_{140}@Au_4$; **D** Diameter of AuNPs from TEM, error bars represent ± S.D. from >100 particles; **E** Hydrodynamic diameter of AuNP from DLS. Characterisation was carried out by LEW and is included for completeness.

Zeta potential measurements showed an increase (from -19.4 mV to -5 mV) upon polymer coating, due to displacement of the citrate stabilising ligands, supporting successful surface coating. To enable chemical characterisation of the surface, XPS

was employed on dried-down nanoparticles (Figure 2.16). A significant increase in carbon and sulfur intensities compared to the 'naked' citrate-particles confirmed the presence of polymer. Finally, TGA confirmed the presence of the polymer coating, with a significant organic mass loss at around 300 °C. Taken together, the above characterisation confirmed successful modification of the gold particle surfaces with the poly(vinyl alcohol).

2.4ii Evaluating the IRI Activity of Multivalent PVA Nanoparticles

These PVA-coated nanoparticles were designed to enable the effect of macromolecular architecture on IRI activity to be probed. Previous results have shown that adding a branch (3-arm versus 2-arm) to polymers of PVA did not lead to any increase in activity.[33] This is in contrast to a 3-fold increase in molecular weight in linear PVAs which increases activity.[30] It has been suggested that activity is decreased by increased branching at equal total molecular weight, due to the additional arm being sterically constrained from aligning with the appropriate crystal face.[21,32] $PVA_{98}@Au_4$ and $PVA_{140}@Au_4$ were screened for IRI activity in PBS buffer, based on their observed stability. IRI activity was evaluated by monitoring the growth of polynucleated ice crystals (using a 'splat' assay)[30,38] at sub-zero temperatures, which enables recrystallisation effects to be separated from nucleation (which PVA has an effect on),[39] using an established method.[30,40,41]

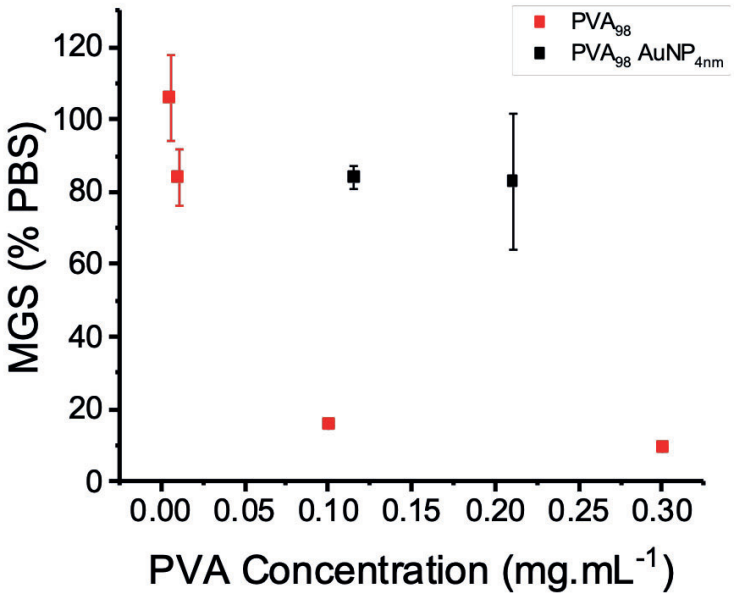

Figure 2.06: Ice recrystallisation inhibition activity of PVA_{98}@Au_4 at decreasing PVA concentrations. While these particles appeared to be stable immediately after synthesis, they appeared to be significantly less stable by the time the IRI assays were performed, with significant discoloration of the solution. MGS = mean grain size reported as an area. Error bars represent ± standard deviation from a minimum of 3 repeats.

Linear PVA showed strong IRI activity, inhibiting all growth <1 $mg.mL^{-1}$, reinforcing that this is the most potent non-protein inhibitor known.[7] Upon testing the gold nanoparticles, it was observed that PVA_{98}@Au_4 was not stable under the assay conditions, with some aggregation occurring. This gave rise to potentially false-negative results with it apparently losing activity (Figure 2.06). From the library of polymers and particles only PVA_{140}@Au_4 was stable in the assay, agreeing with previous observations that tuning the surface of polymer-grafted gold particles is chain length and polymer-type dependent.[37,42,43] In order to ensure all free PVA in solution had been removed, the nanoparticles were washed in PBS until the supernatant

displayed no inherent IRI activity Figure 2.07. The IRI activity of the particles is reported in terms of total PVA concentration (calculated from TGA) to enable the activity per chain to be critically compared, Figure 2.08.

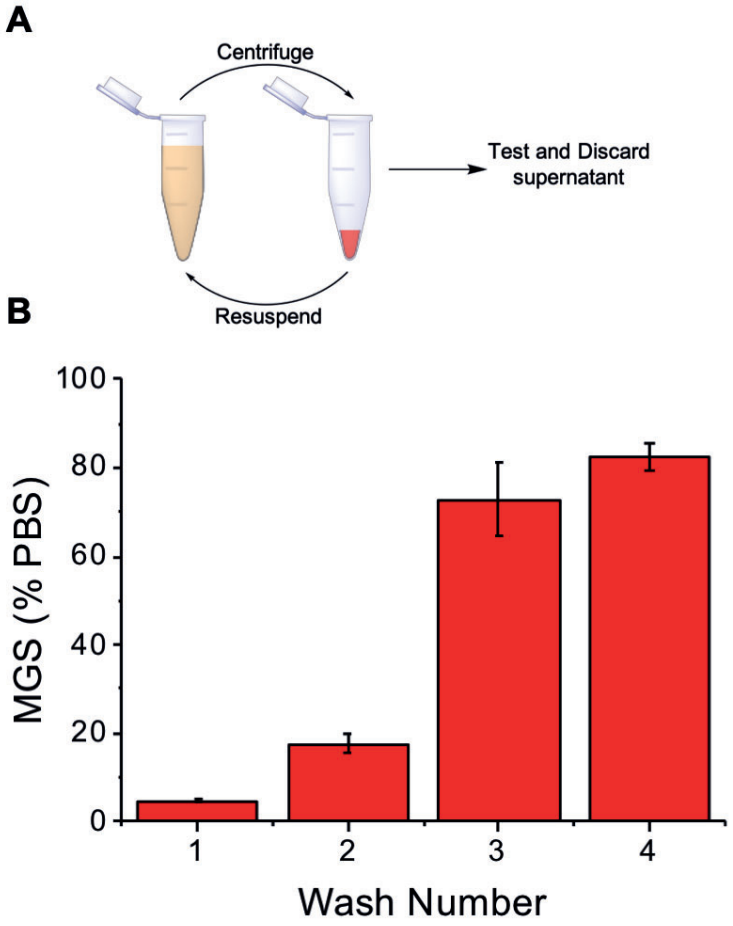

Figure 2.07: A Cartoon illustration of the washing steps used to remove any free PVA from the supernatant, washes were repeated until no PVA was observed by IRI; **B** MGS vs Number of $PVA_{140}@Au_4$ washes, after 4 washes no free PVA was present in the solution. MGS = mean grain size reported as an area. Error bars represent ± standard deviation from a minimum of 3 repeats.

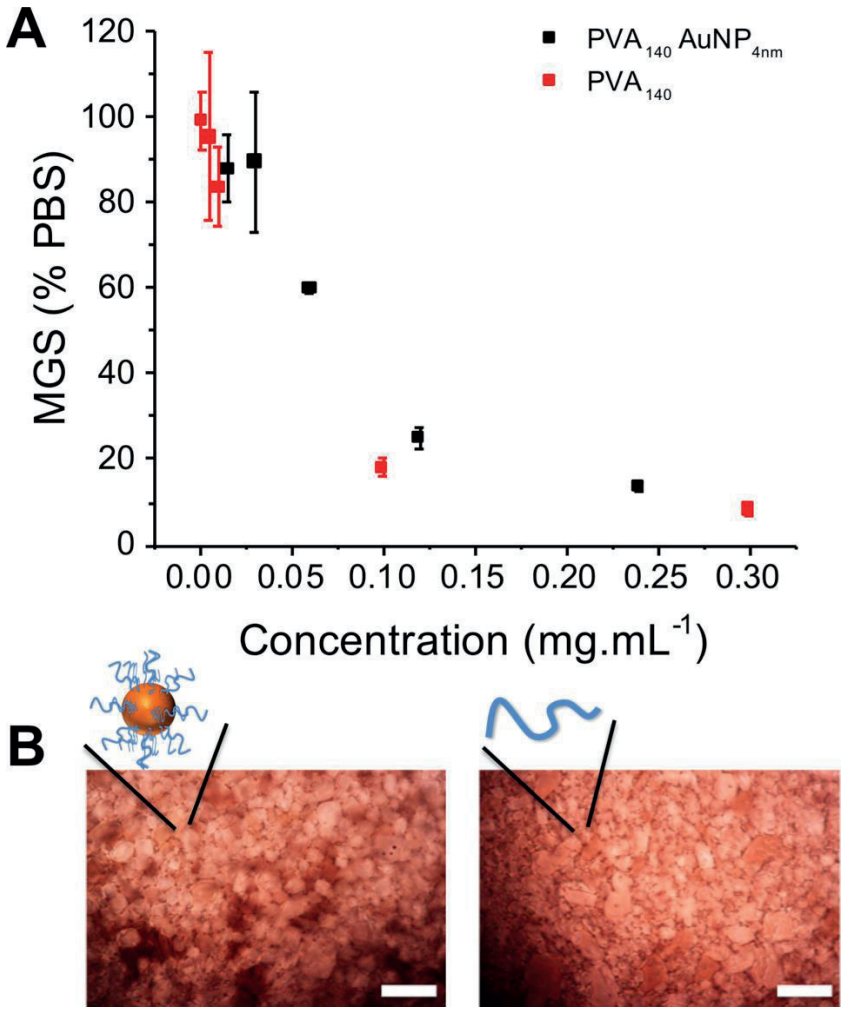

Figure 2.08: A IRI activity of $PVA_{140}@Au_4$ vs concentration, compared to the linear polymer. Concentration reported is of PVA; **B** Example cryomicrographs of ice wafers grown with $PVA_{140}@Au_4$ at 0.12 $mg.mL^{-1}$ and PVA_{140} at 0.1 $mg.mL^{-1}$. Scale bars are 100 µm. MGS = mean grain size reported as an area. Error bars represent ± standard deviation from a minimum of 3 repeats.

Considering the previous reports on polymer architecture removing IRI activity,[30,32] it was remarkable that that $PVA_{140}@Au_4$ was observed to retain all IRI, nearly identical (on a per polymer basis) to that of free PVA chains. As the PVA and particles were tested at different concentrations, and due to the non-linear relationship between concentration and IRI activity, statistical analysis could not be performed reliably. On

a molar basis (assuming one particle is a very large molecule) this would represent a dramatic increase in activity, but such a comparison is not valid for large multivalent systems. The limiting concentration for inhibiting all growth was ~ 0.1 $mg.mL^{-1}$. To explain the retention of activity, the orientation of the PVA in relation to the ice must be considered. Molinaro *et al.* used molecular simulations to hypothesise that PVA can bind to both the primary and secondary prism planes of ice *via* its hydroxyl groups. The distance between hydroxyls in ice on the primary and secondary prismatic faces is 2.76 and 2.74 Å respectively, and between consecutive hydroxyls in PVA is 2.92 Å enabling a good fit for pattern matching (Figure 2.09 A).[20,21] However, for the basal faces, the distance is 4.52 Å. For 3-arm (star) PVA, two arms can bind the prismatic plane but the third arm is perpendicular to the c-axis and cannot form as many hydrogen bonds and hence has no associated activity (Figure 2.09 B). In the present work, the PVA chains are lightly grafted over a large nanoparticle surface, rather than a specific central conjugation point. From thermogravimetric analysis, relatively low grafting densities are obtained, at 8 chains/particle (0.1 $chains.nm^{-2}$). This low density means the polymers are free to interact with the ice faces, and to target the desirable prism faces unlike in highly grafted systems (such as star polymers[33] or bottle-brushes),[32] Figure 2.09 C.

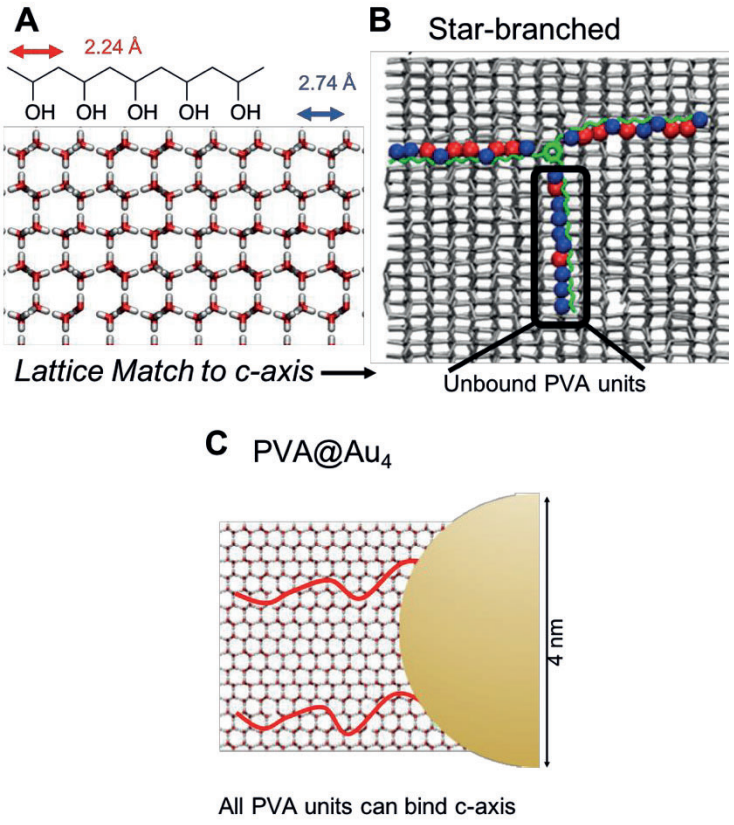

Figure 2.09: Schematic for PVA binding to ice. **A** Ice:PVA lattice matching as proposed by Koop;[20] **B** Simulations suggesting that in 3-arm star PVA, the third arm cannot bind to the correct face, limiting activity;[21] **C** Proposed mechanism for the retention of activity in multivalent PVA nanoparticles.

To demonstrate that the PVA/nanoparticle hybrids were directly interacting with the ice surface, ice shaping experiments were conducted. In this assay, a concentrated sucrose solution (which reduces nucleation and slows growth rates) was used to obtain ice crystals whose growth could be monitored. For aqueous solutions, rounded disc shaped ice crystals were observed (Figure 2.10 A). However for both the PVA and PVA_{140}@$AuNP_4$ faceting was observed and dendritic morphologies were consistent with ice binding and shaping (Figure 2.10 B and C), as seen for dendronised AFP.[44]

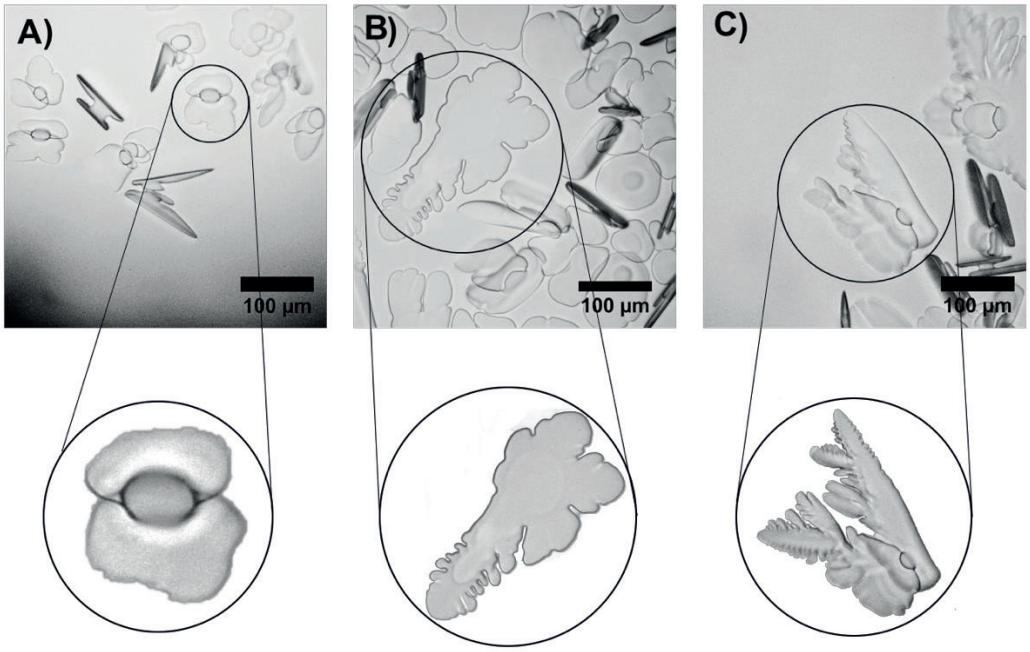

Figure 2.10: Ice shaping assays carried out in 45 % sucrose with zoomed images to demonstrated crystals of interest. **A** No additive at -6 °C; **B** PVA_{140} 0.32 mg.mL^{-1} at -5.5 °C; **C** PVA_{140}@Au4 0.32 mg.mL^{-1} at -4 °C.

2.4iii Evaluating the IRI Activity of PVA Alternatives

Given the marked IRI activity of PVA, we also decided to investigate the specific features of PVA that give rise to this activity, this will hopefully allow us to understand the design rules that may allow us to access more active materials. To that end, a series of polymers with similar structures to PVA were tested and their IRI activities compared. Initially, the importance of the spacing between OH units in PVA was investigated, poly(vinyl alcohol) has been suggested to bind to ice due to its close pattern match between the PVA OH spacing, and the oxygen atoms on the surface of a growing ice crystal.[20] We initially investigated a series of materials which are similar in structure to PVA, however with more flexibility around the pendant groups. Poly(allyl alcohol)[45] and poly(acrylic acid) were tested for their IRI activity, as these

materials have the ability to configure into chains with similar OH spacing as PVA. Polymer synthesis is shown in Scheme 2.02, whilst the structures of the other polymers tested are shown in Figure 2.11.

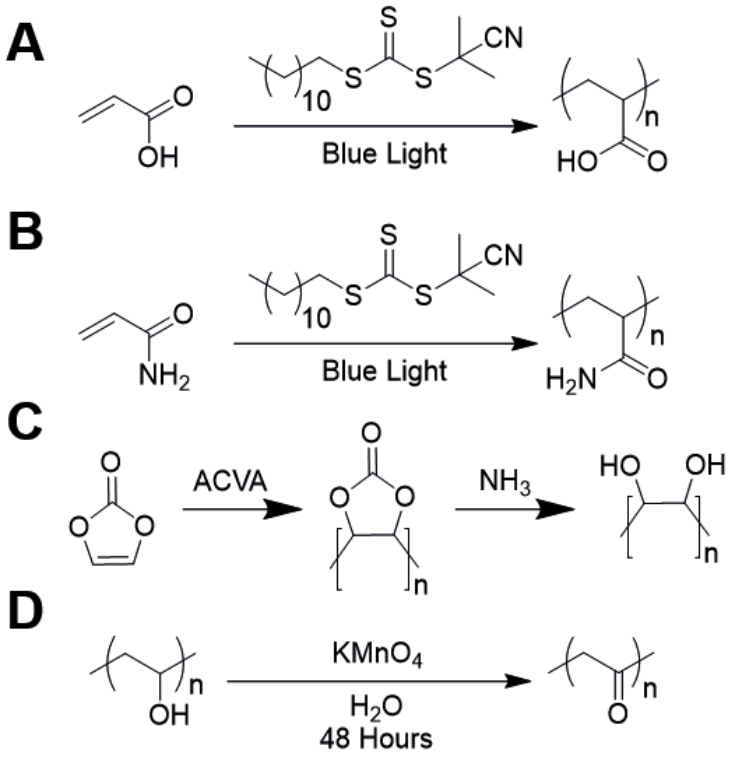

Scheme 2.02: A Synthesis of poly(acrylic acid); **B** Synthesis of poly(acrylamide); **C** Synthesis of poly(methylol) from vinylene carbonate; **D** Synthesis of poly(vinyl ketone) from poly(vinyl alcohol).

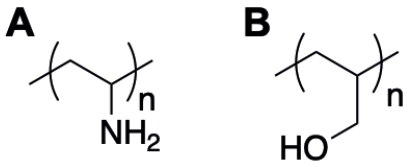

Figure 2.11: The structures of **A** Poly(vinyl amine) and **B** Poly(allyl alcohol) also tested in this work.

Table 2.02: Poly(vinyl alcohol) analogues synthesised.

Polymer	[M]/[CTA] (-)[a]	Conversion (%)[b]	M_n (Theo) ($g.mol^{-1}$)[c]	M_n (SEC) ($g.mol^{-1}$)[d]	*Đ* *(-)*[e]
Poly(acrylic acid)	100	94.2	12000	1040	>4[f]
Poly(acrylamide)	100	45.0	3200	1800	>4[f]
Poly(vinylene carbonate)	100[g]	6[h]	500	12,000	1.52
Poly(vinyl amine)[i]				25,000	
Poly(allyl alcohol)[j]				8300	1.08

(a) Monomer to RAFT agent molar ratio; **(b)** Determined by ^1H NMR using mesitylene as an internal standard; **(c)** Determined from feed ratio and conversion; **(d)** Determined by SEC; **(e)** Đ is M_w/M_n from SEC; **(f)** Significant tailing was observed in the aqueous GPC, leading to high dispersity values (>4); **(g)** Free radical [M]:[Initiator] ratio; **(h)** Determined by mass of polymer produced, NMR suggested negative conversion; **(i)** Purchased from polysciences; **(j)** Provided by Marc Hillmyer.

These materials were tested for IRI activity using the standard 'splat' assay, and it was observed that the activity of these materials was significantly lower than that of PVA. Poly(allyl alcohol) gave a MGS of 39 % at 20 $mg.mL^{-1}$, while poly(acrylic acid) displayed essentially no activity at 60 % MGS. This is the same as observed for an inactive PEG control. For comparison, PVA_{98} which is around the same degree of polymerisation as the allyl alcohol tested, would give similar IRI activity at around 0.05 $mg.mL^{-1}$, a 400 fold concentration difference. Given the significant importance of the backbone spacing on the PVA activity, it was suggested that poly(vinyl amine), another flexible hydrophilic polymer may display similar activity to PVA, however

IRI measurements again suggested that this is not the case, inferring that it is the specific oxygen positioning which is important for optimal ice binding.

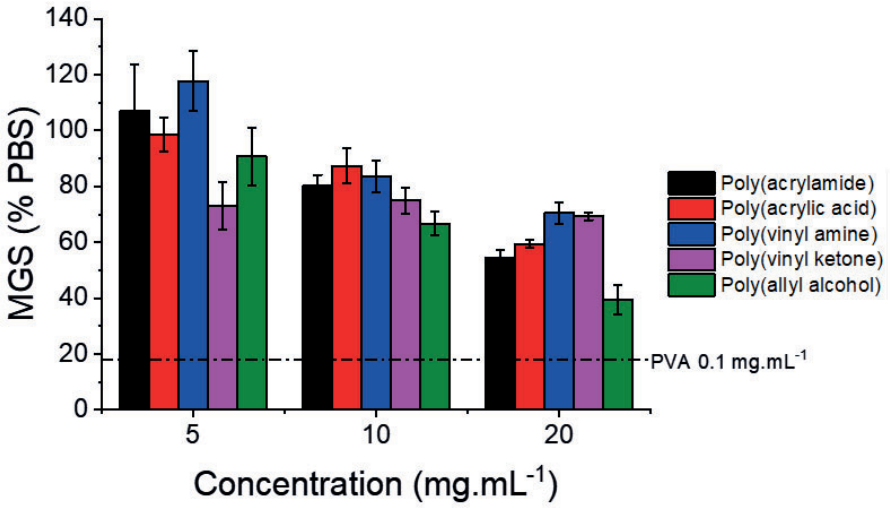

Figure 2.12: IRI activity of the polymers tested. MGS = mean grain size reported as an area. Error bars represent ± standard deviation from a minimum of 3 repeats.

Given these results, the number of OH units in the backbone was investigated as this may allow stronger bonding to the ice surface, and hence greater activity. PVA was compared with poly(methylol), synthesised from the free radical polymerisation of vinylene carbonate followed by deprotection in ammonia, Scheme 2.02. The presence of polymer was confirmed by SEC, and the structure of the final poly(methylol) confirmed by FTIR and ^{1}H NMR. Unfortunately, after synthesis it was discovered that poly(methylol) is insoluble in almost all solvents due to significant intramolecular hydrogen bonding.[46] As a result of this, ^{1}H NMR was conducted in D_3PO_4, and IRI activity could not be tested as pH has a large effect on IRI activity.[47] Attempts to use guanidinium hydrochloride to interrupt the hydrogen bonds and encourage water solubility were unsuccessful.

Given these observations it was determined that investigating the hydrogen bonding between PVA and water may be interesting. Poly(vinyl alcohol) can both donate hydrogen bonds through the H atom, and accept them through the lone pair on the oxygen. Poly(vinyl ketone), which displays very similar spacing of the backbone oxygen but can only accept H bonds, was synthesised *via* the oxidation of PVA using potassium permanganate in water.[48] The resulting structure may engage in keto-enol tautomerism and therefore the dominant form of poly(vinyl ketone) was confirmed by a single peak in the ^{1}H NMR in the region expected for a hydrogen adjacent to a ketone, as well as a strong C=O bond observable by FTIR. The FTIR indicated the presence of an OH peak, at around 3000 cm^{-1} to 3600 cm^{-1}, however the material appeared to be incredibly hygroscopic and therefore this is likely due to the presence of water in the sample, intramolecular hydrogen bonding which, would suggest presence of the enol form, would result in a much lower band (~ 2500-3000 cm^{-1}).[49] IRI results suggest that the simple removal of the ability of PVA to donate a hydrogen bond, significantly reduces its IRI activity, Figure 2.12, with example micrographs shown in Figure 2.13.

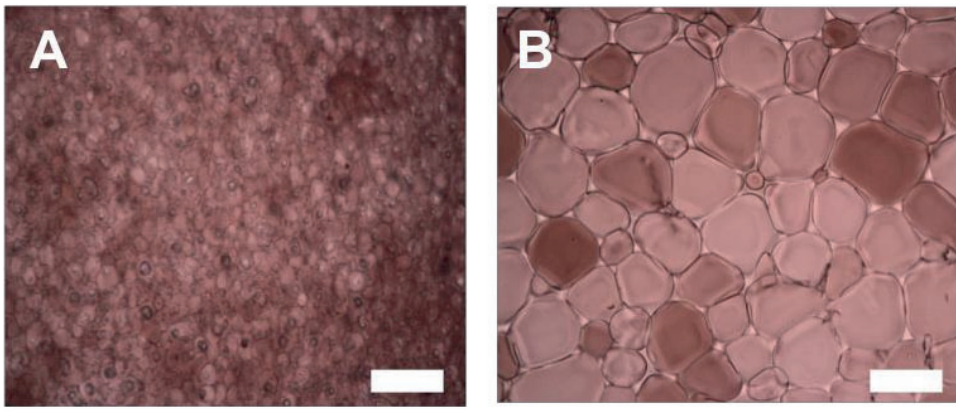

Figure 2.13: Cryomicrographs of **A** PVA_{10} and **B** Poly(vinyl ketone) at 10 $mg.mL^{-1}$. Scale bars are 100 μm.

Taken together, these results demonstrate that PVA is optimally designed to interact with the ice face. The precise spacing of the OH units on the backbone, and the inability of the OH groups to easily rotate out of this orientation, paired with the specific ability of the OH group to interact with the growing ice face, are all crucial for the activity of PVA. Unfortunately, these design rules are incredibly difficult to apply to the synthesis of new materials, as every element of the PVA structure is observed to be required for optimal activity.

							
Concentration (mg.mL)	0.3	20	20	20	20	20	Not Soluble
MGS (% PBS)	9	39	54	59	69	70	

Figure 2.14: Summary of the samples tested in this work. Of the non-PVA materials tested, poly(allyl alcohol) was the most active, however was still much less active than PVA itself.

2.5 Conclusion

We have demonstrated the first synthesis and characterisation of poly(vinyl alcohol) gold nanoparticle hybrids by using RAFT polymerisation and grafting-to methodology. PVA chain lengths were identified which gave colloidally-stable particles, due to the relatively low grafting densities achieved by this strategy, and the surface-bound polymers were observed to retain their full ice recrystallisation inhibition activity. We hypothesise that the low grafting density on the particle surface is beneficial as it enables the polymers to explore the ice surface so each can engage with the correct prism face to allow optimal binding. This hypothesis was supported by ice shaping assays, with addition of the nanoparticles resulting in faceting of the growing ice crystal being observed. These challenge the previous observations, showing that complex architecture can be used to modulate and maintain IRI activity by controlling the PVA density. These results will guide the development not only of more active IRIs, but to also enable their application in more fields where their nanoscopic dimensions, or optical properties are useful, such as in high resolution imaging.

We have also investigated the specific features of PVA which give it its excellent IRI activity and found that all of the structure must be conserved for optimal activity. Altering the spacing and the nature of the hydrophilic group severely limited IRI activity. Until the polymer chemist has the ability to precisely control the location and orientation of side-chains in the solution orientation of the polymer, there is little that can be easily identified as a method by which to improve the IRI activity of other synthetic materials, and therefore alternative classes of cryoprotectant material are more attractive for future development of this field.

2.6 Experimental

Materials

Phosphate-buffered saline (PBS) solutions were prepared using pre-formulated tablets (Sigma-Aldrich) in 200 mL of Milli-Q water (>18.2 Ω mean resistivity) to give [NaCl] = 0.138 M, [KCl] = 0.0027 M, and pH 7.4. Vinyl acetate (>99 %), 4,4'azobis(4-cynaovaleric acid) (>98 %), benzyl bromide (98 %), hydrazine hydrate (78-82 % iodiometric), gold (III) chloride trihydrate (>99.9 %), sodium borohydride (>98 %), 2-cyano-2-propyl dodecyl trithiocarbonate (97 %), potassium permanganate (>99 %), vinylene carbonate (97 %), acrylamide (>99 %) and acrylic acid (99 %) were purchased from Sigma-Aldrich. Vinyl acetate, acrylic acid and vinylene carbonate were filtered through a plug of basic alumina to remove inhibitors prior to use. 4,4'azobis(4-cynaovaleric acid) was recrystallised from methanol and stored at -18 ºC in the dark. Potassium ethyl xanthate (98 %) was purchased from Alfa Aesar. Trisodium citrate and 35 % ammonia solution were purchased from Fisher. Poly(vinyl amine) was purchased from polysciences and dialysed before use. All solvents were purchased from Sigma-Aldrich or VWR and used without further purification.

Physical and Analytical Methods

^{1}H and ^{13}C NMR spectra were recorded on Bruker Avance III HD 300 MHz, HD 400 MHz or HD 500 MHz spectrometers using deuterated solvents obtained from Sigma-Aldrich. Chemical shifts are reported relative to residual non-deuterated solvent. SEC data was recorded on an Agilent 390-LC MDS instrument equipped with differential refractive index (DRI), viscometry (VS), dual angle light scatter (LS) and dual

wavelength UV detectors. The system was equipped with 2 x PLgel Mixed D columns (300 x 7.5 mm) and a PLgel 5 μm guard column. The eluent was DMF with 5 mmol NH_4BF_4 additive. Samples were run at 1 $mL.min^{-1}$ at 50 ºC. Poly(methyl methacrylate) standards (Agilent EasyVials) were used for calibration. Analyte samples were filtered through a nylon membrane with 0.22 μm pore size before injection. Respectively, experimental molar mass ($M_{n,}^{SEC}$) and dispersity (Đ) values of synthesised polymers were determined by conventional calibration using Agilent GPC/SEC software.

Ice wafers were annealed on a Linkam Biological Cryostage BCS196 with T95-Linkpad system controller equipped with a LNP95-Liquid nitrogen cooling pump, using liquid nitrogen as the coolant (Linkam Scientific Instruments UK, Surrey, UK). An Olympus CX41 microscope equipped with a UIS-2 20x/0.45/∞/0-2/FN22 lens (Olympus Ltd, Southend on sea, UK) and a Canon EOS 500D SLR digital camera was used to obtain all images. Image processing was conducted using Image J, which is freely available from http://imagej.nih.gov/ij/.

Ice Recrystallisation Inhibition Assay

A 10 μL droplet of polymer in PBS solution was dropped from 1.4 metres onto a glass microscope coverslip, which was placed on top of an aluminium plate cooled to -78 °C using dry ice. The droplet froze instantly upon impact with the plate, spreading out and forming a thin wafer of ice. This wafer was then placed on a liquid nitrogen cooled cryostage held at -8 °C within the viewing area of the microscope. The wafer was then left to anneal for 30 minutes at -8 °C. The number of crystals in the image was counted using ImageJ, and the area of the field of view divided by this number of crystals to

give the average crystal size per wafer and reported as a percentage (%) of area compared to PBS control.

Ice Shaping Assay - This procedure was performed by Alice Fayter, and is included for completeness.

Samples dissolved in PBS buffer containing 45 % sucrose were sandwiched between two glass coverslips and sealed with immersion oil. Samples were cooled to −50 °C. The temperature was then increased to −8 °C and held for 1 hour to anneal. The samples were then heated at 0.05 °C.min^{-1} until few ice crystals remained and then cooled at 0.05 °C.min^{-1} and the shape of ice crystals observed. Micrographs were obtained every 0.1 °C.

Synthesis of S-Benzyl O-ethyl Carbonodithioate

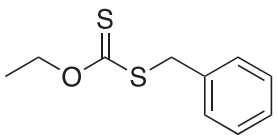

Potassium ethyl xanthate (3 g, 0.0187 mol, 1 eq) was dissolved in 50 mL acetone at 70 °C and stirred, after 30 minutes, benzyl bromide (3.20 g, 0.0187 mol, 1 eq) was added and stirred for 24 hours. During the reaction, a white precipitate is formed, the reaction solution was diluted with a further 50 mL acetone and filtered to remove the solid precipitate. The product was dissolved in dichloromethane (DCM) and washed twice with water at pH 8, followed by brine. The DCM layer was dried with magnesium sulphate, filtered and the solvent removed under vacuum. The resulting yellow oil was then recrystallised in hexane.

Yield: 2.87 g, 72.3 %. ^{1}H NMR ($CDCl_3$): δ = 1.39 (CH_3CH_2O, t, J = 7 Hz, 3H), 4.34 ($C(S)SCH_2C_6H_5$, s, 2H), 4.63 (CH_3CH_2O, q, J = 7 Hz, 2H), 7.31 (Aromatic C-H, m,

5H). ^{13}C NMR ($CDCl_3$): δ = 13 (CH_3CH_2O), 40 ($C(S)CH_2C_6H_5$), 70 (CH_3CH_2O), 127 (*Para* C-H), 128 (*Meta* C-H), 129 (*Ortho* C-H), 135 ($CH_2C(CH)CH$), 213 ($OC(S)S$).

Synthesis of poly(vinyl acetate)$_{98}$

As a representative example, vinyl acetate (3 g, 3.21 mL, 34 mmol, 1000 eq), *S*-benzyl *O*-ethyl carbondithioate (0.074 g, 0.34 mmol, 10 eq.), 4,4'azobis(4-cyanovaleric acid) (0.0098 g, 0.034 mmol, 1 eq.) and mesitylene (0.1 g, 0.086 mL) were added to a 10 mL vial and sealed with a subaseal. The solution was left to degas under nitrogen for 15 minutes, before being placed into an oil bath at 68 °C. The reaction was left for 24 hours before being plunged into liquid nitrogen. Poly(vinyl acetate) was recovered as a sticky yellow oil after precipitation into diethyl ether.

Representative characterisation data for poly(vinyl acetate)$_{98}$**:**

Yield: 1.21 g. ^{1}H NMR (400 MHz, $CDCl_3$) δ = 4.90 – 4.70 ($CH_2CH(OOCH_3)$, br, 1H), 2.07 ($CH_2CH(OOCH_3)$, br, 3H), 1.90-1.60 ($CH_2CH(OOCH_3)$, br, 2H). FTIR: C-H 2954 cm^{-1}, C=O 1729 cm^{-1}, C-O 1407 cm^{-1}. M_n^{SEC}(THF) = 8500 Da, M_w/M_n = 1.37.

Synthesis of poly(vinyl alcohol)$_{98}$

As a representative example, poly(vinyl acetate) (1 g) was dissolved in methanol (5 mL) in a round bottom flask and stirred until dissolved. Hydrazine hydrate solution (15 mL, 78-82 % in water) was added and the reaction heated to 50 °C in an oil bath for 24 hours. The solution was cooled and diluted with water (50 mL) before being purified by dialysis (100-500 Da MWCO) followed by lyophilisation to form a white powder. Representative characterisation data for poly(vinyl alcohol)$_{98}$:

Yield: 0.28g. ^{1}H NMR (400 MHz, D_2O) δ = 4.00 – 3.80 ($CH_2CH(OH)$, br, 1H), 1.80 – 1.30 ($CH_2CH(OH)$, br, 2H). FTIR: O-H 3000-3400 cm^{-1}, C-H 2917 cm^{-1}, C-O 1411 cm^{-1}.

Synthesis of 4 nm gold nanoparticles and subsequent surface conjugation of polymer - This was performed by Laura Wilkins, and is included for completeness.

4 nm citrate-stabilised AuNPs were synthesised as described by Ieong et al.[36] 240 mL of a 0.21 $mmol.L^{-1}$ (0.08 $mg.mL^{-1}$), aqueous solution of $HAuCl_4$ was prepared at room temperature in glassware washed with aqua regia [CAUTION. HANDLE WITH CARE]. 13.8 mg (0.05 mmol) of trisodium citrate was added, followed by 5 mL of an ice-cold 0.1 M (0.5 mmol, 18.5 mg) solution of $NaBH_4$. The solution was stirred at room temperature overnight. Small AuNPs were isolated by taking the supernatant after centrifugation at 13,200 rpm for 10 miutes at 25 °C. 1 mg of polymer was added to 1 mL of Au_4 and the solution was agitated for 60 minutes at room temperature. The solutions were washed three times and concentrated in an Amicon Ultra 0.5 centrifugal filter units with an Ultracel-30 membrane before being re-dispersed in the same volume of PBS.

Synthesis of poly(acrylamide)

Acrylamide (1g, 0.014 mol, 100 eq) was added to a vial containing 2-cyano-2-propyl dodecyl trithiocarbonate (Sigma Aldrich) (49 mg, 0.14 mmol, 1 eq), sealed, and degassed by bubbling under nitrogen for 15 minutes. The vial was then exposed to

blue light for 24 hours at room temperature. The resulting polymer was precipitated into diethyl ether and dried under vacuum.

Yield: 0.77g. ^{1}H NMR ($CDCl_3$): δ = 1.35-1.80 (C*H*$_2$CHCOOH, br), 2.02-2.35 ($CH_2CHCONH_2$, br). $M_n^{SEC}(H_2O)$ = 1900 Da, M_w/M_n = 5.95. FTIR: Amine-NH 3300 (broad), C=O 1649 cm^{-1}, C-N 1319 cm^{-1}.

Synthesis of poly(acrylic acid)

Acrylic acid (1g, 0.014 mol, 100 eq) was added to a vial containing 2-cyano-2-propyl dodecyl trithiocarbonate (Sigma Aldrich) (47 mg, 0.14 mmol, 1 eq), sealed, and degassed by bubbling under nitrogen for 15 minutes. The vial was then exposed to blue light for 24 hours at room temperature. The resulting polymer was precipitated into diethyl ether and dried under vacuum.

Yield: 0.82g. ^{1}H NMR ($CDCl_3$): δ = 1.00-1.63 (C*H*$_2$CHCOOH, br), 1.64-1.87 (C*H*$_2$CHCOOH, br), 2.00-2.42 (C*H*$_2$CHCOOH, br), 3.63-4.49 ($CH_2CHCOOH$, br), 11.94-12.75 (O*H*, br). $M_n^{SEC}(H_2O)$ = 1000 Da, M_w/M_n = 4.93. FTIR: Acid-OH 3024 (broad), C=O 1699 cm^{-1}, C-O 1448 cm^{-1}.

Synthesis of poly(vinyl ketone)

PVA_{98} (0.1 g) was dissolved in water (60 mL) and stirred for 60 minutes. A separate solution was made up of potassium permanganate (7g) in water (60 mL) and the pH adjusted to 12.6. The potassium permanganate solution was added to the PVA solution over two hours using a dropping funnel. After stirring for 48 hours, the solution was dialysed for 48 hours (500-1000 MWCO), after which the solution was filtered and

lyophilized to recover poly(vinyl ketone) (11 mg). The resulting PVK was characterised by ^{1}H NMR and FTIR.

Yield: 11 mg, 11.5%. ^{1}H NMR (D_2O): δ = 1.54-2.08 (C*H*$_2$CO, s). $M_n^{SEC}(H_2O)$ = 450 Da, M_w/M_n = 1.09. FTIR: OH (water) 3716-2601 cm^{-1} , C=O 1554 cm^{-1}, α CH_2 bending 1397 cm^{-1}.

Synthesis of poly(methylol)

Vinylene carbonate (300 mg, 3.49 mmol, 100 eq) was dissolved in DMF (1 mL). 4,4'azobis(4-cyanovaleric acid) (9 mg, 34 μmol, 1 eq) was added and the solution degassed *via* 3 freeze pump thaw cycles. The vessel was flushed with nitrogen and heated to 60 °C with stirring. The reaction was left for 24 hours and the resulting poly(vinylene carbonate) was recovered by precipitation in diethyl ether (18 mg). A small amount was removed for SEC, and the remaining polymer (16 mg) was dissolved in a 35 % ammonia solution (3 mL). After 30 minutes the solution was filtered to recover polymethylol (9mg).

Yield: 9 mg. ^{1}H NMR (D_3PO_4): δ = 5.30-5.45 (C(OH)*H*, br). FTIR: O-H stretching 3617-2968 cm^{-1} , C-H 2941 cm^{-1}, O-H bending 1399 cm^{-1}, C-O 1013 cm^{-1}.

2.7 References

(1) Davies, P. L. Ice-Binding Proteins: A Remarkable Diversity of Structures for Stopping and Starting Ice Growth. *Trends Biochem. Sci.* **2014**, *39* (11), 548–555.

(2) Rothschild, L. J. *Life in Extreme Environments*; Amils, R., Ellis-Evans, C., Hinghofer-Szalkay, H., Eds.; Springer Netherlands: Dordrecht, 2007; Vol. 14.

(3) Harding, M. M.; Anderberg, P. I.; Haymet, A. D. J. "Antifreeze" Glycoproteins from Polar Fish. *Eur. J. Biochem.* **2003**, *270* (7), 1381–1392.

(4) Walters, K. R.; Serianni, A. S.; Sformo, T.; Barnes, B. M.; Duman, J. G. A Nonprotein Thermal Hysteresis-Producing Xylomannan Antifreeze in the Freeze-Tolerant Alaskan Beetle Upis Ceramboides. *Proc. Natl. Acad. Sci.* **2009**, *106* (48), 20210–20215.

(5) Laezza, A.; Casillo, A.; Cosconati, S.; Biggs, C. I.; Fabozzi, A.; Paduano, L.; Iadonisi, A.; Novellino, E.; Gibson, M. I.; Randazzo, A.; Corsaro, M. M.; Bedini, E. Decoration of Chondroitin Polysaccharide with Threonine: Synthesis, Conformational Study, and Ice-Recrystallization Inhibition Activity. *Biomacromolecules* **2017**, *18* (8), 2267–2276.

(6) Celik, Y.; Drori, R.; Pertaya-Braun, N.; Altan, A.; Barton, T.; Bar-Dolev, M.; Groisman, A.; Davies, P. L.; Braslavsky, I. Microfluidic Experiments Reveal That Antifreeze Proteins Bound to Ice Crystals Suffice to Prevent Their Growth. *Proc. Natl. Acad. Sci.* **2013**, *110* (4), 1309–1314.

(7) Biggs, C. I.; Bailey, T. L.; Graham, B.; Stubbs, C.; Fayter, A.; Gibson, M. I. Polymer Mimics of Biomacromolecular Antifreezes. *Nat. Commun.* **2017**, *8* (1), 1546.

(8) Gibson, M. I. Slowing the Growth of Ice with Synthetic Macromolecules: Beyond Antifreeze(Glyco) Proteins. *Polym. Chem.* **2010**, *1* (8), 1141.

(9) Voets, I. K. From Ice-Binding Proteins to Bio-Inspired Antifreeze Materials. *Soft Matter* **2017**, *13* (28), 4808–4823.

(10) Eniade, A.; Purushotham, M.; Ben, R. N.; Wang, J. B.; Horwath, K. A Serendipitous Discovery of Antifreeze Protein-Specific Activity in C-Linked Antifreeze Glycoprotein Analogs. *Cell Biochem. Biophys.* **2003**, *38* (2), 115–124.

(11) Carpenter, J. F.; Hansen, T. N. Antifreeze Protein Modulates Cell Survival during Cryopreservation: Mediation through Influence on Ice Crystal Growth. *Proc. Natl. Acad. Sci.* **2000**, *89* (19), 8953–8957.

(12) Matsumoto, S.; Matsusita, M.; Morita, T.; Kamachi, H.; Tsukiyama, S.; Furukawa, Y.; Koshida, S.; Tachibana, Y.; Nishimura, S.-I.; Todo, S. Effects of Synthetic Antifreeze Glycoprotein Analogue on Islet Cell Survival and Function during Cryopreservation. *Cryobiology* **2006**, *52* (1), 90–98.

(13) Chao, H.; Davies, P. L.; Carpenter, J. F. Effects of Antifreeze Proteins on Red Blood Cell Survival during Cryopreservation. *J. Exp. Biol.* **1996**, *199* (Pt 9), 2071–2076.

(14) Mitchell, D. E.; Lovett, J. R.; Armes, S. P.; Gibson, M. I. Combining Biomimetic Block Copolymer Worms with an Ice-Inhibiting Polymer for the Solvent-Free Cryopreservation of Red Blood Cells. *Angew. Chemie Int. Ed.* **2016**, *55* (8), 2801–2804.

(15) Deller, R. C.; Vatish, M.; Mitchell, D. A.; Gibson, M. I. Synthetic Polymers Enable Non-Vitreous Cellular Cryopreservation by Reducing Ice Crystal

Growth during Thawing. *Nat. Commun.* **2014**, *5*, 3244.

(16) Deller, R. C.; Pessin, J. E.; Vatish, M.; Mitchell, D. A.; Gibson, M. I. Enhanced Non-Vitreous Cryopreservation of Immortalized and Primary Cells by Ice-Growth Inhibiting Polymers. *Biomater. Sci.* **2016**, *47* (7), 935–945.

(17) Graham, B.; Bailey, T. L.; Healey, J. R. J.; Marcellini, M.; Deville, S.; Gibson, M. I. Polyproline as a Minimal Antifreeze Protein Mimic That Enhances the Cryopreservation of Cell Monolayers. *Angew. Chemie Int. Ed.* **2017**, *56* (50), 15941–15944.

(18) Tachibana, Y.; Fletcher, G. L.; Fujitani, N.; Tsuda, S.; Monde, K.; Nishimura, S.-I. Antifreeze Glycoproteins: Elucidation of the Structural Motifs That Are Essential for Antifreeze Activity. *Angew. Chemie Int. Ed.* **2004**, *43* (7), 856–862.

(19) Mochizuki, K.; Molinero, V. Antifreeze Glycoproteins Bind Reversibly to Ice via Hydrophobic Groups. *J. Am. Chem. Soc.* **2018**, *140* (14), 4803–4811.

(20) Budke, C.; Koop, T. Ice Recrystallization Inhibition and Molecular Recognition of Ice Faces by Poly(Vinyl Alcohol). *ChemPhysChem* **2006**, *7* (12), 2601–2606.

(21) Naullage, P. M.; Lupi, L.; Molinero, V. Molecular Recognition of Ice by Fully Flexible Molecules. *J. Phys. Chem. C* **2017**, *121* (48), 26949–26957.

(22) Hakim, A.; Nguyen, J. B.; Basu, K.; Zhu, D. F.; Thakral, D.; Davies, P. L.; Isaacs, F. J.; Modis, Y.; Meng, W. Crystal Structure of an Insect Antifreeze Protein and Its Implications for Ice Binding. *J. Biol. Chem.* **2013**, *288* (17), 12295–12304.

(23) He, Z.; Liu, K.; Wang, J. Bioinspired Materials for Controlling Ice Nucleation,

Growth, and Recrystallization. *Acc. Chem. Res.* **2018**, *51* (5), 1082–1091.

(24) Geng, H.; Liu, X.; Shi, G.; Bai, G.; Ma, J.; Chen, J.; Wu, Z.; Song, Y.; Fang, H.; Wang, J. Graphene Oxide Restricts Growth and Recrystallization of Ice Crystals. *Angew. Chemie Int. Ed.* **2017**, *56* (4), 997–1001.

(25) Mitchell, D. E.; Clarkson, G.; Fox, D. J.; Vipond, R. A.; Scott, P.; Gibson, M. I. Antifreeze Protein Mimetic Metallohelices with Potent Ice Recrystallization Inhibition Activity. *J. Am. Chem. Soc.* **2017**, *139* (29), 9835–9838.

(26) Tam, R. Y.; Ferreira, S. S.; Czechura, P.; Ben, R. N.; Chaytor, J. L. Hydration Index-a Better Parameter for Explaining Small Molecule Hydration in Inhibition of Ice Recrystallization. *J. Am. Chem. Soc.* **2008**, *130* (51), 17494–17501.

(27) Matyjaszewski, K. Atom Transfer Radical Polymerization (ATRP): Current Status and Future Perspectives. *Macromolecules* **2012**, *45* (10), 4015–4039.

(28) Boyer, C.; Bulmus, V.; Davis, T. P.; Ladmiral, V.; Liu, J.; Perrier, S. Bioapplications of RAFT Polymerization. *Chem. Rev.* **2009**, *109* (11), 5402–5436.

(29) Vail, N. S.; Stubbs, C.; Biggs, C. I.; Gibson, M. I. Ultralow Dispersity Poly(Vinyl Alcohol) Reveals Significant Dispersity Effects on Ice Recrystallization Inhibition Activity. *ACS Macro Lett.* **2017**, *6* (9), 1001–1004.

(30) Congdon, T.; Notman, R.; Gibson, M. I. Antifreeze (Glyco)Protein Mimetic Behavior of Poly(Vinyl Alcohol): Detailed Structure Ice Recrystallization Inhibition Activity Study. *Biomacromolecules* **2013**, *14* (5), 1578–1586.

(31) Congdon, T. R.; Notman, R.; Gibson, M. I. Influence of Block Copolymerization on the Antifreeze Protein Mimetic Ice Recrystallization

Inhibition Activity of Poly(Vinyl Alcohol). *Biomacromolecules* **2016**, *17* (9), 3033–3039.

(32) Olijve, L. C.; Hendrix, M. R.; Voets, I. K. Influence of Polymer Chain Architecture of Poly(Vinyl Alcohol) on the Inhibition of Ice Recrystallization. *Macromol. Chem. Phys.* **2016**, *217* (8), 951–958.

(33) Congdon, T. R.; Notman, R.; Gibson, M. I. Synthesis of Star-Branched Poly(Vinyl Alcohol) and Ice Recrystallization Inhibition Activity. *Eur. Polym. J.* **2017**, *88*, 320–327.

(34) Mahatabuddin, S.; Hanada, Y.; Nishimiya, Y.; Miura, A.; Kondo, H.; Davies, P. L.; Tsuda, S. Concentration-Dependent Oligomerization of an Alpha-Helical Antifreeze Polypeptide Makes It Hyperactive. *Sci. Rep.* **2017**, *7* (1), 42501.

(35) Stenzel, M. H.; Cummins, L.; Roberts, G. E.; Davis, T. P.; Vana, P.; Barner-Kowollik, C. Xanthate Mediated Living Polymerization of Vinyl Acetate: A Systematic Variation in MADIX/RAFT Agent Structure. *Macromol. Chem. Phys.* **2003**, *204* (9), 1160–1168.

(36) Ieong, N. S.; Brebis, K.; Daniel, L. E.; O'Reilly, R. K.; Gibson, M. I. The Critical Importance of Size on Thermoresponsive Nanoparticle Transition Temperatures: Gold and Micelle-Based Polymer Nanoparticles. *Chem. Commun.* **2011**, *47* (42), 11627–11629.

(37) Richards, S.-J.; Gibson, M. I. Optimization of the Polymer Coating for Glycosylated Gold Nanoparticle Biosensors to Ensure Stability and Rapid Optical Readouts. *ACS Macro Lett.* **2014**, *3* (10), 1004–1008.

(38) Knight, C. A.; Wen, D.; Laursen, R. A. Nonequilibrium Antifreeze Peptides and the Recrystallization of Ice. *Cryobiology* **1995**, *32* (1), 23–34.

(39) Congdon, T.; Dean, B. T.; Kasperczak-Wright, J.; Biggs, C. I.; Notman, R.; Gibson, M. I. Probing the Biomimetic Ice Nucleation Inhibition Activity of Poly(Vinyl Alcohol) and Comparison to Synthetic and Biological Polymers. *Biomacromolecules* **2015**, *16* (9), 2820–2826.

(40) Graham, B.; Fayter, A. E. R.; Houston, J. E.; Evans, R. C.; Gibson, M. I. Facially Amphipathic Glycopolymers Inhibit Ice Recrystallization. *J. Am. Chem. Soc.* **2018**, *140* (17), 5682–5685.

(41) Inada, T.; Lu, S.-S. Inhibition of Recrystallization of Ice Grains by Adsorption of Poly(Vinyl Alcohol) onto Ice Surfaces. *Cryst. Growth Des.* **2003**, *3* (5), 747–752.

(42) Sze Ieong, N.; Biggs, C. I.; Walker, M.; Gibson, M. I. Comparison of RAFT-Derived Poly(Vinylpyrrolidone) Verses Poly(Oligoethyleneglycol Methacrylate) for the Stabilization of Glycosylated Gold Nanoparticles. *J. Polym. Sci. Part A Polym. Chem.* **2017**, *55* (7), 1200–1208.

(43) Shimmin, R. G.; Schoch, A. B.; Braun, P. V. Polymer Size and Concentration Effects on the Size of Gold Nanoparticles Capped by Polymeric Thiols. *Langmuir* **2004**, *20* (13), 5613–5620.

(44) Stevens, C. A.; Drori, R.; Zalis, S.; Braslavsky, I.; Davies, P. L. Dendrimer-Linked Antifreeze Proteins Have Superior Activity and Thermal Recovery. *Bioconjug. Chem.* **2015**, *26* (9), 1908–1915.

(45) Larsen, M. B.; Wang, S.-J.; Hillmyer, M. A. Poly(Allyl Alcohol) Homo- and Block Polymers by Postpolymerization Reduction of an Activated Polyacrylamide. *J. Am. Chem. Soc.* **2018**, *140* (38), 11911–11915.

(46) Kumru, B.; Bicak, N. Synthesis of Soluble Poly(Vinylene Carbonate) by

Redox-Initiated RAFT Process in Microemulsion and Its Aminolysis Yielding Snow-White Polymethylol. *RSC Adv.* **2015**, *5* (39), 30936–30942.

(47) Burkey, A. A.; Riley, C. L.; Wang, L. K.; Hatridge, T. A.; Lynd, N. A. Understanding Poly(Vinyl Alcohol)-Mediated Ice Recrystallization Inhibition through Ice Adsorption Measurement and PH Effects. *Biomacromolecules* **2018**, *19* (1), 248–255.

(48) Hassan, R. M.; Abd-Alla, M. A. New Coordination Polymers. Part 1. - Novel Synthesis of Poly(Vinyl Ketone) and Characterization as Chelating Agent. *J. Mater. Chem.* **1992**, *2* (6), 609–611.

(49) Williams, D. H.; Fleming, I. *Spectroscopic Methods in Organic Chemistry*, 5th ed.; McGraw-Hill: London, 1995.

2.8 Appendix

Table 2.03: Further characterisation for gold nanoparticles synthesised in this study by LEW.

Particle	ζ potential (mV)[(a)]	SPR_{max} (nm)[(b)]	$Diameter_{TEM}$ (nm)[(c)]	$Diameter_{DLS}$ (nm)[(d)]
$Citrate@Au_4$	-19.4 +/- 2.7 [(e)]	510	3.9 +/- 0.74	4.37
PVA_{98}-Au_4	-5.54 +/- 0.6 [(f)]	522	4.4 +/- 1.4	18.2
PVA_{140}-Au_4	-4.49 +/- 0.4 [(f)]	521	3.6 +/- 0.85	19.4

(a) Averaged over 3 measurements; **(b)** Maximum of SPR peak determined by UV-Vis spectroscopy; **(c)** Taken as the average of 100 particles by TEM; **(d)** Determined by dynamic light scattering, distribution of size by number of particles; **(e)** Solution pH measured as 8.9; **(f)** AuNPs suspended in PBS, pH 7.25.

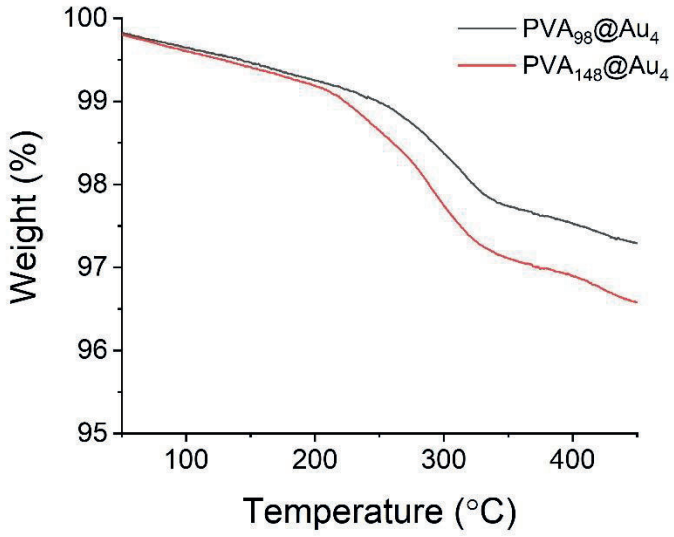

Figure 2.15: TGA analysis of polymer-coated gold nanoparticles. Analysis carried out by LEW and included for completeness.

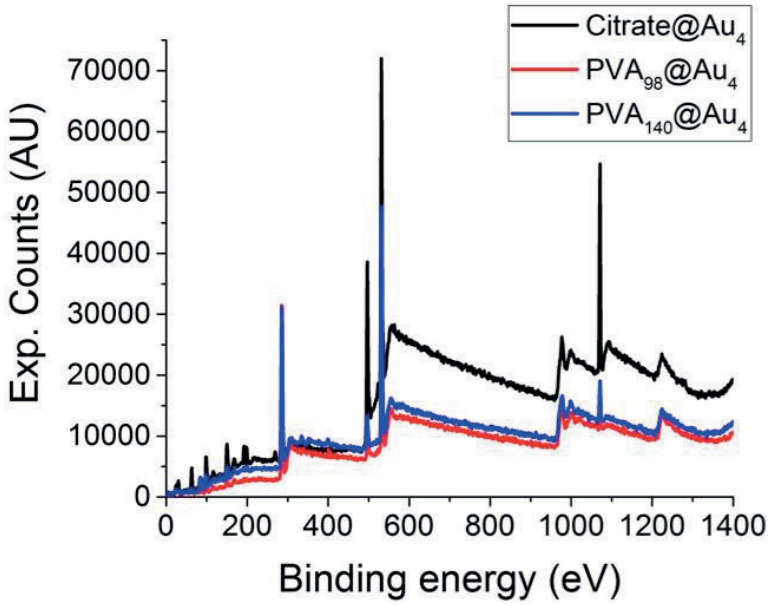

Figure 2.16: XPS survey scans of nanoparticles. Analysis carried out by LEW and included for completeness.

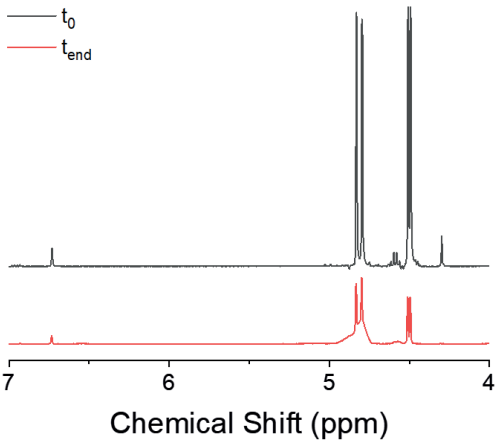

Sample	Mesitylene Integral (6.73ppm)	Vinyl Integral (4.50 ppm)
t_0	1.00	29.01
t_{end}	1.00	9.36
Conversion		67.7%

Figure 2.17: Example of how conversion is determined for the polymers synthesised. The integral of the peak at 4.50 corresponding to one of the vinyl hydrogens in the monomer is monitored relative to an internal standard.

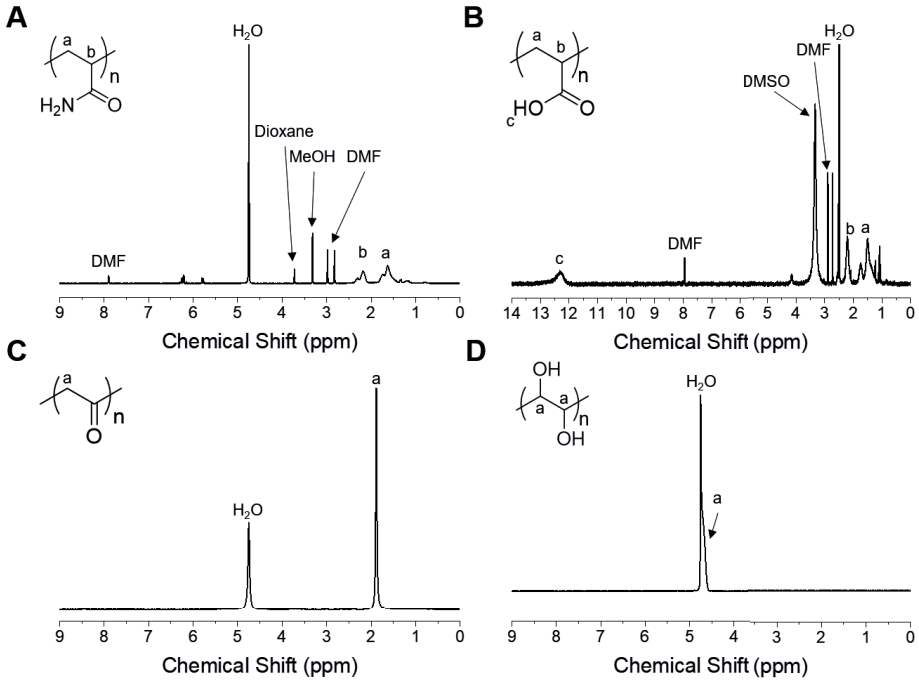

Figure 2.18: ^{1}H NMRs of the PVA-like structures tested. Peaks at 2.88 ppm, 2.96 ppm and 8.02 are DMF, peaks at 3.75 are 1,4-dioxane, peaks at 3.34 ppm are methanol. NMRs were recorded in **A** D_2O; **B** DMSO-d_6; **C** D_2O and **D** D_3PO_4.

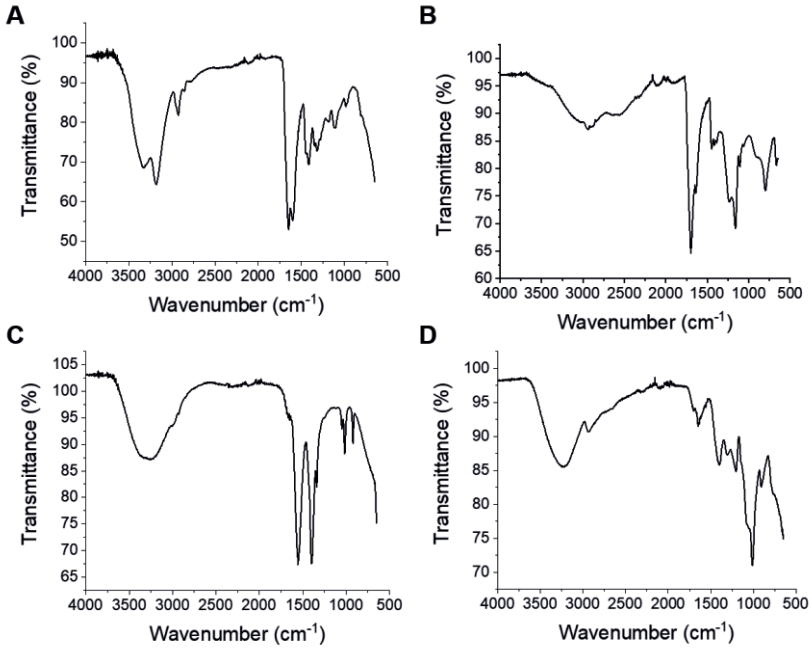

Figure 2.19: FTIR Spectra for the PVA alternatives synthesised. **A** Poly(acrylamide); **B** Poly(acrylic acid); **C** Poly(vinyl ketone); **D** Poly(methylol).

Chapter 3

Synthesis and IRI Activity of Regioregular Poly(ampholytes)

3.1 Abstract

Antifreeze proteins from polar fish species are potent ice recrystallisation inhibitors (IRIs) effectively stopping all ice growth at incredibly low concentrations (<0.1 $mg.mL^{-1}$). Additives which have IRI activity have been shown to enhance cellular cryopreservation with potential to improve the distribution of donor cells and tissue. Poly(ampholytes), polymers with both anionic and cationic side chains, are a rapidly emerging class of polymer cryoprotectants, but their mode of action and the structural features essential for activity are not clear. Here, regioregular poly(ampholytes) are synthesised from maleic anhydride co-polymers to enable stoichiometric installation of the charged groups, ensuring regioregularity which is not possible using conventional random copolymerisation. A modular synthetic strategy is employed to enable the backbone and side chain hydrophobicity to be varied, with side chain hydrophobicity found to have a profound effect on the IRI activity. The activity of the regioregular polymers was found to be superior to those derived from a standard random copolymerisation with statistical incorporation of monomers, demonstrating that sequence composition could modulate the activity of IRI active poly(ampholytes).

3.2 Introduction

Antifreeze (glyco) proteins (AF(G)Ps) have evolved in polar fish species to enable them to survive in sub-zero environments by specifically interacting with ice crystals.[1] AF(G)Ps have three main properties of thermal hysteresis (lowering freezing point but not melting point), dynamic ice shaping (changing morphology of ice crystals) and ice recrystallisation inhibition (IRI) – the inhibition of the growth of already formed ice crystals.[1,2,3] The property of IRI is of particular interest as the growth of ice crystals has been identified as a crucial mechanism of cell death during the thawing of cryopreserved cells and tissues.[4] The addition of AF(G)Ps to cryopreservation solutions was found to give some increase in cell recovery but the effect was limited by the onset of dynamic ice shaping, which leads to ice crystals piercing cell membranes.[5] Consequently, there has been much interest in developing synthetic mimics which have IRI activity to enable the cryostorage of donor tissues and cells.[6,2,7,8] There is an urgent need for new storage mechanisms, with a global shortage of cells such as blood,[9,10,11] which is exacerbated by cells' limited shelf life. Effective cryoprotectants are also important for applications in frozen food.[12,13,14] Current cryopreservation strategies often involve the addition of large quantities of dimethyl sulphoxide (DMSO) which can have negative (toxic) effects on both the cells and the recipient.[15,16]

The most potent polymer-IRI identified to date is poly(vinyl alcohol) (PVA), which can inhibit all ice growth at sub $mg.mL^{-1}$ concentrations, although its exact mechanism is unclear.[17,18] Many other poly-ols have been tested and few have any appreciable activity, suggesting the underlying mechanisms are complex and not just a property of regularly spaced hydroxyl groups.[19,20] Addition of PVA to non-vitrifying cryopreservative solutions has been found to enhance the storage of several cell types

by reducing thawing induced damage.[21,22,23] The role of architecture on PVA's activity has been studied by Gibson and co-workers with the IRI activity increasing with chain length, with a minimum of 10 – 20 units being essential.[24,25] Voets *et al*. found that comb-like PVA's had lower activity compared to linear.[26]

There is increasing evidence that non-hydroxylated polymers (or small molecules) can also display IRI activity, which may give rise to new cryoprotectants. Ben *et al.* have demonstrated that some surfactants are potent IRIs (but not all) and recently a supramolecular IRI was reported.[8] A common feature of these is that hydrophobic domains appear to be crucial to activity, but presented in a manner which does not lead to aggregation. The antimicrobial peptide Nisin A shows potent IRI but only at a pH where its histidine residues are protonated, leading to folding into an amphiphilic shape.[27] Matsumura *et al.* have developed the use of poly(ampholytes) (polymers with both cationic and anionic side chains) as new cryoprotectants enabling the DMSO-free storage of stem cells – a key challenge in regenerative medicine.[28] Gibson *et al.* studied a range of poly(ampholytes) and found that they also display some IRI activity, making them a unique class of polymeric AF(G)P mimics.[29,30] The rationale for poly(ampholyte) IRI activity is currently unclear as they have no obvious ice binding domains, although they do interact with cell membranes, which may enhance their cryoprotective effect.[31] Poly(ampholytes) are an appealing class of polymer to study though, due to their generic nature (e.g any polymer with mixed charges seems to have some activity) and easier synthesis compared to PVA.[32]

All currently described polyampholytes, however, are comprised of either polydisperse polymers (e.g. carboxylated poly(lysine)[28]) or random copolymers with non-stoichiometric ratios of the anionic and cationic groups.[30,31] We have previously shown that both the molecular weight and the ratio of the two charged components

(must be 1:1) are crucial for activity of this emerging class of biomaterials.[30] A further issue is that the sequence distribution of these essential units has not been thoroughly studied (other than both are required). Recent advances in controlled radical polymerisation by Lutz and others have enabled techniques for control over the site of installation of specific functionality into synthetic polymers by kinetic control[33,34] or the synthesis of multiblock copolymers,[35] with improved control over sequence. The most well-known sequence-defined polymers are those based upon maleic anhydride copolymers.[36] Due to maleic anhydride's low propensity to self-propagate, addition of a second monomer enables the formation of perfectly alternating polymers, giving regioregularity. Furthermore the anhydride ring is an ideal platform for post-polymerisation modification[37] to insert adjacent carboxy/amine functionalities to give ampholytes.[29]

Considering the above, the aim of this work was to undertake the first systematic investigation into the role of monomer sequence and location of hydrophobicity on the IRI activity of polyampholytes. Using RAFT polymerisation it was possible to obtain well-defined maleic anhydride containing precursors with a range of comonomers followed by ring-opening of the anhydride using substituted ethanolamines. This allowed us to vary the side chains, whilst ensuring a 1:1 balance of charged units. Quantitative analysis of their IRI activity reveals that side chain hydrophobicity is a powerful tool to enhance activity and comparisons with non-regioregular analogues demonstrates that sequence regulated polymers are more active than random copolymers derived from acrylates. However, their activity is still very weak compared to other synthetic materials e.g. PVA. These findings were then used to inform the development of a new cryoprotectant from a commercial precursor,

which displays excellent post thaw recovery when used for the cryopreservation of red blood cells.

3.3 Results and Discussion

3.3i Polymer Synthesis

To enable the first detailed study on structure-activity relationships in well defined, regioregular polyampholytes, copolymers based on maleic anhydride were designed to give a perfectly alternating structure.[36] A perfectly alternating structure ensures that the positive and negative charges are in an exact stoichiometric ratio (as previous results have shown this to be crucial)[30] as well as avoiding any composition drift or random placement of functionalities associated with post-polymerisation modification or statistical copolymerisation. By judicious choice of the comonomer polymerised with maleic anhydride, the backbone hydrophobicity, as well as side chain hydrophobicity can be sequentially modified. Styrene/MAH (**PS$_x$**) and isopropenyl acetate/MAH (**PIPAC$_x$**) were polymerised using a dithioester RAFT agent and the vinyl acetate/MAH (**VAc$_x$**) using a xanthate (Scheme 3.01). When the PIPAC copolymers were synthesised using the MADIX (Macromolecular Design via the Interchange of Xanthates) agent, larger dispersities were observed, however this was not investigated further. Following polymerisation all polymers were isolated by precipitation and characterised by size exclusion chromatography (SEC) (Table 3.01), ^{1}H NMR and FTIR.

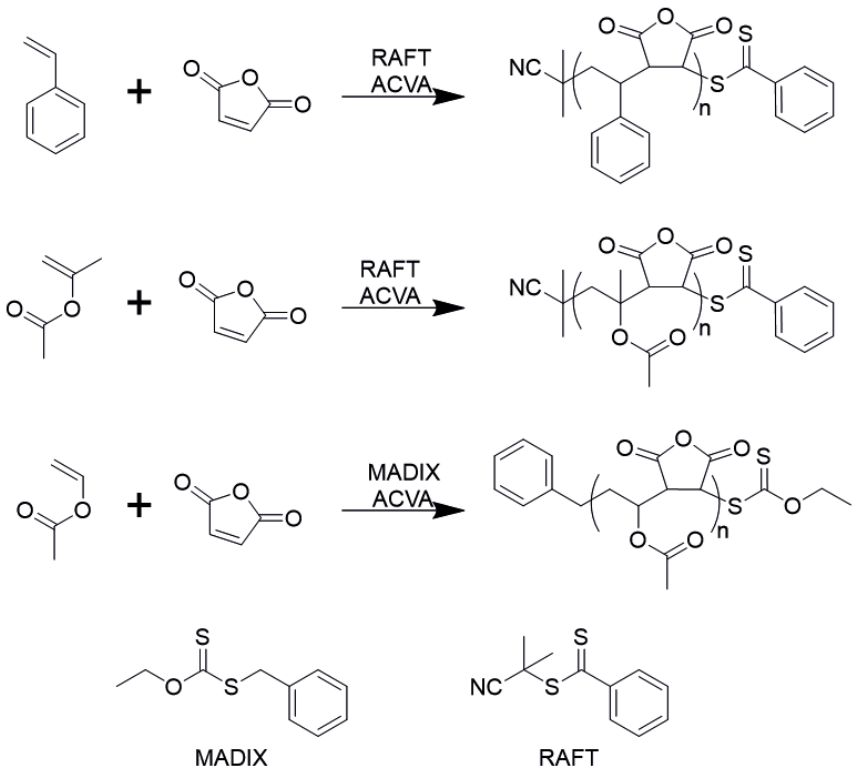

Scheme 3.01: Synthetic route followed for the synthesis of the maleic anhydride polymers in this work. ACVA is 4,4'-Azobis(4-cyanovaleric acid).

To ensure an alternating polymer was formed, a 4-fold excess of the maleic anhydride to comonomer was used (reducing homo-polymer blocks). Vinyl acetate is a deactivated monomer, so is more challenging to polymerise than other common monomers[32] such as acrylates. This, paired with the the non-ideal SEC solvents for these polymers,[32,38] led to observed dispersities being larger than expected for a controlled radical polymerisation. $PVAc_{57}$ demonstrated a bimodal peak in the SEC, possibly due to initiator derived poly(vinyl acetate) homopolymer (Figure 3.01). Attempts to repeat this synthesis afforded polymers with wide dispersities and significant low molecular weight shoulders. Controlled polymerisation of these monomers can also result in deviation from the reported previously reported reactivity ratios,[39] as a result of this, the alternating nature of the polymerisations was investigated.

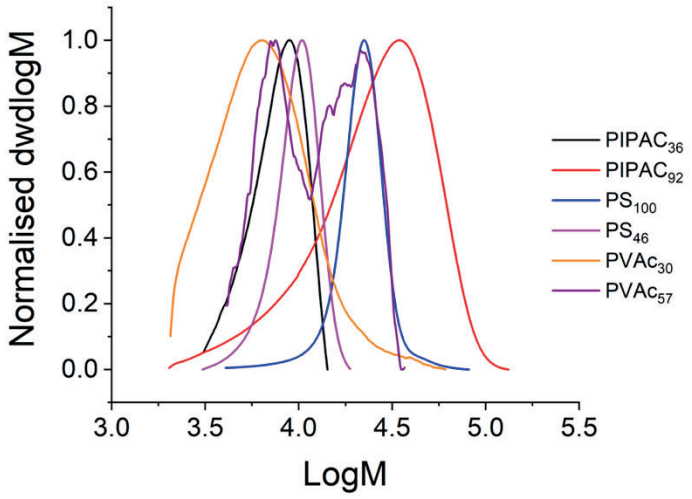

Figure 3.01: Molecular weight distribution from SEC for the copolymers synthesised. SEC was performed in DMF.

Table 3.01: Alternating polymers synthesised.

MA Copolymer[(a)]	[M]: [CTA] (-)[(b)]	M_n (g.mol^{-1}) [(c)]	Đ (-)[(d)]	DP (-)[(e)]
PS_{100}	310	20,300	1.11	100
PS_{46}	150	9,200	1.08	46
$PIPAC_{36}$	100	7,200	1.11	36
$PIPAC_{92}$	420	18,200	1.70	92
$PVAc_{30}$	140	5,600	1.46	30
$PVAc_{57}$	280	10,500	1.34	57

(a) PS100 indicates a poly(styrene-*alt*-maleic anhydride) copolymer with 100 of the alternating repeat units, see Fig 3.1; **(b)** Polymerisable monomer to RAFT agent ratio. 4 equivalents of maleic anhydride were used for every 1 of comonomer to ensure alternating polymerisation; **(c)** Determined by SEC; **(d)** Đ is M_w/M_n from SEC; (**e)** Number average degree of polymerisation from SEC.

In order to determine that the synthesised polymers consisted of a 1:1 ratio of each monomer component, and consequently a perfectly alternating structure as would be predicted by their reactivity ratios, quantitative ^{13}C NMR was employed.

Homopolymers of the non-MAH component should show distinct cross peaks associated with adjacent homopolymer units, e.g. styrene-styrene, due to the influence of the backbone tacticity on this carbon environment, whereas an alternating copolymer should not show any of these. Figure 3.02 A shows styrene homopolymer compared to copolymer with the cross peak clearly not being present in the copolymers. In the case of the shorter VAc copolymer, VAc_{30}, no homopolymer units are present, however in the longer VAc copolymer, VAc_{57}, the presence of a peak at 67.5 ppm suggests a small amount (~6 %) of VAc-VAc adjacent units are present (asterisk, Figure 3.02 B). For PIPAC it was not possible to obtain a homopolymer control (as this monomer does not self-polymerise readily)[32], but the ^{13}C NMR still showed only a single multiplet peak in the region of the PIPAC backbone confirming the alternating structure. Integration of the carbonyl peaks also suggested a 2:1 ratio of anhydride to carbonyl carbons.

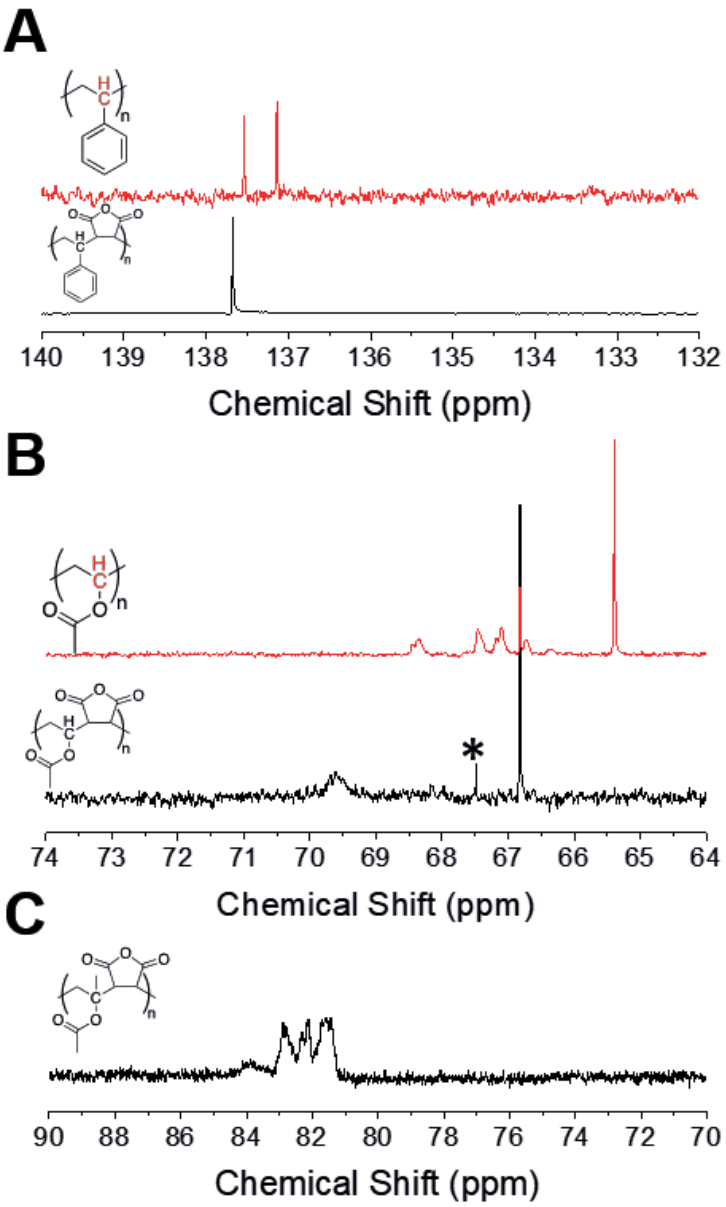

Figure 3.02: ^{13}C NMR sequence analysis of alternating copolymers. * Indicates peak associated with homopolymer. NMRs were run in DMSO-d_6.

3.3ii Polymer Functionalisation and IRI Activity

With these alternating polymers to hand it was necessary to introduce the desired amine functionality, post-polymerisation. *N*-Boc ethanolamine was used as a nucleophile to ring-open the anhydride, which following deprotection with trifluoroacetic acid (TFA), generates the ampholyte structure, Scheme 3.02. An alcohol nucleophile was chosen to prevent the undesired ring-closing reaction

associated with amines (to give a maleimide) which would stop the formation of the carboxylic acid group, essential for IRI activity. To indicate installation of the amine (and for convenience when other side chains are used later) the polymers have been appended with *–NH₂* in our naming convention. (e.g. PS-NH_2 is PS/MA copolymer with primary amine installed side chain).

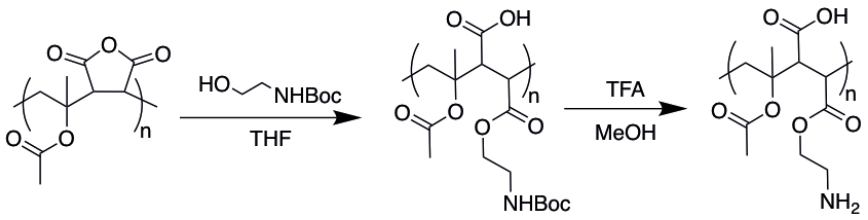

Scheme 3.02: Ring-opening of anhydride and subsequent deprotection.

Successful ring-opening was confirmed by FTIR spectroscopy. The two peaks associated with the anhydride carbonyls (1850 and 1790 cm^{-1}) were quantitatively removed and the installation of an ester and carboxylic acid at lower wavenumber could be seen (Figure 3.03).

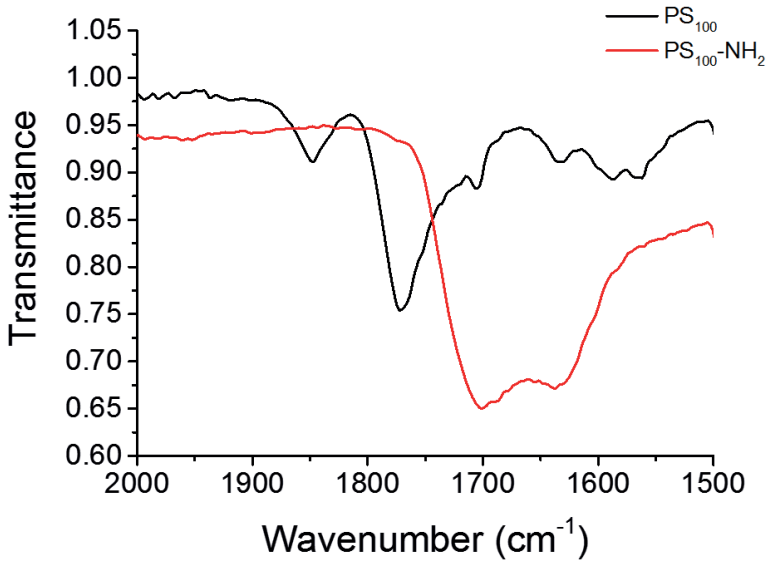

Figure 3.03: Infrared analysis of PS_{100} showing removal of anhydride peaks following ring opening and deprotection. Full spectra are shown in the appendix.

With this library of polyampholytes containing variable chain lengths and backbone hydrophobicities, the ice recrystallisation inhibition (IRI) activity could be evaluated. IRI was measured using the 'splat' assay.[24] Briefly, 10 μL droplets of the polymers in PBS were dropped onto a glass coverslip sat on a chilled (-80 °C) aluminium plate. This generates a large number of <10 micron ice crystals by rapid nucleation, which were then incubated on a cold stage for 30 minutes at -8 °C. The average area of the ice crystals relative to a PBS control can then be determined. Smaller numbers indicate more activity. Polymers were tested at 5, 10 and 20 mg.mL^{-1} and the results of this are shown in Figure 3.04 as a function of concentration. PS_{46}-NH_2 was not water soluble at the concentrations tested, and therefore its IRI activity could not be determined.

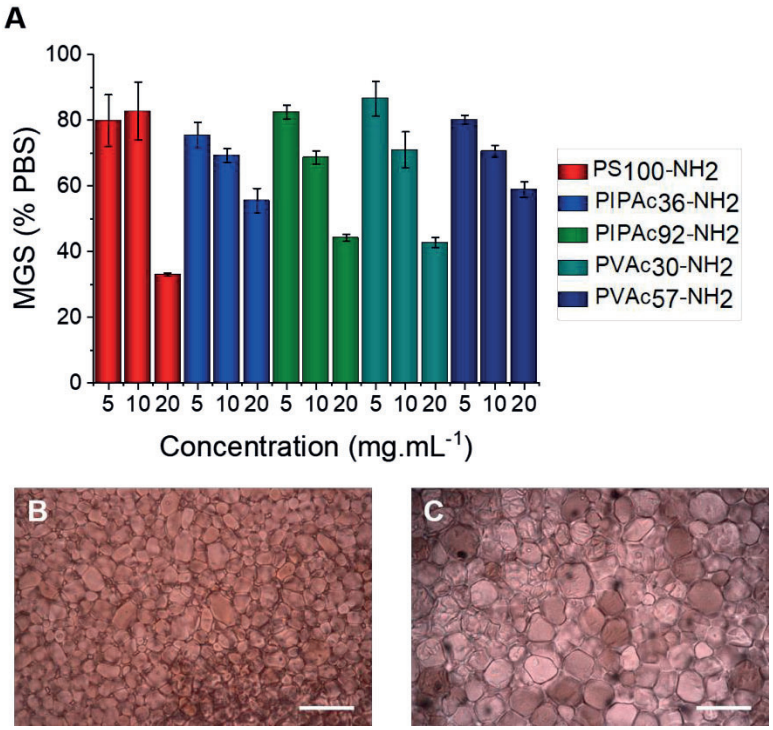

Figure 3.04: IRI activity of amino-side chain poly(ampholytes) with various backbones. **A** IRI activity; **B** Cryo-micrograph of PS_{100}-NH_2 at 20 mg.mL^{-1}; **C** Cryo-micrograph of PEG 20mg.mL^{-1} as a negative control. MGS = mean grain size reported as an area. Error bars represent ± standard deviation from a minimum of 3 repeats. Scale bars are 100 μm.

In line with previous studies on poly(ampholytes) these polymers were weakly active, but as very few synthetic materials have this property, it is still a remarkable observation.[2,6] All the polymers appeared to have similar activity without any strong molecular weight trends observed, with all of them leading to 35 – 50 % crystal areas at the highest concentration (20 mg.mL^{-1}) which is more potent than poly(ampholytes) reported by Matsumura and coworkers.[31] This does not necessarily rule out molecular weight dependence, just in the range tested. Interestingly, the PS-NH_2 copolymers appeared to have higher activity at 20 mg.mL^{-1} compared to the other polymers, but less at lower concentration. Careful analysis of the solutions revealed that the PS-NH_2 were slightly turbid due to some aggregation. This means that the actual concentration of dissolved chains is lower, making a critical comparison challenging. The styrene units, when compared to the other comonomers used in this study, are significantly more hydrophobic and these copolymers are consequently less soluble, demonstrating the delicate balance between hydrophobicity (expected to increase activity) and hydrophilicity (needed to ensure solubility in biological buffers).

The above results showed that modulation of the backbone of the polyampholytes, for the range of materials tested, did not have a large impact on their overall activity. However, the modular synthetic strategy employed here also enables the side chain to be varied. Four amines of varying hydrophobicities were tested, as there is literature evidence suggesting that increasing hydrophobicity will enhance IRI activity in randomly sequenced poly(ampholytes).[31] It was decided that the $IPAc_{92}$ based polymers were to be studied further, as these were more soluble than the PS_{100} samples, as well as ensuring that the polymers tested had a definite alternating structure. Four different amino-alcohols with different hydrophobic chains on the amine were chosen and used to ring open the anhydride unit (Scheme 3.03). Again, FTIR spectroscopy

was used to confirm successful ring-opening and installation of the desired functional groups (Figure 3.05).

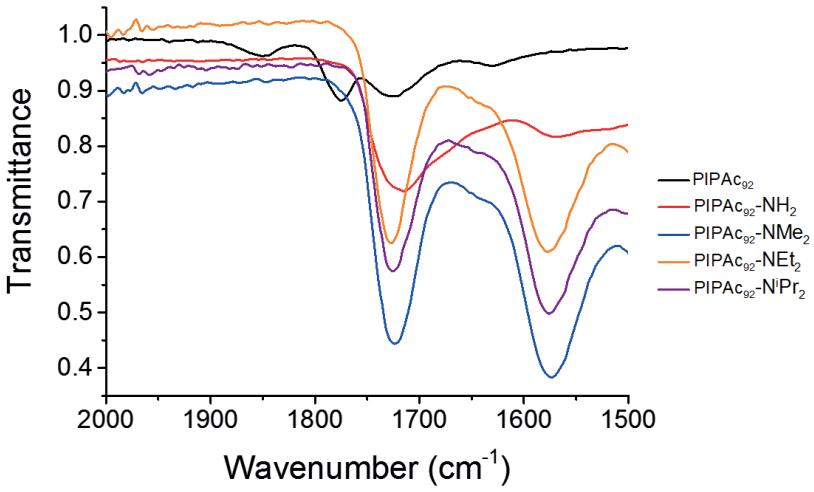

Figure 3.05: FTIR spectra of the functionalised IPAC copolymers.

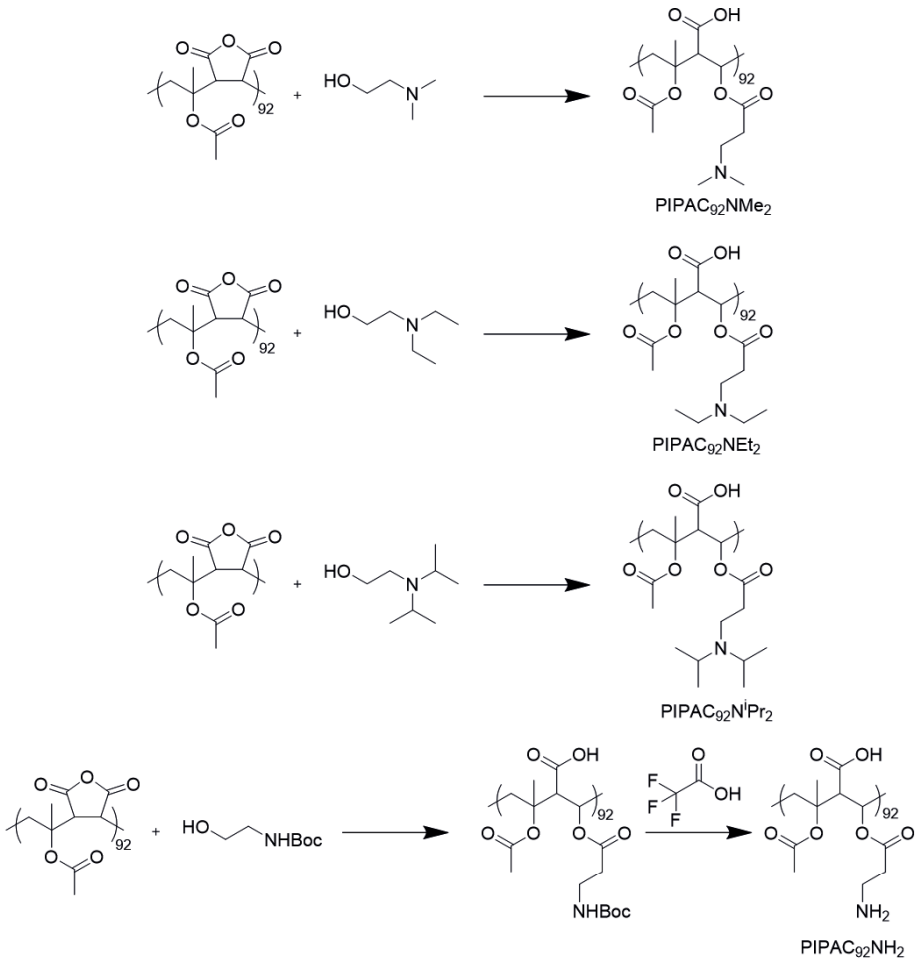

Scheme 3.03: Installation of a range of different amine side chains into alternating copolymers by ring opening of the maleic anhydride unit.

This second set of polymers were tested for IRI activity, as a function of concentration using the same methodology as the first set of polymers (Figure 3.06). For the diethyl, diisopropyl and primary amine, the activity observed was largely identical across concentrations. However, whilst activity was similar at low concentrations, polymers functionalised with the dimethylamino ethanol were dramatically more active at high concentrations, inhibiting nearly all ice growth. This was a remarkable level of activity, and was achieved by accessing a fine balance between backbone hydrophobicity, side chain hydrophobicity and solubility.

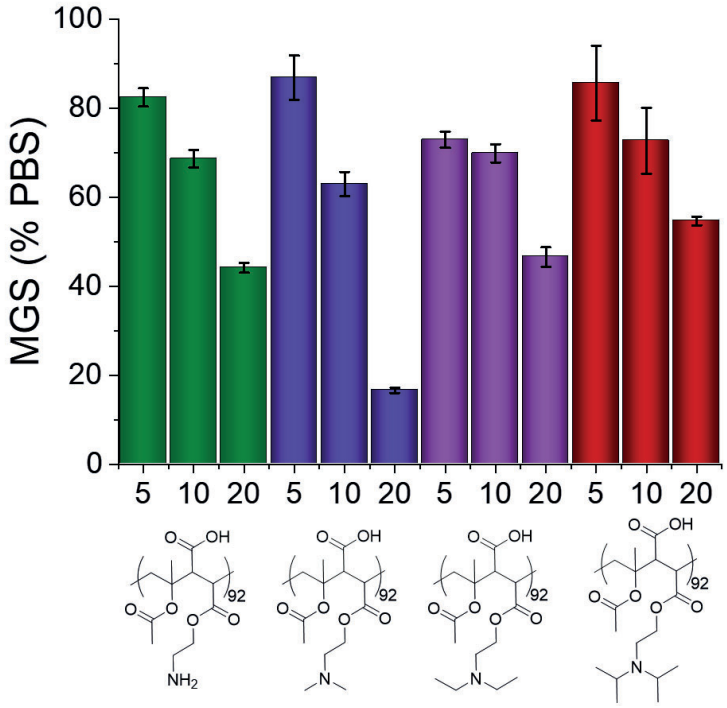

Figure 3.06: IRI activity of side chain modified poly(ampholytes). MGS = mean grain size reported as an area. Error bars represent ± standard deviation from a minimum of 3 repeats.

The data in Figure 3.06 suggests that hydrophobicity plays a role in activity, but the trends are not clear. To obtain a measure of hydrophobicity, the LogP (partition coefficient) for each repeat unit used was calculated and compared to IRI activity

(Figure 3.07). This did not reveal any correlation. IRI activity has been linked to localisation of hydrophobic/hydrophilic domains in native AFPs, small molecules,[40] supramolecular mimics,[8] and in other macromolecules[27] and the LogP does not capture this level of detail but rather just the overall lipophilicity. This observation supports the idea that hydrophobic domains are essential for IRI activity, but that the exact 3-D position of these is crucial and that simply adding 'more hydrophobicity' will not lead to an increase in activity. These results also challenge the assumption that to have potent IRI activity, you must have a good 'match' for a specific face of an ice crystal to enable binding (which is essential for AFP function), this suggests that multiple potential mechanisms can lead to the macroscopic effect of IRI. The poly(ampholytes) used have no obvious binding units for ice, such as hydroxyls, and the individual homopolymers (e.g. poly(amine)) have no activity.[30]

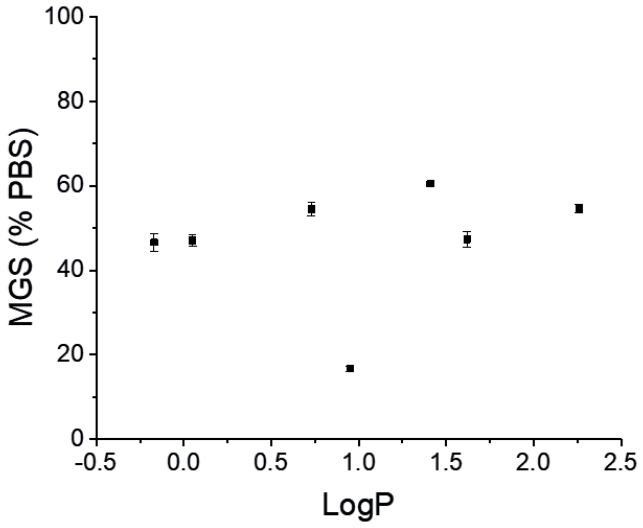

Figure 3.07: Plot of IRI activity vs LogP for the polymers synthesised here at 20 mg.mL^{-1}. LogP was calculated using ChemDraw based on the structure of the repeat unit. MGS = mean grain size reported as an area. Error bars represent ± standard deviation from a minimum of 3 repeats.

To determine if the sequence and placement of the carboxyl/amine groups promoted IRI activity, random sequenced analogues were designed based upon poly(acrylates). The IRI activity of these species was determined and the polymers were compared. These random polymers were less active than their sequence-controlled analogues, which suggested that this precise placement of positive and negatively charged groups is important for IRI activity.

Once the most IRI active species had been identified, $PIPAc_{92}NMe_2$, its ability to act as a cryoprotectant was investigated. Samples were tested using a standard blood cryopreservation assay. Briefly, a polymer solution prepared at double the required concentration was added to an equal volume of red blood cells (RBCs) suspended in phosphate buffered saline at a haematocrit of 30 % (the packed cell volume of red blood cells in a solution). The samples were incubated for 30 minutes in a refrigerator, followed by storage in liquid nitrogen vapour for a further 60 minutes to ensure they were frozen. After this time, the samples were removed and thawed in a water bath at 45 °C for 10 minutes. The thawed samples were then centrifuged for 5 minutes, and the supernatant was added to a solution of NaOH and Triton X-100 in water (AHD solution).[41] This was then pipetted into a flat bottom 96 well plate, and the absorbance recorded at 580 nm. This was then compared to RBCs stored in an unfrozen PBS control and lysis buffer as 0 and 100 % haemolysis values, respectively. The results for $PIPAC_{92}NMe_2$ are shown in figure 3.08. When compared to the current best practice, the observed recoveries are slightly lower than those obtained using glycerol,[42] however the concentrations of polymer used are also much lower (75% recovery is observed in 40% glycerol).

It must be noted, however, that this assay relies on the release of haemoglobin into the supernatant, as a result of damage to the membrane of the cell. During the freezing

and thawing process, cells may be damaged in such a way that no haemoglobin is released, and this will not be reflected by the results of the assay. The assay also does not give any indication of the viability of the cell, i.e. the ability of the red blood cells to successfully carry oxygen is not tested. Despite these limitations, however, this assay is a simple method by which initial cryoprotectant ability can be determined.

The results presented suggests that ampholytes could possibly offer an attractive alternative to glycerol as an effective blood cryoprotectant. These materials were investigated further.

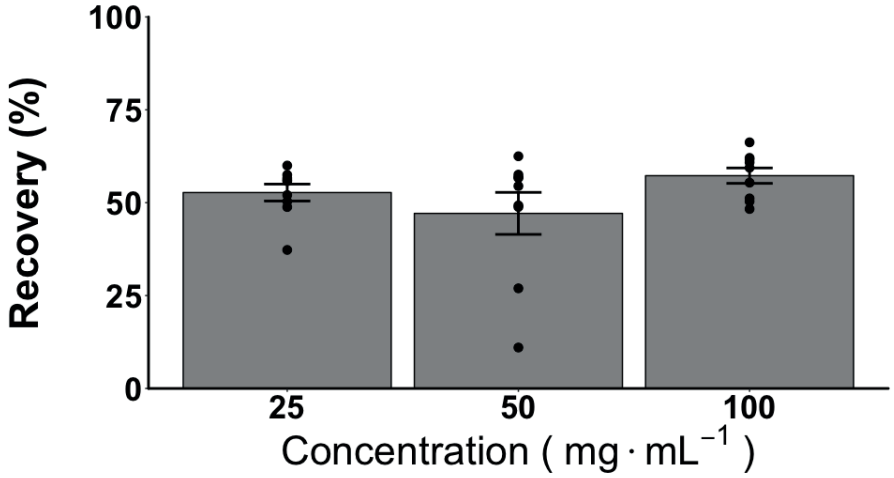

Figure 3.08: Cryoprotectant activity of $PIPAC_{92}NMe_2$ using a fast freezing, fast thawing cryopreservation protocol. Error bars represent ± standard error from a minimum of 3 repeats.

3.3iii Synthesis and Activity of a Scalable Poly(ampholyte) Cryoprotectant

One downside to these synthesised materials, however, is that the initial copolymer is not commercially available, and therefore large-scale synthesis would be relatively expensive, at least initially. Given the observed importance of alternating structure on IRI activity, commercially available alternating copolymers of maleic anhydride were

investigated. Whilst styrene-maleic anhydride is readily available, this material had already been tested and it was determined that it is unlikely to be soluble at the required concentrations for blood cryopreservation (up to 100 $mg.mL^{-1}$). Poly(methyl vinyl ether-*alt*-maleic anhydride) is readily available from Ashland Inc. under the trade name Gantrez and can be purchased for as little as £46 per kilo, and is currently used as a biocompatible adhesive and an ingredient in chewing gum.[43] This copolymer was reacted with the dimethylamino ethanol found previously to generate the most IRI active structure (Scheme 3.04), and the resulting ampholyte tested for hemocompatibility over a 2 hour incubation, during which time little loss in recovery was observed (<10 % lysis at 100 $mg.mL^{-1}$). The samples were then remade, and the blood cryopreservation assay performed using three different molecular weights of the initial copolymer (Figure 3.09).

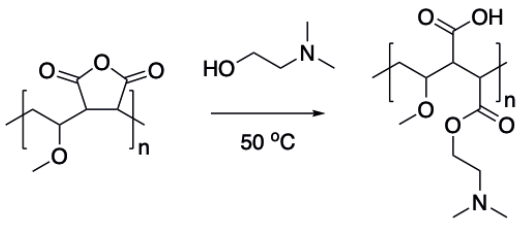

P1 = 20 kDa **P2** = 80 kDa **P3** = 311 kDa

Scheme 3.04: Synthesis of a poly(ampholyte) cryoprotectant from a commercially available precursor.

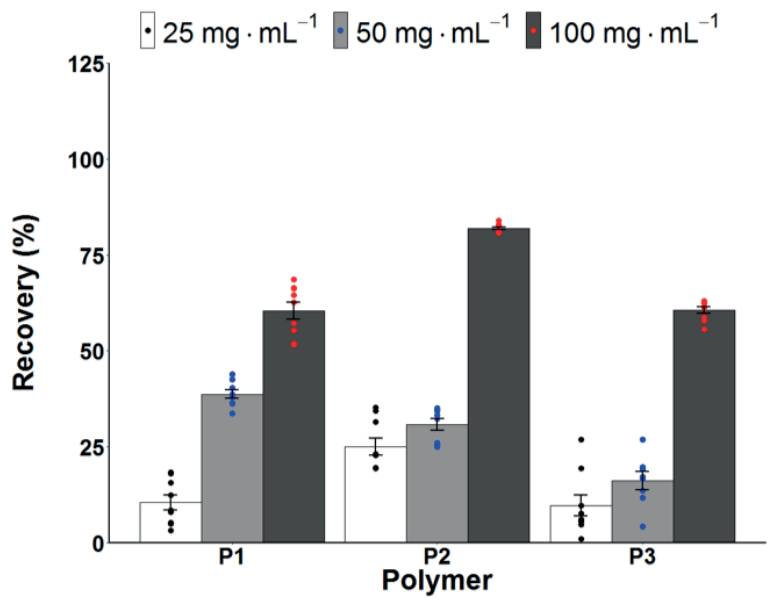

Figure 3.09: Red blood cell post-thaw recovery [defined as ((1-haemolysis)*100)] with cryoprotective polymers. **P1** = 20 kDa, **P2** = 80 kDa, **P3** = 311 kDa. Error bars represent ± standard error from a minimum of 3 repeats.

These materials demonstrated excellent post thaw recovery, greater even than the $PIPAC_{92}NMe_2$ samples tested previously, with the best material (**P2**) achieving around 80 % recovery. In order to investigate the correlation between cryoprotectant effectiveness and IRI activity, the splat assay was again performed with these materials. No significant IRI activity was observed (Figure 3.10), with the best performing polymer (**P3**) being only slightly more active than a negative control (PEG) at 20 $mg.mL^{-1}$.

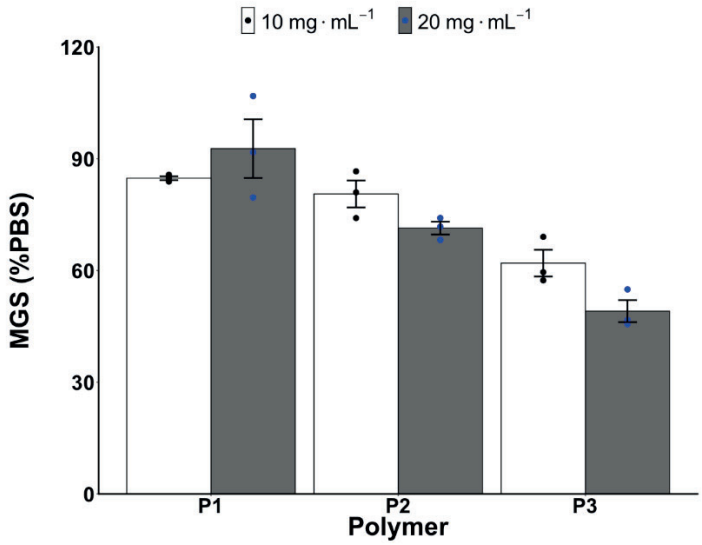

Figure 3.10: IRI activity of poly(ampholytes) synthesised. **P1** = 20 kDa, **P2** = 80 kDa, **P3** = 311 kDa. Error bars represent ± standard deviation from a minimum of 3 repeats.

This agrees with previous reports suggesting that ampholytes do not rely on ice recrystallisation inhibition to enhance cryoprotectant outcomes, they are instead thought to interact with cell membranes, however their exact mechanism of action is not yet understood.[31] The polymers used here are most effective at high concentrations, at which the polymer solutions are highly viscous. An increase in viscosity has been correlated with ice recrystallisation inhibition activity, however very little IRI activity was observed with these materials. The high viscosity of these materials could instead be providing additional structural protection, reducing the mechanical forces experienced by the cells in solution. The viscosities of these materials were not measured, however there was a clear increase in viscosity as the molecular weight of the polymers increased (observed during pipetting samples). The 80 kDa polymer was more active than both the less vicous 20 kDa material, and the significantly more viscous 311 kDa polymer crudely suggesting that if viscosity is

important, for these materials at least a balance is again required. This hypothesis however was not investigated any further.

In an attempt to optimise the freezing recoveries obtained using red blood cells, a number of conditions were investigated. Initial assays were performed using RBC solutions with a 30 % haematocrit, as this is the normal level for the sheep blood tested here. Human blood however has a slightly higher haematocrit level, closer to 50 %, and therefore the effect of a slightly greater haemocrit level on recovery was investigated. Increased haematocrit resulted in a small reduction in RBC recovery (from 78 % to 68 %) and therefore the lower 30 % level was used for all future assays.

Another factor which has a significant influence on the observed recovery are the conditions under which freezing and thawing take place. All previous assays were carried out using a fast freezing and fast thawing process, however for membrane active species, slowing the freezing and thawing process may enable more time for the osmotic pressures inside and outside the cell to equilibrate, potentially increasing cell recovery. All combinations of fast and slow, freezing and thawing were tested, and the results plotted in Figure 3.11. Exact protocols for each freezing condition tested are listed in the experimental section.

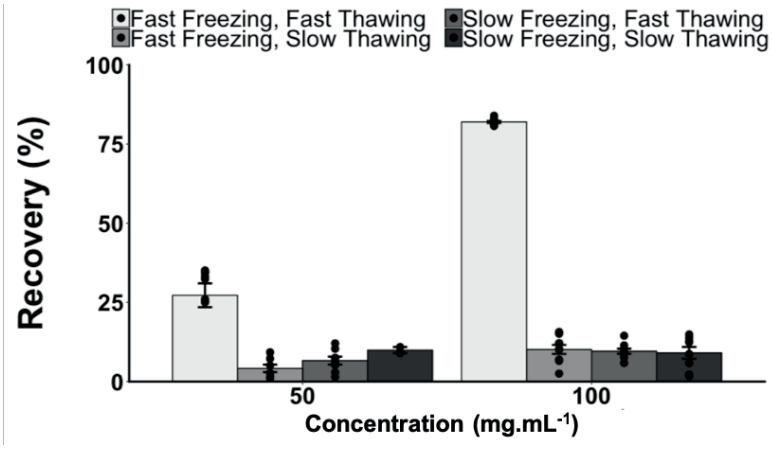

Figure 3.11: Effect of freezing and thawing conditions on recovery using polymer **P2** at two different concentrations. Error bars represent ± standard error from a minimum of 3 repeats.

All freezing and thawing conditions other than the standard fast freezing, fast thawing, showed greatly reduced recovery. This is likely due to the increased time which ice crystals spend at temperatures just below zero, and therefore ice crystals have more time to grow and cause damage to the sample. In an attempt to reduce the concentration of poly(ampholyte), the addition of a co-cryoprotectant was investigated. Varying concentrations of PVA, which is a highly IRI active material, were added to a 50 $mg.mL^{-1}$ ampholyte solution to give a range of cryoprotectant solutions. These solutions were then tested for their cryoprotectant ability. The results are shown in Figure 3.12.

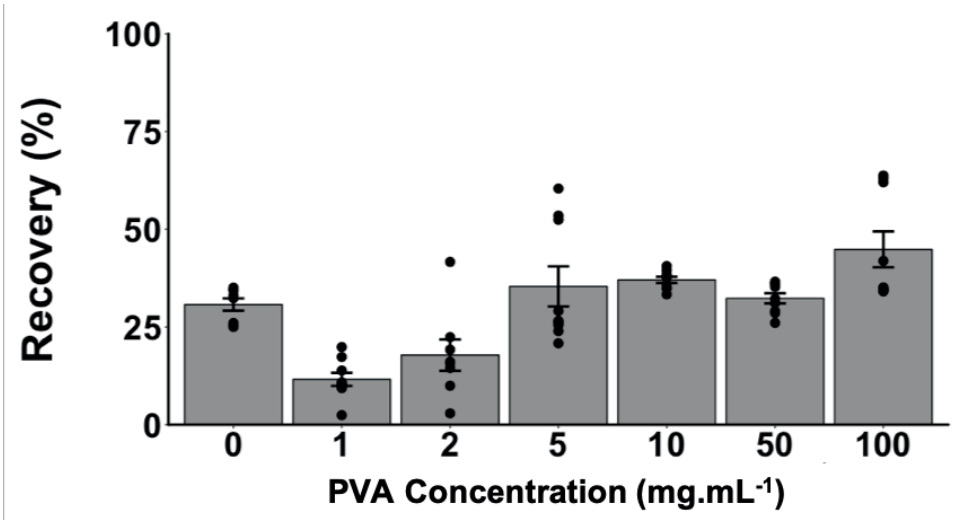

Figure 3.12: Effect of PVA concentration of recovery using ampholyte **P2** at 50 mg.mL^{-1}. Error bars represent ± standard error from a minimum of 3 repeats.

These results suggest that while a marginal improvement can be made by addition of 100 mg.mL^{-1} of PVA, this is not worth the added complexity of using two different cryoprotectants with a greater final cryoprotectant content. These results suggest that the ideal conditions for optimal recovery are 100 mg.mL^{-1} of poly(ampholyte) **P2**, using a fast freezing and fast thawing process, and blood cells at an initial haemocrit of 30 %. Once these conditions had been identified, the reproducibility of the system was investigated. Samples of the polymer and blood were combined and incubated in the fridge or at room temperature for 0 minutes, 15 minutes, 30 minutes or 24 hours, followed by freezing either in liquid nitrogen vapor or submerged in liquid nitrogen. No marked differences were observed between the samples once thawed, suggesting that the processing conditions do not have a significant effect on the recovery observed (Figure 3.13).

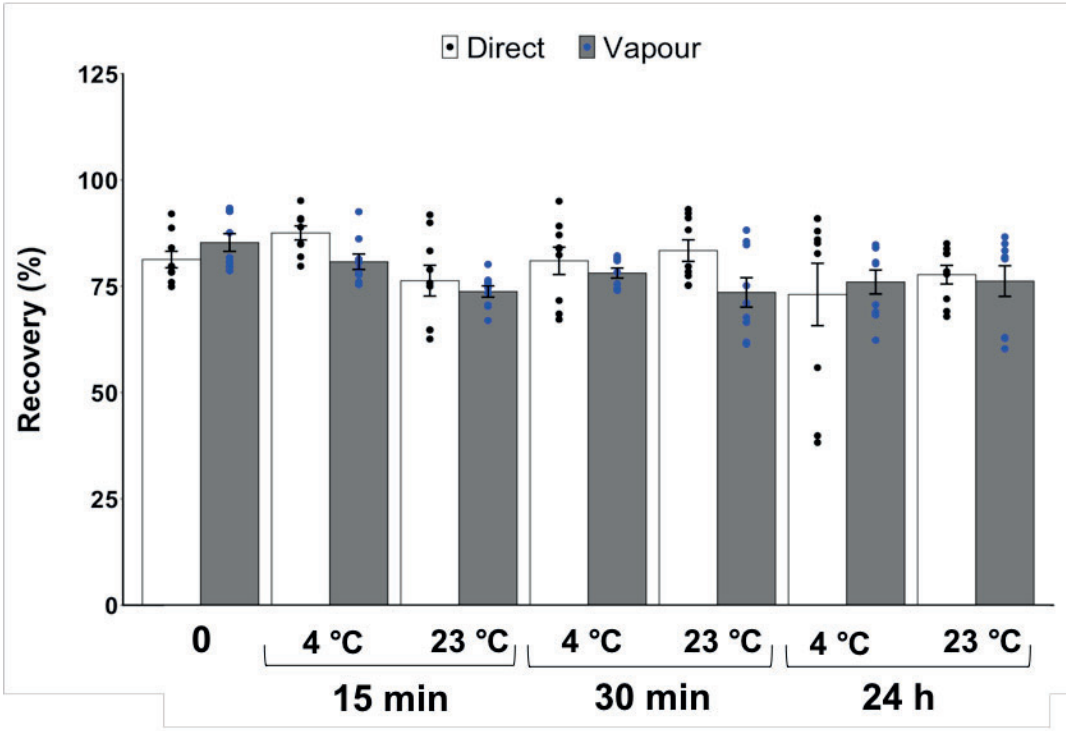

Figure 3.13: Effect of pre-freezing incubation time and temperature on post-thaw recovery with 100 mg.mL^{-1} **P2**. Incubation time (0, 15 min, 30 min, 24 h (24 hours)), incubation temperature (4 ºC or 23 ºC), freezing conditions (directly submerged (direct) or in vapour (vapour) of liq. N_2). Error bars represent ± standard error from a minimum of 3 repeats.

To ensure that the blood cells could be resuspended after freezing, the osmotic fragility of the samples was tested post thaw. Blood was frozen in a 100 mg.mL^{-1} ampholyte solution for two hours, followed by thawing as normal. These samples were then pelleted in a centrifuge and resuspended in PBS solution. Both frozen and unfrozen blood were each added to a serial dilution of salt solutions, and the lysis determined after 30 minutes (Figure 3.14).

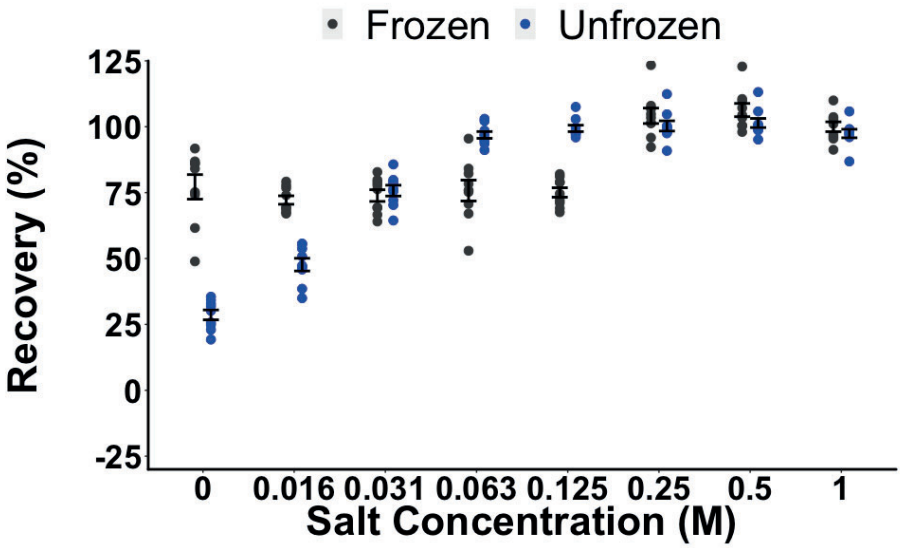

Figure 3.14: Osmotic fragility for blood cells frozen in the presence of 100 mg.mL^{-1} P2 compared to unfrozen cells. Error bars represent ± standard error from a minimum of 3 repeats.

Both frozen and unfrozen cells appeared to be stable at high salt concentrations, at which significant lysis would be expected. In previous studies of haemolysis of red blood cells at high salt concentrations significant dehydration and crenation is observed.[44] Whilst these cells are no longer healthy, if the membrane has not burst, little haemoglobin will be able to leach out into the supernatant. As the AHD assay does not directly measure cell recovery, only haemoglobin loss, this could lead to false positive results for hypertonic solutions. These results suggest that the frozen cells are slightly more sensitive to lower salt concentrations than the unfrozen controls, with some lysis observed at a salt concentration of 0.125 M, however, negligible further lysis was observed. Unfrozen cells appear to undergo some lysis at 0.031 M, with further decreasing salt concentration causing increased lysis. The differences observed between the frozen and unfrozen cells, paired with the unusually low lysis observed at high salt concentrations suggests that while there has been some effect on membrane

integrity, further studies are required to investigate the viability of blood cells cryopreserved using this technique. In spite of these issues, red blood cell cryopreservation is still an attractive screen for identifying interesting cryoprotectant materials which can then be investigated for use as nucleated cell cryoprotectants.

3.4 Conclusion

This study reports the first investigation into the effect of sequence/regiochemistry on the ice recrystallisation inhibition (IRI) activity of polyampholytes, with the intention of mimicking the function of antifreeze (glyco)proteins. Poly(ampholytes) are one of the few classes of material to display this activity, however their mode of action is still unknown. Alternating copolymers were obtained by exploiting the tendency of maleic anhydride to cross-polymerise with a range of hydrophobic comonomers. The anhydride ring could then be opened post-polymerisation to introduce a range of amino-functionalities as well as a carboxylic acid, with an exact 1:1 ratio of functional groups, positioned adjacent to each other. Such control is not possible by a normal radical copolymerisation. Quantitative IRI (ice recrystallisation) assays revealed that the hydrophobic comonomer (styrene) had little impact on the IRI activity which may be due to its dramatic effect on aqueous solubility. Conversely, alkylation of the amines (side chain hydrophobicity) lead to changes in activity. Di-methylation lead to more activity than longer alkyl chains, or a primary amine, demonstrating that although hydrophobicity can increase IRI activity the nature and placement of this must be carefully considered to prevent aggregation/precipitation and to maximise activity. These observations support the concept that spatially segregated hydrophilic/hydrophobic domains are essential to ensure potent IRI in synthetic materials. These findings were then used to help direct the synthesis of a poly(ampholyte) cryoprotectant from a low cost, biocompatible, industrial precursor. The freezing conditions required for this ampholyte were optimised, and the reproducibility of the process demonstrated. The osmotic fragility was determined in order to ensure that the RBCs, once thawed, were not notably more fragile than their unfrozen counterparts. In order to investigate the application of these materials as

effective cryoprotectants further, nucleated cell assays are required. While red blood cells are attractive as an initial screen, they are rarely cryopreserved, and therefore for these materials to be useful, they must be tested with nucleated cell lines. Future investigations into the mechanism of action of these materials would also be incredibly interesting, as this may allow for future structural optimisations to be identified.

3.5 Experimental

Materials

Phosphate-buffered saline (PBS) solutions were prepared using pre-formulated tablets (Sigma-Aldrich) in 200 mL of Milli-Q water (>18.2 Ω mean resistivity) to give [NaCl] = 0.138 M, [KCl] = 0.0027 M, and pH 7.4. Vinyl acetate (>99 %), styrene (>99 %), and isopropenyl acetate (99 %) were purchased from Sigma-Aldrich and were filtered through a plug of basic alumina to remove inhibitors prior to use. 4,4'azobis(4-cynaovaleric acid) (>98 %) was recrystallised from methanol and stored at -18 ºC in the dark. Maleic anhydride (99 %), benzyl bromide (98 %), 2-cyano-2propyl benzodithioate (>97 %), *N*-Boc ethanolamine (98 %), 2-(dimethylamino)ethanol (99.5 %), 2-(diethylamino)ethanol (>99.5 %), 2-(diisopropylamino)ethanol (>99 %) and trifluoroacetic acid (99 %) were purchased from Sigma Aldrich. Potassium ethyl xanthate (98 %) was purchased from Alfa Aesar. All solvents were purchased from VWR or Sigma Aldrich and used without further purification. Initial trial polymerisations were carried out with RAFT agent synthesised by Dr. Tom Congdon, however more was required, and therefore *S*-Benzyl *O*-ethyl Carbonodithioate was synthesised during the course of this work.

Physical and Analytical Methods

^{1}H and ^{13}C NMR spectra were recorded on Bruker Avance III HD 300 MHz, HD 400 MHz or HD 500 MHz spectrometers using deuterated solvents obtained from Sigma-Aldrich. Chemical shifts are reported relative to residual non-deuterated solvent. SEC data was recorded on an Agilent 390-LC MDS instrument equipped with differential refractive index (DRI), viscometry (VS), dual angle light scatter (LS) and dual wavelength UV detectors. The system was equipped with 2 x PLgel Mixed D columns

(300 x 7.5 mm) and a PLgel 5 µm guard column. The eluent was DMF with 5 mmol NH_4BF_4 additive. Samples were run at 1 $mL.min^{-1}$ at 50 °C. Poly(methyl methacrylate) standards (Agilent EasyVials) were used for calibration. Analyte samples were filtered through a nylon membrane with 0.22 µm pore size before injection. Respectively, experimental molar mass ($M_{n,}^{SEC}$) and dispersity (Đ) values of synthesized polymers were determined by conventional calibration using Agilent GPC/SEC software.

Ice wafers were annealed on a Linkam Biological Cryostage BCS196 with T95-Linkpad system controller equipped with a LNP95-Liquid nitrogen cooling pump, using liquid nitrogen as the coolant (Linkam Scientific Instruments UK, Surrey, UK). An Olympus CX41 microscope equipped with a UIS-2 20x/0.45/∞/0-2/FN22 lens (Olympus Ltd, Southend on sea, UK) and a Canon EOS 500D SLR digital camera was used to obtain all images. Image processing was conducted using Image J, which is freely available from http://imagej.nih.gov/ij/. LogP was calculated from the hydrophobicity of the pendant group using ChemDraw Professional 16.0.

Ice Recrystallisation Inhibition Assay

A 10 µL droplet of polymer in PBS solution was dropped from 1.4 metres onto a glass microscope coverslip, which was placed on top of an aluminium plate cooled to -78 °C using dry ice. The droplet froze instantly upon impact with the plate, spreading out and forming a thin wafer of ice. This wafer was then placed on a liquid nitrogen cooled cryostage held at -8 °C within the viewing area of the microscope. The wafer was then left to anneal for 30 minutes at -8 °C. The number of crystals in the image was counted using ImageJ, and the area of the field of view divided by this number of crystals to

give the average crystal size per wafer and reported as a percentage (%) of area compared to PBS control.

Blood Testing Protocol

10 mL Sheep blood in Alsevers solution was added to a 15 mL centrifuge tube and centrifuged at 2000 rpm for 5 minutes to concentrate the solution, 7 mL of the supernatant was removed and replaced with 7 mL PBS solution. Polymer solutions were made at 2X the required concentration to ensure the correct final cryoprotectant concentration. 0.5 mL of the blood solution was added to 0.5 mL of the polymer solutions in 2 mL cryovials. These were then incubated in the fridge for 30 minutes before freezing in liquid nitrogen vapour. After 1 hour, samples were thawed in a water bath at 45 °C for 10 minutes, after which they were transferred to Eppendorf tubes and centrifuged at 2000 rpm for 5 minutes. 40 μL of the supernatant was removed and added to 750 μL of AHD solution. After vortexing, the samples were pipetted into a 96 well plate in triplicate (3 x 200 μL per sample) and the absorbance recorded at 580 nm in the BioTek plate reader. Samples were compared against unfrozen blood cells in PBS and lysis buffer as the 0 and 100 % lysis samples respectively.

Alternative Freezing Conditions

Slow Freezing: Vials were placed into a Mr Frosty (Nalgene) controlled rate freezing container. Cryovials are placed inside, and the container placed in a -80 °C freezer for 24 hours, the Mr Frosty controls the freezing rate to 1 °C/min.

Fast Freezing: Cryovials are plunged into liquid nitrogen until completely frozen and stored for 24 hours.

Slow Thawing: Cryovials containing the frozen blood/polymer mix are placed into a pre-cooled Mr Frosty (-80 °C for 24 hours) and are placed in a refrigerator to slowly warm. After 8 hours, the samples are removed and allowed to warm, to room temperature, after which lysis is determined as normal.

Fast Thawing: Cryovials containing the frozen blood/polymer mix are placed into a water bath set at 45 °C for 10 min, after which lysis is determined as normal.

Osmotic Fragility

20 mL Sheep blood in Alsevers solution was added to a 50 mL centrifuge tube and centrifuged at 2000 rpm for 5 minutes to concentrate the solution, 14 mL of the supernatant was removed and replaced with 14 mL PBS solution. 10 mL of this solution was kept in the refrigerator as a control for unfrozen blood cells in later testing. Polymer solutions were made up at 200 $mg.mL^{-1}$ concentration to ensure the correct final cryoprotectant concentration. Using the remaining 10 mL of blood cells in PBS, 0.5 mL of the blood solution was added to 0.5 mL of the polymer solution in 2 mL cryovials. These were then incubated in the fridge for 30 minutes before freezing above liquid nitrogen vapour. After 1 hour, samples were thawed in a water bath at 45 °C for 10 minutes and recombined into one 15 mL centrifuge tube. This was centrifuged at 2000 rpm for 10 minutes, after which the supernatant was removed, and the sample made up to its original volume with PBS. Salt solutions were prepared at 2 M, 1 M, 0.5 M, 0.25 M, 0.125 M, 0.0625 M and 0.03125 M by serial dilution, as well as pure DI water. 0.2 mL of each salt solution was pipetted into 6 Eppendorf tubes, and 0.2 mL of frozen blood was added to three of these, and unfrozen blood added to the other three. These samples were then left for 20 minutes, after which the samples were centrifuged at 2000 rpm for 5 minutes. 40 μL of the supernatant was

removed and added to 750 μL of AHD solution. After vortexing, the samples were pipetted into a 96 well plate in triplicate (3 x 200 μL per sample) and the absorbance recorded at 580 nm in a plate reader. Samples were compared against unfrozen blood cells stored in PBS and lysis buffer as the 0 and 100 % lysis samples respectively.

Synthesis of *S*-Benzyl *O*-ethyl Carbonodithioate

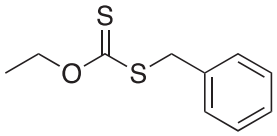

Potassium ethyl xanthate (3 g, 0.0187 mol, 1 eq) was dissolved in 50 mL acetone at 70 °C and stirred, after 30 minutes, benzyl bromide (3.20 g, 0.0187 mol, 1 eq) was added and stirred for 24 hours. During the reaction a white precipitate formed, the reaction solution was diluted with a further 50 mL acetone and filtered to remove the solid precipitate. The product was dissolved in DCM and washed twice with water at pH 8, followed by brine. The DCM layer was dried with magnesium sulphate, filtered and the solvent removed under vacuum. The resulting yellow oil was then recrystallised in hexane.

Yield: 2.87 g, 72.3 %. ^{1}H NMR ($CDCl_3$): δ = 1.39 (CH_3CH_2O, t, J = 7 Hz, 3H), 4.34 ($C(S)SCH_2C_6H_5$, s, 2H), 4.63 (CH_3CH_2O, q, J = 7 Hz, 2H), 7.31 (Aromatic C-H, m, 5H). ^{13}C NMR ($CDCl_3$): δ = 13 (CH_3CH_2O), 40 ($C(S)CH_2C_6H_5$), 70 (CH_3CH_2O), 127 (*Para* C-H), 128 (*Meta* C-H), 129 (*Ortho* C-H), 135 ($CH_2C(CH)CH$), 213 ($OC(S)S$).

Synthesis of poly (maleic anhydride-*alt*-styrene)$_{46}$

2-cyano-2-propyl benzodithioate (7.9 mg, 35 μmol), maleic anhydride (1.0 g, 10.2 mmol), styrene (0.28 g, 2.69 mmol), 4,4′-azobis(4-cyanovaleric acid) (ACVA) (2 mg, 7.17 μmol) and 1,4-dioxane (3 mL) were added to a sealed vial. The solution was

degassed by bubbling N_2 through the solution for 30 minutes, and the reaction was then allowed to polymerise at 80 ºC for 5 hours. The polymerisation reaction was stopped by plunging the resulting solution into liquid nitrogen. Poly(maleic anhydride-*alt*-styrene) was recovered as a pink solid after precipitation into diethyl ether. The diethyl ether was decanted and the solid dried under vacuum overnight forming a pale pink solid.

Yield: 0.28 g. ^{1}H NMR (DMSO): δ = 1.62-2.80 (C*H*$_2$CH(C_6H_5), CH_2C*H*(C_6H_5), br), 2.84-3.97 (CH(C_6H_5)C*H*C(O)OC(O)CH, CH(C_6H_5)CHC(O)OC(O)C*H*, br), 6.80-7.59 (Aromatic C-*H*, br). ^{13}C NMR (DMSO): δ = 33 (*C*H_2CH(C_6H_5)), 43 (CH(C_6H_5)CHC(O)OC(O)*C*H), 51 ((CH(C_6H_5)*C*HC(O)OC(O)CH)), 67 (CH_2*C*H(C_6H_5)), 128 (*C*$_6H_5$), 173 ((CH(C_6H_5)CH*C*(O)OC(O)CH), (CH(C_6H_5)CH*C*(O)O*C*(O)CH)). FTIR Anhydride C=O 1775 cm^{-1}, 1850 cm^{-1}. M_n^{SEC}(DMF) = 9,200 Da, M_w/M_n = 1.08.

Synthesis of poly (maleic anhydride-*alt*-styrene)$_{100}$

2-cyano-2-propyl benzodithioate (3.7 mg, 16 μmol), maleic anhydride (1.0 g, 10.2 mmol), styrene (0.280 g, 2.69 mmol), ACVA (0.94 mg, 3.4 μmol) and 1,4-dioxane (3 mL) were added to a sealed vial. The solution was degassed by bubbling N_2 through the solution for 30 minutes, and the reaction was then allowed to polymerise at 80 ºC for 5 hours. The polymerisation reaction was stopped by plunging the resulting solution into liquid nitrogen. Poly(maleic anhydride-*alt*-styrene) was recovered as a pink solid after precipitation into diethyl ether. The diethyl ether was decanted and the solid dried under vacuum overnight forming a pale pink solid.

Yield: 0.19 g. ^{1}H NMR (DMSO): δ = 1.39-2.76 (C*H*$_2$CH(C_6H_5), CH_2C*H*(C_6H_5), br), 2.79-4.01 (CH(C_6H_5)C*H*C(O)OC(O)CH, CH(C_6H_5)CHC(O)OC(O)C*H*, br), 6.80-7.59

(Aromatic C-*H*, br). ^{13}C NMR (DMSO): δ = 33 (*C*H_2CH(C_6H_5)), 42 (CH(C_6H_5)CHC(O)OC(O)*C*H), 51 ((CH(C_6H_5)*C*HC(O)OC(O)CH)), 66 (CH_2*C*H(C_6H_5)), 129 (Aromatic C), 172 ((CH(C_6H_5)CH*C*(O)OC(O)CH), (CH(C_6H_5)CH*C*(O)O*C*(O)CH)). FTIR Anhydride C=O 1774 cm^{-1}, 1849 cm^{-1}. M_n^{SEC}(DMF) = 20,300 Da, M_w/M_n = 1.11.

Synthesis of poly (maleic anhydride-*alt*-vinyl acetate)$_{30}$

S-benzyl *O*-ethyl carbonodithioate (10 mg, 46 μmol), maleic anhydride (1 g, 10 mmol), vinyl acetate (0.25 g, 2.90 mmol), ACVA (2.6 mg, 9.3 μmol), and 1,4-dioxane (2 mL) were added to a sealed vial. The solution was degassed by bubbling N_2 through the solution for 30 minutes, and the reaction was then allowed to polymerise at 68 ºC for 24 hours. The polymerisation reaction was stopped by plunging the resulting solution into liquid nitrogen. Poly(maleic anhydride-*alt*-vinyl acetate) was recovered as a beige solid after precipitation into diethylether. The diethyl ether was then decanted and the solid dried under vacuum overnight forming a pale beige solid.

Yield: 0.32 g. ^{1}H NMR (DMSO): δ = 1.49-2.42 (C*H*$_2$CH($OCOCH_3$), CH_2CH(OCOC*H*$_3$), br), 2.80-3.71 (CH($OCOCH_3$)CHC(O)OC(O)C*H*, CH($OCOCH_3$)C*H*C(O)OC(O)CH, br), 4.90-5.79 (CH_2C*H*($OCOCH_3$), br). ^{13}C NMR (DMSO): δ = 21 (CH_2CH*(*OCO*C*H$_3$)), 22 (*C*H_2CH($OCOCH_3$)), 32 (CH($OCOCH_3$)CHC(O)OC(O)*C*H), 50 (CH($OCOCH_3$)*C*HC(O)OC(O)CH), 69 (CH_2*C*H($OCOCH_3$), 170 (CH($OCOCH_3$)CH*C*(O)OC(O)CH, CH($OCOCH_3$)CHC(O)O*C*(O)CH), 173 (CH_2CH(O*C*OCH_3)). FTIR: Anhydride C=O 1849 cm^{-1}, 1788 cm^{-1}. M_n^{SEC}(DMF) = 5,600 Da, M_w/M_n = 1.46.

Synthesis of poly (maleic anhydride-*alt*-vinyl acetate)$_{57}$

S-benzyl *O*-ethyl carbonodithioate (5.1 mg, 23 μmol), maleic anhydride (1 g, 10 mmol), vinyl acetate (0.25 g, 2.90 mmol), ACVA (1.3 mg, 4.64 μmol) and 1,4-dioxane (2 mL) were added to a sealed vial. The solution was degassed by bubbling N_2 through the solution for 30 minutes, and the reaction was then allowed to polymerise at 68 ºC for 24 hours. The polymerisation reaction was stopped by plunging the resulting solution into liquid nitrogen. Poly(maleic anhydride-*alt*-vinyl acetate) was recovered as a beige solid after precipitation into diethylether. The diethyl ether was then decanted and the solid dried under vacuum overnight forming a pale beige solid.

Yield: 0.22 g. ^{1}H NMR (DMSO): δ = 1.81-2.14 (C*H*$_2$CH(OCOCH$_3$), CH$_2$CH(OCOC*H*$_3$), br), 2.80-4.00 (CH(OCOCH$_3$)CHC(O)OC(O)C*H*, CH(OCOCH$_3$)C*H*C(O)OC(O)CH, br), 5.09-5.85(CH$_2$C*H*(OCOCH$_3$), br). ^{13}C NMR (DMSO): 21 (CH$_2$CH*(*OCO*C*H$_3$)), 22 (*C*H$_2$CH(OCOCH$_3$)), 33 (CH(OCOCH$_3$)CHC(O)OC(O)*C*H), 50 (CH(OCOCH$_3$)*C*HC(O)OC(O)CH), 69 (CH$_2$*C*H(OCOCH$_3$), 171 (CH(OCOCH$_3$)CH*C*(O)OC(O)CH, CH(OCOCH$_3$)CHC(O)O*C*(O)CH), 173 (CH$_2$CH(O*C*OCH$_3$)). FTIR Anhydride C=O 1849 cm^{-1}, 1776 cm^{-1}. M_n^{SEC}(DMF) = 10,500 Da, M_w/M_n = 1.34.

Synthesis of poly(maleic anhydride-*alt*-isopropenyl acetate)$_{36}$

As a representative example, 2-cyano-2-propyl benzodithioate (14 mg, 65 μmol), maleic anhydride (0.99 g, 10.1 mmol), isopropenyl acetate (0.27 g, 2.70 mmol), ACVA (3.6 mg, 13 μmol) and 1,4-dioxane (2 mL) were added to a sealed vial. The solution was degassed by bubbling N_2 through the solution for 30 minutes, and the reaction was then allowed to polymerise at 68 ºC for 24 hours. The polymerisation reaction was stopped by plunging the resulting solution into liquid nitrogen.

Poly(maleic anhydride-*alt*-isopropenyl acetate) was recovered as a brown solid after precipitation into diethylether. The diethyl ether was then decanted and the solid dried under vacuum overnight forming a brown/black solid.

Yield: 0.24 g. ^{1}H NMR (DMSO): δ = 1.39-1.84 (C(C*H*$_3$)COO, br), 1.84-2.16 (C*H*$_2$C(CH$_3$)OCOCH$_3$, CH$_2$C(CH$_3$)OCOC*H*$_3$, br), 3.45-4.36 (C*H*C(O)OC(O)CH, CHC(O)OC(O)C*H*, br). ^{13}C NMR (DMSO): δ = 22 (CH$_2$C(CH$_3$)OCO*C*H$_3$), 23 (*C*H$_2$C(CH$_3$)OC, CHC(O)OC(O)*C*H), 24 (CH$_2$C(*C*H$_3$)OC), 55 (*C*HC(O)OC(O)CH), 83 (CH$_2$*C*(CH$_3$)OC), 170 (CH*C*(O)OC(O)CH, CHC(O)O*C*(O)CH), 173 (CH$_2$C(CH$_3$)O*C*OCH$_3$). FTIR Anhydride C=O 1845 cm^{-1}, 1748 cm^{-1}. M_n^{SEC}(DMF) = 7,200 Da, M_w/M_n = 1.11.

Synthesis of poly(maleic anhydride-*alt*-isopropenyl acetate)$_{92}$

As a representative example, 2-cyano-2-propyl benzodithioate (3.4 mg, 15 μmol), maleic anhydride (0.99 g,10.1 mmol), isopropenyl acetate (0.27 g, 2.70 mmol), ACVA (0.86 mg, 3.01 μmol) and 1,4-dioxane (2 mL) were added to a sealed vial. The solution was degassed by bubbling N_2 through the solution for 30 minutes, and the reaction was then allowed to polymerise at 68 ºC for 24 hours. The polymerisation reaction was stopped by plunging the resulting solution into liquid nitrogen. Poly(maleic anhydride-*alt*-isopropenyl acetate) was recovered as a brown solid after precipitation into diethylether. The diethyl ether was then decanted and the solid dried under vacuum overnight forming a brown/black solid.

Yield: 0.22 g. ^{1}H NMR (DMSO): δ = 1.29-1.84 (C(C*H*$_3$)COO, br), 1.84-2.07 (C*H*$_2$C(CH$_3$)OCOCH$_3$, CH$_2$C(CH$_3$)OCOC*H*$_3$, br), 3.44-4.40 (C*H*C(O)OC(O)CH, CHC(O)OC(O)C*H*, br). ^{13}C NMR (DMSO): δ = 21 (CH$_2$C(CH$_3$)OCO*C*H$_3$), 22 (*C*H$_2$C(CH$_3$)OC, CHC(O)OC(O)*C*H), 24 (CH$_2$C(*C*H$_3$)OC), 54 (*C*HC(O)OC(O)CH),

82 ($CH_2C(CH_3)OC$), 170 ($CHC(O)OC(O)CH$, $CHC(O)OC(O)CH$), 173 ($CH_2C(CH_3)OCOCH_3$). FTIR Anhydride C=O 1845 cm^{-1}, 1774 cm^{-1}. M_n^{SEC}(DMF) = 18,200 Da, M_w/M_n = 1.70.

Post-polymerisation modification of poly(maleic anhydride-*alt*-styrene) with N-Boc ethanolamine and subsequent deprotection

As a representative example, poly(maleic anhydride-*alt*-styrene) (0.06 g), was dissolved in THF (1 mL). After dissolution, N-boc ethanolamine (0.32 g, 1.99 mmol) was added in excess. The solution was stirred for 24 hours at 40 ºC. The product was diluted with water and dialysed (Fisher, 1000-3500 Da MWCO) for 48 hours (7 water changes). The water was removed under reduced pressure and the solid dissolved in methanol (2 mL) before addition of excess trifluoroacetic acid (2 g, 17 mmol). The resulting solution was again concentrated *in vacuo,* dissolved in water and dialysed (Fisher, 1000-3500 Da MWCO) for 48 hours (7 water changes). The resulting product was then freeze dried to evolve a white solid.

Yield: 19 mg. ^{1}H NMR (DMSO): δ = 1.46-2.00 ($CH_2CH(C_6H_5)$, br), 2.06 – 2.96 ($CH_2CH(C_6H_5)$, br), 3.11-3.67 ($CHC(OCOH)CH(COOCH_2)$, $CHC(OCOH)CH(COOCH_2)$, $CH(COOCH_2CH_2NH_2)$, $CH(COOCH_2CH_2NH_2)$, br), 6.50-7.61 (Aromatic C-*H*, br). FTIR Ring opened C=O 1711 cm^{-1} (broad), Carboxylate (O=C-O^-) 1645 cm^{-1} (broad), Alcohol O-H 2764 –3710 cm^{-1}.

Post-polymerisation modification of poly (maleic anhydride-*alt*-vinyl acetate) with N-Boc ethanolamine and subsequent deprotection

As a representative example, poly(maleic anhydride-*alt*-vinyl acetate) (0.05 g), was dissolved in THF (1 mL). After dissolution, N-boc ethanolamine (0.32 g, 1.99 mmol)

was added in excess. The solution was stirred for 24 hours at 40 °C. The product was diluted with water and dialysed (Fisher, 1000-3500 Da MWCO) for 48 hours (7 water changes). The water was removed under reduced pressure and the solid dissolved in methanol (2 mL) before addition of excess trifluoroacetic acid (2 g, 17 mmol). The resulting solution was again concentrated *in vacuo,* dissolved in water and dialysed (Fisher, 1000-3500 Da MWCO) for 48 hours (7 water changes). The resulting product was then freeze dried to evolve a white solid.

Yield: 17 mg. ^{1}H NMR (DMSO): δ = 1.50-2.35 (C*H*$_2$CHOCOCH$_3$, CH$_2$CHOCOC*H*$_3$, br), 2.49-2.98 (C*H*(COOH)CHCOOC, CH(COOH)C*H*COOC, br), 3.03 (CHCOOCH$_2$C*H*$_2$NH$_2$, t), 3.72 (CHCOOC*H*$_2$CH$_2$NH$_2$, t), 4.98-5.46 (CH$_2$C*H*OCOCH$_3$). FTIR Ring opened C=O 1731 cm^{-1} (broad), Carboxylate (O=C-O$^-$) 1570 cm^{-1} (broad), Alcohol O-H 2952 – 3696 cm^{-1}.

Post-polymerisation modification of poly (maleic anhydride-*alt*-isopropenyl acetate) with N-Boc ethanolamine and subsequent deprotection

As a representative example, poly(maleic anhydride-*alt*-isopropenyl acetate) (0.05 g), was dissolved in THF (1 mL). After dissolution, N-boc ethanolamine (0.32 g, 1.99 mmol) was added in excess. The solution was stirred for 24 hours at 40 °C. The product was diluted with water and dialysed (Fisher, 1000-3500 Da MWCO) for 48 hours (7 water changes). The water was removed under reduced pressure and the solid dissolved in methanol (2mL) before addition of excess trifluoroacetic acid (2 g, 17 mmol). The resulting solution was again concentrated *in vacuo,* dissolved in water and dialysed (Fisher, 1000-3500 Da MWCO) for 48 hours (7 water changes). The resulting product was then freeze dried to evolve a white solid.

Yield: 22 mg. ^{1}H NMR (D_2O): δ = 1.42-1.76 ($CH_2C(CH_3)OCOCH_3$, br), 1.76-2.11 ($CH_2C(CH_3)OCOCH_3$, $CH_2C(CH_3)OCOCH_3$, $CH_2CH_2NH_2$, br), 3.04 ($OCH_2CH_2NH_2$, t, J = 5 Hz), 3.19-3.42 (CH(COOH)CH(CO), br), 3.57-3.69 (CH(COOH)CH(CO), br), 3.73 ($OCH_2CH_2NH_2$, t, J = 5 Hz). FTIR Ring opened C=O 1712 cm^{-1} (broad), Carboxylate (O=C-O$^-$) 1570 cm^{-1} (broad), Alcohol O-H 2707 – 3695 cm^{-1}.

Post-polymerisation modification of poly (maleic anhydride-*alt*-isopropenyl acetate) with dimethylamino ethanol

As a representative example, poly(maleic anhydride-*alt*-isopropenyl acetate) (0.05 g), was dissolved in THF (1 mL) followed by the addition of water (0.5 mL). After dissolution, Dimethylamino ethanol (0.25 g, 2.80 mmol) was added in excess. The solution was stirred for 24 hours at 40 °C. The product was diluted with water and dialysed (Fisher, 1000-3500 Da MWCO) for 48 hours (7 water changes). The resulting product was then freeze dried to evolve a white solid.

Yield: 29 mg. ^{1}H NMR (D_2O): δ = 1.30-1.76 ($CH_2C(CH_3)OCOCH_3$, br), 1.83-2.14 ($CH_2C(CH_3)OCOCH_3$, $CH_2C(CH_3)OCOCH_3$,br), 2.71-2.96 ($N(CH_3)_2$), 3.14 ($OCH_2CH_2N(CH_3)_2$, t, J = 5 Hz), 3.26-3.59 (CH(COOH)CH(CO), br), 3.79 ($OCH_2CH_2N(CH_3)_2$, t, J = 5 Hz), 4.13-4.45 (CH(COOH)CH(CO), br). FTIR Ring opened C=O 1724 cm^{-1} (broad), Carboxylate (O=C-O$^-$) 1573 cm^{-1} (broad), Alcohol O-H 3059 – 3690 cm^{-1}.

Post-polymerisation modification of poly (maleic anhydride-*alt*-isopropenyl acetate) with diethylamino ethanol

As a representative example, poly(maleic anhydride-*alt*-isopropenyl acetate) (0.05 g), was dissolved in THF (1 mL) and water (0.5 mL). After dissolution, Diethylamino

ethanol (0.30 g, 2.56 mmol) was added in excess. The solution was stirred for 24 hours at 40 °C. The product was diluted with water and dialysed (Fisher, 1000-3500 Da MWCO) for 48 hours (7 water changes). The resulting product was then freeze dried to evolve a white solid.

Yield: 19mg. ^{1}H NMR (D_2O): δ = 1.00-1.31 ($N(CH_2C\mathit{H}_3)_2$, br), 1.31-1.72 ($CH_2C(C\mathit{H}_3)OCOCH_3$, br), 1.82-2.13 ($C\mathit{H}_2C(CH_3)OCOCH_3$, $CH_2C(CH_3)OCOC\mathit{H}_3$, br), 3.04-3.28 ($N(C\mathit{H}_2CH_3)_2$, $OCH_2C\mathit{H}_2N(CH_3)_2$, br), 3.28-3.62 ($C\mathit{H}$(COOH)CH(CO), br), 3.79 ($OCH_2C\mathit{H}_2N(C\mathit{H}_2CH_3)_2$, t, J = 5 Hz) , 4.10-4.59 (CH(COOH)C*H*(CO), br). FTIR Ring opened C=O 1724 cm^{-1} (broad), Carboxylate ($O=C-O^-$) 1575 cm^{-1} (broad), Alcohol O-H 3077 – 3685 cm^{-1}.

Post-polymerisation modification of poly (maleic anhydride-*alt*-isopropenyl acetate) with diisopropylamino ethanol

As a representative example, poly(maleic anhydride-*alt*-isopropenyl acetate) (0.05 g), was dissolved in THF (1 mL) and water (0.5 mL). After dissolution, Diisopropylamino ethanol (0.30 g, 2.06 mmol) was added in excess. The solution was stirred for 24 hours at 40 °C. The product was diluted with water and dialysed (Fisher, 1000-3500 Da MWCO) for 48 hours (7 water changes). The resulting product was then freeze dried to evolve a white solid.

Yield: 17 mg. ^{1}H NMR (D_2O): δ = 1.12-1.40 ($N(CH(C\mathit{H}_3)_2)_2$, br), 1.41-1.73 ($CH_2C(C\mathit{H}_3)OCOCH_3$, br), 1.81-2.12 ($C\mathit{H}_2C(CH_3)OCOCH_3$, $CH_2C(CH_3)OCOC\mathit{H}_3$, br), 3.11 ($OCH_2C\mathit{H}_2N(CH(CH_3)_2)_2$, t, J = 5 Hz), 3.18-3.50 ($C\mathit{H}$(COOH)CH(CO), br), 3.59 ($OCH_2CH_2N(C\mathit{H}(CH_3)_2)_2$, m, J = 6 Hz), 3.76 ($OC\mathit{H}_2CH_2N(CH(CH_3)_2)_2$, t, J = 5 Hz), 4.04-4.54 (CH(COOH)C*H*(CO), br). FTIR Ring opened C=O 1724 cm^{-1} (broad), Carboxylate ($O=C-O^-$) 1575 cm^{-1} (broad), Alcohol O-H 3073 – 3701 cm^{-1}.

Synthesis of Poly(methyl vinyl ether-*alt*-maleic anhydride) based poly(ampholytes) (P1, P2, P3)

As a representative example, poly(methyl vinyl ether-*alt*-maleic anhydride), average M_n ~80,000 Da, (1 g) was dissolved in tetrahydrofuran (50 mL) and heated to 50 °C with stirring. After dissolution, dimethylamino ethanol (2 g) was added in excess, forming a pink waxy solid, which was allowed to stir for 30 minutes. 50 mL water was added, and the reaction left to stir overnight followed by purification in dialysis tubing (Spectrapor, 12 – 14 kDa MWCO) for 48 hours with 7 water changes. The resulting solution was freeze-dried to evolve a white solid.

Yield: 1.03 g. ^{1}H NMR (DMSO): **δ** = 1.31 – 2.00 ($CH_2CH(OCH_3)CH_2$, br), 2.42 ($(CH_3)_2NCH_2$, s), 2.50 ($CH_2CH(OCH_3)CH_2$, s), 2.66 (NCH_2CH_2COO, t, J = 6 Hz), 3.11 – 3.37 ($CH_2CH(OCH_3)CH_2$, br), 3.41 – 4.41 ($CH(OCH_3)CH(COOH)CH(COOC)$, $CH(OCH_3)CH(COOH)CH(COOC)$, br), 3.56 ($NCH_2CH_2COO$, t, J = 6 Hz). ^{13}C NMR (DMSO): 42 ($(CH_3)_2NCH_2$), 55 (NCH_2CH_2COO), 58 (NCH_2CH_2COO). FTIR: C-O1220 cm^{-1}, C-N 1342 cm^{-1}, Carboxylate (O=C-O$^-$) 1560 cm^{-1}, C=O 1724 cm^{-1}, Ammonium (Me_2N-H$^+$) 2364 cm^{-1}.

3.6 References

(1) Harding, M. M.; Anderberg, P. I.; Haymet, A. D. J. "Antifreeze" Glycoproteins from Polar Fish. *Eur. J. Biochem.* **2003**, *270* (7), 1381–1392.

(2) Balcerzak, A. K.; Capicciotti, C. J.; Briard, J. G.; Ben, R. N. Designing Ice Recrystallization Inhibitors: From Antifreeze (Glyco)Proteins to Small Molecules. *RSC Adv.* **2014**, *4* (80), 42682–42696.

(3) Venketesh, S.; Dayananda, C. Properties, Potentials, and Prospects of Antifreeze Proteins. *Crit. Rev. Biotechnol.* **2008**, *28* (1), 57–82.

(4) Capicciotti, C. J.; Kurach, J. D. R.; Turner, T. R.; Mancini, R. S.; Acker, J. P.; Ben, R. N. Small Molecule Ice Recrystallization Inhibitors Enable Freezing of Human Red Blood Cells with Reduced Glycerol Concentrations. *Sci. Rep.* **2015**, *5* (1), 9692.

(5) Chao, H.; Davies, P. L.; Carpenter, J. F. Effects of Antifreeze Proteins on Red Blood Cell Survival during Cryopreservation. *J. Exp. Biol.* **1996**, *199* (Pt 9), 2071–2076.

(6) Gibson, M. I. Slowing the Growth of Ice with Synthetic Macromolecules: Beyond Antifreeze(Glyco) Proteins. *Polym. Chem.* **2010**, *1* (8), 1141.

(7) Leclère, M.; Kwok, B. K.; Wu, L. K.; Allan, D. S.; Ben, R. N. C-Linked Antifreeze Glycoprotein (C-AFGP) Analogues as Novel Cryoprotectants. *Bioconjug. Chem.* **2011**, *22* (9), 1804–1810.

(8) Drori, R.; Li, C.; Hu, C.; Raiteri, P.; Rohl, A. L.; Ward, M. D.; Kahr, B. A Supramolecular Ice Growth Inhibitor. *J. Am. Chem. Soc.* **2016**, *138* (40), 13396–13401.

(9) Currie, L.; Livesey, S.; Harper, J.; Connor, J. Cryopreservation of Single-Donor Platelets with a Reduced Dimethyl Sulfoxide Concentration by the Addition of

Second-Messenger Effectors: Enhanced Retention of in Vitro Functional Activity. *Transfusion* **1998**, *38* (2), 160–167.

(10) Polge, C.; Smith, A. U.; Parkes, A. S. Revival of Spermatozoa after Vitrification and Dehydration at Low Temperatures. *Nature* **1949**, *164* (4172), 666–666.

(11) Baust, J. M.; Gao, D.; Baust, J. G. Cryopreservation. *Organogenesis* **2009**, *5* (3), 90–96.

(12) Ustun, N. S.; Turhan, S. Antifreeze Proteins: Characteristics, Function, Mechanism of Action, Sources and Application to Foods. *J. Food Process. Preserv.* **2015**, *39* (6), 3189–3197.

(13) Lindner, N. M.; Oldroyd, J. R.; Sztehlo, A.; Towell, D. J. Frozen Confectionery Product Comprising Ice Structuring Proteins. WO2005058058 A1, 2004.

(14) Sidebottom, C.; Buckley, S.; Pudney, P.; Twigg, S.; Jarman, C.; Holt, C.; Telford, J.; McArthur, A.; Worrall, D.; Hubbard, R.; Lillford, P. Heat-Stable Antifreeze Protein from Grass. *Nature* **2000**, *406* (6793), 256–256.

(15) Iwatani, M.; Ikegami, K.; Kremenska, Y.; Hattori, N.; Tanaka, S.; Yagi, S.; Shiota, K. Dimethyl Sulfoxide Has an Impact on Epigenetic Profile in Mouse Embryoid Body. *Stem Cells* **2006**, *24* (11), 2549–2556.

(16) Shu, Z.; Heimfeld, S.; Gao, D. Hematopoietic SCT with Cryopreserved Grafts: Adverse Reactions after Transplantation and Cryoprotectant Removal before Infusion. *Bone Marrow Transplant.* **2014**, *49* (4), 469–476.

(17) Inada, T.; Lu, S.-S. Inhibition of Recrystallization of Ice Grains by Adsorption of Poly(Vinyl Alcohol) onto Ice Surfaces. *Cryst. Growth Des.* **2003**, *3* (5), 747–752.

(18) Budke, C.; Koop, T. Ice Recrystallization Inhibition and Molecular Recognition

of Ice Faces by Poly(Vinyl Alcohol). *ChemPhysChem* **2006**, *7* (12), 2601–2606.

(19) Gibson, M. I.; Barker, C. A.; Spain, S. G.; Albertin, L.; Cameron, N. R. Inhibition of Ice Crystal Growth by Synthetic Glycopolymers: Implications for the Rational Design of Antifreeze Glycoprotein Mimics. *Biomacromolecules* **2009**, *10* (2), 328–333.

(20) Deller, R. C.; Congdon, T.; Sahid, M. A.; Morgan, M.; Vatish, M.; Mitchell, D. A.; Notman, R.; Gibson, M. I. Ice Recrystallisation Inhibition by Polyols: Comparison of Molecular and Macromolecular Inhibitors and Role of Hydrophobic Units. *Biomater. Sci.* **2013**, *1* (5), 478.

(21) Deller, R. C.; Vatish, M.; Mitchell, D. A.; Gibson, M. I. Glycerol-Free Cryopreservation of Red Blood Cells Enabled by Ice-Recrystallization-Inhibiting Polymers. *ACS Biomater. Sci. Eng.* **2015**, *1* (9), 789–794.

(22) Deller, R. C.; Vatish, M.; Mitchell, D. A.; Gibson, M. I. Synthetic Polymers Enable Non-Vitreous Cellular Cryopreservation by Reducing Ice Crystal Growth during Thawing. *Nat. Commun.* **2014**, *5*, 3244.

(23) Deller, R. C.; Pessin, J. E.; Vatish, M.; Mitchell, D. A.; Gibson, M. I. Enhanced Non-Vitreous Cryopreservation of Immortalized and Primary Cells by Ice-Growth Inhibiting Polymers. *Biomater. Sci.* **2016**, *47* (7), 935–945.

(24) Congdon, T.; Notman, R.; Gibson, M. I. Antifreeze (Glyco)Protein Mimetic Behavior of Poly(Vinyl Alcohol): Detailed Structure Ice Recrystallization Inhibition Activity Study. *Biomacromolecules* **2013**, *14* (5), 1578–1586.

(25) Phillips, D. J.; Congdon, T. R.; Gibson, M. I. Activation of Ice Recrystallization Inhibition Activity of Poly(Vinyl Alcohol) Using a Supramolecular Trigger. *Polym. Chem.* **2016**, *7* (9), 1701.

(26) Olijve, L. C.; Hendrix, M. R.; Voets, I. K. Influence of Polymer Chain Architecture of Poly(Vinyl Alcohol) on the Inhibition of Ice Recrystallization. *Macromol. Chem. Phys.* **2016**, *217* (8), 951–958.

(27) Mitchell, D. E.; Gibson, M. I. Latent Ice Recrystallization Inhibition Activity in Nonantifreeze Proteins: Ca 2+ -Activated Plant Lectins and Cation-Activated Antimicrobial Peptides. *Biomacromolecules* **2015**, *16* (10), 3411–3416.

(28) Matsumura, K.; Hyon, S.-H. H. Polyampholytes as Low Toxic Efficient Cryoprotective Agents with Antifreeze Protein Properties. *Biomaterials* **2009**, *30* (27), 4842–4849.

(29) Mitchell, D. E.; Cameron, N. R.; Gibson, M. I. Rational, yet Simple, Design and Synthesis of an Antifreeze-Protein Inspired Polymer for Cellular Cryopreservation. *Chem. Commun.* **2015**, *51* (65), 12977–12980.

(30) Mitchell, D. E.; Lilliman, M.; Spain, S. G.; Gibson, M. I. Quantitative Study on the Antifreeze Protein Mimetic Ice Growth Inhibition Properties of Poly(Ampholytes) Derived from Vinyl-Based Polymers. *Biomater. Sci.* **2014**, *2* (12), 1787–1795.

(31) Rajan, R.; Hayashi, F.; Nagashima, T.; Matsumura, K. Toward a Molecular Understanding of the Mechanism of Cryopreservation by Polyampholytes: Cell Membrane Interactions and Hydrophobicity. *Biomacromolecules* **2016**, *17* (5), 1882–1893.

(32) Harrisson, S.; Liu, X.; Ollagnier, J.-N.; Coutelier, O.; Marty, J.-D.; Destarac, M. RAFT Polymerization of Vinyl Esters: Synthesis and Applications. *Polymers* **2014**, *6* (5), 1437–1488.

(33) Schmidt, B. V. K. J.; Fechler, N.; Falkenhagen, J.; Lutz, J.-F. Controlled Folding of Synthetic Polymer Chains through the Formation of Positionable

Covalent Bridges. *Nat. Chem.* **2011**, *3* (3), 234–238.

(34) Moatsou, D.; Hansell, C. F.; O'Reilly, R. K. Precision Polymers: A Kinetic Approach for Functional Poly(Norbornenes). *Chem. Sci.* **2014**, *5* (6), 2246–2250.

(35) Gody, G.; Barbey, R.; Danial, M.; Perrier, S. Ultrafast RAFT Polymerization: Multiblock Copolymers within Minutes. *Polym. Chem.* **2015**, *6* (9), 1502–1511.

(36) Rätzsch, M. Alternating Maleic Anhydride Copolymers. *Prog. Polym. Sci.* **1988**, *13* (4), 277–337.

(37) Gauthier, M. A.; Gibson, M. I.; Klok, H.-A. Synthesis of Functional Polymers by Post-Polymerization Modification. *Angew. Chemie Int. Ed.* **2009**, *48* (1), 48–58.

(38) Stenzel, M. H.; Cummins, L.; Roberts, G. E.; Davis, T. P.; Vana, P.; Barner-Kowollik, C. Xanthate Mediated Living Polymerization of Vinyl Acetate: A Systematic Variation in MADIX/RAFT Agent Structure. *Macromol. Chem. Phys.* **2003**, *204* (9), 1160–1168.

(39) Smets, M. C.; Wilde, D. . Copolymerisation de l'Anhydride Maleique Avec Differents Monomeres Vinyliques. *J. Polym. Sci.* **1950**, *5* (2), 253–258.

(40) Capicciotti, C. J.; Leclère, M.; Perras, F. A.; Bryce, D. L.; Paulin, H.; Harden, J.; Liu, Y.; Ben, R. N. Potent Inhibition of Ice Recrystallization by Low Molecular Weight Carbohydrate-Based Surfactants and Hydrogelators. *Chem. Sci.* **2012**, *3* (5), 1408–1416.

(41) Wolf, H. U.; Lang, W.; Zander, R. Alkaline Haematin D-575, a New Tool for the Determination of Haemoglobin as an Alternative to the Cyanhaemiglobin Method. II. Standardisation of the Method Using Pure Chlorohaemin. *Clin. Chim. Acta* **1984**, *136* (1), 95–104.

(42) Valeri, C. R.; Ragno, G.; Pivacek, L. E.; Cassidy, G. P.; Srey, R.; Hansson-Wicher, M.; Leavy, M. E. An Experiment with Glycerol-Frozen Red Blood Cells Stored at -80°C for up to 37 Years. *Vox Sang.* **2003**, *79* (3), 168–174.

(43) European Food Safety Authority (EFSA), Parma, I. Scientific Opinion on the Safety of "Methyl Vinyl Ether-Maleic Anhydride Copolymer" (Chewing Gum Base Ingredient) as a Novel Food Ingredient. *EFSA J.* **2013**, *11* (3423), 1–17.

(44) Goodhead, L. K.; MacMillan, F. M. Measuring Osmosis and Hemolysis of Red Blood Cells. *Adv. Physiol. Educ.* **2017**, *41* (2), 298–305.

3.7 Appendix

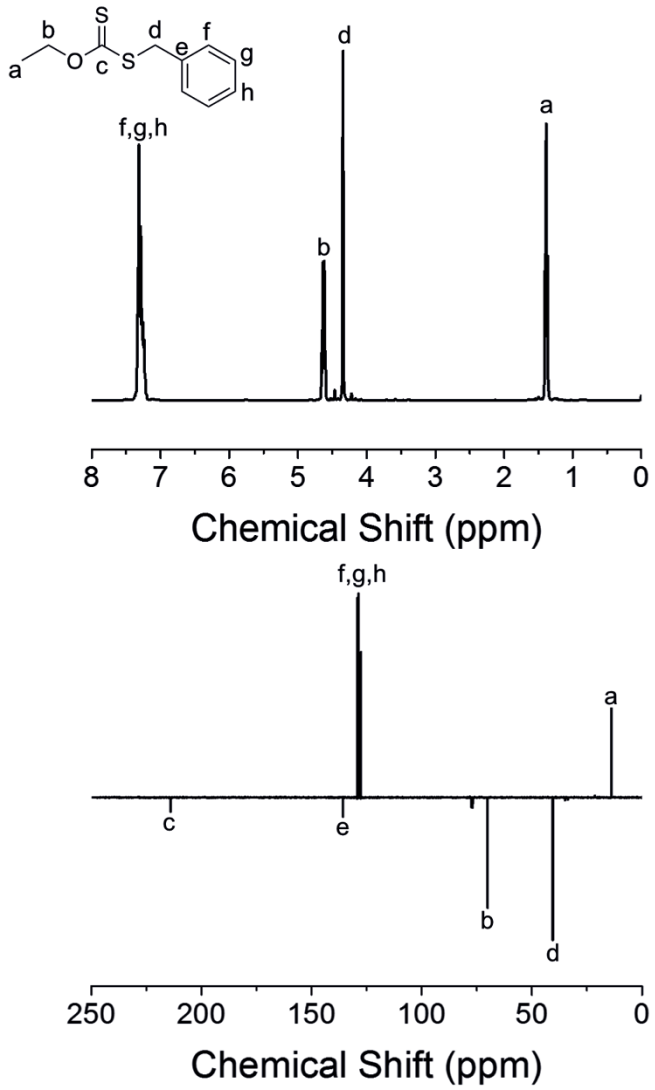

Figure 3.15: ^{1}H and ^{13}C NMR of the MADIX agent synthesised. Peaks at 77 ppm in the ^{13}C NMR are due to chloroform.

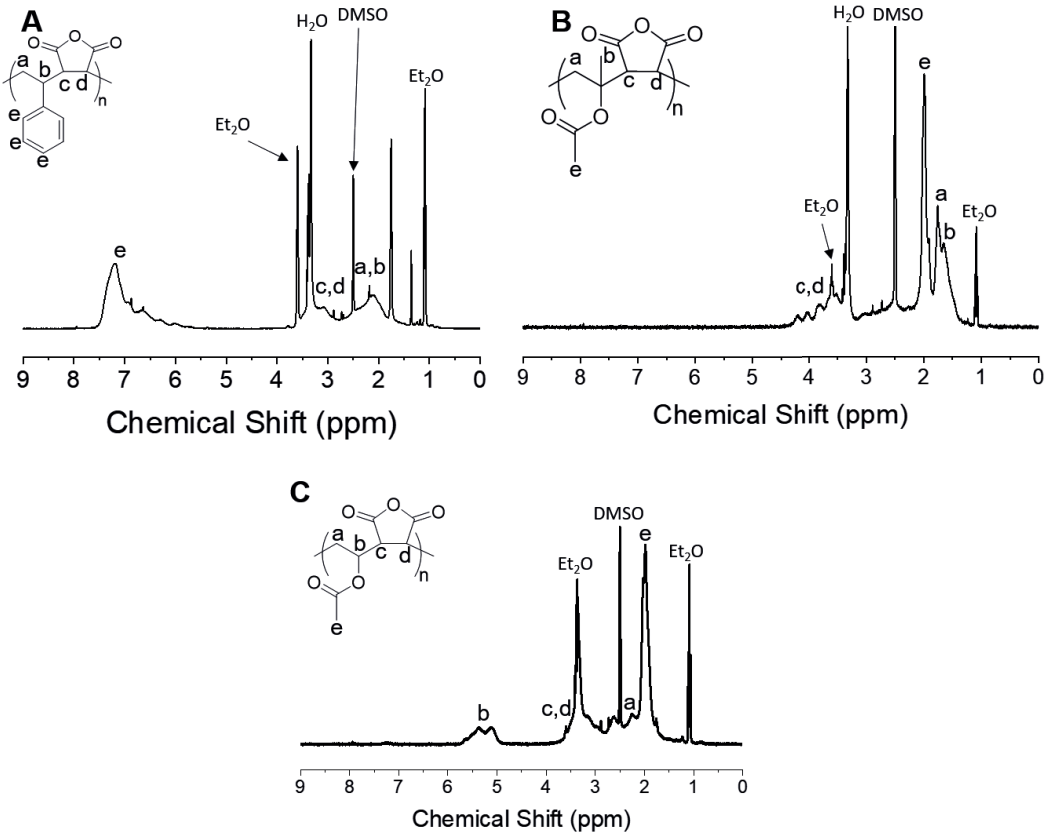

Figure 3.16: ^{1}H NMR of the MA copolymers synthesised: **A** PSMA; **B** PIPACMA and **C** VAcMA. NMRs were run in DMSO.

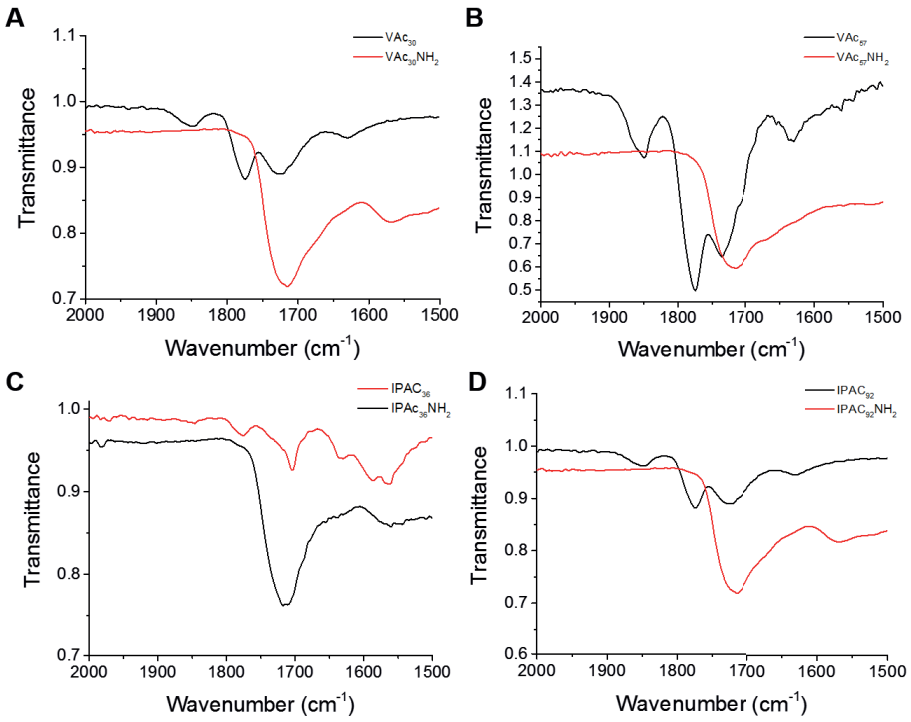

Figure 3.17: FTIR spectra for the copolymers and their NH_2 derivatives, the loss of the anhydride peak at ~ 1850 cm^{-1} and formation of a broad peak at ~1725 cm^{-1} suggests successful modification. **A** VAc_{30}; **B** VAc_{57}; **C** $IPAC_{36}$; **D** $IPAC_{92}$.

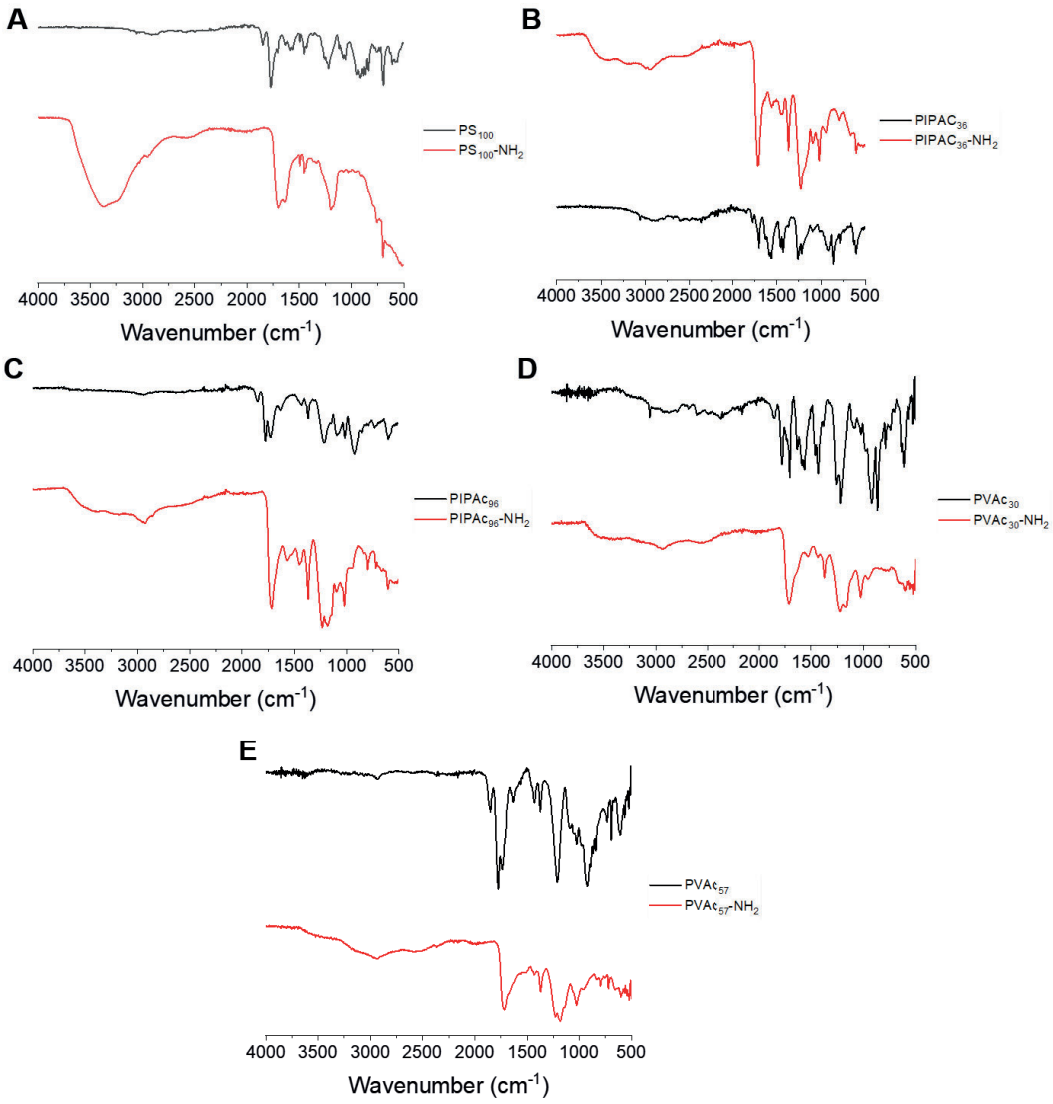

Figure 3.18: Full FTIR spectra for the ethanolamine functionalised polymers. **A** PS_{100}; **B** $PIPAC_{36}$ **C** $PIPAC_{92}$ **D** $PVAc_{30}$; **E** $PVAc_{57}$.

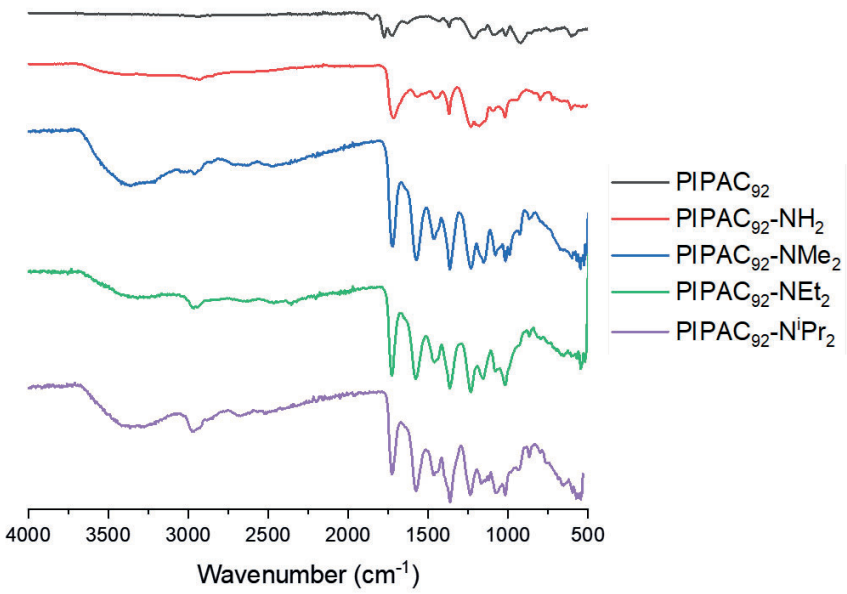

Figure 3.19: FTIR spectra for the functionalised $PIPAC_{92}$ copolymers.

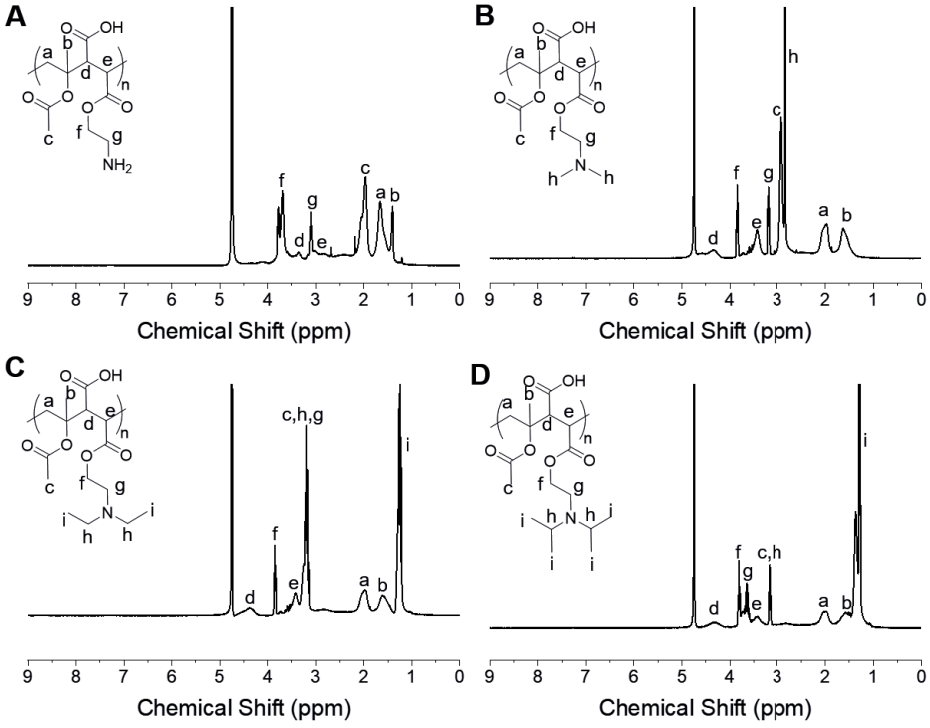

Figure 3.20: ^{1}H NMR for the functionalised $PIPAC_{92}$ copolymers. Polymers were functionalised with **A** Ethanolamine; **B** Dimethylamino ethanol; **C** Diethylaminoethanol and **D** Diisopropylamino ethanol. NMRs were run in D_2O.

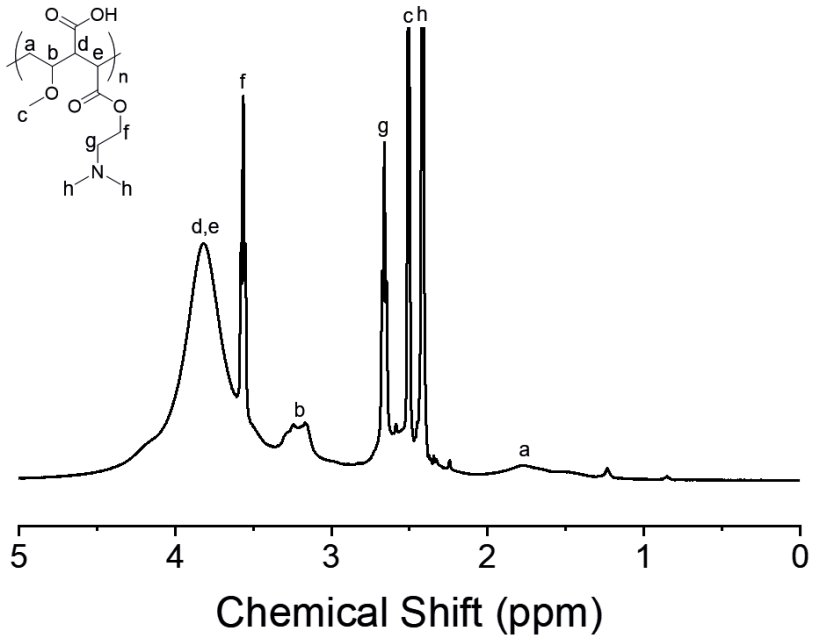

Figure 3.21: ^{1}H NMR of the of Poly(methyl vinyl ether-*alt*-maleic anhydride) ampholyte after ring opening with dimethylamino ethanol.

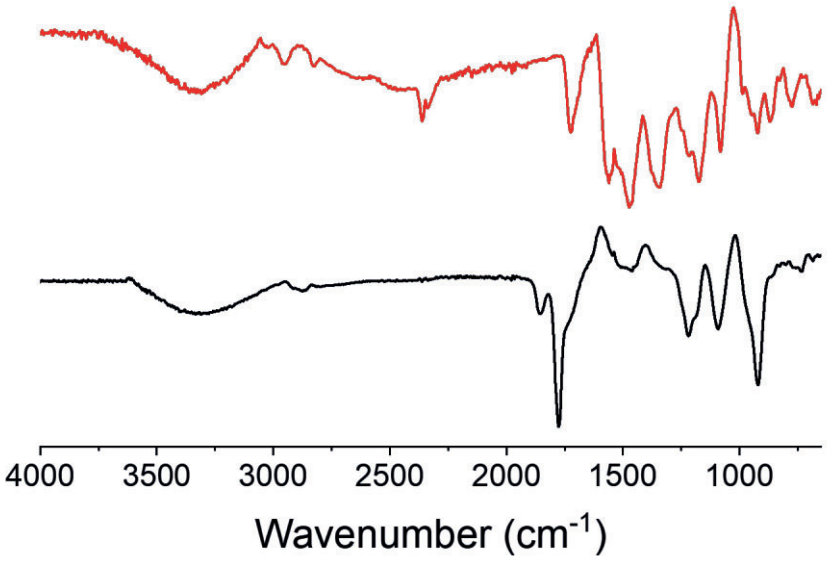

Figure 3.22: FTIR of Poly(methyl vinyl ether-*alt*-maleic anhydride) (black) and of the poly(ampholyte) produced after reaction with dimethylamino ethanol (red).

Chapter 4

Development of High Throughput Oxygen Tolerant Photoiniferter Polymerisation and Evaluation of Poly(ampholyte) Libraries

4.1 Abstract

Polymeric materials have been shown to have the potential to act as highly effective cryoprotectants, however the huge chemical space of synthetic polymers means that in most studies only a small parameter range can be realistically synthesised in a short time. This means that the 'best' observed formulations may not actually be optimum. High throughput experimentation in this area is traditionally limited by the need for de-oxygenation in radical polymerisations, but advances in photopolymerisation now provide opportunities for 'in air' polymerisations. Here, we demonstrate a simple protocol using liquid handling robots (or multichannel pipettes) with blue-light photolysis of a RAFT agent and tertiary amine deoxygenation to enable the synthesis of polymer libraries in industry-standard 96-well plates, and with no specialised infrastructure or degassing step. The role of solvents and the amine deoxygenator are explored to optimise the polymerisation, particularly to look at alternatives to dimethyl sulfoxide (DMSO) for hydrophobic monomer copolymerisation. DMSO has been shown to aid the degassing process but is not easy to remove, and hence prevents isolation of pure polymer. Using dioxane, in-plate evaporation or precipitation of the

tertiary amine allowed isolation of polymers in-plate, facilitating the workflow. As an example of the throughput, in just under 40 hours, 392 polymers were synthesised and subsequently analysed direct from plates by a 96-well plate-sampling SEC system to demonstrate reproducibility. Due to less efficient degassing in dioxane (compared to DMSO) the molecular weight and dispersity control was limited in all cases (with acrylates giving the lowest dispersities) but the key aim of this system is to access 100's of polymers quickly and in a format to enable testing. This method will enable easy exploration of chemical space and development of screening libraries to identify hits for further study using precision polymerisation methods. This technique was then used to synthesise a library of poly(ampholytes) of poly(dimethylaminoethyl methacrylate-*co*-methacrylic acid) (DMAEMA-MAA) to identify the optimal copolymer ratio, and then a series of 120 different terpolymers were synthesised with increasing content of hydrophilic or hydrophobic comonomer.

4.2 Introduction

To match the complex function and structures of biomacromolecules using synthetic materials, it is essential to incorporate increased diversity of monomer components to generate copolymers of increasing complexity.[1–4] For example, recent advances in sequence controlled[5,6] and multi-block[7,8] copolymers have led to emergent biological and biomimetic function, and there is a need to explore polymer formulations for many pharmaceutical applications.[9] However, there is a major challenge associated with the huge chemical space to be explored, which scales dramatically when comonomers are used. As a result of this, high-throughput methods are required for material discovery and to elucidate structure-activity relationships between materials and their properties.[10–13] Despite the ease and convenience of modern controlled radical polymerisation (CRP) methods (*i.e.* reversible addition fragmentation chain transfer (RAFT), atom transfer radical polymerisation (ATRP)), reagent addition, degassing and crucially the isolation, purification and transfer of the polymers into assay-ready formats are still bottlenecks for translation to truly high-throughput systems. Polymer investigations typically use panels of 10's of polymers, which represents a very small proportion of the investigable chemical space. This means that specific formulations with emergent properties are often missed and the sample size is very small when compared to commercially available standard libraries for drug discovery or biological screening.

Schubert and co-workers reported protocols for the high-throughput synthesis of multiblock copolymers using RAFT polymerisation, initiated thermally by an azo-initiator. The system required the synthesiser to be placed in an inert environment and necessitated that all reagents were kept under a constant flow of nitrogen.[14] Desterac reported the use of a parallel synthesiser to prepare various acrylate copolymers *via* a

MADIX process.[15] However, these systems require specialist infrastructures to enable closed-to-air preparations that are not always available. Inert high-throughput techniques have also been applied using a variety of controlled radical techniques including ATRP and cationic ring opening polymerisation (CROP).[16,17] These strategies using robotic methods in inert atmospheres have also been reviewed by Schubert.[18] Alexander and co-workers have exploited robotics to print diverse libraries of cross-linked copolymers onto surfaces to discover new materials to resist bacterial fouling[19] or for stem cell expansion.[11] Langer and co-workers have used step-growth polymerisation methods to explore large (140 polymers) libraries to identify gene transfection vectors. The advantage of this method is that only solvent needs to be removed at the end of the reaction. A high-throughput screen was successful in identifying copolymers for solubilisation of low-solubility pharmaceuticals, which could not have been easily achieved by rational design alone.[20]

When screening polymers for biological applications, it is essential that the polymers can be easily transferred into the format needed for testing – especially multi-well plates used in most biological testing. Otherwise, manual handling and weighing of 100's of polymers creates a process bottleneck. Ideally, in the prototype stage, reactions should be conducted in the multi-well plate format enabling direct transfer from the synthetic medium to the testing.[21,22] There has been considerable recent interest in the development of oxygen tolerant, or intrinsically oxygen-depleting polymerisation methods. One example employed enzymatic degassing; glucose oxidase (GOx) was used to remove oxygen in the polymerisation of hydroxyethyl acrylate, generating narrow dispersity polymers in methanol/PBS solutions.[23] These materials reached conversions of >90 % in three hours, and when paired with a liquid handling robot allowed controlled, high-throughput synthesis of polymers from a

variety of water soluble monomers[24] and in complex solvent mixtures.[25] This GOx strategy has also been exploited by Matyjaszewski to enable oxygen tolerant ATRP.[26] However, separating the enzyme from the product polymers is non-trivial and it does not work in organic solvents, which are essential if hydrophobic (co)monomers are to be used. An early report of using light to initiate a controlled living radical polymerisation was reported by Hawker and co-workers in 2012. Using an iridium catalyst, excellent control over the polymerisation of methyl methacrylate was achieved, demonstrating that the propagation occurs only when the light is switched on, and the chain remains dormant without this external stimulus.[27] Boyer and co-workers expanded the scope of potential monomers compatible with oxygen tolerant polymerisation through the development of PET-RAFT (photo-induced electron transfer, reversible addition fragmentation transfer) which allows the polymerisation of a wide variety of hydrophobic and hydrophilic monomers.[28–30] This process involves the use of a photocatalyst to reduce the chain transfer agent, generating a radical species which can then initiate the polymerisation. This technique was applied by Boyer for the high-throughput synthesis of a range of functionalised linear polymers as well as more complex 3-arm and 4-arm star polymers.[31] The polymerisation of less activated monomers has been demonstrated using this technique, with the iridium catalysed polymerisation of vinyl acetate shown to proceed equally well in both degassed and oxygen rich conditions.[32] Boyer also pioneered the development of an oxygen tolerant, enzyme free, technique for the synthesis of complex polymer architectures in aqueous media using Eosin Y and ascorbic acid. The applicability of this technique to high-throughput polymerisation was also demonstrated, carrying out reactions in 96-well plates at a range of ultralow volumes for the synthesis of arm-first star polymers.[30] Photopolymerisation is also emerging as

a tool to enable the synthesis of hybrid materials containing proteins (that could be sensitive to traditional thermal polymerisation).[33–35] The multi-functional nature of these photocatalysts allows a variety of mechanisms to be exploited. Sumerlin and Boyer investigated the possible reaction mechanisms involved in aqueous PET-RAFT polymerisations using Eosin Y by varying the intensity and color of the light source used to initiate the polymerisation, as well as in the presence and absence of a tertiary amine. Under different irradiation conditions, the photocatalyst could be either oxidised or reduced, leading to different initiation and reversible-termination steps. When no photocatalyst was present, the trithiocarbonate initiates *via* direct photolysis to generate an initiating species that could then also act as the chain transfer agent.[36–38]

One alternative to these PET-RAFT strategies was introduced by Qiao and co-workers. It involves the use of a sacrificial tertiary amine to reduce a photo-irradiated RAFT agent, which in turn converts dissolved oxygen to superoxide. The formed superoxide is hypothesised to be irreversibly trapped by reacting with DMSO in the system.[39] This system is appealing due to its simplicity and there being no need for additional photo-catalysts or enzymes. Xu *et. al* have also used tertiary amines in their photo-irradiated systems, noting a significant increase in rate of propagation when present.[28] Qiao's method has been adapted for the screening of cationic polymers, and their derivatives, as antimicrobials.[40] One downside to this strategy is the need for DMSO in the reaction mixture. DMSO has a high boiling point (189 °C) and hence polymers need to be either precipitated, which is not always easy in high-throughput and may require several different solvent systems, or prepared sufficiently concentrated for dilution at the point of assaying for function.[41,42] Hemocompatibility (blood toxicity) assays, for example requires a final DMSO concentration typically

below 1 %[43] to avoid false negatives, and hence alternatives to DMSO as the screening solvent are desirable.

One class of materials for which a combinatorial approach would be interesting are cryoprotective poly(ampholytes). Carboxylated poly(L-lysine) was first observed to be an effective cryoprotectant in 2009,[44] and since its discovery, a number of new materials have been investigated. While it has been shown that both charge ratio[44,45] and hydrophobicity[46] are important, only a very small number of different materials have ever actually been tested, and the exact mechanism by which they work is not well understood, meaning that rational design of these materials is difficult.[47] Most papers report testing on less than 15 different materials, with copolymers of dimethylaminoethyl methacrylate (DMAEMA) and methacrylic acid (MAA) being among the most common vinyl derived species investigated.[46,48] Terpolymers of DMAEMA MAA containing up to 10% octyl methacrylate, butyl methacrylate or 2-hydroxyethyl methacrylate have been tested, but given the number of potential vinyl monomers which could be incorporated, and the exact balance of hydrophobicity required being important but not well understood, a combinatorial approach may help to further our understanding of the design rules required to access the optimal activity of these materials.

Considering this, we wanted to explore the limits and scope of the tertiary amine-degassing method for high-throughput combinatorial polymer synthesis as it is synthetically simple and crucially does not involve the addition of persistent toxic or photo-active components (other than the chain transfer agent, which is incorporated into polymer) that may interfere with downstream assays.

We have developed a DMSO free photopolymerisation system that when paired with a liquid handling robot, enables the generation of polymer arrays in multi-well plates.

Adapting the solvent conditions enables in-plate parallel purification and easy vacuum-removal of solvent. To demonstrate the utility of this method a library of almost 400 polymers were synthesised in <40 hours within microplates using liquid handling systems. This system allows access to a wide variety of polymers with little processing and high recoveries (~10 g per plate). This does not allow for full control over molecular weight or dispersity, but enables an easy route to obtain large compositional diversity with no specific infrastructure required, to generate new lead materials for further study. We discuss the limitations of this technique in respect to monomer selectivity and polymer characteristics, as well as its use to generate a library of poly(ampholytes). The ability of these materials to act as blood cryoprotectants was evaluated using a modified high throughput assay, and the most and least active materials synthesised using traditional RAFT polymerisation, followed by determination of their IRI and cryoprotectant activity using standard assays.

4.3 Results and Discussion

4.3i High Throughput Method Development

The key goal of this study was to explore the use and limits of tertiary amine additives to enable intrinsic oxygen-degassing, using trithiocarbonates as iniferters within an easy to use system for high-throughput 'in air' polymer discovery that would be achievable without expensive infrastructure. The aim is not to make the polymers with the lowest dispersities nor the 'most controlled', but to have a method to speed up the synthesis, purification, and discovery process using multi-well plates without needing specialised infrastructure which can be easily translated to a traditional RAFT polymerisation to further probe 'hits' emerging from screening. 96-well plates are industry standard and compatible with liquid handling systems, multichannel pipettes and high-throughput biological screening, and are hence useful vessels for conducting polymerisations in.[21,22,30] Conventional radical polymerisation requires degassing, but there is no practical method to degas many plates at once. In addition, the degassing of the stock solutions and then inert atmosphere transfer, while possible, is made easier by the use a glove box or similar and hence presents a barrier to accessibility. To enable a simpler high-throughput method, poly(propylene) deep-well 96-well (2 mL/well) plates were chosen as the reaction vessels with blue light (LED) irradiation and tertiary amines, adapted from Qiao and co-workers.[39,40] In all cases no degassing of any components was employed. Pleasingly, an initial test showed the formation of polymer, proving that the system could work when open to air, but could suffer from solvent evaporation due to the heat generated by the LED lights. Therefore, reaction vessels were covered with TiterTops (a solvent resistant, adhesive plastic cover) to protect the LED lights from solvent evaporation; these are not airtight and the deep

well plates had significant headspace in each well. For initial tests, *N*-hydroxyethylacrylamide (HEA) was used as the monomer in dioxane with 2-cyano-2-propyl dodecyl trithiocarbonate (CPDTC) as the iniferter and triethanolamine (TEOA) as the tertiary amine oxygen scavenger (Figure 4.01 A).[39] These initial conditions were chosen carefully: Tertiary amine containing monomers (*e.g.* dimethylaminoethyl methacrylate) have been used previously[39,40] but for this work it was important to ensure only the additive (TEOA) could contribute to the degassing, not the monomer itself, which would increase the effective tertiary amine concentration. Dioxane was chosen as the solvent, rather than DMSO, as for library syntheses dioxane is far easier to remove under vacuum than DMSO, *vide infra*. Aqueous solutions were not suitable as that would exclude hydrophobic monomers, which are important in several screening situations, such as for antimicrobial materials.[40]

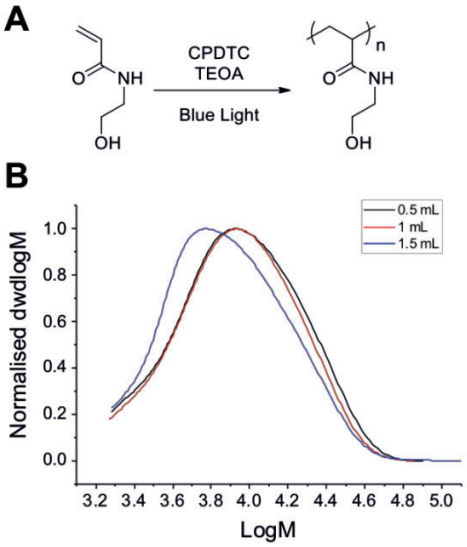

Figure 4.01: A Reaction scheme for HEA polymerisations to determine appropriate reaction volumes and TEOA concentrations; **B** MW distribution from SEC of the poly(HEA) produced to identify the effect of headspace volume on polymerisation. Samples are labelled by total volume of reaction. These samples were produced using 20 wt % monomer, 2 M TEOA, [M]:[I] ratio of 100:1 and dioxane as solvent. SEC was carried out in DMF.

Initial polymerisations were conducted with total volumes of 0.5, 1 or 1.5 mL to enable the headspace effects to be probed, as this has been found to be crucial in degassing ATRP/SET by reducing the rate of re-oxygenation.[49] Using the same stock solution for each volume, with a [M]:[Iniferter] ratio of 100:1, and [M] = 2 M we saw no substantial differences in the polymers produced (Figure 4.01 B). This suggests that total volume was not crucial and that this factor was dependent on diffusion barriers to oxygen, as has been reported by Johnson and co-workers.[50] Following this, the TEOA concentration was systematically varied. The TEOA is hypothesised by Qiao to be consumed in the oxygen scavenging mechanism by enabling electron transfer to the irradiated trithiocarbonate anion. The radical trithiocarbonate anion is then in turn oxidised through a reaction with dissolved oxygen, regenerating the neutral trithiocarbonate and reducing the oxygen to superoxide, in which the oxygen radical is present as a singlet species. This singlet oxygen species is thought to be less reactive to other radicals and is unable to terminate the polymerisation.[39] This has been shown by Boyer, and others.[50,51]

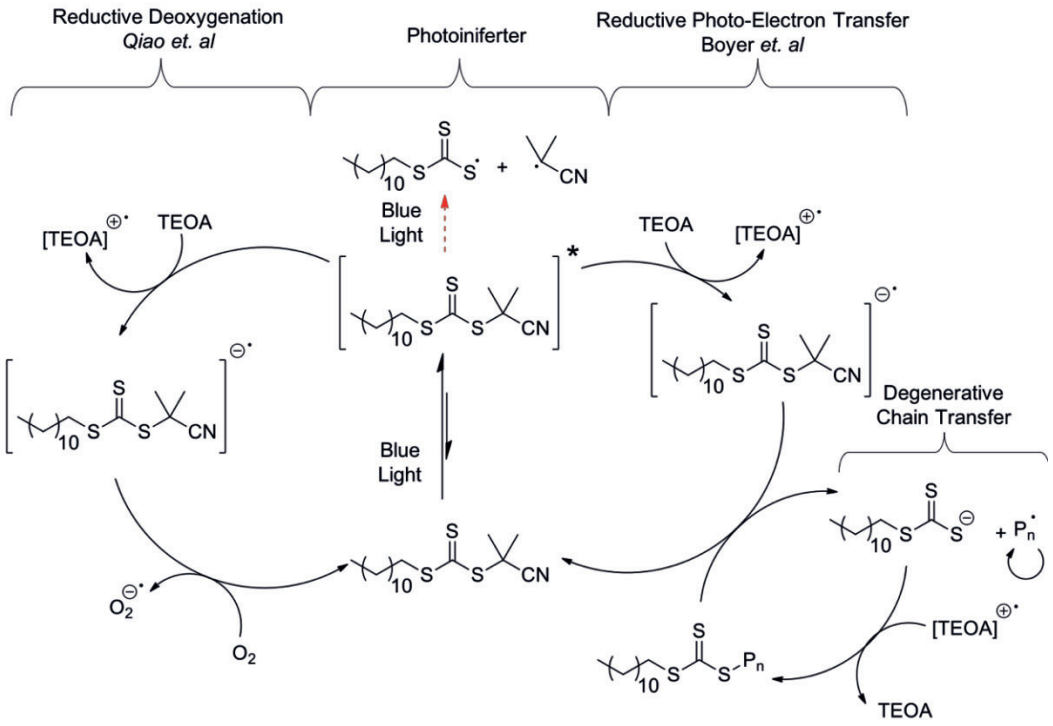

Figure 4.02: Proposed mechanism for the tertiary amine-promoted deoxygenation and propagation of the reaction. Reductive deoxygenation as proposed by Qiao,[39] and reductive photo-electron transfer as proposed by Boyer.[36] Intense blue light may also promote photolysis of the photodegradable iniferter (dashed red line) leading to an iniferter polymerisation mechanism.

Figure 4.02 summarises the reactions hypothesised to occur when the trithiocarbonate is irradiated with blue light in the presence of TEOA. It can be assumed that the reductive deoxygenation pathway is favoured when there is oxygen present, as this has been widely seen in radical polymerisations in the presence of residual oxygen, and is commonly referred to as the inhibition time; *i.e.* the time taken for any radicals generated in the system to react with oxygen, after which propagation can occur. When the oxygen concentration is sufficiently reduced, the system will then favour the reductive photo-electron transfer pathway, leading to propagation of the polymerisation *via* a degenerative chain transfer process. The ability of these trithiocarbonate species to engage in tertiary amine catalysed, photoinduced

polymerisation has been demonstrated previously in a fully degassed system.[52] In addition, it is possible that a percentage of the photodegradable iniferter undergoes direct photolysis, forming two radical species which would then propagate the polymerisation, and in a perfectly degassed system would lead to well-controlled polymer, but in an open system with residual oxygen, could terminate and become uncontrolled. We hypothesise that this may be one reason for the limited molecular weight control and dispersity seen in this system (*vide infra*).

HEA was polymerised in 0.5 mL total volume, with [M]:[I] = 100:1 and the resulting polymers characterised by SEC (Figure 4.03). Increasing the TEOA concentration from 0.22 M to 4.43 M led to a reduction in molecular weight from 13,000 to 6,000 $g.mol^{-1}$. Figure 4.02 suggests that an increased TEOA concentration would increase the concentration of both the radical anion form of the iniferter and the radical cation amine. This radical cation reduces propagation by promoting conversion of the active degenerative chain transfer species to the inert form. Polymer dispersity also reduces with the addition of more TEOA (from 2.03 to 1.45), suggesting the polymerisation is more controlled with increasing concentration of degassing agent.

One downside of a high throughput approach is that for the methodology to be useful, it must also be possible to analyse the products of the reaction in a sufficiently high throughput manner. Determining the conversion reached is usually done by NMR, however this is not ideal for the analysis of 100s of samples, therefore a representative experiment was carried out. MMA was polymerised in a standard plate experiment, however with samples removed and analysed before and after the polymerisation. Sufficiently high conversion was reported for the technique to be useful (> 90%), and therefore all future analysis was done using a high throughput SEC instrument to confirm the presence of polymer, however the exact structure was not confirmed. We

believe that this still useful for a screening methodology however, where libraries are used to inform the selection of materials of future interest, which can be synthesised by more conventional techniques and analysed more completely.

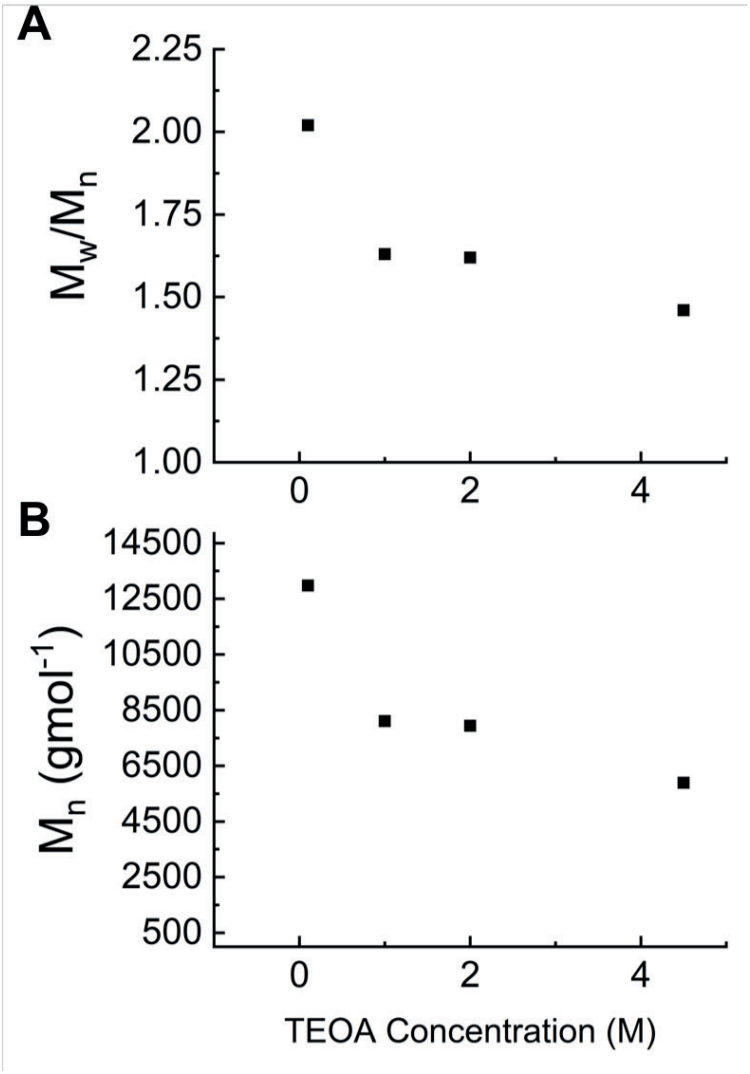

Figure 4.03: Polymerisation of HEA at 20 wt % monomer using CPDTC as the iniferter and dioxane as the solvent. A [M]:[I] ratio of 100:1 was used. TEOA concentration was varied and the resulting dispersity (**A**) and molecular weight (**B**) of the polymers produced is shown. TEOA was tested at concentrations between 0.22 M and 4.43 M at room temperature. SEC was carried out in DMF.

When no amine was present in the reaction, a small amount of very high molecular weight polymer was formed (DP >900), likely due to an incredibly fast free radical

reaction before the diffusion of oxygen into the system caused termination and no further polymerisation. This agrees with the findings of Sumerlin and co-workers, who investigated the photopolymerisation mechanisms followed by trithiocarbonates under various wavelengths of irradiation, demonstrating that in a fully degassed ideal system, trithiocarbonates follow a photoiniferter mechanism under blue light.[36] One hypothesis for the observation that lower dispersities are obtained with DMSO is that the superoxide irreversibly reacts with DMSO forming dimethylsulfone, and would be unable to reoxidise back into triplet oxygen, which could then terminate the polymerisation. In this system more TEOA is needed to continually remove oxygen, as there is no DMSO to scavenge this oxygen.[39] Control experiments using 10 % (v/v in final monomer, dioxane, iniferter, TEOA mixture) DMSO produced polymers with slightly lower dispersity (Đ = 1.86) than the DMSO free polymerisations (Đ = 2.12), but not as low as a degassed control (Đ = 1.50), suggesting DMSO provides more efficient degassing than the amine alone (Figure 4.04). However, conducting this work without DMSO is crucial to facilitate a true high-throughput approach where polymer can be easily isolated. Even higher TEOA concentrations could not be explored due to high viscosities incompatible with the liquid handling robot.

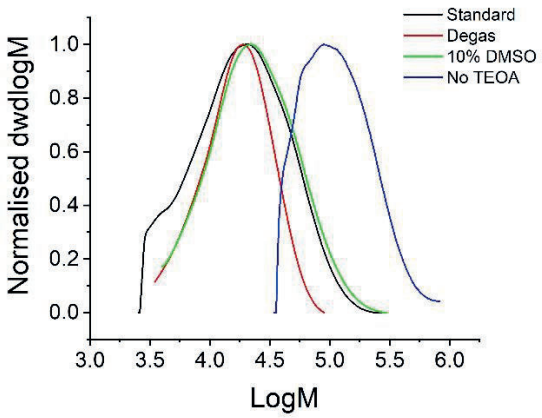

Figure 4.04: MW distributions from SEC of the PMMA synthesised in a series of control reactions. Samples are labelled according to the conditions of the reaction, a control with no iniferter produced no polymer. These samples were produced using 20 wt % monomer a [M]:[I] ratio of 100:1 and dioxane as solvent. SEC was carried out in DMF.

The data above confirms that pHEA can be obtained in dioxane (easier to remove due to its lower boiling point = 101 °C), rather than DMSO. The dispersity values are relatively high, but it is important to highlight that this is the development of a screening tool to enable quick access to 100's of polymers for initial screening, after which conventional RAFT (or other CRP methods) can be used to study the molecular weight dependent properties of the leads in detail. To explore the library-orientated approach further, 96-well plate photopolymerisations (no degassing step) were explored using a liquid handling robot system to distribute the components. For this the following monomers were used; dimethylaminoethyl methacrylate (DMAEMA), hydroxyethyl acrylamide (HEA), methyl acrylate (MA) and *N*-isopropyl methacrylamide (NIPMAM) with at least 48 repeats of each to determine uniformity and reproducibility of the product. A TEOA concentration of 2 M was used and [M]:[I] of 100:1 using CPDTC with blue light irradiation for 24 hours in the indicated solvents.

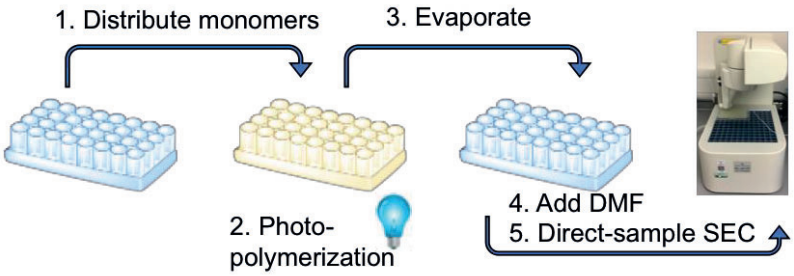

Figure 4.05: Preparation and sampling procedure for high-throughput SEC.

To enable analysis of such a large number of samples, a SEC instrument was modified in house to enable sampling directly from the 96-well plates, alongside rapid SEC columns (Figure 4.05). To facilitate data analysis and reproducibility, M_p (the molecular weight at the maximum of the peak) was extracted as this could be automatically determined by a simple spreadsheet code, whereas M_n requires more extensive data processing.

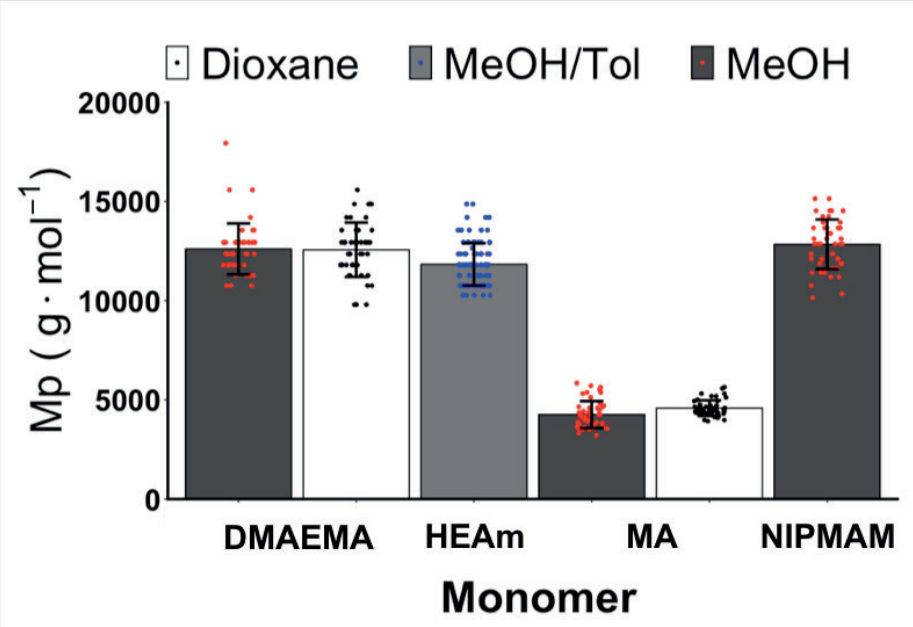

Figure 4.06: M_p of polymers obtained using indicated solvents and monomers. Individual values are shown as datapoints, the height of the bar is the mean value, and the error bars represent ± the standard error from a minimum of 48 repeats. SEC was carried out in DMF.

The results are shown in Figure 4.06 as the average as well as each individual polymer data point – this set alone contains 392 polymers, which is larger than most soluble polymer libraries.[14,23] The solvent used had little difference on the observed molecular weights, suggesting these are not involved in the oxygen scavenging (unlike DMSO), and that the system is not a free radical process, where solvent has a major effect on molecular weight. To enable detailed characterisation, five random samples from each monomer/solvent combination were selected and analysed in detail by conventional SEC (Table 4.01).

Table 4.01: Accurate polymer analysis for solvent and monomer versatility determination.

Monomer	Solvent	M_n (g.mol^{-1})[a]	M_w (g.mol^{-1})[b]	Đ (-)[c]
DMAEMA	MeOH	7400	12000	1.60
		5800	9800	1.68
		7600	11200	1.47
		7300	11800	1.61
		6300	10800	1.74
	Dioxane	6600	11800	1.78
		6300	11300	1.77
		7100	13,000	1.87
		6300	11200	1.77
		6500	12000	1.83
HEA	1:1 MeOH/Tol	5600	10800	1.91
		5400	10200	1.91
		7300	13300	1.82
		6000	12000	1.91
		5000	9400	1.88
MA	MeOH	4800	5900	1.23
		4300	5100	1.19
		4200	5900	1.23
		4700	5600	1.19
		4200	4800	1.14
	Dioxane	3900	4400	1.11
		3900	4300	1.09
		4000	4500	1.10
		4000	4800	1.19
		4200	4800	1.15

(a) M_n is number average molecular weight from SEC; **(b)** M_w is weight average molecular weight from SEC; **(c)** Đ is M_w/M_n from SEC. SEC was carried out in DMF. No M_n(theo) is reported as conversion was not determined for these samples.

This confirmed that there was little variation from sample to sample. In the case of methyl acrylate, lower dispersities (Đ <1.2) were observed than the other polymers (Đ >1.5), most likely due to the higher rate of polymerisation typical of acrylates, meaning that there was less termination due to reaction with reformed oxygen and hence this method might be particularly useful for acrylates. As all previous reactions had been carried out at a single [M]:[I] ratio (100:1), the ability of this technique to target varying molecular weights was investigated. A range of other monomers covering the most common types were explored (methacrylate, acrylate, acrylamide, methacrylamide); methyl methacrylate (MMA), MA, *N*-isopropylacrylamide (NIPAM) and *N*-isopropylmethacrylamide (NIPMAM) were selected, again avoiding tertiary amine containing species. Polymers were prepared using 20 wt % monomer, in 0.5 mL total volume, and dioxane as the solvent, with a [M]:[I] ratios of 100:1 and 50:1, and a final TEOA concentration of 2 M. After 24 hours irradiation, polymers were analysed using high-throughput SEC (Figure 4.07).

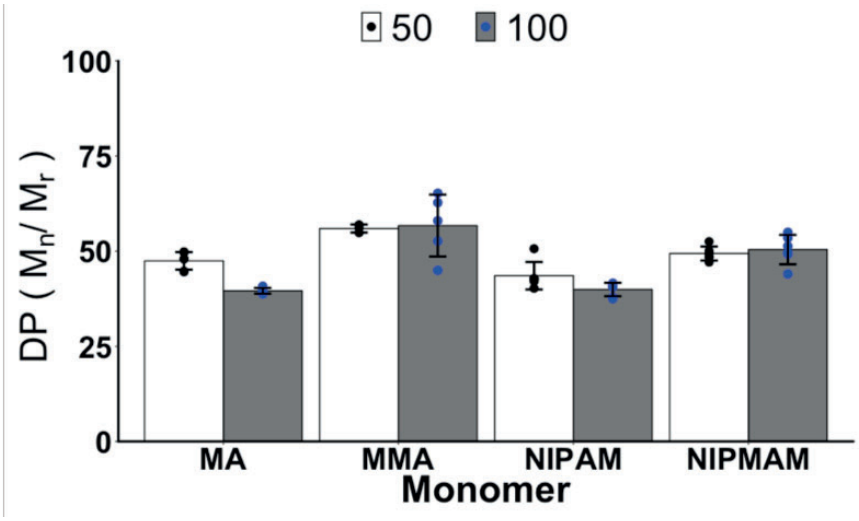

Figure 4.07: Obtained DP vs targeted DP (from feed ratio) for a range of monomers, M_r is the molecular weight of the monomer. Individual values are shown as data points, the height of the bar is the mean value, and the error bars represent ± the standard error from a minimum of 5 repeats. SEC was carried out in DMF.

Across the four monomers selected, there was no difference between the molecular weights of the polymers resulting from each [M]:[I] ratio tested and therefore this lack of molecular weight control required further investigation. One method by which control could be introduced is by reducing the initiator concentration, (which in this case is also the chain transfer agent) decreasing the rate of termination and therefore providing better control over the products of the reaction. However, if trithiocarbonate concentration is reduced too much, irreversible deactivation of the chain transfer agent can occur.[53] Methyl methacrylate was polymerised at varying monomer concentrations from 20 to 2.5 wt %, covering a range of initiator concentrations from 0.04 M to 0.001 M. While slightly lower dispersities were observed in samples made at lower monomer concentrations, again little molecular weight control was observed. Figure 4.08 shows the polymer DP vs targeted DP from the high throughput SEC system, while table 4.02 shows SEC data from one sample of each run on a standard SEC system.

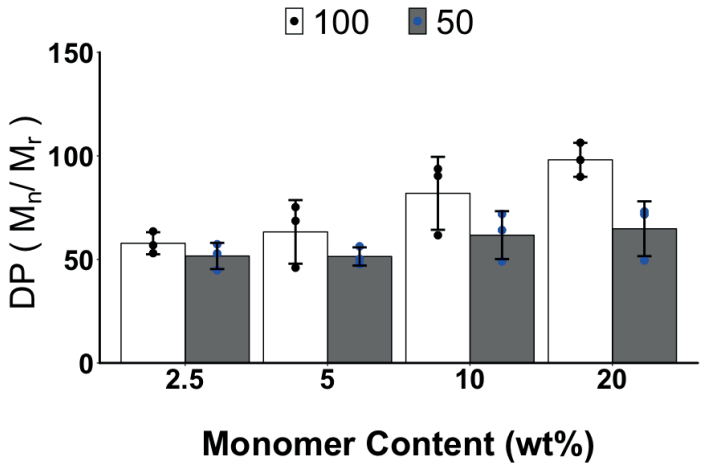

Figure 4.08: Obtained degree of polymerisation for PMMA samples made with varying monomer content, using indicated [M]:[I] ratios. Polymers were made in deep well plates with a final TEOA concentration of 2 M, with dioxane as solvent. Individual values are shown as data points, the height of the bar is the mean value, and the error bars represent ± the standard error from a minimum of 3 repeats. SEC was carried out in DMF.

Table 4.02: SEC data for PMMA samples made with varying monomer contents.

Concentration (wt %)[a]	[M]:[I] (-)[b]	M_n (g.mol^{-1}) [c]	M_w (g.mol^{-1})[d]	Đ (-)[e]
20 %	50	5600	10000	1.84
	100	8400	20000	2.32
10 %	50	6300	12000	1.98
	100	8500	18000	2.12
5 %	50	5300	9800	1.89
	100	7300	14000	1.96
2.50 %	50	5600	11000	1.93
	100	8900	15000	1.69

(a) Wt % monomer present in initial reaction solution; **(b)** Monomer to initiator/chain transfer agent ratio; **(c)** M_n is number average molecular weight from SEC; **(d)** M_w is weight average molecular weight from SEC; **(e)** Đ is M_w/M_n from SEC. SEC was carried out in DMF. No M_n(theo) is reported as conversion was not determined for these samples.

In order to ensure that the initiation was not due to side reactions of another species, therefore altering the [M]:[I] ratio and hence the molecular weight of the polymer, a control experiment with no iniferter was carried out, this afforded no polymer after 24 hours irradiation. These observations agree with the findings of both Qiao[54] and Boyer;[31] that only the efficient and irreversible removal of dissolved oxygen can enable a truly controlled/living polymerisation, and that a dynamic system that allows triplet oxygen to reform will always suffer from termination events.

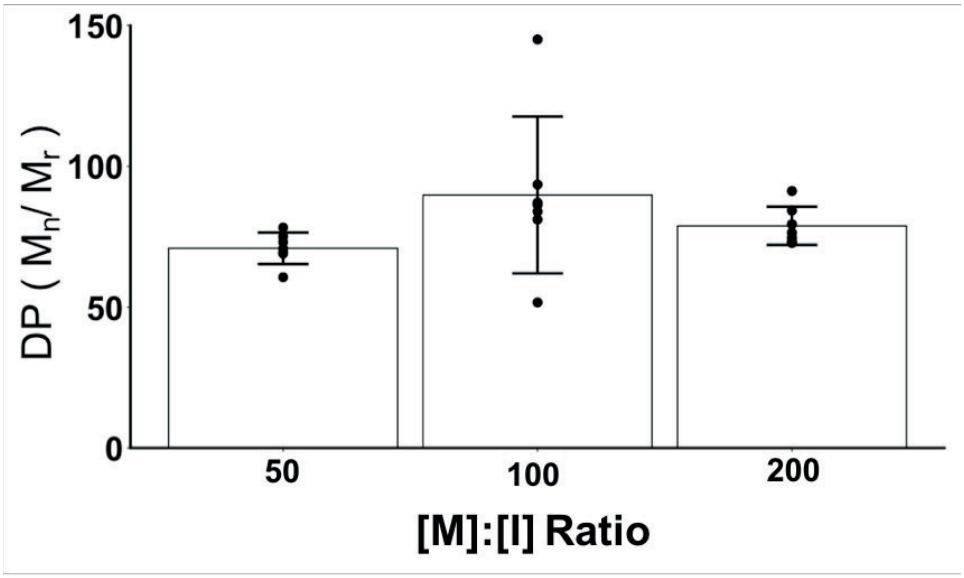

Figure 4.09: Obtained degree of polymerisation for polymers made with a constant radical concentration. All reactions had a final iniferter concentration of 0.02 M, and monomer content was varied accordingly to target three different [M]:[I] ratios. Individual values are shown as data points, the height of the bar is the mean value, and the error bars represent ± the standard error from a minimum of 5 repeats. SEC was carried out in DMF.

To further investigate the effect of radical concentration, reactions with the same total radical concentration (*i.e.* initiator concentration) were carried out, varying the monomer concentration to target different molecular weights. This should allow for

identical rates of radical generation across all targeted [M]:[I] values. Again, little control over the polymerisation was observed, with polymers from all three reaction conditions generating materials of similar molecular weight and dispersity (Table 4.03). Previous photoiniferter polymerisations of acrylates have found that using a constant radical concentration and variable monomer concentrations allowed multiple molecular weights to be accessed. The reported polymerisations demonstrated an initial linear character, however deviation from this behavior was observed at higher conversions due to unidentified side reactions leading to termination.[55] Photoiniferter polymerisations using NIPAM and MAA have also demonstrated this two stage kinetic process, with an initially living character up to ~60 % conversion, after which termination reactions dominate and significantly slow the observed molecular weight increase.[56,57] These side reactions, along with those which occur as a result of reformed oxygen, may lead to the lack of molecular weight control observed here, and therefore the kinetics of the polymerisation was investigated further.

Table 4.03: SEC Data for PMMA samples made at a constant radical concentration.

[M]:[I] (-)[a]	M_n (g.mol^{-1})[b]	DP (-)[c]	Đ (-)[d]
50	7800	78	1.75
	7300	73	1.64
	7500	75	1.69
	7000	70	1.73
	6100	61	1.72
	6900	69	1.73
	7100	71	1.78
100	5200	52	1.39
	15000	150	1.55
	8100	81	1.81
	8600	86	1.92
	8700	87	1.89
	9400	94	1.95
	8400	84	1.99
200	8000	80	1.62
	7700	77	1.47
	7500	75	1.49
	7300	73	1.44
	7300	73	1.39
	8500	85	1.71
	9100	91	1.58

(a) Monomer to iniferter ratio; **(b)** M_n is number average molecular weight from SEC; **(c)** DP is M_n/M_r **(d)** Đ is M_w/M_n from SEC. SEC was carried out in DMF. No M_n(theo) is reported as conversion was not determined for these samples.

Polymers were prepared as before, with the addition of a small amount of DMF as an internal NMR standard. Using methyl methacrylate at 20 wt % in dioxane at two [M]:[I] ratios (100 and 50), it was found that within 24 hours conversion had reached

90 %, with 99 % reached after 28 hours. This ensures that there is little monomer remaining, which is important for the polymerisation of high boiling point materials, as the monomer may have adverse effects on assays using material directly sampled from the plates. Kinetic plots are shown in Figure 4.10, and display a sharp initial increase in molecular weight at low conversion, which suggests slow initiation (*i.e.* the majority of irradiated RAFT agent is initially employed converting oxygen to superoxide), and a non-linear increase in molecular weight with conversion infers that the polymerisation is likely following a free radical mechanism. The eventual slowing of $Ln[M_0/M_t]$ suggests an increase in the rate of termination after 5 hours, possibly due to superoxide reverting to the triplet state and interfering with the reaction, paired with the loss of control associated with high conversion iniferter polymerisations discussed above. The latter is consistent with other reports of iniferter reactions in which side reactions dominate later timepoints, even in fully degassed systems. It is important to again note, that for combinatorial approaches full conversion (ensuring no residual monomer) is more important than stopping the reaction during the linear phase but having to then add a purification step.

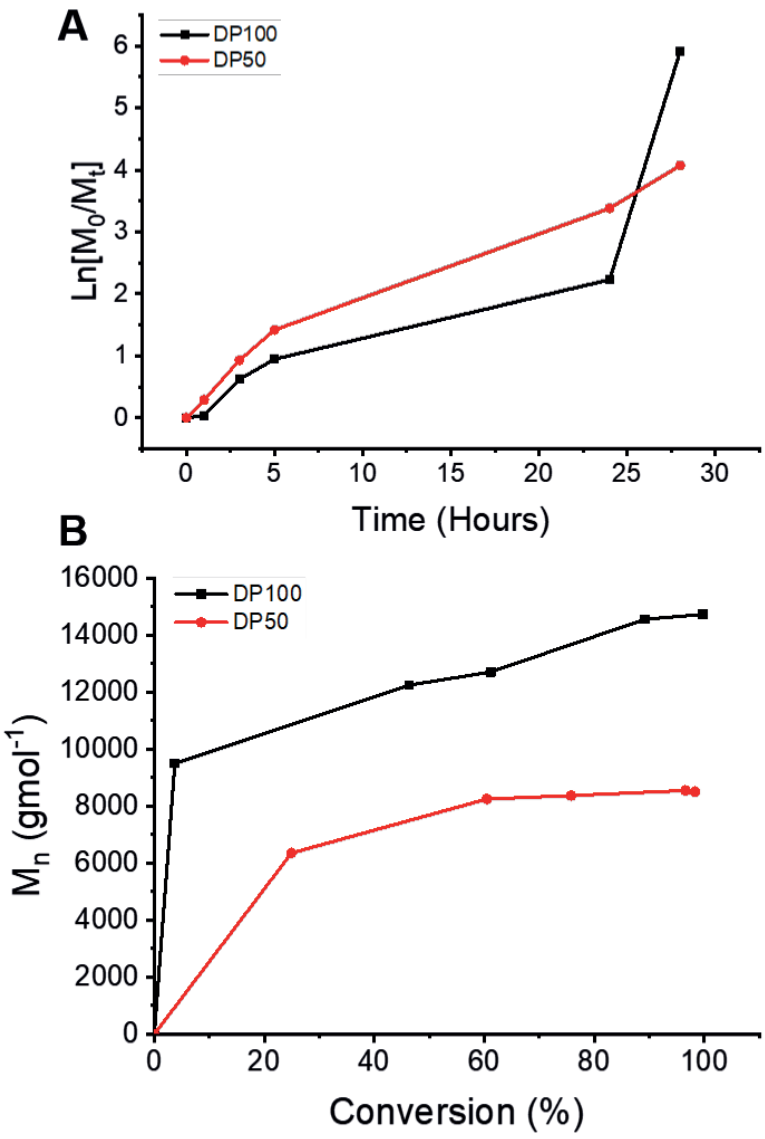

Figure 4.10: Kinetic plots for the polymerisation of MMA at 20 wt % monomer in dioxane, using CPDTC as the iniferter and a final TEOA concentration of 2 M. **A** Semi-logarithmic plot; **B** Evolution of M_n versus conversion. M_n was determined by SEC in DMF.

The above results show that the photoiniferter method can be used for high throughput polymerisations of a range of monomer types without the need for DMSO, assuming control of molecular weight by variation of [monomer]:[iniferter] is not essential – which is true for many screening applications but this point must be taken into account when using this protocol. However, a key reason for moving from DMSO was to

facilitate a simple and in-plate isolation of the polymers, as the dialysis of hundreds of polymers is not straightforward. There is also the need to remove TEOA for most applications (although not always essential depending on the concentration required for subsequent testing)[40] to enable isolation of pure polymer. Addition of HCl in organic solvent precipitates the TEOA as the insoluble salt, leaving the polymer dissolved in the dioxane/HCl mix, and the 96-well plate can be centrifuged followed by simple removal of the supernatant by liquid handling robot or similar, followed by drying. Figure 4.11 shows ^{1}H NMR spectra of precipitated TEOA and supernatant polymer, showing essentially quantitative removal in a single step which is again compatible with our approach of only using liquid handing robot at each step.

As an alternative to TEOA, triethylamine (TEA) was explored as the tertiary amine scavenger with a lower boiling point. In a trial experiment after 24 hours, MMA polymerisations in 2 M TEA reached 80 % conversion. TEA has a much lower boiling point (89 °C *vs* 335 °C for TEOA) and can be easily removed by drying the polymer plates under vacuum. It is important to note that due to the heat generated by lights, additional cooling is required during the polymerisation to prevent evaporation of the amine. These polymerisations were successfully conducted by cooling the plate using a thermocycler but this is an important consideration to ensure successful polymerisation. An advantage of this process is that it also removes any solvent from the reaction allowing isolation of polymer in a single step.

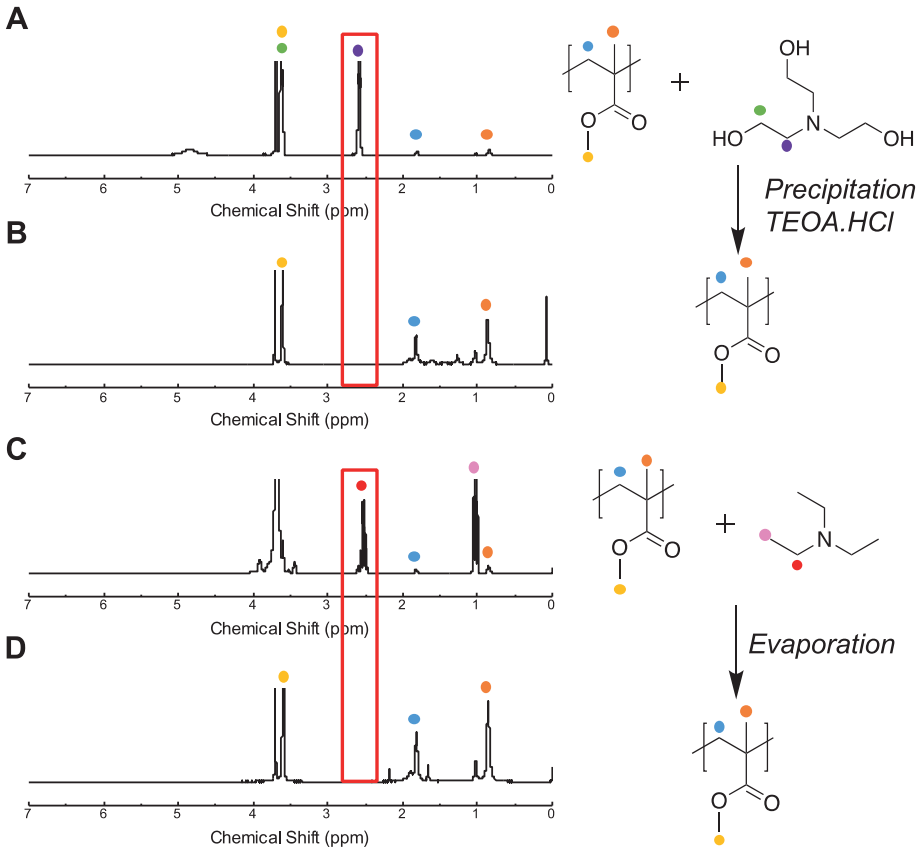

Figure 4.11: Oxygen scavenger removal demonstrated by ^{1}H NMR spectroscopy ($CDCl_3$). **A** PMMA and TEOA; **B** PMMA and TEOA supernatant after the addition of HCl; **C** PMMA and TEA; **D** PMMA and TEA after drying under vacuum for 24 hours. The peak at 3.70 ppm is residual dioxane. The highlighted area (red box) shows the region in which the characteristic $(CH_2)_3N$ peak is located.

4.3ii Synthesis of a Library of Poly(ampholytes)

Given the ease with which this method allows the generation of a large number of polymers with wide diversity, we decided to use this technique to investigate the effect of polymer composition on poly(ampholyte) cryoprotectant activity. As with previous ampholyte polymers, dimethylaminoethyl methacrylate and methacrylic acid were chosen as the cationic and anionic component respectively. Attempts to incorporate a permanently charged [2-(Acryloyloxy)ethyl]trimethylammonium chloride monomer

into the chain afforded no conversion, and this was not investigated further. The rate of polymerisation of these two monomers was studied for a 50:50 sample over 8 hours, after which full monomer conversion (>99.9 %) was observed (Figure 4.12). As can be seen from the first order kinetic plot, there is a significant induction period at the start of the reaction, likely caused by the degassing phase of the reaction. DMAEMA was converted more quickly, suggesting that the resulting polymer will have a gradient microstructure, however methods to prevent this such as a monomer feed would be impractical in a plate, more important for this screening methodology was that full conversion of both monomers was successfully observed.

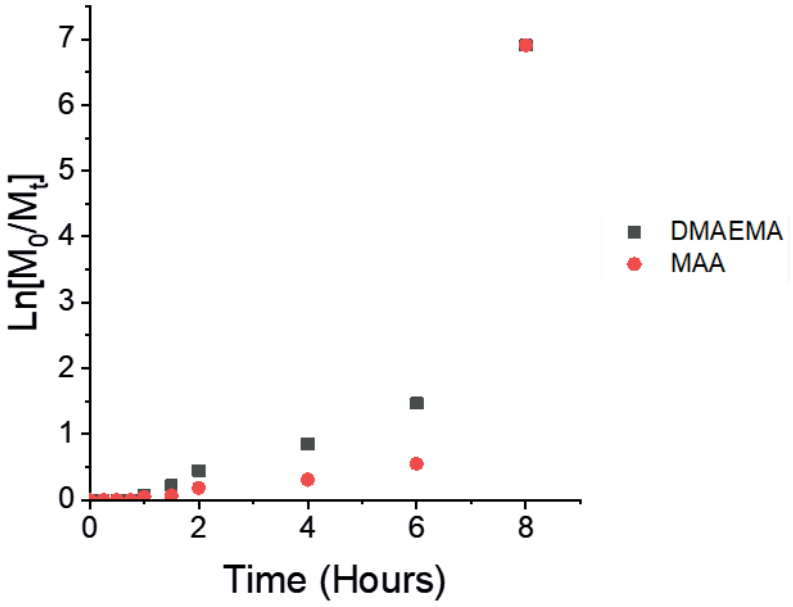

Figure 4.12: First order kinetic plot for the copolymerisation of DMAEMA and MAA.

Once it was demonstrated that this method enabled full conversion of both monomers under blue light irradiation, the effect of TEOA concentration on cryoprotectant activity was investigated. This is essential to ensure that samples can be taken directly from the reaction mixture for high throughput testing. TEOA concentrations were tested using 100 mg.mL^{-1} of a dimethylamino ethanol ring opened poly(methyl vinyl

ether-*alt*-maleic anhydride) copolymer using concentrations of up to 1 M TEOA. At all concentrations tested, addition of TEOA did not result in a notable reduction in RBC recovery post thaw (Figure 4.13). TEOA is widely reported to be non-toxic,[58,59] however concentrations as high as 1 M would be expected to cause some level of cell damage. This could however be causing the same hypertonic damage as observed by the blood cells using high salt concentrations,[60] whereby crenation of the cell results in cell damage but without release of hemoglobin into the supernatant.

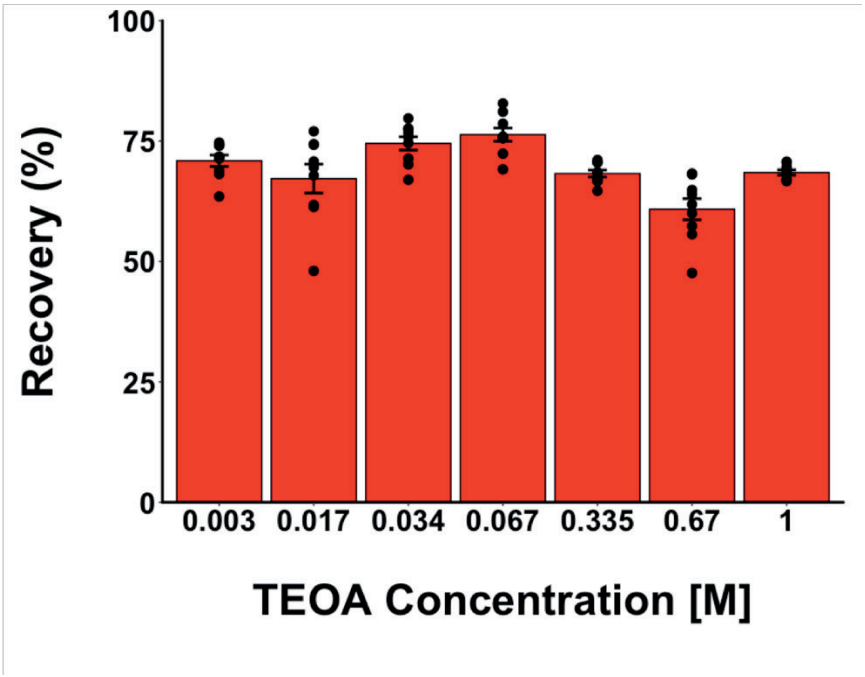

Figure 4.13: The effect of TEOA concentration on blood cell recovery after incubation for 30 minutes, followed by cryopreservation using a known poly(ampholyte). Individual values are shown as data points, the height of the bar is the mean value, and the error bars represent ± the standard error from a minimum of 6 repeats.

Due to the charged nature of these materials, the pH at which they are tested must also be considered, as this can greatly affect the protonation/deprotonation of the monomers. It was determined that to correct the pH of the final dissolved polymers

(synthesised in a 0.5 M TEOA solution, pH ~10) to pH 7.4, addition of 0.5 mL PBS corrected to pH 0.3 was required. An initial plate of polymers were synthesised using 0.5 M TEOA (final cryopreservation assay concentration 0.18 M, within the range tested), with 10 % increments of DMAEMA:MAA from 70:30 to 30:70 being used. Polymers were prepared using a liquid handling robot in dioxane, and reacted for 24 hours, followed by drying. 2 samples of each combination were agitated in DMF for 24 hours, after which they were analysed by SEC. As MAA content increased, samples became less DMF soluble, and therefore these materials gave a much lower intensity response in the SEC (Figure 4.14).

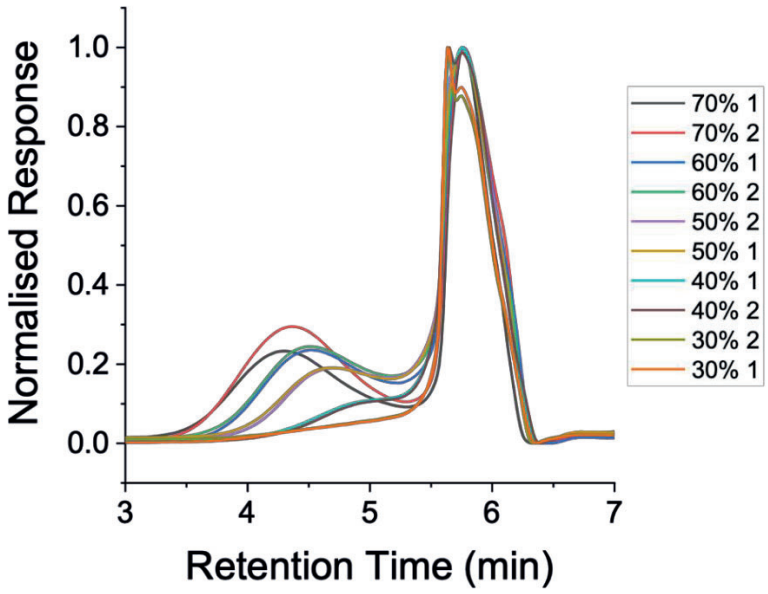

Figure 4.14: Retention time vs normalised RI for the samples tested, SEC was carried out in DMF with a flow rate of 2 ml/min using a single PL: Rapide F column. Samples are named according to the DMAEMA content, with two samples of each composition being analysed. The peak between 5.50 and 6.30 minutes is the solvent peak.

The remaining 14 samples of each material were dissolved in 0.5 mL pH 0.3 PBS and made up to 700 µL using standard PBS to give a final polymer concentration of 142

mg.mL^{-1}, and final pH of 7.4. These samples were then tested for cryoprotectant activity using a blood freezing assay modified for high throughput testing. As can be seen from the results (Figure 4.15), increased DMAEMA content resulted in increased recovery, however above 50%, no statistically significant difference was observed between the samples ($P < 0.05$). When the pKa of the monomers is considered relative to the pH of the solution, it was estimated that a 50:50 ratio of charges is obtained at an initial monomer content of between 50 % and 60 % DMAEMA. The calculated percentage of charged units for each monomer type and at each feed ratio is shown in Table 4.04.

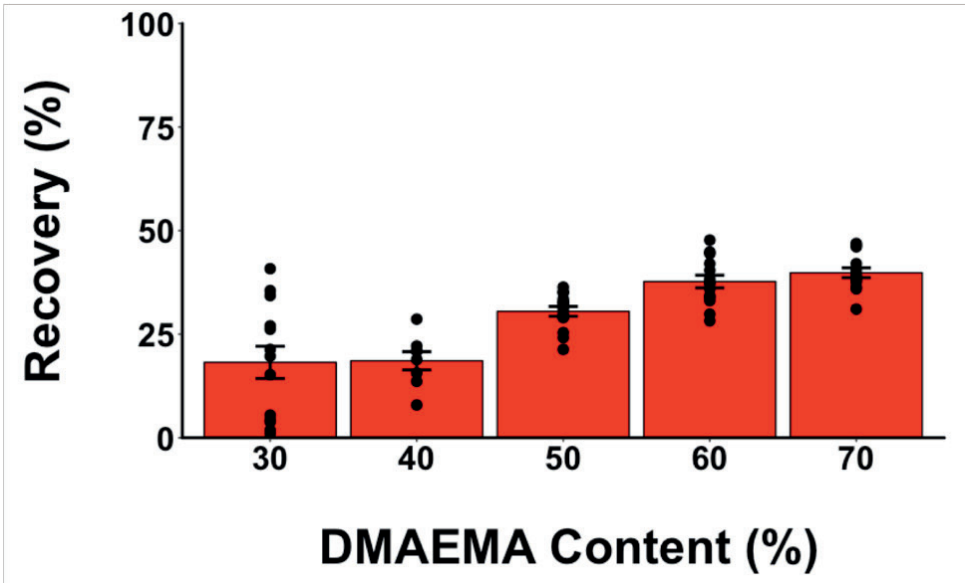

Figure 4.15: The effect of polymer composition on blood cell recovery at 71 mg.mL^{-1}. Polymers were copolymers of DMAEMA MAA. Individual values are shown as data points, the height of the bar is the mean value, and the error bars represent ± the standard error from a minimum of 12 repeats.

Table 4.04: Calculated percentage of charged units for each monomer type at the monomer feed ratios tested and a solution pH of 7.4.

Monomer Ratio[(a)]	DMAEMA		MAA
	Charged (%)[(b)]	Neutral (%)[(c)]	Charged (%)[(d)]
70:30	63	7	30
60:40	54	6	40
50:50	45	5	50
40:60	36	4	60
30:70	27	3	70

(a) Ratio of monomers in initial feed, DMAEMA:MAA respectively; **(b)** percentage of charged units of DMAEMA present relative to the whole polymer using a pKa value of 8.4;[61] **(c)** percentage of uncharged units of DMAEMA present; **(d)** percentage of uncharged units of MAA present relative to the whole polymer using a pKa value of 4.9.[62]

Of the polymer compositions tested, $DMAEMA_{70\%}MAA_{30\%}$ and $DMAEMA_{60\%}MAA_{40\%}$ were the most active, displaying essentially the same activity. In order to try and maintain the most equal ratio of monomers in the feed, $DMAEMA_{60\%}MAA_{40\%}$ was chosen for further investigations. Twelve possible comonomers were selected and incorporated in concentrations from 2-20 % at 2 % intervals, generating 120 different poly(ampholytes). These samples were again made up to 700 μL at pH 7.4 and tested in triplicate using the same high throughput assay as before. Unfortunately, one plate (containing 60 of the samples) gave inconsistent results for the PBS control used as 0 % lysis, and therefore this plate was omitted from further analysis. The results are shown below in Figure 4.16. Plotting LogP of each polymer vs the recovery showed no correlation between hydrophobicity and recovery. (Figure 4.26)

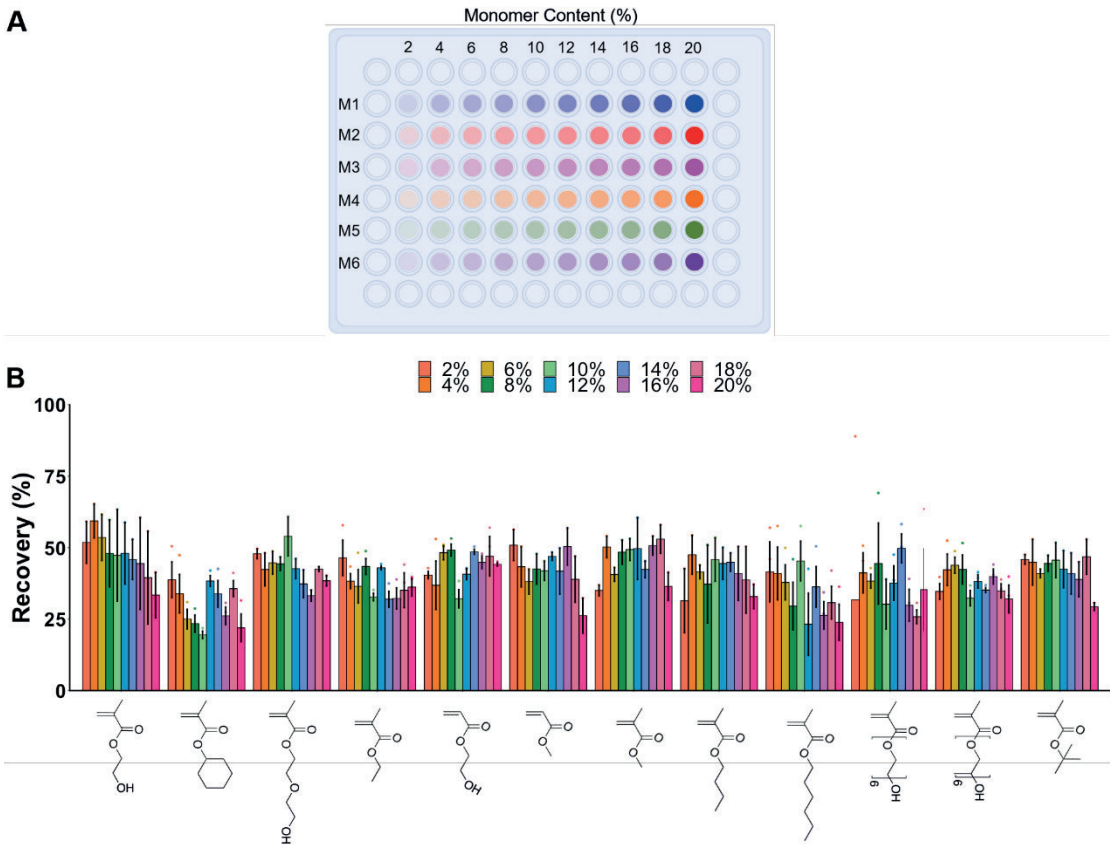

Figure 4.16: A Schematic of the polymer libraries produced in 96 well plates. Each row corresponds to a different termonomer (M1 – M6), with each column containing a different termonomer content (2 to 20 %); **B** Red blood cell cryoprotectant activity of a library of 120 ampholytes screened as part of this work. Bars are coloured according to the % incorporation of the termonomer shown. Individual values are shown as data points, the height of the bar is the mean value, and the error bars represent ± the standard error from a minimum of 2 repeats.

Whilst all samples appear to become less active as termonomer content is increased, some samples appear to have enhanced activity with inclusion of a small amount of termonomer. 2-Hydroxy ethyl methacrylate (HEMA) appeared to show the most significant enhancement, with the 4 % sample showing a 20 % improvement over the copolymer alone. Statistical analysis identified 497 significant differences ($P < 0.05$), with the largest and most significant ($P = 0.0002$) being between these two materials.

The terpolymer containing 10 % cyclohexyl methacrylate appeared to show the least activity. These results are in stark contrast to the findings of Matsumura, who found that in a copolymer of 1:1 DMAEMA:MAA the addition of 5% hydroxyethyl methacrylate significantly reduced the viability of L929 cells post thaw, when compared to the initial copolymer. Conversely, the incorporation of 5% octyl methacrylate, a significantly more hydrophobic monomer, led to an increase in post thaw viability.[48] These results suggest that the optimal features required for cryopreservation of red blood cells may be different to those required for nucleated cells.

Further investigation of these materials is required to ensure that these results are due to the material itself, and not an unintended side product formed during the high throughput process. This screening methodology should not be used without further investigation of materials made *via* conventional methods due to the lack of characterisation data for the plated materials. Three different molecular weights of 4 % HEMA terpolymer, as the most active, were synthesised using standard, thermally initiated and fully degassed RAFT polymerisation, along with one sample of 10 % cyclohexyl methacrylate (the worst performing polymer). The remainder of the monomer feed was made up of a 60:40 mix of DMAEMA MAA. These samples were tested for IRI activity, as well as on a larger scale blood experiment to determine the validity of this screening process and evaluate its ability to provide new potential lead compounds. To ensure that all monomer had been incorporated, polymerisations were carried out to high conversion (>95 % in all cases).

The molecular weight of the resulting polymers was determined by SEC in DMF, which showed there to be very little difference in molecular weight between the samples made at [M]:[I] ratios of 100:1 and 200:1. This is possibly due to DMF not

being an ideal solvent for these samples, and therefore initial dissolution and filtering as part of the sample preparation may have removed higher molecular weight material. Characterisation data is shown in Table 4.05.

Table 4.05: 'Hit' polymers synthesised as a result of preliminary library investigations.

Polymer[(a)]	**[M]/[I] (-)[(b)]**	**Conversion (%)[(c)]**	**M_n (Theoretical) ($g.mol^{-1}$) [(d)]**	**M_n (SEC) ($g.mol^{-1}$) [(e)]**	***Đ*[(f)]**
4% $HEMA_{50}$	50	100	6,400	10,000	1.48
4% $HEMA_{100}$	100	97	12,000	15,000	1.57
4% $HEMA_{200}$	200	98	25,000	15,000	1.84
10% $CyMA_{100}$	100	96	12000	16,000	1.39

(a) Sample names are determined according to the termonomer used, and the [M]:[I] ratio of the initial monomer feed; **(b)** Monomer to Iniferter molar ratio; **(c)** Determined by ^1H NMR using DMF as an internal standard; **(d)** Determined from feed ratio and conversion; **(e)** Determined by SEC; **(f)** Đ is M_w/M_n from SEC. SEC was carried out in DMF.

Once the polymers had been synthesised, they were tested for both cryoprotectant activity and IRI activity, in order to see if there was again any correlation. Whilst all polymers showed weak activity, there appeared to be little difference in IRI activity between the most active 4% HEMA containing material (32 % MGS) , and the least active CyMA containing species (41 % MGS). IRI data is shown in Figure 4.17.

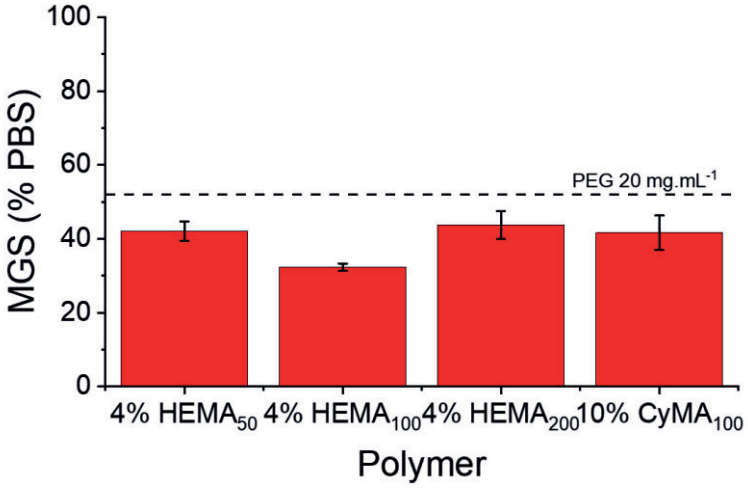

Figure 4.17: IRI activity of the 'hit' polymers produced in this work. PEG at 20 mg.mL^{-1} is included as an example of a negative control. MGS = Mean grain size reported as an area. The height of the bar is the mean value, and the error bars represent ± the standard deviation from a minimum of 3 repeats.

These polymers were then tested for cryoprotectant activity using the standard blood testing assay at two concentrations of 100 and 50 mg.mL^{-1}. The results are shown in Figure 4.18. 4 % $HEMA_{200}$ appears to be the most active cryoprotectant, with the highest recovery at both concentrations tested, while the worst sample from the initial screen, the 10 % cyclohexyl methacrylate polymer, gave the lowest average recovery at both concentrations. Interestingly, the most IRI active sample corresponded to the lowest recovery, reinforcing the findings using poly(methyl vinyl ether-*alt*-maleic anhydride) based ampholytes, suggesting that the IRI activity of these materials is not indicative of the cryoprotectant effectiveness.

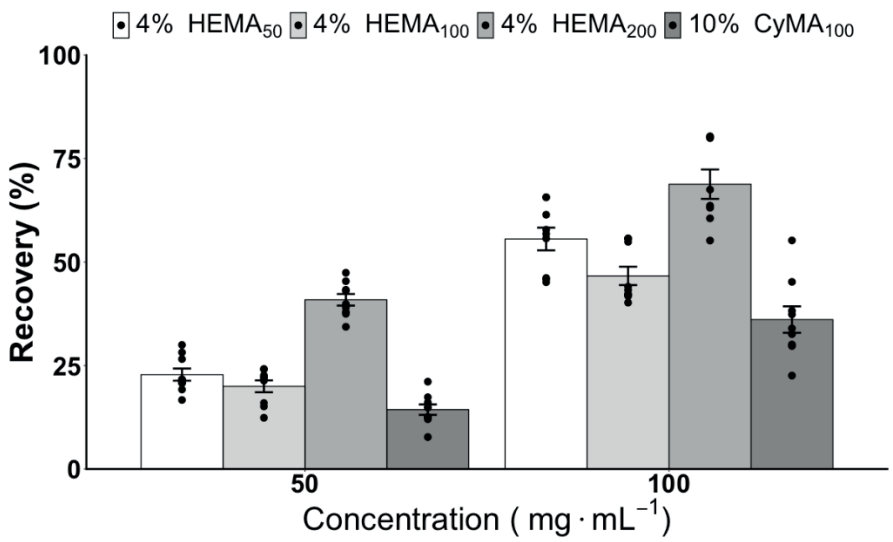

Figure 4.18: Cryoprotectant activity of the polymers synthesised using standard RAFT polymerisation, guided by the results of the poly(ampholyte) library. Individual values are shown as data points, the height of the bar is the mean value, and the error bars represent ± the standard error from a minimum of 9 repeats.

Red blood cell cryopreservation is a simple, low cost screening procedure for the identification of materials which may act as effective cryoprotectants for nucleated cell storage. Poly(ampholytes), which are known to be highly active cryoprotectants, have the potential to occupy a massive chemical space, and therefore being able to synthesise and identify the most active materials drastically increases the efficiency of the workflow, allowing large numbers of samples to be tested in a relatively short time frame. This is in contrast to cryopreservation assays using nucleated cells, which often require multiple days to screen a small concentration range of a single material. Evaluating the activity of the most and least active materials found here using nucleated cells, will allow the impact of high throughput RBC screening to be further evaluated, however these experiments have not yet been conducted.

4.4 Conclusion

Here we demonstrate a useful, but easily accessible, method to enable the synthesis of large polymer libraries within multi-well plates simply using blue light and tertiary amines as intrinsic deoxygenators. Using this method, ~ 400 polymers were made in <40 hours, and is easily scalable to larger libraries. The role of the tertiary amine was investigated and shown that high concentrations provided polymers with a narrower molecular weight distribution. Whilst this method uses a 'RAFT' agent, it is clear that this reaction has the hallmarks of an iniferter mechanism, with high degrees of termination at higher degrees of conversion. The possibility of the reaction to proceed in tandem *via* a reductive photo-electron transfer (PET-RAFT) mechanism further complicates any attempt at confirming a mechanism and optimising the system to deliver predictable molecular weight distributions. Hence control over the system in terms of predictable molecular weight from [Monomer]/[Iniferter] ratios is limited, but for certain monomer classes (*i.e.* acrylates) low dispersity can be achieved. We therefore propose that this technique is a starting point for the synthesis of a library of polymers with varying monomer composition that does not require any complex purification, for rapid screening. Once the monomer composition leads have been identified, standard living/CRP techniques can be used to investigate the effect of molecular weight on the lead polymers. This approach requires far fewer polymers to be made to screen a reasonable molecular weight range and would be suitable for many biological screening applications where monomer composition of the polymer usually is the primary differentiator of function. The reproducibility of the method was tested by running >40 repeats of each monomer/solvent combination. Using a modified plate-sampling SEC system, the variance was shown to be small and the position of the reaction in the 96-well plate had no effect on its outcome, which is crucial for

screening. Dioxane was found to be a suitable solvent, with the advantage that it is easy to remove by simple evaporation at the end of the reaction. It was also shown how the tertiary amines (triethanolamine and triethylamine) can be removed from the product using a single-step purification in-plate enabling isolation of pure polymers, which is not easily achieved by other in-plate methods. The power of this method lies in its simplicity, rapidity, and scalability to enable libraries of differently functional polymers to emerge to screen for function.

This technique was then used to enable the synthesis of a library of poly(ampholyte) terpolymers which, when paired with high throughput blood screening, allowed the identification of a small number of potential lead compounds for further development. These species were synthesised using standard RAFT polymerisation and tested for both cryoprotectant and IRI activity, as found previously, IRI activity was observed to be a poor indicator of cryoprotectant activity for poly(ampholytes).

In order to develop these findings further, nucleated cell assays are required. The work presented here has suggested that, for poly(ampholytes) at least, IRI activity is not necessarily a good indicator of cryoprotectant activity. To investigate this finding fully, future assays using nucleated cells are required to compare the cryoprotective activity of both highly IRI active materials, and those which display little IRI activity, but excellent blood recovery. The findings of this future work would enable the validity of these initial observations to be explored further.

4.5 Experimental

Materials

N-Hydroxyethyl acrylamide (97 %), methyl methacrylate (99 %), methyl acrylate (99 %), *N*-isopropylacrylamide (97 %), *N*-isopropylmethacrylamide (97 %), 2-(dimethylamino)ethyl methacrylate (98 %), 2-Hydroxyethyl methacrylate (97 %), di(ethylene glycol) methyl ether metharylate (95 %), ethyl methacrylate (99 %), hydroxyethyl acrylate (96 %), ^{n}butyl methacrylate (99 %), poly(ethylene glycol) methyl ether methacrylate and poly(propylene glycol) methyl ether methacrylate, triethanolamine (TEOA) (98 %), triethylamine (TEA) (>99.5 %), 2-cyano-2-propyl dodecyltrithiocarbonate (97 %), 2,2'-azobis(2-methylpropionitrile) (98 %) and all solvents were purchased from Sigma-Aldrich and used without further purification. were purchased from Sigma-Aldrich. Cyclohexyl methacrylate (97 %) and hexyl methacrylate (97 %) were purchased from Acros. All monomers were filtered through a plug of basic alumina to remove inhibitors prior to use. Alkaline Haematin D-575 (AHD) solution is made up of 0.4 g sodium hydroxide, and 2.5 g Triton X-100 dissolved in 100 mL deionised water.

Physical and Analytical Methods

^{1}H NMR spectra were recorded on Bruker DPX-300 and DPX-400 spectrometers using deuterated solvents purchased from Sigma-Aldrich. Chemical shifts are reported relative to residual non- deuterated solvent. Infrared data was recorded on a Bruker Vector 22 GI003097. SEC was carried out in DMF and run on an Agilent 1260 Infinity II- MDS instrument equipped with differential refractive index (DRI), Viscometry (VS), Light scattering (LS) and variable wavelength UV detectors,. The system was equipped with 2 x PLgel Mixed D columns (300 x 7.5 mm) and a PLgel 5 μm guard

column. The eluent was DMF with 5 mM NH_4BF_4 additive. Samples were run at 1 $mL.min^{-1}$ at 50 °C. Poly(methyl methacrylate) (Agilent EasiVials) were used to create a third order calibration between 500 - 2,000,000 Da for calibration. Analyte samples were filtered through a nylon filter with 0.22 μm pore size before injection. Respectively, experimental molar mass ($M_{n,}^{SEC}$) and dispersity ($Đ$) values of synthesised polymers were determined by conventional calibration using Agilent GPC/SEC software. High throughput SEC was carried out on a PL SEC 50 Plus with a differential refractive index (DRI) detector. The system was equipped with either a single PL Rapide F (10 x 100 mm) column, 2x PL Rapide M (7.5 x 150 mm) columns or a combination of PL Rapide M (7.5 mm x 150 mm) and PL Rapide F (10 x 100 mm) columns. The eluent was DMF with 1 % LiBr as the additive. Samples were run at 50 °C at either 2 $mL.min^{-1}$ (for 10 mm diameter columns) or 1 $mL.min^{-1}$ (for 7.5mm columns) based on column set respectively. Poly(methyl methacrylate) standards (Agilent EasiVials) were used for calibration to create a third order calibration between 500 - 1,000,000 Da. Respectively, experimental molar mass ($M_{n,}^{SEC}$) and dispersity ($Đ$) values of synthesised polymers were determined by conventional calibration using Agilent GPC/SEC software. Polymers were prepared using a Gilson Pipette Max 268, with 200 µL and 20 µL pipette heads.

Pipette Error

As solutions were pipetted using a system designed for water, the ability of a pipette to accurately measure 1 mL dioxane was tested. 1 mL was aspirated 5 times and each time weighed into a clean vial. Given the density of dioxane, a mass of 1.033 g is expected. Values recorded: 1.021 g, 1.028 g, 1.024 g, 1.030 g, 1.024 g. These values give an average of 1.025 g, and a standard deviation of 0.0032 g. This suggests that

the values are likely close to the desired volume, and that the values measured are consistent. However, we would recommend testing solutions before use to ensure consistent pipetting volumes.

Determination of the effect of headspace

Into a 20 mL vial was added *N*-hydroxyethyl acrylamide (2.34 g), triethanolamine (3.02 g), dioxane (5.15 mL) and 2-cyano-2-propyl dodecyl trithiocarbonate (39 μL). This solution was mixed until homogenous, and then 0.5 mL, 1 mL and 1.5mL pipetted into separate wells of a 2.2 mL deep 96 well plate. The plate was then covered with a TiterTop and wrapped in blue LED lights. The reaction was allowed to proceed for 24 hours after which the lights were removed and the plate dried under vacuum for 24 hours to remove dioxane. 1 mL DMF was added to each of the three wells and the plate shaken for 6 hours. These samples were then filtered, diluted to 2 $mg.mL^{-1}$ and analysed by SEC in DMF.

0.5 mL Sample: M_n^{SEC}(DMF): 7,000 Da, M_w/M_n = 1.62. 1 mL Sample: M_n^{SEC}(DMF): 6,200 Da, M_w/M_n = 1.60. 1.5 mL Sample: M_n^{SEC}(DMF): 6,900 Da, M_w/M_n = 1.58.

Determination of optimal TEOA concentration

As a representative example, a 0.22 M TEOA solution was prepared by the addition of *N*-hydroxyethyl acrylamide (1.28 g), TEOA (0.165 g), dioxane (3.67 mL) and 2-cyano-2-propyl dodecyl trithiocarbonate (iniferter) (21 μL) into a vial. This solution was mixed until homogenous, and then 0.5 mL was pipetted into a 2.2 mL deep 96 well plate. The other solutions at concentrations of 1.07 M, 2.03 M and 4.43 M were added to individual wells. The plate was then covered with a TiterTop and wrapped in blue LED lights. The reaction was allowed to proceed for 24 hours after which the

lights were removed and the plate dried under vacuum for 24 hours to remove dioxane. 1mL DMF was added to each of the three wells and the plate shaken for 6 hours. These samples were then filtered, diluted to 2 $mg.mL^{-1}$ and analysed by SEC in DMF.

0.22 M Sample: M_n^{SEC}(DMF): 13,000 Da, M_w/M_n = 2.03. 1.07 M Sample: M_n^{SEC}(DMF): 8,000 Da, M_w/M_n = 1.62. 2.03 M Sample: M_n^{SEC}(DMF): 8,000 Da, M_w/M_n = 1.62. 4.43 M Sample: M_n^{SEC}(DMF): 6,000 Da, M_w/M_n = 1.45.

Table 4.06: Composition of each stock solution for each concentration of TEOA.

Concentration (M)[(a)]	HEA (g)[(b)]	TEOA (g)[(c)]	Dioxane (mL)[(d)]	Iniferter (µL)[(e)]
0.22	1.28	0.165	3.67	21
1.07	1.23	0.796	3.16	20
2.03	1.17	1.51	2.58	19
4.43	1.02	3.30	1.13	17

(a) Concentration of TEOA tested; **(b)** Mass of hydroxyethyl acrylamide added to stock solution; **(c)** Mass of TEOA added to stock solution; **(d)** Volume of dioxane added to stock solution; **(e)** Volume of 2-cyano-2-propyl dodecyl trithiocarbonate added to stock solution.

Determination of Monomer and Solvent Versatility

As a representative example, to the first column of a 4-column reservoir in a liquid handling robot was added 2-(dimethylamino)ethyl methacrylate (50 mL). To the second column of the reservoir was added 2-cyano-2-propyl dodecyl trithiocarbonate (144 µL) , TEOA (9.47 g), and methanol (8.83 mL). To the third column of the reservoir was added 2-cyano-2-propyl dodecyl trithiocarbonate (103 µL), TEOA (8.91 g), and dioxane (12.96 mL). 210 µL of monomer was added to wells A1:H6, and 150 µL to wells A7:H12 of a 96 well plate, followed by 290 µL of the methanol solution

to wells A1:H6, and 350 μL of the dioxane solution to each of wells A7:H12. The plate was then covered with a TiterTop and wrapped in blue LED lights. The reaction was allowed to proceed for 24 hours after which the lights were removed and the plate dried under vacuum for 24 hours to remove the solvent. The plate was then placed back into the liquid handling robot and 1mL DMF was added to each well. This plate was then agitated for 6 hours, followed by the addition of 200 μL of this solution to the corresponding well of an empty polypropylene 96 well plate. These samples were then analysed by high throughout GPC and the M_p of each peak picked out and plotted in Figure 4.06.

Table 4.07: Composition of each stock solution used in the polymerisations carried out to determine monomer and solvent versatility.

Monomer[a]	**Solvent[b]**	**Monomer Reservoir**		**Solvent Reservoir**			
		Monomer (mL)[c]	**Volume (μL)[d]**	**TEOA (g)[e]**	**Solvent (mL)[f]**	**Iniferter (μL)[g]**	**Volume (μL)[h]**
DMAEMA	MeOH	25	210	9.47	8.83	144	290
	Dioxane	25	150	8.91	12.96	103	350
MA	MeOH	25	146	9.44	12.61	188	354
	Dioxane	25	94	9.34	15.92	121	406
HEA	MeOH/Tol	50	108	18.63	30.21	242	392

(a) Monomer polymerised; **(b)** Polymerisation solvent; **(c)** Volume of monomer added to reservoir; **(d)** Volume of monomer added from monomer reservoir to plate; **(e)** Mass of TEOA added; **(f)** Volume of solvent added to reservoir; **(g)** Volume of 2-cyano-2-propyl dodecyltrithiocarbonate added to reservoir; **(h)** Volume of solvent/TEOA/Iniferter added from solvent reservoir to plate.

Polymerisation of NIPMAM (solid monomer)

Into a 250 mL conical flask was added *N*-isopropylmethacrylamide (15.6g), triethanolamine (18.27 g), Methanol (27.90 mL) and 2-cyano-2-propyl dodecyl trithiocarbonate (237 μL). This solution was mixed until homogenous, and then added to the first column of a 4-column reservoir. 500 μL of this solution was added into each well of a 96 well deep well plate. The plate was then covered with a TiterTop and wrapped in blue LED lights. The reaction was allowed to proceed for 24 hours after which the lights were removed and the plate dried under vacuum for 24 hours to remove dioxane. The plate was then placed back into the liquid handling robot and 1mL DMF was added to each well. This plate was then agitated for 6 hours, followed by the addition of 200 μL of this solution to the corresponding well of an empty polypropylene 96 well plate. These samples were then analysed by high throughout GPC and the M_p of each peak picked out and plotted in Figure 4.07.

Variable molecular weight polymerisations

To a 12-column reservoir in a liquid handling robot was added MMA (10 mL) (col 1), a solution made up of TEOA (3.06 g), dioxane (5.03 mL) and 2-cyano-2-propyl dodecyl trithiocarbonate (39 μL) (col 2), a solution made up of TEOA (3.06 g), dioxane (4.99 mL) and 2-cyano-2-propyl dodecyl trithiocarbonate (79 μL) (col 3), MA (10 mL) (col 4), a solution made up of TEOA (3.11 g), dioxane (5.31 mL) and 2-cyano-2-propyl dodecyl trithiocarbonate (40 μL) (col 5), a solution made up of TEOA (3.11 g), dioxane (5.26 mL) and 2-cyano-2-propyl dodecyl trithiocarbonate (81 μL) (col 6), a solution containing NIPAM (2.26 g), TEOA (2.98 g), dioxane (5.05 mL) and 2-cyano-2-propyl dodecyl trithiocarbonate (39 μL) (col 7), a solution containing

NIPAM (2.26 g), TEOA (2.98 g), dioxane (5.02 mL) and 2-cyano-2-propyl dodecyl trithiocarbonate (77 μL) (col 8), a solution containing NIPMAM (2.46 g), TEOA (2.88 g), dioxane (4.93 mL) and 2-cyano-2-propyl dodecyl trithiocarbonate (37 μL) (col 9) and a solution containing NIPMAM (2.46 g), TEOA (2.88 g), dioxane (4.90 mL) and 2-cyano-2-propyl dodecyl trithiocarbonate (75 μL) (col 10). 110 μL from column 1 was pipetted into wells A2:B7 of a deep well 96 well plate, followed by 390 μL of column 2 into A2:A7, and 390 μL of column 3 into B2:B7. 94 μL from column 4 was pipetted into wells C2:D7, followed by 406 μL of column 5 into C2:C7, and 406 μL of column 6 into D2:D7. 500 μL of column 7 was pipetted into wells E2:E7, 500 μL of column 8 was pipetted into wells F2:F7, 500 μL of column 9 was pipetted into wells G2:G7 and finally 500 μL of column 10 was pipetted into wells H2:H7. The plate was then covered with a TiterTop and wrapped in blue LED lights. The reaction was allowed to proceed for 24 hours after which the lights were removed and the plate dried under vacuum for 24 hours to remove dioxane. The plate was then placed back into the liquid handling robot and 1mL DMF was added to each well. This plate was then agitated for 6 hours, followed by the addition of 200 μL of this solution to the corresponding well of an empty polypropylene 96 well plate. These samples were then analysed by high throughout GPC, and the DP of the polymers plotted in Figure 4.07.

Table 4.08: Solutions made for the liquid monomers used for molecular weight targeting.

Monomer[a]	[M]:[I] (-)[b]	Monomer Reservoir		Solvent Reservoir			
		Monomer (mL)[c]	Volume (µL)[d]	TEOA (g)[e]	Solvent (mL)[f]	Iniferter (µL)[g]	Volume (µL)[h]
MMA	100	10	110	3.06	5.03	39	390
	50	10	110	3.06	4.99	79	390
MA	100	10	94	3.11	5.31	40	406
	50	10	94	3.11	5.26	81	406

(a) Monomer polymerised; **(b)** Monomer to iniferter ratio; **(c)** Volume of monomer added to reservoir; **(d)** Volume of monomer added from monomer reservoir to plate; **(e)** Mass of TEOA added to reservoir; **(f)** Volume of dioxane added to reservoir; **(g)** Volume of 2-cyano-2-propyl dodecyl trithiocarbonate added to reservoir; Volume of solvent/TEOA/Iniferter added from solvent reservoir to plate.

Table 4.09: Solutions made for the solid monomers used for molecular weight targeting.

Monomer[a]	[M]:[I] (-)[b]	Solvent Reservoir				
		Monomer (g)[c]	TEOA (g)[d]	Solvent (mL)[e]	Iniferter (µL)[f]	Volume (µL)[g]
NIPAM	100	2.26	2.98	5.05	39	500
	50	2.26	2.98	5.02	77	500
NIPMAM	100	2.46	2.88	4.93	37	500
	50	2.46	2.88	4.90	75	500

(a) Monomer polymerised; **(b)** Monomer to iniferter ratio; **(c)** Mass of monomer added to reservoir; **(d)** Mass of TEOA added to reservoir; **(e)** Volume of dioxane added to

reservoir; **(f)** Volume of 2-cyano-2-propyl dodecyl trithiocarbonate added to reservoir; **(g)** Volume of monomer/solvent/TEOA/iniferter added from solvent reservoir to plate.

Variable monomer concentration polymerisations

To a 12-column reservoir in a liquid handling robot was added: MMA (20 mL) (col 1), a solution containing TEOA (1.5 g), dioxane (2.57 mL) and 2-cyano-2-propyl dodecyl trithiocarbonate (19 μL) (col 2), a solution containing TEOA (1.5 g), dioxane (2.54 mL) and2-cyano-2-propyl dodecyl trithiocarbonate (38 μL) (col 3), a solution containing TEOA (1.5 g), dioxane (3.10 mL) and 2-cyano-2-propyl dodecyl trithiocarbonate (10 μL) (col 4), a solution containing TEOA (1.55 g), dioxane (3.04 mL) and 2-cyano-2-propyl dodecyl trithiocarbonate (20 μL) (col 5), a solution containing TEOA (1.49 g), dioxane (3.38 mL) and 2-cyano-2-propyl dodecyl trithiocarbonate (5 μL) (col 6), a solution containing TEOA (1.55 g), dioxane (3.33 mL) and 2-cyano-2-propyl dodecyl trithiocarbonate (10 μL) (col 7), a solution containing TEOA (1.49 g), dioxane (3.52 mL) and 2-cyano-2-propyl dodecyl trithiocarbonate (2.5 μL) (col 8) and a solution containing TEOA(1.49 g), dioxane (3.52 mL) and 2-cyano-2-propyl dodecyl trithiocarbonate (5 μL) (col 9). 216 μL from column 1 was pipetted into wells A2:B7 of a deep well 96 well plate, followed by 284 μL of column 2 into A2:A7, and 284 μL of column 3 into B2:B7. 111 μL from column 1 was pipetted into wells C2:D7, followed by 389 μL of column 4 into C2:C7, and 389 μL of column 5 into D2:D7. 55 μL from column 1 was pipetted into wells E2:F7, followed by 445 μL of column 6 into E2:E7, and 445 μL of column 7 into F2:F7. 111 μL from column 1 was pipetted into wells G2:H7, followed by 472 μL of column 8 into G2:G7, and 472 μL of column 9 into H2:H7. The plate was then covered with a TiterTop and wrapped in blue LED lights. The reaction was allowed to proceed for 24 hours after which the lights were removed and the plate dried under vacuum for 24

hours to remove dioxane. The plate was then placed back into the liquid handling robot and 1 mL DMF was added to each well. This plate was then agitated for 6 hours, followed by the addition of 200 μL of this solution to the corresponding well of an empty polypropylene 96 well plate. These samples were then analysed by high throughout GPC, and the M_p of the polymers plotted in Figure 4.08.

Table 4.10: Solutions made up for the monomer content variation plates and the amount added into each well.

Wt % Monomer[(a)]	[M]:[I] (-)[(b)]	Monomer Added (μL)[(c)]	Solvent Reservoir			
			TEOA (g)[(d)]	Solvent (mL)[(e)]	Iniferter (μL)[(f)]	Volume (μL)[(g)]
20	100	110	1.5	2.57	19	390
	50	110	1.5	2.54	38	390
10	100	55	1.5	3.10	10	445
	50	55	1.55	3.04	20	445
5	100	28	1.49	3.38	5.0	472
	50	28	1.55	3.33	10	472
2.5	100	14	1.49	3.52	2.5	486
	50	14	1.49	3.52	5.0	486

(a) Wt % MMA present in the polymerisation reaction; **(b)** Monomer to iniferter ratio; **(c)** Volume of monomer added to each polymerisation; **(d)** Mass of TEOA added to reservoir; **(e)** Volume of dioxane added to reservoir; **(f)** Volume of 2-cyano-2-propyl dodecyl trithiocarbonate added to reservoir; **(g)** Volume of solvent/TEOA/iniferter added from solvent reservoir to plate.

Polymerisations with a constant radical concentration

To a 4-column reservoir in a liquid handling robot was added: MMA (10 mL) (col 1), a solution containing TEOA (1.5 g), dioxane (3.1 mL) and 2-cyano-2-propyl dodecyl

trithiocarbonate (20 μL) (col 2), a solution containing TEOA (1.5 g), dioxane (2.54 mL) and 2-cyano-2-propyl dodecyl trithiocarbonate (20 μL) (col 3) and a solution containing TEOA (1.5 g), dioxane (1.44 mL) and 2-cyano-2-propyl dodecyl trithiocarbonate (20 μL) (col 4). 51 μL of MMA from column 1 was added to wells B2:B7 of a deep well 96 well plate, followed by 103 μL to wells C2:C7 and 206 μL to wells D3:D7. These wells were then made up to 500 μL with the corresponding TEOA/dioxane/iniferter solution, 449 μL of the solution in column 2 was added to wells B2:B7, followed by 397 μL from column 3 to wells C2:C7, and finally 296 μL from column 4 to wells D2:D7. The plate was then covered with a TiterTop and wrapped in blue LED lights. The reaction was allowed to proceed for 24 hours after which the lights were removed and the plate dried under vacuum for 24 hours to remove dioxane. The plate was then placed back into the liquid handling robot and 1mL DMF was added to each well. This plate was then agitated for 6 hours, followed by the addition of 200 μL of this solution to the corresponding well of an empty polypropylene 96 well plate. These samples were then analysed by high throughout SEC, and the DP of the polymers plotted in Figure 4.09.

Table 4.11: Solutions made up to examine the molecular weight control of the polymerisation using a constant radical concentration.

[M]:[I] (-)[a]	Monomer added (µL)[b]	Solvent Reservoir			
		TEOA (g)[c]	Solvent (mL)[d]	Iniferter (µL)[e]	Volume (µL)[f]
50	51	1.5	3.10	20	449
100	103	1.5	2.54	20	397
200	206	1.5	1.44	20	296

(a) Monomer to iniferter ratio; **(b)** Volume of monomer added to each polymerisation; **(c)** Mass of TEOA added to reservoir; **(d)** Volume of dioxane added to reservoir; **(e)** Volume of 2-cyano-2-propyl dodecyl trithiocarbonate added to reservoir; **(f)** Volume of solvent/TEOA/iniferter added from solvent reservoir to plate.

Conversion Experiments

As a representative example, to a 20 mL vial was added MMA (1.01 g), TEOA (1.50 g), dioxane (2.57 mL), 2-cyano-2-propyl dodecyl trithiocarbonate (19.5 µL) and DMF (50 µL) and mixed until homogeneous. 500 µL of this solution was pipetted into wells B2:B7 of a deep well 96 well plate. A small sample of this stock solution was analysed by NMR as a t0 sample. The plate was then covered with a TiterTop and wrapped in blue LED lights. At various timepoints, the plate was uncovered and the contents of one well was removed, followed by analysis by NMR and GPC. After 28 hours the reaction was stopped. Conversion was determined by integration of the vinyl peaks against the DMF standard. Conversion was plotted against molecular weight, and reaction time against the $Ln[M_o/M_n]$ in order to investigate the kinetics of the reaction. This is shown in Figure 4.10.

Amine Free Control Polymerisation

To a 10 mL vial was added methyl methacrylate (0.5 g), dioxane (1.95 mL) and 2-cyano-2-propyl dodecyl trithiocarbonate (10 μL). This solution was stirred and then 0.5 mL pipetted into a vial, a sample was removed for NMR and the vial was left open to air and irradiated for 24 hours. After this time, another NMR was taken and the sample was dried under vacuum and the sample dissolved in DMF followed by SEC analysis. M_n^{SEC}(DMF) = 95,000 Da, M_w/M_n = 1.51. Conversion = 10 %.

Degassed Control Experiment

To a 10 mL vial was added methyl methacrylate (0.5 g), triethanolamine (0.74 g), dioxane (1.28 mL) and 2-cyano-2-propyl dodecyl trithiocarbonate (10 μL). This solution was stirred and then 0.5 mL pipetted into a vial, the vial was sparged with nitrogen for 5 minutes and a sample removed for NMR, followed by irradiation for 24 hours. After this time, another NMR sample was removed and the sample was diluted with more dioxane and transferred to a 2 mL Eppendorf, 0.1 mL HCl was added and the sample centrifuged to remove the amine. The resulting solution was dried and the sample dissolved in DMF followed by SEC analysis. M_n^{SEC}(DMF) = 13,500 Da, M_w/M_n = 1.50. Conversion = 94 %.

Standard Control Experiment

To a 10 mL vial was added methyl methacrylate (0.5 g), triethanolamine (0.74 g), dioxane (1.28 mL) and 2-cyano-2-propyl dodecyl trithiocarbonate (10 μL). This solution was stirred and then 0.5 mL pipetted into a vial, the vial was left open to air and irradiated for 24 hours. After this time, the sample was diluted with more dioxane and transferred to a 2 mL Eppendorf, 0.1 mL HCl was added and the sample

centrifuged to remove the amine. The resulting solution was dried and the sample dissolved in DMF followed by SEC analysis. M_n^{SEC}(DMF) = 12,400 Da, M_w/M_n = 2.12. Conversion = 93 %.

10 % DMSO Control Experiment

To a 10 mL vial was added methyl methacrylate (0.5 g), triethanolamine (0.74 g), dioxane (1.03 mL), DMSO (0.25 mL) and 2-cyano-2-propyl dodecyl trithiocarbonate (10 μL). This solution was stirred and then 0.5 mL pipetted into a vial, a sample was removed for NMR and the vial was left open to air and irradiated for 24 hours. After this time, another NMR was taken and the sample was diluted with more dioxane and transferred to a 2 mL Eppendorf, 0.1 mL HCl was added and the sample centrifuged to remove the amine. The resulting solution was dried and the sample dissolved in DMF followed by SEC analysis. M_n^{SEC}(DMF) = 17,000 Da, M_w/M_n = 1.86. Conversion = 80 %.

No Iniferter Control Experiment

To a 10 mL vial was added methyl methacrylate (0.5 g), triethanolamine (0.74 g) and dioxane (1.28 mL). This solution was stirred and then 0.5 mL pipetted into a vial, a sample was removed for NMR and the vial was left open to air and irradiated for 24 hours. After this time, another NMR was taken, and the sample was diluted with more dioxane and transferred to a 2 mL Eppendorf, 0.1 mL HCl was added and the sample centrifuged to remove the amine. The resulting solution was dried and the sample dissolved in DMF followed by SEC analysis. SEC DMF: No polymer observed. Conversion = 2 % (most likely due to evaporation of the monomer).

TEA Test Experiment

To a 10 mL vial was added methyl methacrylate (0.5 g), triethylamine (0.5 g), dioxane (1.25 mL) and 2-cyano-2-propyl dodecyl trithiocarbonate (10 μL). This solution was stirred and then 0.5 mL pipetted into one well of a 96 well plate placed onto a thermocycler set at 4 °C, the plate was sealed with a TiterTop and irradiated for 24 hours. After this time, the sample was diluted with more dioxane and transferred to a 2 mL Eppendorf, 0.1 mL HCl was added and the sample centrifuged to remove the amine. The resulting solution was dried and the sample dissolved in DMF followed by SEC analysis. M_n^{SEC}(DMF) = 14,600 Da, M_w/M_n = 1.93. Conversion = 80 %.

Conversion of DMAEMA MAA Copolymers

To a 12-column reservoir in a liquid handling robot was added DMAEMA (15 mL) (col 1), MAA (15 mL) (col 2), a solution of 0.6 M TEOA in dioxane (15 mL) (col 3). To a 1.5 mL Eppendorf in a liquid handling robot was added a 10 wt % solution of 2-cyano-2-propyl dodecyl trithiocarbonate in dioxane. 70 μL of DMAEMA was added to wells B2:B10, followed by 35 μL of MA, 368 μL of the TEOA/dioxane solution, and 27 μL of the iniferter solution. 10 μL of DMF was added to each well as an NMR standard. The plate was then covered with a TiterTop and wrapped in blue LED lights. At a number of timepoints, the entire contents of the well were removed and dissolved in deuterated chloroform. Conversion was determined by disappearance of the monomer vinyl peak. The results are shown in Figure 4.12.

Synthesis of DMAEMA MAA Copolymers

To a 12-column reservoir in a liquid handling robot was added DMAEMA (15 mL) (col 1), MAA (15 mL) (col 2), a solution of 0.6 M TEOA in dioxane (30 mL) (divided

between col 3 and col 4). To two 1.5 mL Eppendorfs in a liquid handling robot was added a 10 wt % solution of 2-cyano-2-propyl dodecyl trithiocarbonate in dioxane. 86 µL of DMAEMA from column 1 was added to wells A1:H2 of a deep well 96 well plate, followed by 78 µL to wells A3:H4, 70 µL to wells A5:H6, 59 µL to wells A7:H8 and 47 µL to wells A9:H10. 19 µL of MAA from column 2 was added to wells A1:H2, followed by 26 µL to wells A3:H4, 35 µL to wells A5:H6, 44 µL to wells A7:H8 and 55 µL to wells A9:H10. 368 µL of the TEOA/dioxane solution was added to wells A1:H10, followed by 27 µL of the iniferter solution to each of wells A1:H10. The plate was then covered with a TiterTop and wrapped in blue LED lights. The reaction was allowed to proceed for 24 hours after which the lights were removed and the plate dried under vacuum for 24 hours to remove dioxane. The plate was then placed back into the liquid handling robot and 700 µL PBS corrected to pH 0.3 was added to wells A1:G10. DMF containing 1 % LiBr (1 mL) was added to wells H1:H10. The plate was agitated for 24 hours to encourage complete dissolution. 200 µL was removed from wells H1:H10 and analysed by high throughput SEC. 100 µL was removed from wells A1:G10 and transferred to a 96 well round bottom polypropylene plate for cryopreservation screening.

$DMAEMA_{0.7}MAA_{0.3}$ 1- M_n^{SEC}(DMF): 3,000 M_w/M_n: 2.03; 2 - M_n^{SEC}(DMF): 3,100 M_w/M_n: 2.09. $DMAEMA_{0.6}MAA_{0.4}$ 1- M_n^{SEC}(DMF): 2,500 M_w/M_n: 1.71; 2 - M_n^{SEC}(DMF): 2,500 M_w/M_n: 1.72. $DMAEMA_{0.5}MAA_{0.5}$ 1- M_n^{SEC}(DMF): 2,000 M_w/M_n: 1.45; 2 - M_n^{SEC}(DMF): 2,100 M_w/M_n: 1.40. $DMAEMA_{0.4}MAA_{0.6}$ 1- M_n^{SEC}(DMF): 1,500 M_w/M_n: 1.34; 2 - M_n^{SEC}(DMF): 1,600 M_w/M_n: 1.35. $DMAEMA_{0.3}MAA_{0.7}$ 1- M_n^{SEC}(DMF): 1,100 M_w/M_n: 1.77; 2 - M_n^{SEC}(DMF): 1,000 M_w/M_n: 1.69.

Synthesis of DMAEMA MAA Terpolymers

To a 12-column reservoir in a liquid handling robot was added DMAEMA (15 mL) (col 1), MAA (15 mL) (col 2), a solution of 0.6 M TEOA in dioxane (30 mL) (divided between col 3 and col 4). To two 1.5 mL Eppendorfs in a liquid handling robot was added a 10 wt % solution of 2-cyano-2-propyl dodecyl trithiocarbonate in dioxane. The corresponding termonomer for each row was added to wells A2:G2 of a deep well 96 well plate (1.5 mL). 6 monomers per run, repeated twice with 12 termonomers total. 63 μL of DMAEMA was added to wells B2:G11, followed by 21 μL MAA, 390 μL of the TEOA/dioxane solution, and 27 μL iniferter solution. This was then followed by 14 μL DMAEMA to B2:G2, 12 μL to B3:G3, 11 μL to B4:G4, 9 μL to B5:G5, 8 μL to B6:G6, 6 μL to B7:G7, 5 μL to B8:G8, 3 μL to B9:G9 and 2 μL to B10 to G10. 5 μL MAA was added to B2:G2, followed by 4 μL to B3:G3, 3 μL to B4:G4, 3 μL to B5:G5, 3 μL to B6:G6, 2 μL to B7:G7, 2 μL to B8:G8, 1 μL to B9:G9 and 1 μL to B10 to G10. 2 μL of termonomer was added to B2:G2, followed by 4 μL to B3:G3, 6 μL to B4:G4, 8 μL to B5:G5, 10 μL to B6:G6, 12 μL to B7:G7, 14 μL to B8:G8, 16 μL to B9:G9 and 18 μL to B10 to G10 and 20 μL to B11 to G11. The plate was then covered with a TiterTop and wrapped in blue LED lights. The reaction was allowed to proceed for 24 hours after which the lights were removed, and the plate dried under vacuum for 24 hours to remove dioxane. The plate was then placed back into the liquid handling robot and 500 μL PBS corrected to pH 0.3, followed by 200 μL standard PBS was added to wells B2:G11. The plate was agitated for 24 hours, followed by removal of 300 μL of each sample for blood testing in triplicate. The remaining polymers were freeze dried, and dissolved in DMF followed by high throughput SEC. SEC traces are shown in the appendix (Figure 4.24 and 4.25).

Termonomers used were: 2-hydroxyethyl methacrylate, cyclohexyl methacrylate, di(ethylene glycol) methyl ether methacrylate, ethyl methacrylate, hydroxyethyl acrylate, methyl acrylate, methyl methacrylate, ^{n}butyl methacrylate, ^{n}hexyl methacrylate, poly(ethylene glycol) methyl ether methacrylate, poly(propylene glycol) methyl ether methacrylate and ^{t}butyl methacrylate.

In order to compensate for density differences as a result of the robot working with volumes, termonomer additions were initially individually calculated. It was determined, however, that no density compensation leads to a difference of less than 2 mg polymer between the least and most dense at the end of the reaction (assuming 100 % conversion). This was however much more intensive to programme, and therefore universal addition volumes were generated using the average density of all of the monomers used.

High Throughput Blood Screening

100 mg polymer in each well of a 96 well plate was dissolved in 700 μL PBS and agitated until complete dissolution was observed. 100 μL was removed from each the wells and pipetted into a standard polypropylene 96 well plate in triplicate. 10 mL Sheep blood in Alsevers solution was added to a 15 mL centrifuge tube and centrifuged at 2000 rpm for 5 minutes to concentrate the solution, 7 mL of the supernatant was removed and replaced with 7 mL PBS solution. 100 μL of blood was added to each well of the same 3x 96 well plates, and the plates covered with TiterTops. The plates were agitated for 10 minutes to ensure mixing, and then suspended above liquid nitrogen for 20 minutes until fully frozen. Each plate was then warmed at 45 ºC for 15 minutes on a plate warmer. The plate was removed, and the

PBS and Lysis buffer controls added (100 μL PBS or Lysis buffer mixed with 100 μL blood respectively). The plate was centrifuged at 3700 rpm for 5 minutes, and then 8 μL removed from each well and pipetted into a 96 well flat bottom plate already containing 200 μL AHD solution in each well. The absorbance at 580 nm was then determined using a plate reader, and the results averaged across the three plates.

Synthesis of 4 % HEMA Copolymers

As a representative example, 2-hydroxyethyl methacrylate (0.057 g, 0.44 mmol, 2eq), 2-(dimethylamino)ethyl methacrylate (1 g, 6.4 mmol, 28.8 eq), methacrylic acid (0.36 g, 4.2 mmol, 19.2 eq), 2-cyano-2-propyl dodecyl trithiocarbonate (0.076 g, 0.22 mmol, 1 eq), 2,2'-azobis(2-methylpropionitrile) (0.007 g, 0.044 mmol, 0.2 eq), dioxane (2 mL) as solvent, and DMF (20 μL) as an NMR standard were added to a vial. A stirrer bar was added, the vial sealed with a subaseal, and the solution bubbled with nitrogen for 10 minutes. After this time, a small sample was removed to determine conversion, and the vial was placed into an oil bath set to 68 ºC. After 24 hours, another sample was taken for conversion, and the resulting polymer plunged into liquid nitrogen to stop the reaction. The polymer was dissolved in water, and then precipitated into methanol 3 times followed by lyophilisation. The resulting polymer was analysed by ^{1}H NMR, FTIR and SEC. Representative characterisation data for $HEMA_{50}$:

Yield: 0.57g. ^{1}H NMR (400 MHz, D_2O): **δ** = 0.55 – 1.44 ($CH_2C(CH_3)$, br), 1.44 – 2.17 ($CH_2C(CH_3)$, br), 2.36 – 2.89 ($(CH_3)_2NCH_2CH_2O$, br), 2.94 – 3.50 ($(CH_3)_2NCH_2CH_2O$, br), 3.69 – 3.84 ($HOCH_2CH_2O$, br), 3.94 – 4.06 ($HOCH_2CH_2O$, br), 4.03-4.07 ($(CH_3)_2NCH_2CH_2O$, br). FTIR: C-O 1148 cm^{-1}, $C(O)O^-$ symmetric stretch 1388 cm^{-1}, $C(O)O^-$ asymmetric stretch 1570 cm^{-1}, C=O 1716 cm^{-1}, $N(CH_3)H^+$ 2152 cm^{-1}, OH 3100-3500 cm^{-1}. M_n^{SEC}(DMF) = 10,000 Da, M_w/M_n = 1.48.

Synthesis of 10 % CyMA Copolymers

As a representative example, cyclohexyl methacrylate (0.20 g, 1.2 mmol, 10eq), 2-(dimethylamino)ethyl methacrylate (1 g, 6.4 mmol, 54 eq), methacrylic acid (0.36 g, 4.2 mmol, 36 eq), 2-cyano-2-propyl dodecyl trithiocarbonate (0.041 g, 0.11 mmol, 1 eq), 2,2'-azobis(2-methylpropionitrile) (0.004 g, 0.024 mmol, 0.2 eq), dioxane (2 mL) as solvent, and DMF (20 μL) as an NMR standard were added to a vial. A stirrer bar was added, the vial sealed with a subaseal, and the solution bubbled with nitrogen for 10 minutes. After this time, a small sample was removed to determine conversion, and the vial was placed into an oil bath set to 68 ºC. After 24 hours, another sample was taken for conversion, and the resulting polymer plunged into liquid nitrogen to stop the reaction. The polymer was dissolved in water, and then precipitated into methanol 3 times followed by lyophilisation. The resulting polymer was analysed by ^{1}H NMR, FTIR and SEC. Representative characterisation data for $CyMA_{100}$:

Yield: 0.77g. ^{1}H NMR (400 MHz, D_2O): **δ** = 0.62 – 1.26 ($CH_2C(CH_3)$, br), 1.26 – 1.59 (cyclohexyl C-H, br), 1.59 – 2.24 ($CH_2C(CH_3)$, br), 2.40 – 3.00 ($(CH_3)_2NCH_2CH_2O$, br), 3.01 – 3.61 ($HOCH_2CH_2O$, br), 3.99 – 4.52 ($HOCH_2CH_2O$, br). FTIR: C-O 1143 cm^{-1}, $C(O)O^-$ symmetric stretch 1384 cm^{-1}, C-O 1465 cm^{-1}, $C(O)O^-$ asymmetric stretch 1575 cm^{-1}, C=O 1714 cm^{-1}, $N(CH_3)H^+$ 2167 cm^{-1}, OH 3100-3600 cm^{-1}. M_n^{SEC}(DMF) = 15,000 Da, M_w/M_n = 1.39.

Ice Recrystallisation Inhibition Assay

A 10 μL droplet of polymer in PBS solution was dropped from 1.4 metres onto a glass microscope coverslip, which was placed on top of an aluminium plate cooled to -78 °C using dry ice. The droplet froze instantly upon impact with the plate, spreading out and forming a thin wafer of ice. This wafer was then placed on a liquid nitrogen cooled

cryostage held at -8 °C within the viewing area of the microscope. The wafer was then left to anneal for 30 minutes at -8 °C. The number of crystals in the image was counted using ImageJ, and the area of the field of view divided by this number of crystals to give the average crystal size per wafer and reported as a percentage (%) of area compared to PBS control.

Blood Testing Protocol

10 mL Sheep blood in Alsevers solution was added to a 15 mL centrifuge tube and centrifuged at 2000 rpm for 5 minutes to concentrate the solution, 7 mL of the supernatant was removed and replaced with 7 mL PBS solution. Polymer solutions were made at 2X the required concentration to ensure the correct final cryoprotectant concentration. 0.5 mL of the blood solution was added to 0.5 mL of the polymer solutions in 2 mL cryovials. These were then incubated in the fridge for 30 minutes before freezing above liquid nitrogen vapour. After 1 hour, samples were thawed in a water bath at 45 °C for 10 minutes, after which they were transferred to Eppendorf tubes and centrifuged at 2000 rpm for 5 minutes. 40 μL of the supernatant was removed and added to 750 μL of AHD solution. After vortexing, the samples were pipetted into a 96 well plate in triplicate (3 x 200 μL per sample) and the absorbance recorded at 580 nm in a BioTek plate reader. Samples were compared against unfrozen PBS and lysis buffer samples as the 0 and 100 % lysis samples respectively.

4.6 References

(1) Boyer, C.; Bulmus, V.; Davis, T. P.; Ladmiral, V.; Liu, J.; Perrier, S. Bioapplications of RAFT Polymerization. *Chem. Rev.* **2009**, *109* (11), 5402–5436.

(2) Cobo, I.; Li, M.; Sumerlin, B. S.; Perrier, S. Smart Hybrid Materials by Conjugation of Responsive Polymers to Biomacromolecules. *Nat. Mater.* **2015**, *14* (2), 143–159.

(3) Biggs, C. I.; Bailey, T. L.; Graham, B.; Stubbs, C.; Fayter, A.; Gibson, M. I. Polymer Mimics of Biomacromolecular Antifreezes. *Nat. Commun.* **2017**, *8* (1), 1546.

(4) Lutz, J.-F. An Introduction to Sequence-Controlled Polymers. In *Sequence-Controlled Polymers: Synthesis, Self-Assembly, and Properties*; 2014; Vol. 1170, pp 1–11.

(5) Zydziak, N.; Konrad, W.; Feist, F.; Afonin, S.; Weidner, S.; Barner-Kowollik, C. Coding and Decoding Libraries of Sequence-Defined Functional Copolymers Synthesized via Photoligation. *Nat. Commun.* **2016**, *7* (1), 13672.

(6) Martens, S.; Van Den Begin, J.; Madder, A.; Du Prez, F. E.; Espeel, P. Automated Synthesis of Monodisperse Oligomers, Featuring Sequence Control and Tailored Functionalization. *J. Am. Chem. Soc.* **2016**, *138* (43), 14182–14185.

(7) Gody, G.; Barbey, R.; Danial, M.; Perrier, S. Ultrafast RAFT Polymerization: Multiblock Copolymers within Minutes. *Polym. Chem.* **2015**, *6* (9), 1502–1511.

(8) Engelis, N. G.; Anastasaki, A.; Nurumbetov, G.; Truong, N. P.; Nikolaou, V.; Shegiwal, A.; Whittaker, M. R.; Davis, T. P.; Haddleton, D. M. Sequence-Controlled Methacrylic Multiblock Copolymers via Sulfur-Free RAFT

Emulsion Polymerization. *Nat. Chem.* **2017**, *9* (2), 171–178.

(9) Ting, J. M.; Porter, W. W.; Mecca, J. M.; Bates, F. S.; Reineke, T. M. Advances in Polymer Design for Enhancing Oral Drug Solubility and Delivery. *Bioconjug. Chem.* **2018**, *29* (4), 939–952.

(10) Anderson, D. G.; Lynn, D. M.; Langer, R. Semi-Automated Synthesis and Screening of a Large Library of Degradable Cationic Polymers for Gene Delivery. *Angew. Chemie Int. Ed.* **2003**, *42* (27), 3153–3158.

(11) Mei, Y.; Saha, K.; Bogatyrev, S. R.; Yang, J.; Hook, A. L.; Kalcioglu, Z. I.; Cho, S. W.; Mitalipova, M.; Pyzocha, N.; Rojas, F.; Van Vliet, K. J.; Davies, M. C.; Alexander, M. R.; Langer, R.; Jaenisch, R.; Anderson, D. G. Combinatorial Development of Biomaterials for Clonal Growth of Human Pluripotent Stem Cells. *Nat. Mater.* **2010**, *9* (9), 768–778.

(12) Greenaway, R. L.; Santolini, V.; Bennison, M. J.; Alston, B. M.; Pugh, C. J.; Little, M. A.; Miklitz, M.; Eden-Rump, E. G. B.; Clowes, R.; Shakil, A.; Cuthbertson, H. J.; Armstrong, H.; Briggs, M. E.; Jelfs, K. E.; Cooper, A. I. High-Throughput Discovery of Organic Cages and Catenanes Using Computational Screening Fused with Robotic Synthesis. *Nat. Commun.* **2018**, *9* (1), 1–11.

(13) Bray, C. L.; Tan, B.; Wood, C. D.; Cooper, A. I. High-Throughput Solubility Measurements of Polymer Libraries in Supercritical Carbon Dioxide. *J. Mater. Chem.* **2005**, *15* (4), 456–459.

(14) Haven, J. J.; Guerrero-Sanchez, C.; Keddie, D. J.; Moad, G.; Thang, S. H.; Schubert, U. S. One Pot Synthesis of Higher Order Quasi-Block Copolymer Libraries via Sequential RAFT Polymerization in an Automated Synthesizer. *Polym. Chem.* **2014**, *5* (18), 5236–5246.

(15) Chapon, P.; Mignaud, C.; Lizarraga, G.; Destarac, M. Automated Parallel Synthesis of MADIX (Co)Polymers. *Macromol. Rapid Commun.* **2003**, *24* (1), 87–91.

(16) Zhang, H.; Fijten, M. W. M.; Hoogenboom, R.; Reinierkens, R.; Schubert, U. S. Application of a Parallel Synthetic Approach in Atom-Transfer Radical Polymerization: Set-up and Feasibility Demonstration. *Macromol. Rapid Commun.* **2003**, *24* (1), 81–86.

(17) Hoogenboom, R.; Fijten, M. W. M.; Meier, M. A. R.; Schubert, U. S. Living Cationic Polymerizations Utilizing an Automated Synthesizer : High-Throughput Synthesis of Polyoxazolines. **2003**, 92–97.

(18) Hoogenboom, R.; Schubert, U. S. The Fast and the Curious : High-Throughput Experimentation. *Polymer (Guildf).* **2003**, *41*, 2425–2434.

(19) Hook, A. L.; Chang, C. Y.; Yang, J.; Luckett, J.; Cockayne, A.; Atkinson, S.; Mei, Y.; Bayston, R.; Irvine, D. J.; Langer, R.; Anderson, D. G.; Williams, P.; Davies, M. C.; Alexander, M. R. Combinatorial Discovery of Polymers Resistant to Bacterial Attachment. *Nat. Biotechnol.* **2012**, *30* (9), 868–875.

(20) Ting, J. M.; Tale, S.; Purchel, A. A.; Jones, S. D.; Widanapathirana, L.; Tolstyka, Z. P.; Guo, L.; Guillaudeu, S. J.; Bates, F. S.; Reineke, T. M. High-Throughput Excipient Discovery Enables Oral Delivery of Poorly Soluble Pharmaceuticals. *ACS Cent. Sci.* **2016**, *2* (10), 748–755.

(21) Weissleder, R.; Kelly, K.; Sun, E. Y.; Shtatland, T.; Josephson, L. Cell-Specific Targeting of Nanoparticles by Multivalent Attachment of Small Molecules. *Nat. Biotechnol.* **2005**, *23* (11), 1418–1423.

(22) Janzen, W. P. Screening Technologies for Small Molecule Discovery: The State of the Art. *Chem. Biol.* **2014**, *21* (9), 1162–1170.

(23) Chapman, R.; Gormley, A. J.; Herpoldt, K. L.; Stevens, M. M. Highly Controlled Open Vessel RAFT Polymerizations by Enzyme Degassing. *Macromolecules* **2014**, *47* (24), 8541–8547.

(24) Chapman, R.; Gormley, A. J.; Stenzel, M. H.; Stevens, M. M. Combinatorial Low-Volume Synthesis of Well-Defined Polymers by Enzyme Degassing. *Angew. Chemie Int. Ed.* **2016**, *55* (14), 4500–4503.

(25) Schneiderman, D. K.; Ting, J. M.; Purchel, A. A.; Miranda, R.; Tirrell, M. V.; Reineke, T. M.; Rowan, S. J. Open-to-Air RAFT Polymerization in Complex Solvents: From Whisky to Fermentation Broth. *ACS Macro Lett.* **2018**, *7* (4), 406–411.

(26) Enciso, A. E.; Fu, L.; Russell, A. J.; Matyjaszewski, K. A Breathing Atom-Transfer Radical Polymerization: Fully Oxygen-Tolerant Polymerization Inspired by Aerobic Respiration of Cells. *Angew. Chemie Int. Ed.* **2018**, *57* (4), 933–936.

(27) Fors, B. P.; Hawker, C. J. Control of a Living Radical Polymerization of Methacrylates by Light. *Angew. Chemie Int. Ed.* **2012**, *51* (35), 8850–8853.

(28) Xu, J.; Shanmugam, S.; Duong, H. T.; Boyer, C. Organo-Photocatalysts for Photoinduced Electron Transfer-Reversible Addition–Fragmentation Chain Transfer (PET-RAFT) Polymerization. *Polym. Chem.* **2015**, *6* (31), 5615–5624.

(29) Gormley, A. J.; Yeow, J.; Ng, G.; Conway, Ó.; Boyer, C.; Chapman, R. An Oxygen-Tolerant PET-RAFT Polymerization for Screening Structure-Activity Relationships. *Angew. Chemie Int. Ed.* **2018**, *57* (6), 1557–1562.

(30) Yeow, J.; Chapman, R.; Xu, J.; Boyer, C. Oxygen Tolerant Photopolymerization for Ultralow Volumes. *Polym. Chem.* **2017**, *8* (34), 5012–5022.

(31) Gormley, A. J.; Yeow, J.; Ng, G.; Conway, Ó.; Boyer, C.; Chapman, R. An Oxygen-Tolerant PET-RAFT Polymerization for Screening Structure–Activity Relationships. *Angew. Chemie Int. Ed.* **2018**, *57* (6), 1557–1562.

(32) Shanmugam, S.; Xu, J.; Boyer, C. Photoinduced Electron Transfer-Reversible Addition-Fragmentation Chain Transfer (PET-RAFT) Polymerization of Vinyl Acetate and N-Vinylpyrrolidinone: Kinetic and Oxygen Tolerance Study. *Macromolecules* **2014**, *47* (15), 4930–4942.

(33) Blackman, L. D.; Varlas, S.; Arno, M. C.; Fayter, A.; Gibson, M. I.; O'Reilly, R. K. Permeable Protein-Loaded Polymersome Cascade Nanoreactors by Polymerization-Induced Self-Assembly. *ACS Macro Lett.* **2017**, *6* (11), 1263–1267.

(34) Blackman, L. D.; Varlas, S.; Arno, M. C.; Houston, Z. H.; Fletcher, N. L.; Thurecht, K. J.; Hasan, M.; Gibson, M. I.; O'Reilly, R. K. Confinement of Therapeutic Enzymes in Selectively Permeable Polymer Vesicles by Polymerization-Induced Self-Assembly (PISA) Reduces Antibody Binding and Proteolytic Susceptibility. *ACS Cent. Sci.* **2018**, *4* (6), 718–723.

(35) Tucker, B. S.; Coughlin, M. L.; Figg, C. A.; Sumerlin, B. S. Grafting-From Proteins Using Metal-Free PET–RAFT Polymerizations under Mild Visible-Light Irradiation. *ACS Macro Lett.* **2017**, *6* (4), 452–457.

(36) Figg, C. A.; Hickman, J. D.; Scheutz, G. M.; Shanmugam, S.; Carmean, R. N.; Tucker, B. S.; Boyer, C.; Sumerlin, B. S. Color-Coding Visible Light Polymerizations to Elucidate the Activation of Trithiocarbonates Using Eosin Y. *Macromolecules* **2018**, *51* (4), 1370–1376.

(37) Stubbs, C.; Congdon, T. R.; Gibson, M. I. Photo-Polymerisation and Study of the Ice Recrystallisation Inhibition of Hydrophobically Modified Poly(Vinyl

Pyrrolidone) Co-Polymers. *Eur. Polym. J.* **2019**, *110*, 330–336.

(38) Blackman, L. D.; Doncom, K. E. B.; Gibson, M. I.; O'Reilly, R. K. Comparison of Photo- and Thermally Initiated Polymerization-Induced Self-Assembly: A Lack of End Group Fidelity Drives the Formation of Higher Order Morphologies. *Polym. Chem.* **2017**, *8* (18), 2860–2871.

(39) Fu, Q.; Xie, K.; McKenzie, T. G.; Qiao, G. G. Trithiocarbonates as Intrinsic Photoredox Catalysts and RAFT Agents for Oxygen Tolerant Controlled Radical Polymerization. *Polym. Chem.* **2017**, *8* (9), 1519–1526.

(40) Richards, S.-J.; Jones, A.; Tomás, R. M. F.; Gibson, M. I. Photochemical "In-Air" Combinatorial Discovery of Antimicrobial Co-Polymers. *Chem. Eur. J.* **2018**, *24* (52), 13758–13761.

(41) Pal, R.; Mamidi, M. K.; Das, A. K.; Bhonde, R. Diverse Effects of Dimethyl Sulfoxide (DMSO) on the Differentiation Potential of Human Embryonic Stem Cells. *Arch. Toxicol.* **2012**, *86* (4), 651–661.

(42) Thaler, R.; Spitzer, S.; Karlic, H.; Klaushofer, K.; Varga, F. DMSO Is a Strong Inducer of DNA Hydroxymethylation in Pre-Osteoblastic MC3T3-E1 Cells. *Epigenetics* **2012**, *7* (6), 635–651.

(43) Yi, X.; Liu, M.; Luo, Q.; Zhuo, H.; Cao, H.; Wang, J.; Han, Y. Toxic Effects of Dimethyl Sulfoxide on Red Blood Cells, Platelets, and Vascular Endothelial Cells in Vitro. *FEBS Open Bio* **2017**, *7* (4), 485–494.

(44) Matsumura, K.; Hyon, S.-H. H. Polyampholytes as Low Toxic Efficient Cryoprotective Agents with Antifreeze Protein Properties. *Biomaterials* **2009**, *30* (27), 4842–4849.

(45) Mitchell, D. E.; Lilliman, M.; Spain, S. G.; Gibson, M. I. Quantitative Study on the Antifreeze Protein Mimetic Ice Growth Inhibition Properties of

Poly(Ampholytes) Derived from Vinyl-Based Polymers. *Biomater. Sci.* **2014**, *2* (12), 1787–1795.

(46) Rajan, R.; Kazuaki, M. Preparation of Novel Synthetic Cryoprotectants. *Cryobiol. cryotechnology* **2014**, *60* (2), 99–103.

(47) Rajan, R.; Hayashi, F.; Nagashima, T.; Matsumura, K. Toward a Molecular Understanding of the Mechanism of Cryopreservation by Polyampholytes: Cell Membrane Interactions and Hydrophobicity. *Biomacromolecules* **2016**, *17* (5), 1882–1893.

(48) Rajan, R.; Jain, M.; Matsumura, K. Cryoprotective Properties of Completely Synthetic Polyampholytes via Reversible Addition-Fragmentation Chain Transfer (RAFT) Polymerization and the Effects of Hydrophobicity. *J. Biomater. Sci. Polym. Ed.* **2013**, *24* (August 2015), 1767–1780.

(49) Liarou, E.; Whitfield, R.; Anastasaki, A.; Engelis, N. G.; Jones, G. R.; Velonia, K.; Haddleton, D. M. Copper-Mediated Polymerization without External Deoxygenation or Oxygen Scavengers. *Angew. Chemie Int. Ed.* **2018**, *57* (29), 8998–9002.

(50) Lamb, J.; Qin, K. P.; Johnson, J. A. Visible-Light Mediated, Additive-Free, and Open-to-Air Controlled Radical Polymerization of Acrylates and Acrylamides. *Polym. Chem.* **2019**, *00*, 1–3.

(51) Ouannes, C.; Wilson, T. Quenching of Singlet Oxygen by Tertiary Aliphatic Amines. Effect of DABCO. *J. Am. Chem. Soc.* **1968**, *90* (23), 6527–6528.

(52) McKenzie, T. G.; Fu, Q.; Uchiyama, M.; Satoh, K.; Xu, J.; Boyer, C.; Kamigaito, M.; Qiao, G. G. Beyond Traditional RAFT: Alternative Activation of Thiocarbonylthio Compounds for Controlled Polymerization. *Adv. Sci.* **2016**, *3* (9), 1–9.

(53) Wang, H.; Li, Q.; Dai, J.; Du, F.; Zheng, H.; Bai, R. Real-Time and in Situ Investigation of “Living”/Controlled Photopolymerization in the Presence of a Trithiocarbonate. *Macromolecules* **2013**, *46* (7), 2576–2582.

(54) Fu, Q.; Xie, K.; McKenzie, T. G.; Qiao, G. G. Trithiocarbonates as Intrinsic Photoredox Catalysts and RAFT Agents for Oxygen Tolerant Controlled Radical Polymerization. *Polym. Chem.* **2017**, *8* (9), 1519–1526.

(55) Lambrinos, P.; Tardi, M.; Polton, A.; Sigwalt, P. The Mechanism of the Polymerization of n.Butyl Acrylate Initiated with N,N-Diethyl Dithiocarbamate Derivatives. *Eur. Polym. J.* **1990**, *26* (10), 1125–1135.

(56) Ishizu, K.; Khan, R. A.; Furukawa, T.; Furo, M. Controlled Radical Polymerization of N-Isopropylacrylamide Initiated by Photofunctional 2-(N,N-Diethyldithiocarbamyl)Isobutyric Acid Sodium Salt in Aqueous Medium. *J. Appl. Polym. Sci.* **2004**, *91* (5), 3233–3238.

(57) Ishizu, K.; Katsuhara, H.; Itoya, K. Controlled Radical Polymerization of Methacrylic Acid Initiated by Diethyldithio-Carbamate-Mediated Iniferter. *J. Polym. Sci. Part A Polym. Chem.* **2005**, *43* (1), 230–233.

(58) Gamer, A. O.; Rossbacher, R.; Kaufmann, W.; van Ravenzwaay, B. The Inhalation Toxicity of Di- and Triethanolamine upon Repeated Exposure. *Food Chem. Toxicol.* **2008**, *46* (6), 2173–2183.

(59) Depass, L. R.; Fowler, E. H.; Leung, H. W. Subchronic Dermal Toxicity Study of Triethanolamine in C3H/HeJ Mice. *Food Chem. Toxicol.* **1995**, *33* (8).

(60) Goodhead, L. K.; MacMillan, F. M. Measuring Osmosis and Hemolysis of Red Blood Cells. *Adv. Physiol. Educ.* **2017**, *41* (2), 298–305.

(61) Van Tomme, S. R.; van Steenbergen, M. J.; De Smedt, S. C.; van Nostrum, C. F.; Hennink, W. E. Self-Gelling Hydrogels Based on Oppositely Charged

Dextran Microspheres. *Biomaterials* **2005**, *26* (14), 2129–2135.

(62) Fisher, S.; Kunin, R. Effect of Cross-Linking on the Properties of Carboxylic Polymers. I. Apparent Dissociation Constants of Acrylic and Methacrylic Acid Polymers. *J. Phys. Chem.* **1956**, *60* (8), 1030–1032.

4.7 Appendix

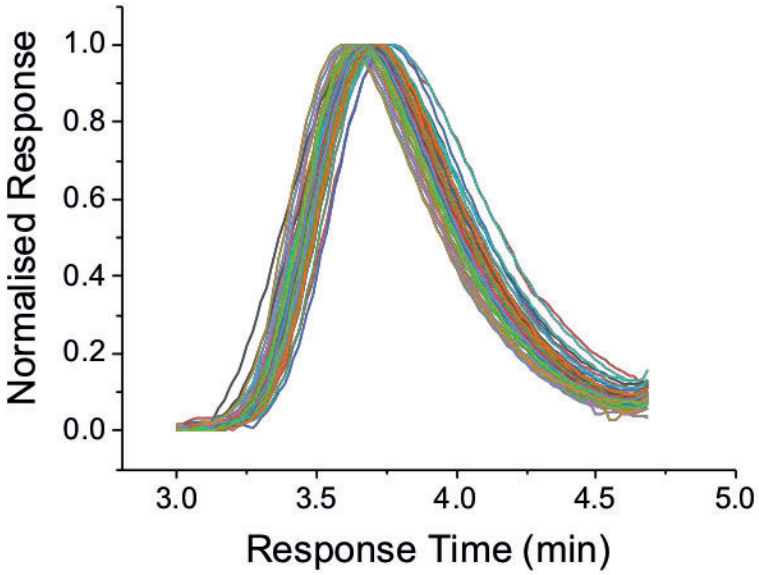

Figure 4.19: SEC Traces in DMF for poly(DMAEMA) samples made using 20 wt % monomer, 2 M TEOA, [M]:[I] ratio of 100:1 and dioxane as solvent.

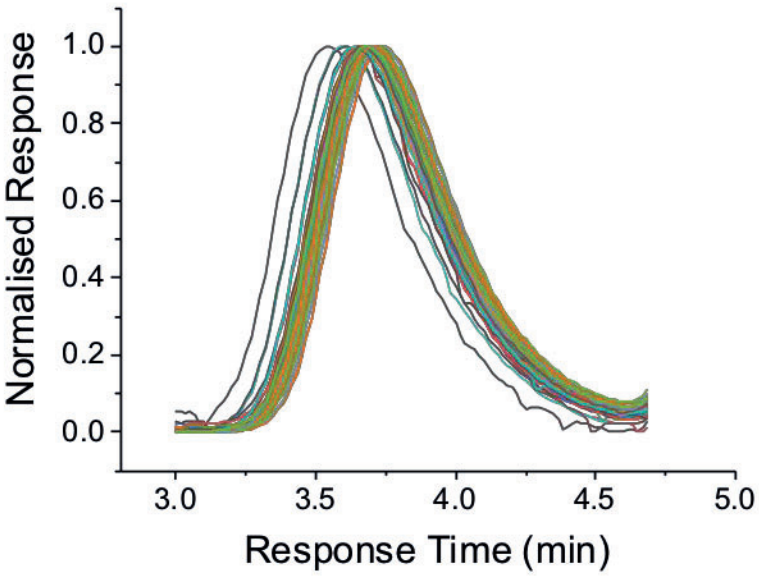

Figure 4.20: SEC Traces in DMF for poly(DMAEMA) samples made using 20 wt % monomer, 2 M TEOA, [M]:[I] ratio of 100:1 and methanol as solvent.

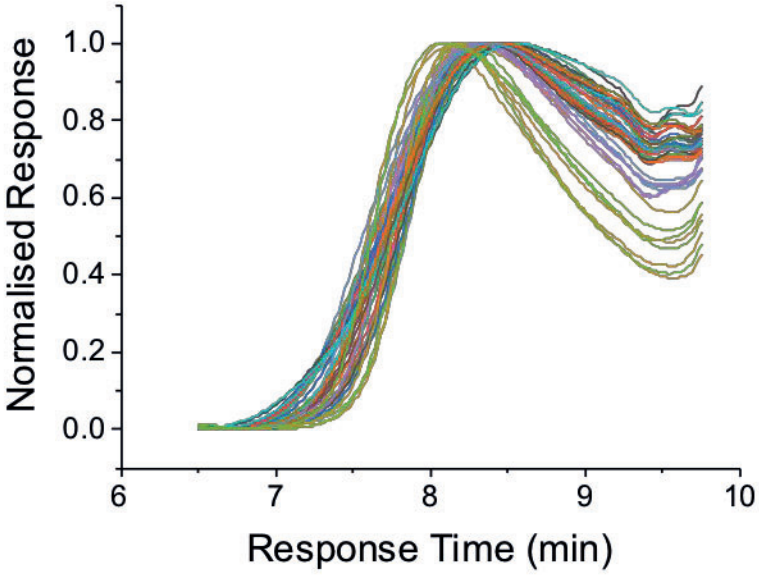

Figure 4.21: SEC Traces in DMF for poly(MA) samples made using 20 wt % monomer, 2 M TEOA, [M]:[I] ratio of 100:1 and dioxane as solvent.

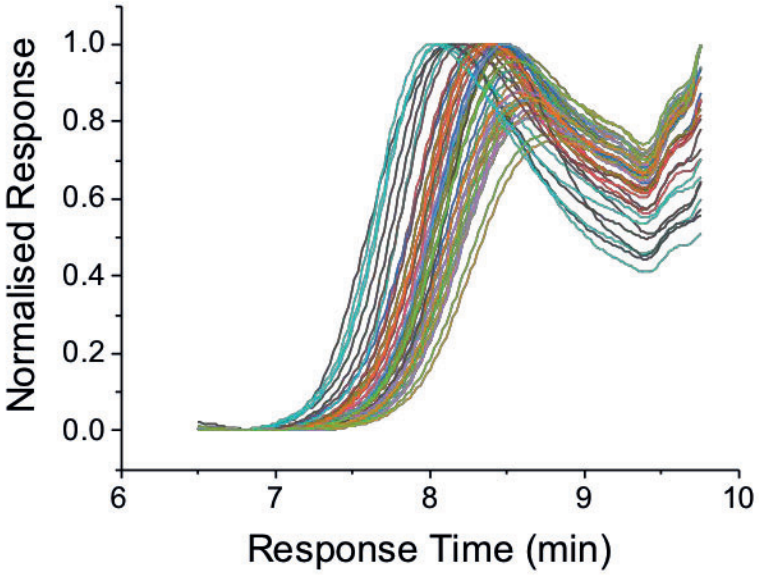

Figure 4.22: SEC Traces in DMF for poly(MA) samples made using 20 wt % monomer, 2 M TEOA, [M]:[I] ratio of 100:1 and methanol as solvent.

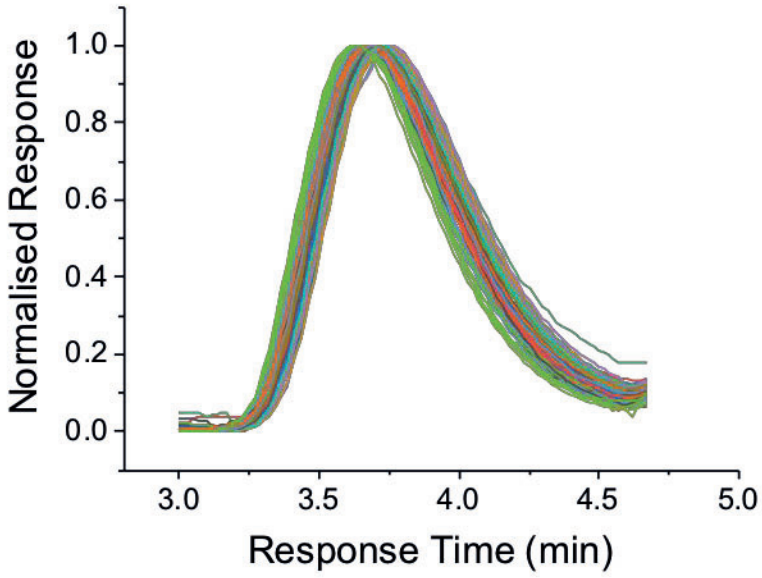

Figure 4.23: SEC Traces in DMF for poly(HEA) samples made using 20 wt % monomer, 2 M TEOA, [M]:[I] ratio of 100:1 and a 1:1 mix of methanol/toluene as solvent.

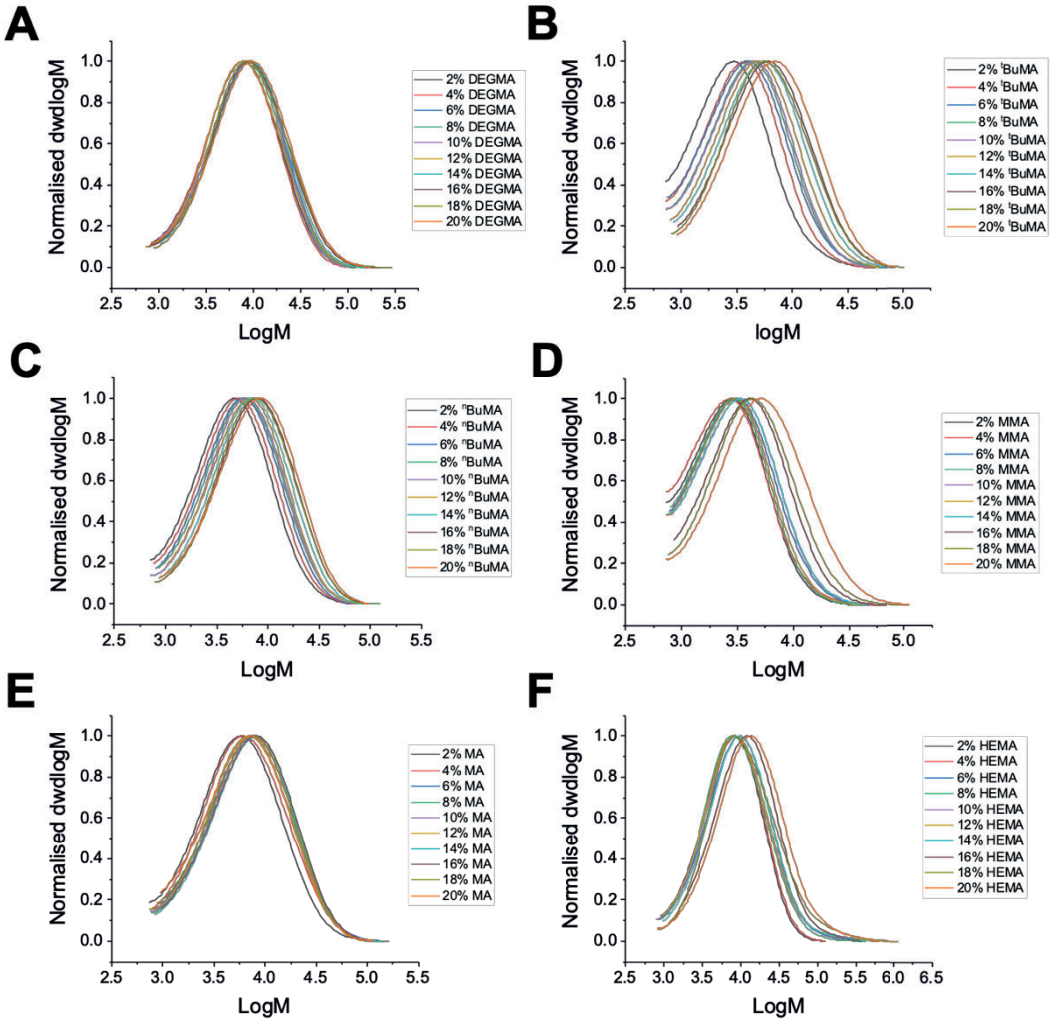

Figure 4.24: Molecular weight distributions from high throughput SEC for the first plate of poly(ampholytes) synthesised. **A** DEGMA; **B** ^{t}BuMA; **C** ^{n}BuMA; **D** MMA; **E** MA; **F** HEMA. SEC was carried out in DMF.

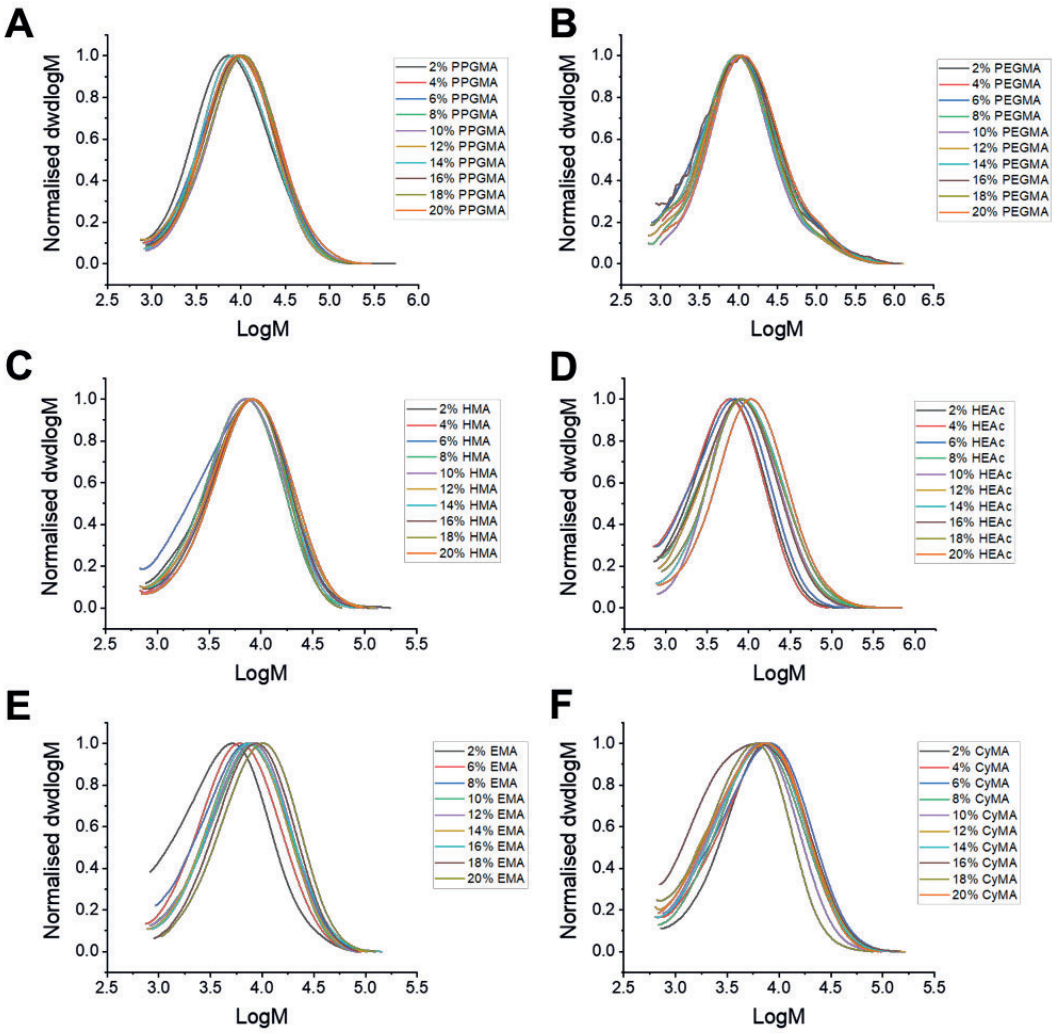

Figure 4.25: Molecular weight distributions from high throughput SEC for the second plate of poly(ampholytes) synthesised. **A** PPGMA; **B** PEGMA; **C** HMA; **D** HEAc; **E** EMA; **F** CyMA. SEC was carried out in DMF.

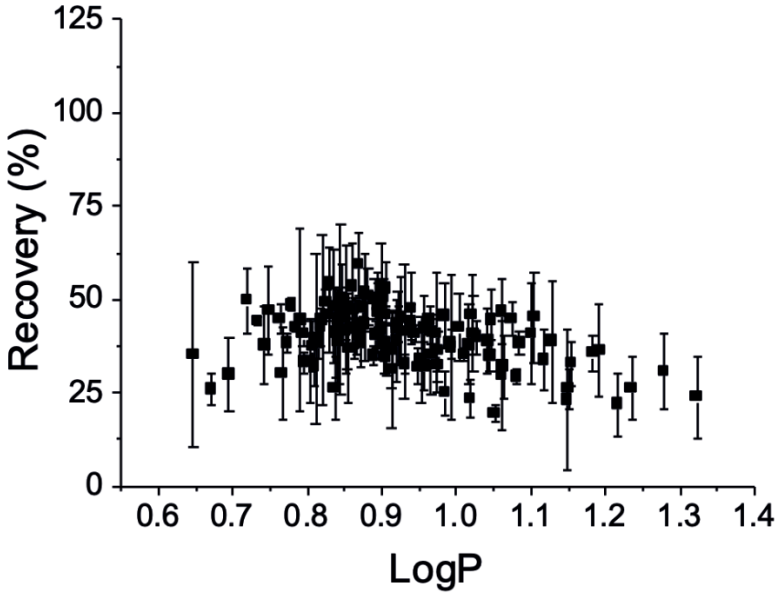

Figure 4.26: Plot of LogP vs Recovery for the library of poly(ampholyte) terpolymers synthesised.

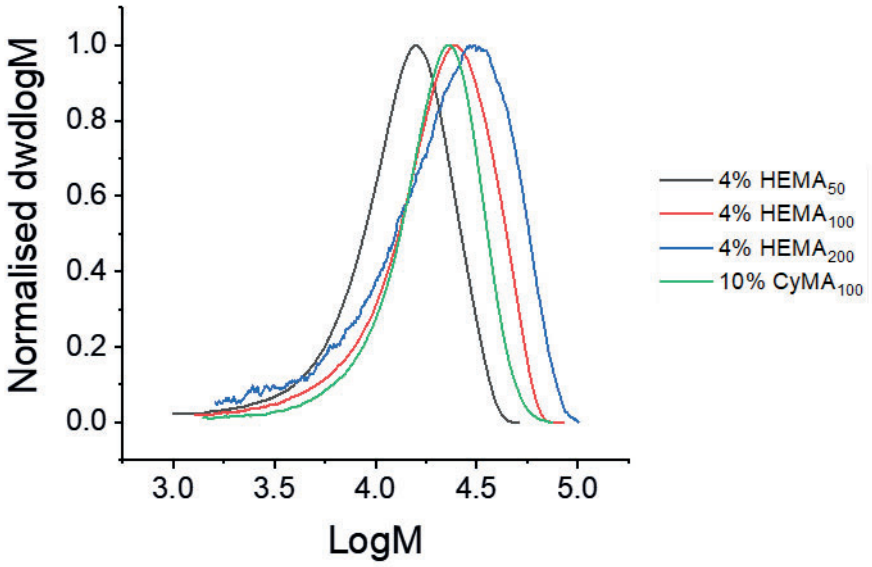

Figure 4.27: Molecular weight distribution from SEC for the 4 polymers synthesised by traditional RAFT polymerisation shown to be most interesting from the library. SEC was carried out in DMF.

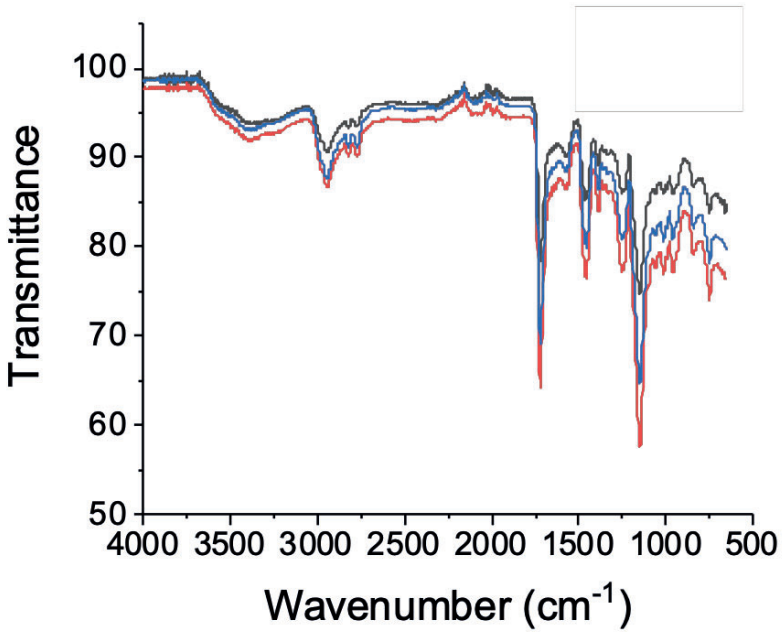

Figure 4.28: FTIR of the three DMAEMA-MAA-HEMA terpolymers synthesised at 3 different [M]:[CTA] ratios: 4% $HEMA_{50}$ (black), 4% $HEMA_{100}$ (red) and 4% $HEMA_{200}$ (blue).

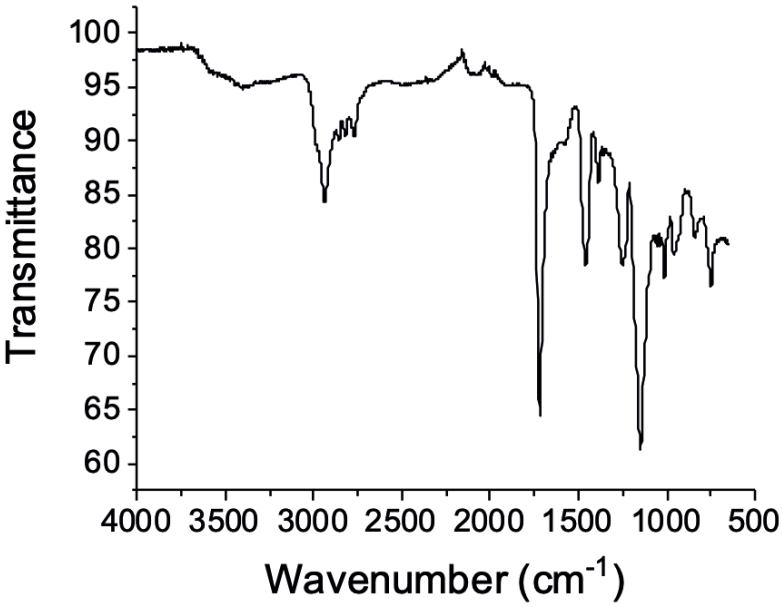

Figure 4.29: FTIR of the 10 % cyclohexyl methacrylate terpolymer synthesised as part of this work (10% $CyMA_{100}$).

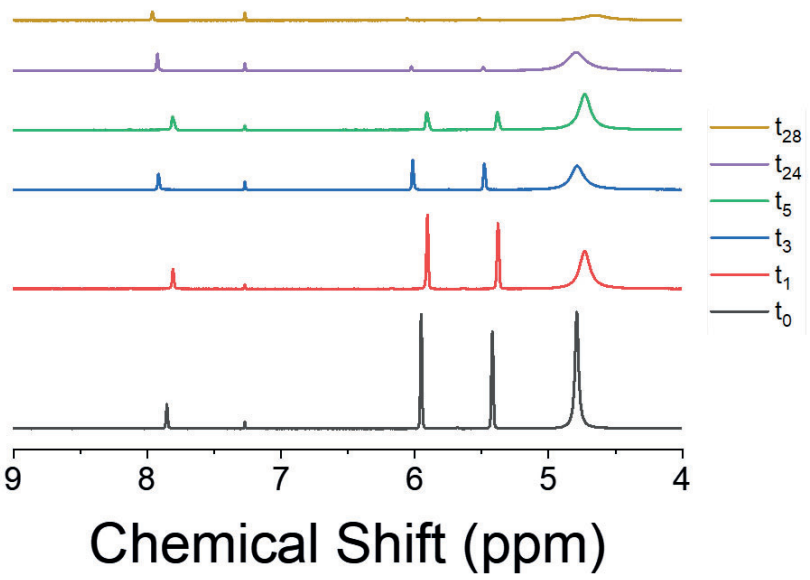

Figure 4.30: Example of the conversion NMRs used to generate the kinetic plots shown in figure 4.10. NMRs were run in $CDCl_3$ and vinyl peaks (5.49 ppm and 6.02 ppm) were monitored relative to the DMF proton at 8.00 ppm.

Chapter 5

Evaluating the Effect of Hydrophobicity on Weakly IRI Active Materials *via* Photopolymerisation of *N*-vinylpyrrolidone

5.1 Abstract

Antifreeze proteins modulate the formation and growth of ice in biological systems, enabling extremophiles to survive in sub-zero temperatures. A common feature is their rigidity, with segregated hydrophobic and hydrophilic domains. It has been demonstrated that increased hydrophobicity in rigid, facially amphipathic, synthetic polymers enhances ice recrystallisation inhibition (IRI) activity but this has not been evaluated in uncharged flexible systems. In this work, photoiniferter polymerisation is used to obtain well-defined poly(*N*-vinylpyrrolidone) copolymers to probe the impact of hydrophobicity on ice recrystallisation inhibition in a fully flexible polymer system, to increase our understanding of how to mimic antifreeze proteins. It is observed that PVP homopolymers demonstrate no significant IRI and that hydrophobic comonomers give very modest changes in IRI, demonstrating that the spacial segregation of 'philicities' is crucial, and not just the overall hydrophobic content of the polymer. These results will help design the next generation of IRI active polymers for cryopreservation applications as well as aid our understanding of how biomacromolecules can inhibit ice growth.

5.2 Introduction

The formation and growth of ice is a major problem in the engineering,[1] aerospace,[2] and medical[3,4] fields. Nature has evolved a diverse series of biomacromolecules which can prevent or promote ice formation[5–7] or prevent seeded ice crystals from growing further.[8,9] Ice growth is a particular issue in the cryopreservation of cells,[10,11] contributing to cell death post-thaw and hence any materials (biological or synthetic) which can modulate this may find a role within the biological cold-chain, including emerging cell-based therapies[12–14] and also for proteins[15] and bacteria.[16] Synthetic polymers which can mimic the function of antifreeze (glyco)proteins (AF(G)Ps) have emerged,[17–19] especially ice recrystallisation inhibition (IRI), but the design rules to enable the discovery of new materials remain elusive. The most IRI active synthetic macromolecule identified to date is poly(vinyl alcohol)[20,21] which has few structural similarities to either AFP or AFGP, and recent results support a distinct mechanism involving hydrogen bonding *via* a precise spacing match between hydroxyls on the PVA chain and the prism plane of ice.[22,23] Drori *et al.* have demonstrated that safranin-O can self-assemble into fibres leading to remarkable IRI and ice shaping ability[24] highlighting that there are potentially many mechanisms of interaction with a growing ice face which may lead to the macroscopic effect of ice growth inhibition.

A common feature of all IRI active materials (large or small molecules) is that they have a balance between hydrophilic and hydrophobic contributions which seems to be essential, or at least highly desirable. Mitchell *et al.* showed that self-assembled metallohelices were potent IRIs despite having no obvious hydrogen bonding motifs, and that the most active had segregated hydrophilic and hydrophobic domains across their surface.[25] Facially amphiphilic rigid glycopolymers (derived from ROMP polymerisation) have definite IRI activity (50 % or greater inhibition of ice growth),[26]

in contrast to fully flexible glycopolymers from methacrylate monomers[27] which can freely rotate around the backbone, supporting the need for segregated 'philicities' for at least one mechanism of ice growth inhibition. Hydroxyl groups (as in PVA) are also not essential; Ben *et al.* have developed lysine derivatives where IRI activity increases with hydrophobicity, but not with the critical micelle concentration, ruling out micellisation as a factor.[28,29] Crucially, these compounds do not lead to ice shaping, implying that ice-face binding may not be essential for inhibiting growth, but instead limiting the rate of exchange at the semi-ordered layer,[30] although this has not been proven yet.

The challenging nature of the ice-water interface and the lack of understanding of ice nucleation makes the rational design of new polymeric AF(G)P mimics challenging.[31] In contrast to ice inhibition, there are many examples of kinetic hydrate inhibitors (KHI) for gas hydrates, with polymers containing amides being particularly important[32,33] including poly(*N*-vinylpyrrolidone) (PVP). This suggests that vinyl lactams maybe good candidates for exploring new IRI active polymers. Many KHI are based on lesser activated monomers (LAMs) which are more challenging to polymerise by controlled radical polymerisation. The radical created during initiation and propagation is much more reactive than the monomer itself, leading to a variety of side reactions during the polymerisation, with a high propensity for chain transfer to both solvent and monomer.[34] In a conventional RAFT polymerisation, the conjugation of the RAFT agent would be enough to generate a stable material, leading to the end of the polymerisation reaction. The addition of a much less stable Z group is required in order to prevent this deactivation, and thus xanthates, *N*-aryl dithiocarbonates, or dithionapththalates,[35] which provide less stability to the radical are required, as opposed to the usual di- or tri- thiocarbonates.[36]

It is currently not clear if vinyl lactams could be repurposed for ice growth inhibition, inspired by their use as kinetic hydrate inhibitors. Considering this, the aim of this work was to systematically explore if the ice recrystallisation activity of inactive PVP homopolymers could be modulated through the introduction of statistically distributed hydrophobic groups as has been shown to be beneficial for materials with distinct, but weak, IRI activity.[26,28] Photoinifirter polymerisation was used to obtain poly(*N*-vinylpyrrolidone), and copolymers with poly(vinyl acetate), at room temperature. After deprotection of the acetate groups, esterification enabled the introduction of a range of side chains, whilst ensuring identical molecular weight distributions. IRI activity measurements showed that IRI activity was not induced, confirming that local rigidity and facial amphiphilicity are crucial, rather than just the addition of a simple hydrophobic comonomer.

5.3 Results and Discussion

5.3i Photoiniferter Polymerisation of *N*-vinylpyrrolidone

Homopolymers of poly(*N*-vinylpyrrolidone) display no IRI activity other than that expected on a colligative level and are therefore an interesting starting point due to their ability to be copolymerised with other less activated monomers allowing the modulation of hydrophobicity post-polymerisation. Photopolymerisation is a rapidly emerging tool in polymer synthesis enabling temporal control and milder reaction conditions compared to traditional thermal initiation methods.[37,38] Xanthates have been reported to enable RAFT/MADIX polymerisation of LAMs using visible light *via* direct photolysis,[39] but also by photoredox catalysis known as photoinduced electron-transfer: PET-RAFT.[40] A particular advantage of these photochemical methods is the ability to conduct the polymerisation in the presence of oxygen[41–43] and at room temperature, which helps avoid the thermally-induced side reactions associated with high temperature polymerisation of less activated monomers like vinyl acetate, for example.[44] As a result of these advantages, the photopolymerisation of *N*-vinylpyrrolidone using a xanthate chain transfer agent was explored. In this process a photolabile MADIX agent is chosen which, when exposed to blue light, generates the radical species necessary to initiate the polymerisation.[41,45] This MADIX agent can then act as both a chain transfer agent and a terminating agent, leading to good control over the polymerisation.[46]

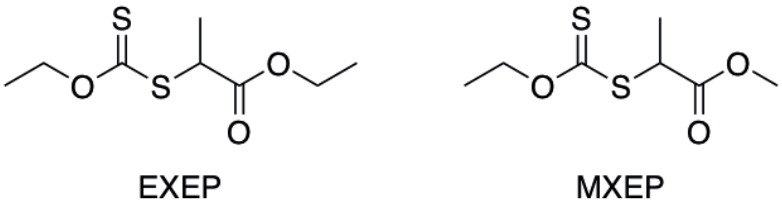

Figure 5.01: Structures of MADIX agents used for the photopolymerisation of LAMs.

Ethyl 2-((ethoxycarbonothioyl)thio)propanoate (EXEP), the structure of which is shown in Figure 5.01, has previously been shown to initiate and control the polymerisation of vinyl acetate using only blue light and hence was the starting point.[47] In this work, the methyl ester derivative was synthesised from readily available potassium ethyl xanthate and 2-methyl bromopropionate, and this was used for all polymerisations due to its easy synthesis and purification. Purity of the MXEP was determined by ^{1}H and ^{13}C NMR in $CDCl_3$, these are shown in Figure 5.02.

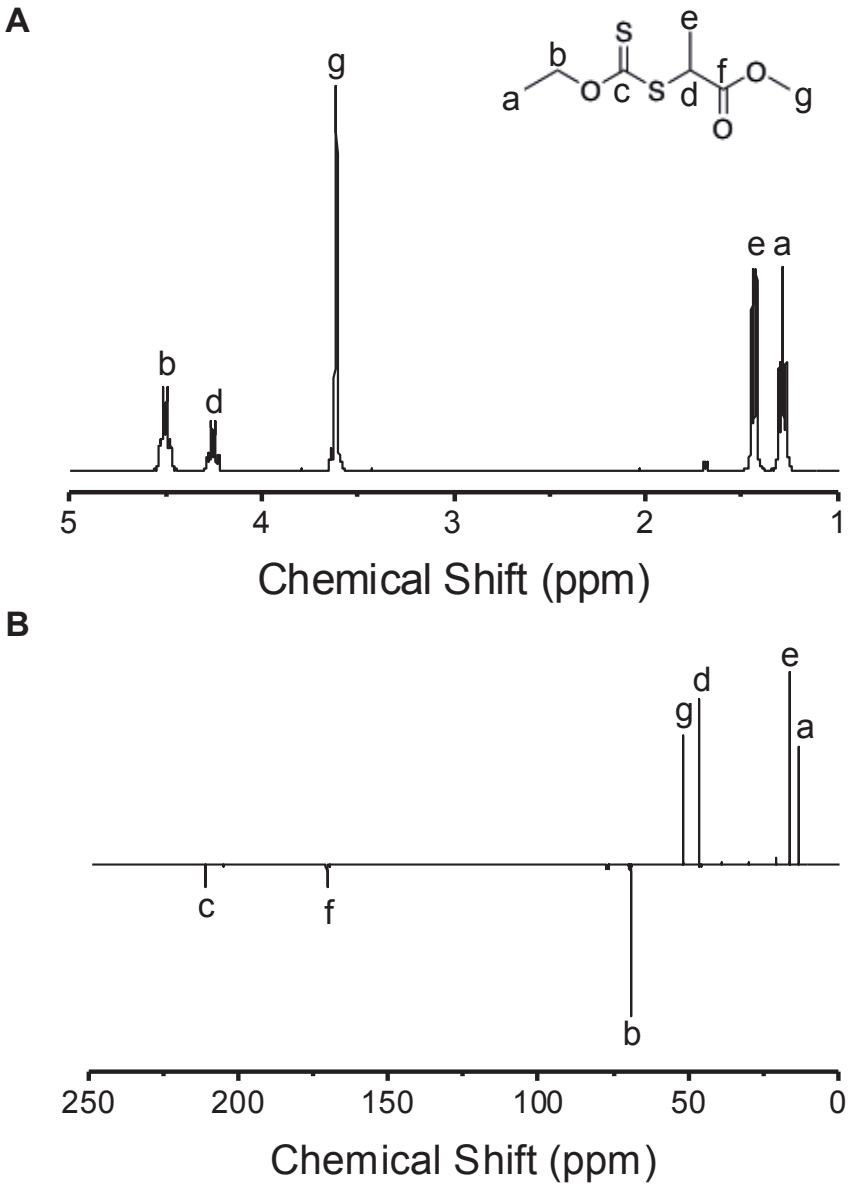

Figure 5.02: ^{1}H (**A**) and ^{13}C (**B**) NMR and of MXEP. NMR was performed in $CDCl_3$.

Initial attempts to polymerise *N*-vinylpyrrolidone under blue light without deoxygenation using a tertiary amine oxygen scavenger failed to afford polymer and were not explored further.[41,45] To overcome this, bulk solutions of monomer/CTA were placed in the reaction vessel and degassed using N_2, followed by irradiation using blue light, Scheme 5.01.

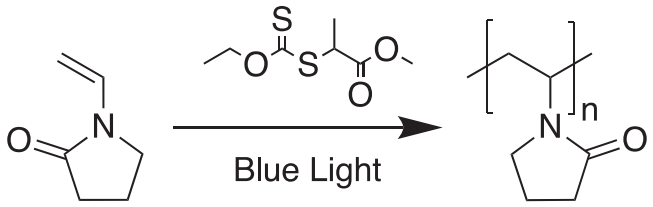

Scheme 5.01: Reaction scheme for the bulk polymerisation of *N*-vinylpyrrolidone using MXEP.

In our screening we observed that this led to polymer formation at room temperature (with no added initiator), and that the polymers typically had lower dispersities (Đ <1.3) however low concentration of polymer in SEC could also contribute to these values being lower.[20] It is believed that this is the first example of VP photopolymerisation using the direct photolysis of a MADIX agent. As a result of this simple synthetic procedure, a panel of PVP homopolymers with targeted degrees of polymerisation from 25 to 100 were obtained using this method, the characterisation data for these materials is shown in Table 5.01.

Table 5.01: PVP homopolymers synthesised in this work

Sample[(a)]	[VP]:[MXEP] (-)[(b)]	Conv (%)[(c)]	M_n (Theo) ($g.mol^{-1}$)[(d)]	M_n (SEC) ($g.mol^{-1}$)[(e)]	M_n (NMR) ($g.mol^{-1}$)[(f)]	Đ (-)[(g)]
PVP_{14}	20	44	980	1500	1300	1.22
PVP_{29}	50	N/A[(h)]	N/A	3200	2800	1.30
PVP_{62}	100	29	3223	6900	5500	1.32

(a) Sample names are determined according to the number average degree of polymerisation (DP) determined by SEC; **(b)** Monomer to MADIX agent molar ratio; **(c)** Determined by ^{1}H NMR using mesitylene as an internal standard; **(d)** Determined by targeted MW multiplied by conversion; **(e)** Determined by SEC; **(f)** Determined by end group analysis; **(g)** Đ is M_w/M_n from SEC; **(h)** Conversion could not be determined as the initial timepoint NMR was not sufficiently concentrated to show the vinyl peaks with reliable integration values. SEC was performed in DMF.

In order to determine polymer molecular weight, SEC was used. SEC was carried out in DMF and molecular weight determined against a poly(methyl methacrylate) calibration. SEC molecular weights were larger than expected, as is commonly seen for PVP, which is difficult to accurately measure in SEC, as it has unusual elution behaviour in commonly used solvents[20,48,49] (other than hexafluoro-isoproanol).[48,49] SEC traces for the materials described in Table 5.01 are shown in Figure 5.03.

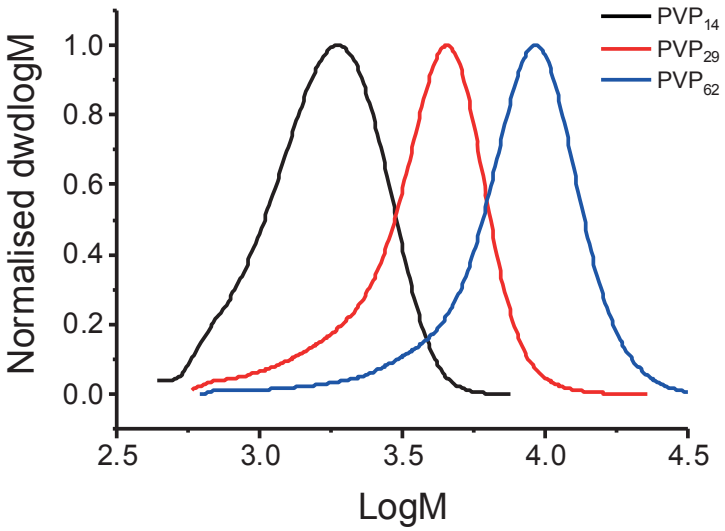

Figure 5.03: Molecular weight distribution from SEC of PVP Homopolymers made in this work. SEC was performed in DMF.

Once the polymers had been synthesised, their intrinsic IRI activity was measured. This is evaluated through the use of a splat assay.[20,29] In short, this involves seeding a polynucleated wafer of small ice crystals (<10 μm) which are then annealed at – 8 °C for 30 minutes, before their size is measured relative to a PBS control, ordinarily, polymers are tested at decreasing concentrations until no activity is observed. A negative control of poly(ethylene glycol), which has no IRI activity, was used to rule out colligative effects, as high concentrations of any material will also limit the rate of ice growth (Figure 5.04).[27] Any activity greater than this level, at the same

concentration, is thought to be due to some interaction between the polymer and the growing ice face.

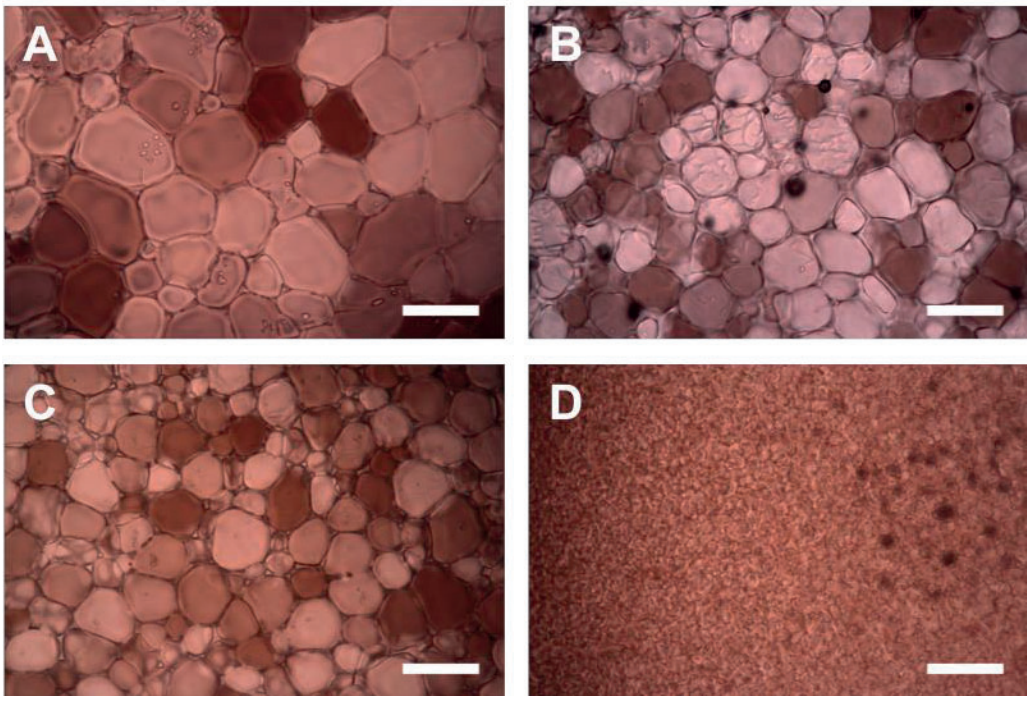

Figure 5.04: Example microscope images taken after 30 minutes annealing at -8 °C. **A** PBS 0.01 M; **B** PEG 20 mg.mL^{-1}; **C** PVP_{14} 20 mg.mL^{-1}; **D** PVA_{148} 0.3 mg.mL^{-1}. All scale bars are 100 µM. PVA is included as an example of the image expected for an IRI active material.

When compared to the negative control (PEG), at both 10 and 20 mg.mL^{-1}, none of the polymers demonstrated significant IRI activity (Figure 5.05). Increasing the molecular weight of the polymer also has no effect on the activity of the material, contrary to what is observed with other IRI active polymers such as PVA (Figure 5.04 D).[20] These results presented the opportunity to explore if IRI activity can be induced by the increase of hydrophobicity. It is important to highlight very few materials have IRI activity, and several recent reviews summarise these.[5,17,18]

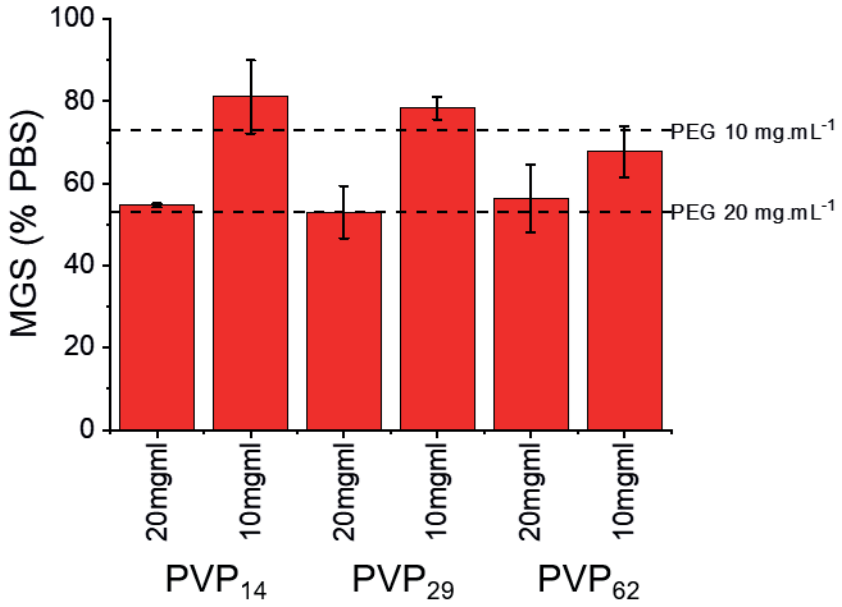

Figure 5.05: IRI activity of PVP homopolymers. Dashed lines indicated the activity of PEG at the concentration indicated. MGS = mean grain size reported as an area. Error bars represent ± standard deviation from a minimum of 3 repeats.

5.3ii Determining the IRI activity of Copolymers of *N*-vinylpyrrolidone with Vinyl Acetate

Previous reports have demonstrated that the activity of moderately IRI active materials can be increased through the incorporation of more hydrophobic units.[26,50] In order to investigate whether this phenomenon is observed in non-IRI active materials, *N*-vinylpyrrolidone was copolymerised with vinyl acetate, at varying monomer ratios from 5 to 15 mol % VAc. A single molecular weight was targeted, with all polymerisations being carried out at a total monomer to CTA ratio of 100:1. The polymers prepared are shown in Table 5.02.

Table 5.02: PVPVAc Copolymers synthesised with varying VAc content.

Sample[(a)]	[VP]: [CTA] (-)[(b)]	[VAc]: [CTA] (-)[(c)]	$Conv_{VP}$ (%)[(d)]	$Conv_{VAc}$ (%)[(e)]	M_n (Theo) ($g.mol^{-1}$) [(f)]	M_n (SEC) ($g.mol^{-1}$) [(g)]	Đ (-)[(h)]
$PVP_{52}VAc_3$	90	10	58	29	7300	7000	1.48
$PVP_{52}VAc_6$	80	20	65	32	6100	6200	1.43
$PVP_{57}VAc_{10}$	75	25	76	43	7700	6100	1.47

(a) Sample names are determined according to the number average degree of polymerisation of each monomer determined by conversion; **(b)** Vinylpyrrolidone to RAFT agent molar ratio; **(c)** Vinyl acetate to RAFT agent molar ratio; **(d)** Vinylpyrrolidone conversion determined by ^{1}H NMR using mesitylene as an internal standard; **(e)** Vinyl acetate conversion determined by ^{1}H NMR using mesitylene as an internal standard; **(f)** Determined by targeted MW multiplied by conversion; **(g)** Determined by SEC; **(h)** Đ is M_w/M_n from SEC.

VAc was chosen as it is also a less activated monomer (LAM), and is suitable for xanthate copolymerisation,[20,36] but is also more hydrophobic than PVP. The VAc units also offer a functional handle for post-polymerisation modification (described below). ^{1}H NMR spectroscopy was used to determine the final composition of the produced polymers. As greater VAc content was required, a greater proportion of VAc was necessitated in the initial monomer feed, this is expected due to the relative reactivity ratios for these monomers (vinylpyrrolidone r = 3.30, vinyl acetate r = 0.205).[51] Polymerisations were also quenched before full VP conversion in an attempt to discourage extended blocks of VAc, and a gradient like microstructure in the final copolymer. Characterisation data for these materials is shown in Table 5.02, and the SEC traces, again in DMF, are shown in Figure 5.06. Unfortunately, molecular weight

could not be determined by NMR due to overlap between the end group and vinyl acetate protons.

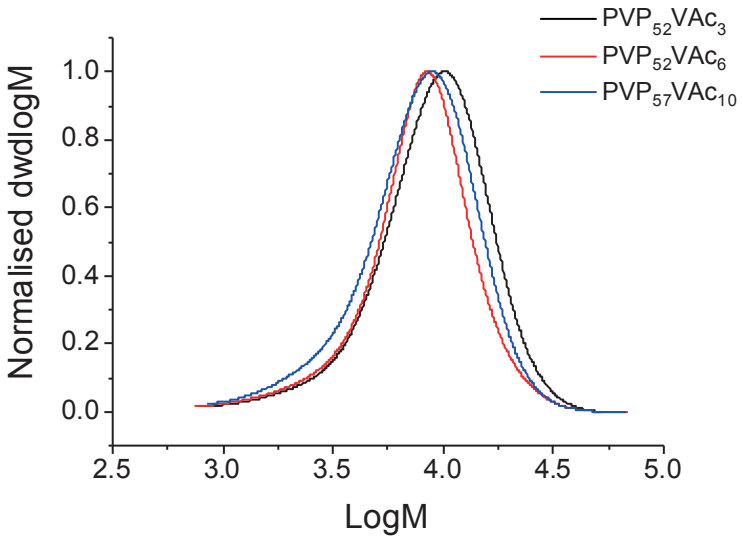

Figure 5.06: Molecular weight distribution from SEC for the polymers described in Table 5.2 Polymers were produced at the same molecular weight with varying VAc incorporation. SEC was performed in DMF.

These polymers were subsequently evaluated for IRI activity as described above. There was a small (but statistically insignificant) increase in the IRI activity (decrease in mean grain size) as the VAc content was increased, which suggested that either copolymerisation cannot increase the IRI activity, or that the VAc itself was insufficiently hydrophobic, Figure 5.07. Considering these results, a greater degree of introduced hydrophobicity was required to enable this concept to be further probed. Greater VAc incorporation was avoided as this would create solubility issues when further functionalisation was attempted, which may give rise to negative results due to solubility, instead of a lack of IRI activity.[52]

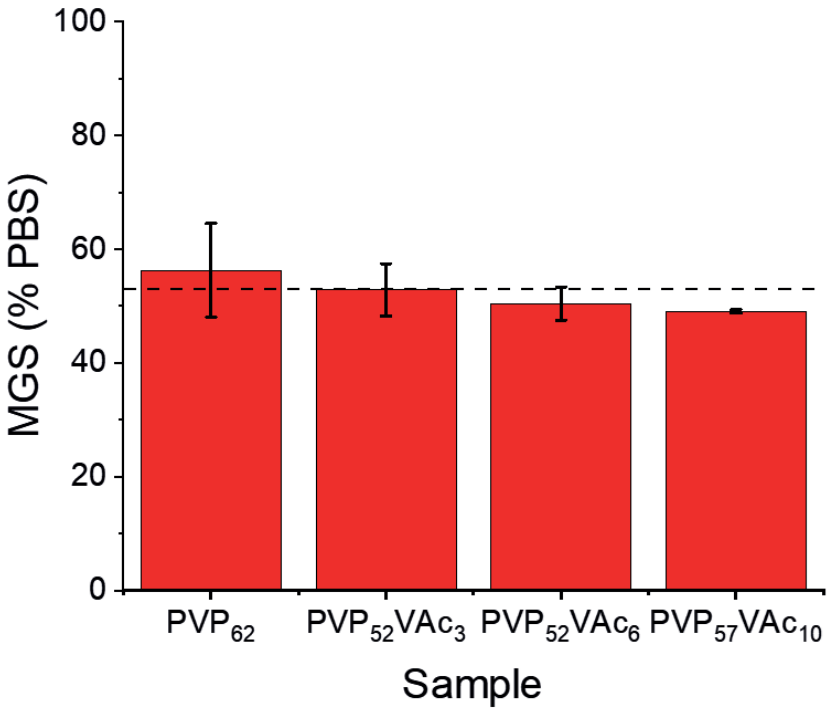

Figure 5.07: IRI activity of PVP-*co*-VAc polymers tested at 20 mg.mL^{-1} and compared to a PVP_{62} homopolymer. MGS = mean grain size reported as an area. The dashed line indicates the activity of 20 mg.mL^{-1} PEG. Error bars represent ± standard deviation from a minimum of 3 repeats.

To enable a higher degree of hydrophobicity to be probed, a range of 5 mol % VAc copolymers were synthesised at varying molecular weights. Samples were prepared using three different [M]:[I] ratios, 200, 100 and 50:1, and characterisation data for these materials is shown in Table 5.03, with SEC traces shown in Figure 5.08 B.

Table 5.03: 5% VAc copolymers synthesised at three different molecular weights.

Sample[(a)]	**[VP]: [CTA] (-)**[(b)]	**[VAc]: [CTA] (-)**[(c)]	**$Conv_{VP}$**[d]**(%)**[(d)]	**$Conv_{VAc}$ (%)**[(e)]	**M_n (Theo) ($g.mol^{-1}$)** [(f)]	**M_n (SEC) ($g.mol^{-1}$)** [(g)]	**Đ (-)**[(h)]
$PVP_{24}VAc_2$	40	10	59	20	5700	3600	1.49
$PVP_{52}VAc_3$	90	10	58	29	7300	7000	1.48
$PVP_{106}VAc_5$	190	10	56	53	13000	13000	1.65

(a) Sample names are determined according to the number average degree of polymerisation of each monomer determined by conversion; **(b)** Vinylpyrrolidone to RAFT agent molar ratio; **(c)** Vinyl acetate to RAFT agent molar ratio; **(d)** Vinylpyrrolidone conversion determined by ^{1}H NMR using mesitylene as an internal standard; **(e)** Vinyl acetate conversion determined by ^{1}H NMR using mesitylene as an internal standard; **(f)** Determined by targeted MW multiplied by conversion; **(g)** Determined by SEC; **(h)** Đ is M_w/M_n from SEC. SEC was performed in DMF.

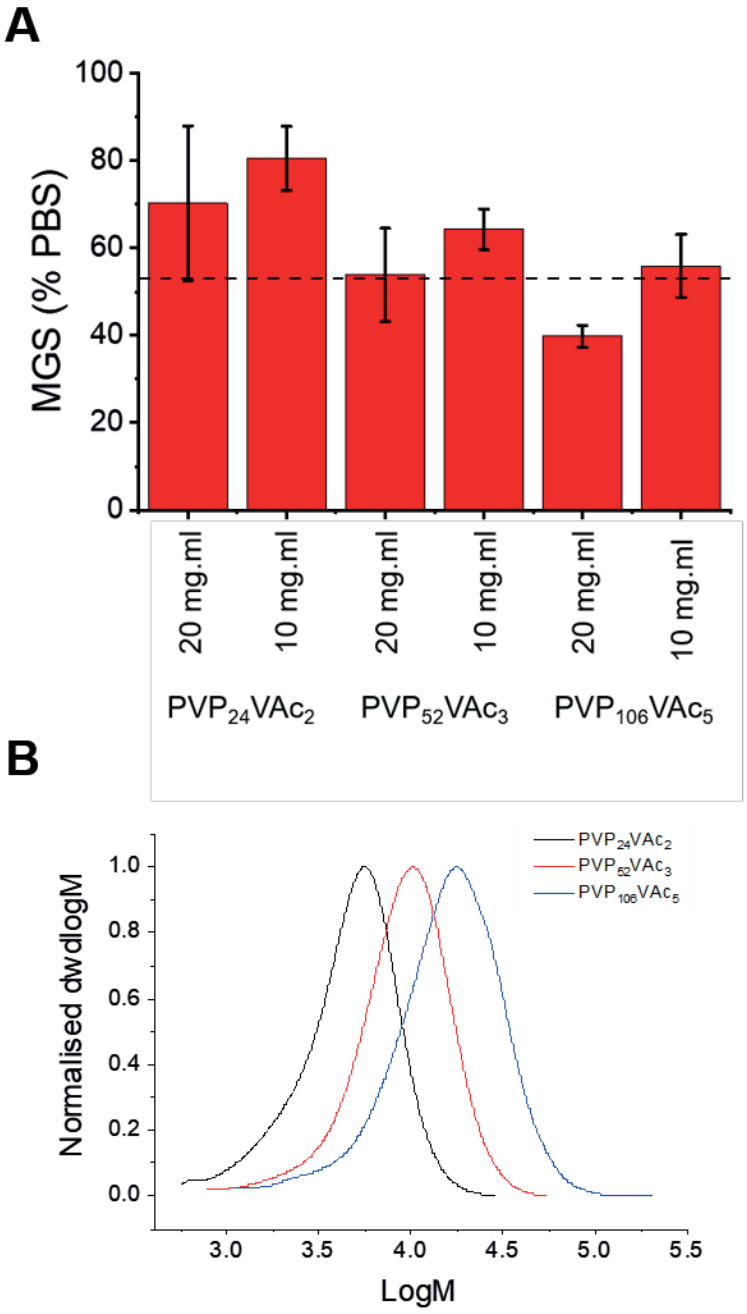

Figure 5.08: A Impact of VAc content on IRI activity as a function of DP. MGS = mean grain size reported as an area. The dashed line indicates the activity of 20 mg.mL^{-1} PEG. Error bars represent ± standard deviation from a minimum of 3 repeats; **B** Molecular weight distribution from SEC of polymers described in Table 5.03. SEC was performed in DMF.

Again, these samples were tested for IRI activity using the standard splat assay, and the results are shown in Figure 5.09. Increasing the molecular weight again resulted in little difference between the samples, demonstrating no significant molecular weight dependence in the PVP-*co*-VAc polymers, unlike other IRI active materials.[14,20,22,53] The longer polymers appeared to be more readily soluble, and therefore these were selected for further functionalisation and testing.

5.3iii Evaluating the IRI activity of Hydrophobically Modified Poly(*N*-vinylpyrrolidone-co-vinyl acetate)

A sample of $PVP_{106}VAc_5$ was deprotected by stirring with hydrazine at 50 °C in methanol, and quantitative removal of the acetate groups was confirmed by IR and ^{13}C NMR, as shown in Figure 5.09. ^{1}H NMR, which is usually used to determine degree of hydrolysis, could not be used as the vinyl alcohol repeat unit peaks are obscured by the protons of the vinylpyrrolidone repeat unit. The hydroxyl group was subsequently esterified using a range of acyl chlorides of varying hydrophobicity, from propionyl to 4-fluorobenzoyl chloride (Scheme 5.02) generating a library of diversely functionalised PVP copolymers. For the benzoyl, valeroyl and propionyl polymers, successful functionalisation was confirmed by the loss of the VA backbone peaks at 37 and 119 ppm in the ^{13}C NMR, and the formation of new backbone peaks at 62 and 72 ppm, as well as the appearance of new aromatic or alkyl protons in the ^{1}H NMR as appropriate. In the case of 4-fluorobenzoyl functionalised materials, ^{19}F NMR was used, and the formation of a single peak at -106 ppm confirmed the presence of the fluorinated group in the polymer.

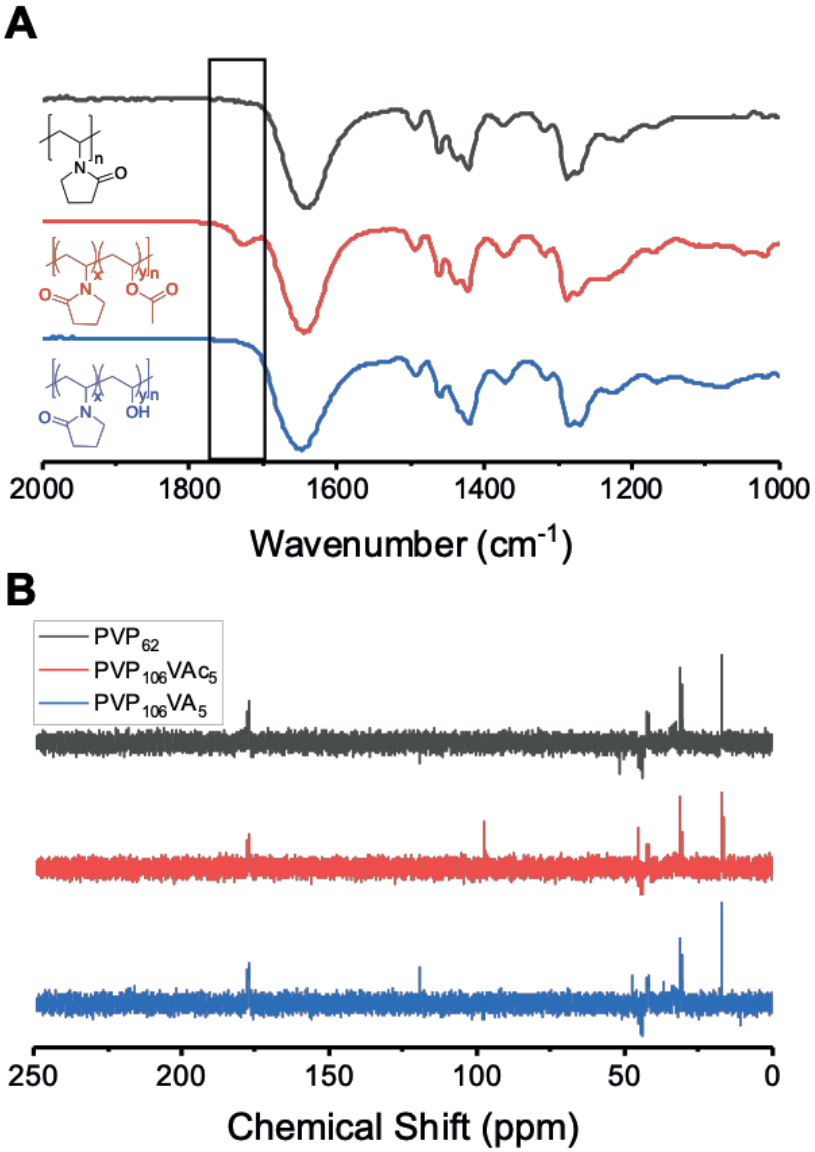

Figure 5.09: Characterisation of PVP, PVP-*co*-VAc and PVP-*co*-VA. **A** Infrared spectra showing the introduction of the acetate group, and its subsequent removal after treatment with hydrazine. Vinyl acetate ester unit is highlighted; **B** ^{13}C NMR of Poly(N-vinylpyrrolidone), Poly(N-vinylpyrrolidone-co-vinyl acetate) and Poly(N-vinylpyrrolidone-co-vinyl alcohol). The additional methyl peak at 16 ppm and backbone carbon at 97 ppm indicate successful incorporation of the vinyl acetate monomer. The subsequent loss of these peaks after deprotection, and new peaks at 37 ppm and 47 ppm corresponding to the backbone carbons of the vinyl acetate unit demonstrate successful deprotection. NMRs were run in $CDCl_3$.

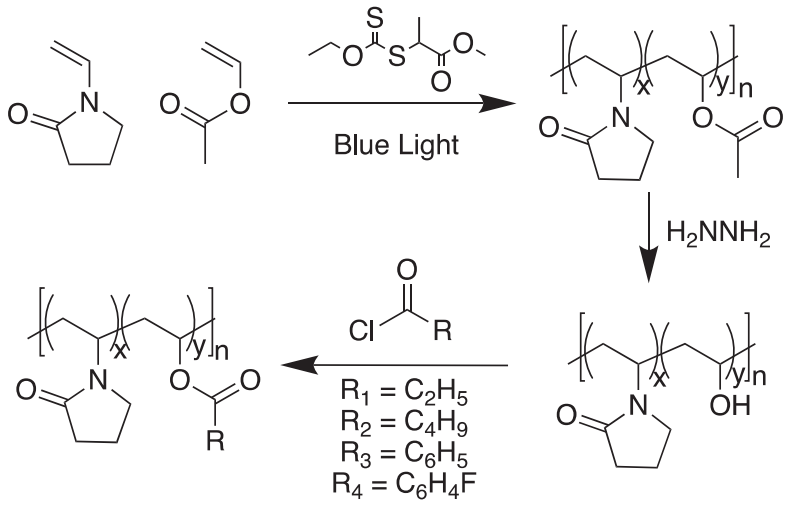

Scheme 5.02: Reaction scheme for the deprotection of PVP-*co*-VAc, and the subsequent functionalisation using acyl chlorides.

The resulting copolymers were again tested for IRI activity using a splat assay, and the results plotted in figure 5.10 A. In all cases, no significant difference between the IRI activity was observed, independent of the comonomer unit. Plotting the mean grain size at 20 $mg.mL^{-1}$ against the calculated partition coefficient for the hydrophobic monomer (LogP), showed there was no observable correlation between comonomer hydrophobicity and IRI activity (Figure 5.10 B). These observations are in contrast to what is observed for rigid polymers, such as those derived from ROMP (ring opening metathesis polymerisation) where subtle changes to the hydrophobic unit have a dramatic impact,[26] and also in emerging self-assembled systems.[24,25] This difference has been linked to the need to segregate the hydrophobic units from the hydrophilic to introduce IRI activity.

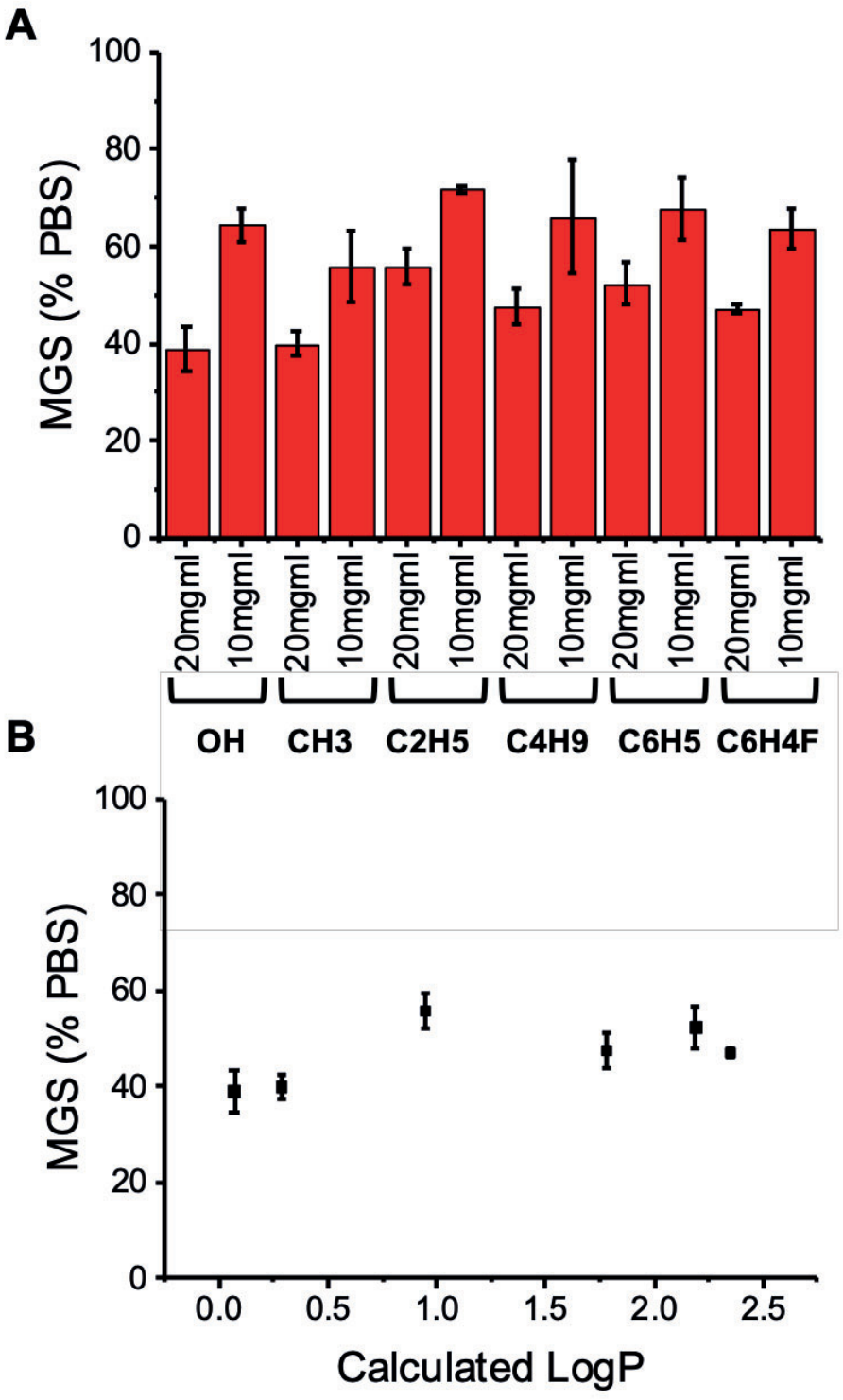

Figure 5.10: IRI activity of hydrophobically modified PVP copolymers. **A** IRI activity of all functionalised copolymers synthesised; **B** Mean grain size verses calculated LogP of the hydrophobic comonomer. MGS = mean grain size reported as an area. Error bars represent ± standard deviation from a minimum of 3 repeats.

Similar results have been observed in small molecule IRI agents from Ben *et al*., where in some cases greater hydrophobicity led to increased IRI, but in others it failed to do so.[28] The addition of alkyl chains from one to six carbons did not increase IRI activity, however between seven and sixteen carbon long chains, IRI activity increased and solubility decreased, suggesting a fine balance between hydrophobicity and solubility is required.[9] When compared to the above results, in which the materials contained an obvious hydroxyl rich binding motif, this suggests that activity cannot be induced in an inactive material simply by the introduction of hydrophobic groups, but that more precise methods are required. Modelling experiments have demonstrated that AGFP binds to ice *via* its hydrophobic face,[54] however these results also suggest that hydrophobic domains are not enough, and that the 3D presentation and control of these hydrophobic faces is important for the binding of the material to the growing ice face, and therefore its ability to inhibit ice recrystallisation.

5.4 Conclusion

Herein, the ice growth inhibition potential of poly(*N*-vinylpyrrolidone), as a homopolymer and as a hydrophobically modified copolymer has been sequentially explored. A photopolymerisation method using xanthates as photoiniferters/RAFT agents was used, enabling intrinsic blue-light initiated polymerisation in bulk, reaching higher degrees of conversation and lower dispersities than is typically obtained using thermal methods. Copolymers of vinyl acetate (another lesser activated monomer) were also synthesised, which after deprotection enabled sequential side-chain modification of the polymer using a range of acyl chlorides. Ice recrystallisation inhibition assays showed that homo PVP demonstrated no IRI activity compared with negative controls and was therefore a good substrate for further modification. The incorporation of hydrophobic groups failed to lead to any significant increases in activity. This is in contrast to previous reports on rigid-rod polymers and small molecule IRI agents, where introducing hydrophobicity increases activity. These observations support a hypothesis that hydrophobicity alone is not enough to induce ice growth inhibition, and the placement and distribution of the units is crucial. The approach used here did not segregate hydrophobic units, and hence adds support to emerging concepts that the spacial segregation of the hydrophilic and hydrophobic components is a key feature of all macromolecular IRI agents. These results will help guide the development of the next generation of IRI agents, especially focussing efforts towards the development of defined and inflexible copolymers. One potential development of this work would be to create block copolymers of the hydrophobic and hydrophilic monomers, in order to investigate the role of separated domains of hydrophobicity and hydrophilicity. This would allow further conclusions to be drawn about the role of hydrophobicity in highly IRI active materials.

5.5 Experimental

Materials

Phosphate-buffered saline (PBS) solutions were prepared using pre-formulated tablets (Sigma-Aldrich) in 200 mL of Milli-Q water (>18.2 Ω mean resistivity) to give [NaCl] = 0.138 M, [KCl] = 0.0027 M, and pH 7.4. Vinyl acetate (>99 %), 2-vinylpyrrolidone (>99 %), methyl bromoacetate (97 %), fluorobenzoyl chloride (98 %), benzoyl chloride (99 %), valeroyl chloride (98 %), propionyl chloride (98 %), polyethylene glycol (average M_n 4,600 Da), mesitylene (98 %) and hydrazine hydrate solution (78-82 % in water) were purchased from Sigma-Aldrich. Vinyl acetate was filtered through a plug of basic alumina to remove inhibitors prior to use. Potassium ethyl xanthate (98 %) was purchased from Alfa Aesar. All solvents were purchased from VWR or Sigma Aldrich and reagents were used without further purification unless indicated.

Physical and Analytical Methods

^{1}H and ^{13}C NMR spectra were recorded on Bruker Avance III HD 300 MHz, HD 400 MHz or HD 500 MHz spectrometers using deuterated solvents obtained from Sigma-Aldrich. Chemical shifts are reported relative to residual non-deuterated solvent. SEC data was recorded on an Agilent 390-LC MDS instrument equipped with differential refractive index (DRI), viscometry (VS), dual angle light scatter (LS) and dual wavelength UV detectors. The system was equipped with 2 x PLgel Mixed D columns (300 x 7.5 mm) and a PLgel 5 μm guard column. The eluent was DMF with 5 mmol NH_4BF_4 additive. Samples were run at 1 $mL.min^{-1}$ at 50 °C. Poly(methyl methacrylate) standards (Agilent EasyVials) were used for calibration. Analyte samples were filtered through a nylon membrane with 0.22 μm pore size before

injection. Respectively, experimental molar mass ($M_{n,SEC}$) and dispersity (Đ) values of synthesized polymers were determined by conventional calibration using Agilent GPC/SEC software.

Ice wafers were annealed on a Linkam Biological Cryostage BCS196 with T95-Linkpad system controller equipped with a LNP95-Liquid nitrogen cooling pump, using liquid nitrogen as the coolant (Linkam Scientific Instruments UK, Surrey, UK). An Olympus CX41 microscope equipped with a UIS-2 20x/0.45/∞/0-2/FN22 lens (Olympus Ltd, Southend on sea, UK) and a Canon EOS 500D SLR digital camera was used to obtain all images. Image processing was conducted using Image J, which is freely available from http://imagej.nih.gov/ij/. LogP was calculated from the hydrophobicity of the pendant group using ChemDraw Professional 16.0.

Ice Recrystallisation Inhibition Assay

A 10 μL droplet of polymer in PBS solution was dropped from 1.4 metres onto a glass microscope coverslip, which was placed on top of an aluminium plate cooled to -78 °C using dry ice. The droplet froze instantly upon impact with the plate, spreading out and forming a thin wafer of ice. This wafer was then placed on a liquid nitrogen cooled cryostage held at -8 °C within the viewing are of the microscope. The wafer was then left to anneal for 30 minutes at -8 °C. The number of crystals in the image was counted, again using ImageJ, and the area of the field of view divided by this number of crystals to give the average crystal size per wafer and reported as a percentage (%) of area compared to PBS control.

Synthesis of methyl 2-((ethoxycarbonothioyl)thio)propanoate (MXEP)

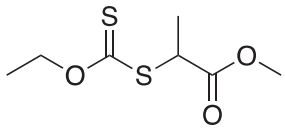

Acetone (70 mL) was added to a round bottom flask equipped with a stirrer bar. Potassium ethyl xanthate (3 g, 19 mmol, 1 eq) was added and stirred until dissolution. After 30 minutes, Methyl 2-bromopropionate (2.84 g, 19 mmol, 1 eq) was added and the solution left for 24 hours. The resulting solution was filtered, washed with cold ethanol, and the filtrate concentrated *in vacuo*. The resulting yellow oil was purified on a column of silica with hexane:ethyl acetate (9:1) as eluent. The fractions were concentrated and dried under vacuum.

Yield 2.84 g 71 %. ^{1}H NMR (400 MHz, $CDCl_3$): **δ** = 1.30 (CH_3CH_2O, t, J = 7 Hz, 3H), 1.45 ($SCH(CH_3)CO$, d, J = 7 Hz, 3H), 3.62 ($COOCH_3$, s, 3H), 4.27 ($SCH(CH_3)CO$, q, J = 7 Hz, 1H), 4.52 (CH_3CH_2O, q, J = 7 Hz, 2H). ^{13}C NMR (400 MHz, $CDCl_3$): **δ** = 14 (CH_3CHO), 18 ($SCH(CH_3)CO$), 47 ($SCH(CH_3)CO$), 55 ($COOCH_3$), 70 (CH_3CH_2O), 173 ($SCH(CH_3)COO$), 211 ($OC(S)S$).

Synthesis of PVP homopolymers

As a representative example, 2-vinylpyrrolidone (1 g, 9 mmol, 100 eq), MXEP (0.018 g, 0.09 mmol, 1 eq) and Mesitylene (20 μL) were added to a 20 mL vial and sealed with a subaseal. The solution was degassed and a sample taken for ^{1}H NMR. The vial was wrapped with blue LEDs and left to react for 24 hours. After which, another sample was taken for NMR, and conversion determined by analysing the mesitylene

standard. The resulting polymer was precipitated three times into hexane, dried and dissolved in water, followed by lyophilisation to evolve a fine white powder.

Yield: 0.202 g. ^{1}H NMR (400 MHz, D_2O): **δ** = 1.39-1.83 (C*H*$_2$CH(C_4H_6NO), br, 2H), 1.84-2.07 (NCH$_2$C*H*$_2$CH$_2$CO, br, 2H), 2.08-2.50 (NCH$_2$CH$_2$C*H*$_2$CO, br, 2H), 2.93-3.38 (NC*H*$_2$CH$_2$CH$_2$CO, br, 2H), 3.41-3.86 (CH$_2$C*H*(C_4H_6NO), br 1H). ^{13}C NMR (400 MHz, $CDCl_3$): **δ** = 17 (NCH$_2$*C*H$_2$CH$_2$CO), 31 (NCH$_2$CH$_2$*C*H$_2$CO), 34 (*C*H$_2$CH(C_4H_6NO)), 42 (N*C*H$_2$CH$_2$CH$_2$CO), 44-46 (CH$_2$*C*H(C_4H_6NO)), 177 (NCH$_2$CH$_2$CH$_2$*C*O). IR Lactam C-H 2959 cm^{-1}, C=O 1642 cm^{-1}. M_n^{SEC}(DMF) = 6,900 Da, M_w/M_n = 1.32.

Synthesis of PVP-PVAc copolymers

As a representative example, 2-vinylpyrrolidone (1 g, 9 mmol, 90 eq), vinyl acetate (0.086 g, 1 mmol, 10 eq), MXEP (0.02 g, 0.1 mmol) and Mesitylene (20 μL) were added to a 20 mL vial and sealed with a subaseal. The solution was degassed and a sample taken for ^{1}H NMR. The vial was wrapped with blue LEDs and left to react for 24 hours. At the end of the reaction, another sample was taken for NMR, and conversion determined by analysing the mesitylene standard. The resulting polymer was precipitated three times into hexane, dried and dissolved in water, followed by lyophilisation to evolve a fine white powder.

Yield: 0. 426g. ^{1}H NMR (400 MHz, $CDCl_3$): **δ** = 1.09-1.22 (C*H*$_3$COOCH, br), 1.39-1.84 (C*H*$_2$CH(C_4H_6NO), C*H*$_2$CH(O)CH$_2$, br), 1.86-2.09 (NCH$_2$C*H*$_2$CH$_2$CO, br), 2.10-2.53 (NCH$_2$CH$_2$C*H*$_2$CO, br), 2.93-3.39 (NC*H*$_2$CH$_2$CH$_2$CO, br), 3.40-3.93 (CH$_2$C*H*(C_4H_6NO), br), 4.51-4.63 (CH$_3$C*H*(O)CH$_2$, br). ^{13}C NMR (400 MHz, $CDCl_3$): **δ** = 16 (*C*H$_3$COOCH), 17(NCH$_2$*C*H$_2$CH$_2$CO), 31 (NCH$_2$CH$_2$*C*H$_2$CO), 34 (*C*H$_2$CH(C_4H_6NO), 42 (N*C*H$_2$CH$_2$CH$_2$CO), 44-45 (CH$_2$C*H*(C_4H_6NO), 46

($CH_2CHOCOCH_3$), 97 ($CH_2CHOCOCH_3$), 177 ($NCH_2CH_2CH_2CO$), 178 (CH_3COO). IR Lactam C=O 1646 cm^{-1}, Acetate C=O 1729 cm^{-1}. M_n^{SEC}(DMF) = 7,000 Da, M_w/M_n = 1.48.

Deprotection of PVP-PVAc Copolymers

Poly(2-vinylpyrrolidone-*co*-vinyl acetate) (0.5 g) was added to a round bottom flask and dissolved in methanol (10 mL) with stirring. The flask was heated to 50 °C and hydrazine (10 mL) added. The reaction was left for 24 hours, after which the solvent was concentrated *in vacuo* and the polymer/methanol solution precipitated into diethyl ether. Solvent was removed and the sample dissolved in water followed by lyophilisation to produce a fine white powder.

Yield: 0.382 g. ^{1}H NMR (400 MHz, $CDCl_3$): **δ** = 1.27-1.80 ($CH_2CH(C_4H_6NO)$, CH_2CHOH, br), 1.80-2.07 ($NCH_2CH_2CH_2CO$, br), 2.09-2.58 ($NCH_2CH_2CH_2CO$, br), 2.83-3.39 ($NCH_2CH_2CH_2CO$, br), 3.40-3.93 ($CH_2CH(C_4H_6NO)$, CH_2CHOH, br). ^{13}C NMR (400 MHz, $CDCl_3$): **δ** = 17 ($NCH_2CH_2CH_2CO$), 31 ($NCH_2CH_2CH_2CO$), 34 ($CH_2CH(C_4H_6NO)$, 37 (CH_2CHOH), 42 ($NCH_2CH_2CH_2CO$), 44-45 ($CH_2CH(C_4H_6NO)$, 47 (CH_2CHOH), 177 ($NCH_2CH_2CH_2CO$). IR Lactam C=O 1648 cm^{-1}. M_n^{SEC}(DMF) = 4,100 Da, M_w/M_n = 3.33.

Functionalisation of PVP-PVA Copolymers with Benzoyl Chloride

Poly(N-vinylpyrrolidone-*co*-vinyl alcohol) (150 mg) was dissolved in dimethylformamide (10 mL) with stirring and left to dissolve. After 30 minutes, triethylamine (20 mg) and benzoyl chloride (45 mg) was added and left to react for 3 hours. After which the polymer was concentrated *in vacuo* and precipitated three times into diethyl ether and dried under vacuum. The polymer was then dissolved in water

and purified using centrifugal dialysis (3000 Da MWCO, Millipore) followed by lyophilisation.

Yield: 27 mg. ^{1}H NMR (400 MHz, D_2O): **δ** = 1.29-1.84 (C*H*$_2$CH(C_4H_6NO), C*H*$_2$CHOCO, br), 1.85-2.09 (NCH$_2$C*H*$_2$CH$_2$CO, br), 2.10-2.53 (NCH$_2$CH$_2$C*H*$_2$CO, br), 2.91-3.41 (NC*H*$_2$CH$_2$CH$_2$CO, br), 3.42-4.18 (CH$_2$C*H*(C_4H_6NO), CH$_2$C*H*OCO, br), 7.44-7.55 (meta-CH, br), 7.57-7.65 (para-CH, br), 7.72-7.83 (ortho-CH, br). ^{13}C NMR (400 MHz, $CDCl_3$): **δ** = 17 (NCH$_2$*C*H$_2$CH$_2$CO), 31 (NCH$_2$CH$_2$*C*H$_2$CO), 34 (*C*H$_2$CH(C_4H_6NO), 62 (*C*H$_2$CHOCO), 42 (N*C*H$_2$CH$_2$CH$_2$CO), 44-45 (CH$_2$*C*H(C_4H_6NO), 72 (CH$_2$*C*HOCO), 127 (meta-*C*H), 127 (ortho-*C*H, para-*C*H), 177 (NCH$_2$CH$_2$CH$_2$*C*O), 178 ($OCOC_6H_5$).

Functionalisation of PVP-PVA Copolymers with 4-Fluorobenzoyl Chloride

Poly(N-vinylpyrrolidone-*co*-vinyl alcohol) (150 mg) was dissolved in dimethylformamide (10 mL) with stirring and left to dissolve. After 30 minutes, triethylamine (20 mg) and 4-fluorobenzoyl chloride (55 mg) was added and left to react for 3 hours. After which the polymer was concentrated *in vacuo* and precipitated three times into diethyl ether and dried under vacuum. The polymer was then dissolved in water and purified using centrifugal dialysis (3000 Da MWCO, Millipore) followed by lyophilisation.

Yield: 33 mg. ^{1}H NMR (400 MHz, D_2O): **δ** = 1.30-1.84 (C*H*$_2$CH(C_4H_6NO), C*H*$_2$CHOCO, br), 1.85-2.08 (NCH$_2$C*H*$_2$CH$_2$CO, br), 2.09-2.60 (NCH$_2$CH$_2$C*H*$_2$CO, br), 2.96-3.39 (NC*H*$_2$CH$_2$CH$_2$CO, CH$_2$C*H*O br), 3.40-4.09 (CH$_2$C*H*(C_4H_6NO), CH$_2$C*H*OCO, br), 7.10-7.30 (meta-CH, br), 7.75-7.90 (ortho-CH, br). ^{19}F NMR decoupled (400 MHz, D_2O): **δ** = -106 (para-CF, s, 1F).

Functionalisation of PVP-PVA Copolymers with Propionyl Chloride

Poly(N-vinylpyrrolidone-*co*-vinyl alcohol) (150 mg) was dissolved in dimethylformamide (10 mL) with stirring and left to dissolve. After 30 minutes, triethylamine (20 mg) and propionyl chloride (30 mg) was added and left to react for 3 hours. After which the polymer was concentrated *in vacuo* and precipitated into diethyl ether (x3) and dried under vacuum. The polymer was then dissolved in water and purified using centrifugal dialysis (3000 Da MWCO, Millipore) followed by lyophilisation.

Yield: 39 mg. ^{1}H NMR (400 MHz, D_2O): **δ** = 1.34-1.85 ($CH_2CH(C_4H_6NO)$, CH_2CHOCO, br), 1.86-2.07 ($NCH_2CH_2CH_2CO$, br), 2.09-2.59 ($NCH_2CH_2CH_2CO$, CH_3CH_2COO br), 2.90-3.38 ($NCH_2CH_2CH_2CO$, CH_2CHO br), 3.40-4.10 ($CH_2CH(C_4H_6NO)$, CH_2CHOCO, CH_3CH_2COO, br). ^{13}C NMR (400 MHz, D_2O): **δ** = 18 ($NCH_2CH_2CH_2CO$, CH_3CH_2COO), 32 ($NCH_2CH_2CH_2CO$), 34 (CH_2CHOCO, $CH_2CH(C_4H_6NO)$), 42 ($NCH_2CH_2CH_2CO$), 44 ($CH_2CH(C_4H_6NO)$, 46 (CH_2CHOCO), 62 (CH_3CH_2COO), 177 (CH_3CH_2COO, $NCH_2CH_2CH_2CO$).

Functionalisation of PVP-PVA Copolymers with Valeroyl Chloride

Poly(N-vinylpyrrolidone-*co*-vinyl alcohol) (150 mg) was dissolved in dimethylformamide (10 mL) with stirring and left to dissolve. After 30 minutes, triethylamine (20 mg) and propionyl chloride (35 mg) was added and left to react for 3 hours. After which the polymer was concentrated *in vacuo* and precipitated into diethyl ether (x3) and dried under vacuum. The polymer was then dissolved in water and purified using centrifugal dialysis (3000 Da MWCO, Millipore) followed by lyophilisation.

Yield: 26 mg. ^{1}H NMR (400 MHz, D_2O): **δ** = 1.35-1.84 (C*H*$_2$CH(C_4H_6NO), C*H*$_2$CHOCO, br), 1.83-2.08 (NCH$_2$C*H*$_2$CH$_2$CO, C*H*$_3$CH$_2$CH$_2$COO, CH$_3$C*H*$_2$CH$_2$COO, br), 2.09-2.67 (NCH$_2$CH$_2$C*H*$_2$CO, C*H*$_3$CH$_2$COO br), 2.90-3.37 (NC*H*$_2$CH$_2$CH$_2$CO, CH$_2$C*H*O br), 3.39-4.10 (CH$_2$C*H*(C_4H_6NO), CH$_2$C*H*OCO, CH$_3$CH$_2$C*H*$_2$COO, br). ^{13}C NMR (400 MHz, D_2O): **δ** = 17 (*C*H$_3$CH$_2$CH$_2$COO, CH$_3$*C*H$_2$C*H*$_2$COO, NCH$_2$*C*H$_2$CH$_2$CO), 32 (NCH$_2$CH$_2$*C*H$_2$CO), 34 (*C*H$_2$CHOCO, *C*H$_2$CH(C_4H_6NO)), 42 (N*C*H$_2$CH$_2$CH$_2$CO), 44 (CH$_2$C*H*(C_4H_6NO), 46 (*C*H$_2$CHOCO), 63 (CH$_3$*C*H$_2$COO), 177 (CH$_3$CH$_2$CH$_2$*C*OO, NCH$_2$CH$_2$CH$_2$*C*O).

5.6 References

(1) Parent, O.; Ilinca, A. Anti-Icing and de-Icing Techniques for Wind Turbines: Critical Review. *Cold Reg. Sci. Technol.* **2011**, *65* (1), 88–96.

(2) Valarezo, W. O.; Lynch, F. T.; McGhee, R. J. Aerodynamic Performance Effects Due to Small Leading-Edge Ice (Roughness) on Wings and Tails. *J. Aircr.* **1993**, *30* (6), 807–812.

(3) Morris, G. J.; Acton, E. Controlled Ice Nucleation in Cryopreservation - A Review. *Cryobiology* **2013**, *66* (2), 85–92.

(4) Fowler, A.; Toner, M. Cryo-Injury and Biopreservation. *Ann. N. Y. Acad. Sci.* **2005**, *1066* (1), 119–135.

(5) He, Z.; Liu, K.; Wang, J. Bioinspired Materials for Controlling Ice Nucleation, Growth, and Recrystallization. *Acc. Chem. Res.* **2018**, *51* (5), 1082–1091.

(6) Maki, L. R.; Galyan, E. L.; Chang-Chien, M. M.; Caldwell, D. R. Ice Nucleation Induced by Pseudomonas Syringae. *Appl. Microbiol.* **1974**, *28* (3), 456–459.

(7) Dreischmeier, K.; Budke, C.; Wiehemeier, L.; Kottke, T.; Koop, T. Boreal Pollen Contain Ice-Nucleating as Well as Ice-Binding 'Antifreeze' Polysaccharides. *Sci. Rep.* **2017**, *7* (1), 41890.

(8) Ben, R. N. Antifreeze Glycoproteins-Preventing the Growth of Ice. *ChemBioChem* **2001**, *2* (3), 161–166.

(9) Balcerzak, A. K.; Capicciotti, C. J.; Briard, J. G.; Ben, R. N. Designing Ice Recrystallization Inhibitors: From Antifreeze (Glyco)Proteins to Small Molecules. *RSC Adv.* **2014**, *4* (80), 42682–42696.

(10) Mazur, P. Cryobiology: The Freezing of Biological Systems. *Science* **1970**, *168* (3934), 939–949.

(11) Koshimoto, C.; Mazur, P. Effects of Warming Rate, Temperature, and Antifreeze Proteins on the Survival of Mouse Spermatozoa Frozen at an Optimal Rate. *Cryobiology* **2002**, *45* (1), 49–59.

(12) Bender, E. Cell-Based Therapy: Cells on Trial. *Nature* **2016**, *540* (7634), 106–108.

(13) Baust, J. M.; Gao, D.; Baust, J. G. Cryopreservation. *Organogenesis* **2009**, *5* (3), 90–96.

(14) Graham, B.; Bailey, T. L.; Healey, J. R. J.; Marcellini, M.; Deville, S.; Gibson, M. I. Polyproline as a Minimal Antifreeze Protein Mimic That Enhances the Cryopreservation of Cell Monolayers. *Angew. Chemie Int. Ed.* **2017**, *56* (50), 15941–15944.

(15) Lee, J.; Lin, E.-W.; Lau, U. Y.; Hedrick, J. L.; Bat, E.; Maynard, H. D. Trehalose Glycopolymers as Excipients for Protein Stabilization. *Biomacromolecules* **2013**, *14* (8), 2561–2569.

(16) Hasan, M.; Fayter, A. E. R.; Gibson, M. I. Ice Recrystallization Inhibiting Polymers Enable Glycerol-Free Cryopreservation of Microorganisms. *Biomacromolecules* **2018**, *19* (8), 3371–3376.

(17) Biggs, C. I.; Bailey, T. L.; Graham, B.; Stubbs, C.; Fayter, A.; Gibson, M. I. Polymer Mimics of Biomacromolecular Antifreezes. *Nat. Commun.* **2017**, *8* (1), 1546.

(18) Voets, I. K. From Ice-Binding Proteins to Bio-Inspired Antifreeze Materials. *Soft Matter* **2017**, *13* (28), 4808–4823.

(19) Gibson, M. I. Slowing the Growth of Ice with Synthetic Macromolecules: Beyond Antifreeze(Glyco) Proteins. *Polym. Chem.* **2010**, *1* (8), 1141.

(20) Congdon, T.; Notman, R.; Gibson, M. I. Antifreeze (Glyco)Protein Mimetic

Behavior of Poly(Vinyl Alcohol): Detailed Structure Ice Recrystallization Inhibition Activity Study. *Biomacromolecules* **2013**, *14* (5), 1578–1586.

(21) Inada, T.; Lu, S.-S. Inhibition of Recrystallization of Ice Grains by Adsorption of Poly(Vinyl Alcohol) onto Ice Surfaces. *Cryst. Growth Des.* **2003**, *3* (5), 747–752.

(22) Budke, C.; Koop, T. Ice Recrystallization Inhibition and Molecular Recognition of Ice Faces by Poly(Vinyl Alcohol). *ChemPhysChem* **2006**, *7* (12), 2601–2606.

(23) Naullage, P. M.; Lupi, L.; Molinero, V. Molecular Recognition of Ice by Fully Flexible Molecules. *J. Phys. Chem. C* **2017**, *121* (48), 26949–26957.

(24) Drori, R.; Li, C.; Hu, C.; Raiteri, P.; Rohl, A. L.; Ward, M. D.; Kahr, B. A Supramolecular Ice Growth Inhibitor. *J. Am. Chem. Soc.* **2016**, *138* (40), 13396–13401.

(25) Mitchell, D. E.; Clarkson, G.; Fox, D. J.; Vipond, R. A.; Scott, P.; Gibson, M. I. Antifreeze Protein Mimetic Metallohelices with Potent Ice Recrystallization Inhibition Activity. *J. Am. Chem. Soc.* **2017**, *139* (29), 9835–9838.

(26) Graham, B.; Fayter, A. E. R.; Houston, J. E.; Evans, R. C.; Gibson, M. I. Facially Amphipathic Glycopolymers Inhibit Ice Recrystallization. *J. Am. Chem. Soc.* **2018**, *140* (17), 5682–5685.

(27) Gibson, M. I.; Barker, C. A.; Spain, S. G.; Albertin, L.; Cameron, N. R. Inhibition of Ice Crystal Growth by Synthetic Glycopolymers: Implications for the Rational Design of Antifreeze Glycoprotein Mimics. *Biomacromolecules* **2009**, *10* (2), 328–333.

(28) Capicciotti, C. J.; Leclère, M.; Perras, F. A.; Bryce, D. L.; Paulin, H.; Harden, J.; Liu, Y.; Ben, R. N. Potent Inhibition of Ice Recrystallization by Low

Molecular Weight Carbohydrate-Based Surfactants and Hydrogelators. *Chem. Sci.* **2012**, *3* (5), 1408–1416.

(29) Balcerzak, A. K.; Febbraro, M.; Ben, R. N. The Importance of Hydrophobic Moieties in Ice Recrystallization Inhibitors. *RSC Adv.* **2013**, *3* (10), 3232–3236.

(30) Czechura, P.; Tam, R. Y.; Dimitrijevic, E.; Murphy, A. V.; Ben, R. N. The Importance of Hydration for Inhibiting Ice Recrystallization with C-Linked Antifreeze Glycoproteins. *J. Am. Chem. Soc.* **2008**, *130* (10), 2928–2929.

(31) Kiselev, A.; Bachmann, F.; Pedevilla, P.; Cox, S. J.; Michaelides, A.; Gerthsen, D.; Leisner, T. Active Sites in Heterogeneous Ice Nucleation—the Example of K-Rich Feldspars. *Science* **2017**, *355* (6323), 367–371.

(32) Zhang, Q.; Kelland, M. A. Study of the Kinetic Hydrate Inhibitor Performance of Poly(N -Vinylcaprolactam) and Poly(N -Isopropylmethacrylamide) with Varying End Caps. *Energy and Fuels* **2018**, *32* (9), 9211–9219.

(33) Kelland, M. A. History of the Development of Low Dosage Hydrate Inhibitors. *Energy & Fuels* **2006**, *20* (3), 825–847.

(34) Harrisson, S.; Liu, X.; Ollagnier, J.-N.; Coutelier, O.; Marty, J.-D.; Destarac, M. RAFT Polymerization of Vinyl Esters: Synthesis and Applications. *Polymers* **2014**, *6* (5), 1437–1488.

(35) Liu, Q.; Wu, H.; Zhang, L.; Zhou, Y.; Zhang, W.; Pan, X.; Zhang, Z.; Zhu, X. RAFT Polymerization of N-Vinylpyrrolidone Mediated by Cyanoprop-2-Yl-1-Dithionaphthalate in the Presence of a Fluoroalcohol: The Possibility of Altering Monomer Properties by Hydrogen Bonding? *Polym. Chem.* **2016**, *7* (11), 2015–2021.

(36) Stenzel, M. H.; Cummins, L.; Roberts, G. E.; Davis, T. P.; Vana, P.; Barner-Kowollik, C. Xanthate Mediated Living Polymerization of Vinyl Acetate: A

Systematic Variation in MADIX/RAFT Agent Structure. *Macromol. Chem. Phys.* **2003**, *204* (9), 1160–1168.

(37) Perrier, S. 50th Anniversary Perspective : RAFT Polymerization—A User Guide. *Macromolecules* **2017**, *50* (19), 7433–7447.

(38) Corrigan, N.; Yeow, J.; Judzewitsch, P.; Xu, J.; Boyer, C. A. J. M. Seeing the Light: Advancing Materials Chemistry through Photopolymerization. *Angew. Chemie Int. Ed.* **2018**.

(39) Khan, M. Y.; Cho, M.-S.; Kwark, Y.-J. Dual Roles of a Xanthate as a Radical Source and Chain Transfer Agent in the Photoinitiated RAFT Polymerization of Vinyl Acetate. *Macromolecules* **2014**, *47* (6), 1929–1934.

(40) Xu, J.; Jung, K.; Atme, A.; Shanmugam, S.; Boyer, C. A Robust and Versatile Photoinduced Living Polymerization of Conjugated and Unconjugated Monomers and Its Oxygen Tolerance. *J. Am. Chem. Soc.* **2014**, *136* (14), 5508–5519.

(41) Richards, S.-J.; Jones, A.; Tomás, R. M. F.; Gibson, M. I. Photochemical "In-Air" Combinatorial Discovery of Antimicrobial Co-Polymers. *Chem. Eur. J.* **2018**, *24* (52), 13758–13761.

(42) Chapman, R.; Gormley, A. J.; Stenzel, M. H.; Stevens, M. M. Combinatorial Low-Volume Synthesis of Well-Defined Polymers by Enzyme Degassing. *Angew. Chemie Int. Ed.* **2016**, *55* (14), 4500–4503.

(43) Yeow, J.; Chapman, R.; Xu, J.; Boyer, C. Oxygen Tolerant Photopolymerization for Ultralow Volumes. *Polym. Chem.* **2017**, *8* (34), 5012–5022.

(44) Britton, D.; Heatley, F.; Lovell, P. A. Chain Transfer to Polymer in Free-Radical Bulk and Emulsion Polymerization of Vinyl Acetate Studied by NMR

Spectroscopy. *Macromolecules* **1998**, *31* (9), 2828–2837.

(45) Fu, Q.; Xie, K.; McKenzie, T. G.; Qiao, G. G. Trithiocarbonates as Intrinsic Photoredox Catalysts and RAFT Agents for Oxygen Tolerant Controlled Radical Polymerization. *Polym. Chem.* **2017**, *8* (9), 1519–1526.

(46) Figg, C. A.; Hickman, J. D.; Scheutz, G. M.; Shanmugam, S.; Carmean, R. N.; Tucker, B. S.; Boyer, C.; Sumerlin, B. S. Color-Coding Visible Light Polymerizations to Elucidate the Activation of Trithiocarbonates Using Eosin Y. *Macromolecules* **2018**, *51* (4), 1370–1376.

(47) Ding, C.; Fan, C.; Jiang, G.; Pan, X.; Zhang, Z.; Zhu, J.; Zhu, X. Photocatalyst-Free and Blue Light-Induced RAFT Polymerization of Vinyl Acetate at Ambient Temperature. *Macromol. Rapid Commun.* **2015**, *36* (24), 2181–2185.

(48) Ieong, N. S.; Redhead, M.; Bosquillon, C.; Alexander, C.; Kelland, M.; O'Reilly, R. K. The Missing Lactam-Thermoresponsive and Biocompatible Poly(N -Vinylpiperidone) Polymers by Xanthate-Mediated RAFT Polymerization. *Macromolecules* **2011**, *44* (4), 886–893.

(49) Ieong, N. S.; Brebis, K.; Daniel, L. E.; O'Reilly, R. K.; Gibson, M. I. The Critical Importance of Size on Thermoresponsive Nanoparticle Transition Temperatures: Gold and Micelle-Based Polymer Nanoparticles. *Chem. Commun.* **2011**, *47* (42), 11627–11629.

(50) Rajan, R.; Jain, M.; Matsumura, K. Cryoprotective Properties of Completely Synthetic Polyampholytes via Reversible Addition-Fragmentation Chain Transfer (RAFT) Polymerization and the Effects of Hydrophobicity. *J. Biomater. Sci. Polym. Ed.* **2013**, *24* (August 2015), 1767–1780.

(51) Bork, J. F.; Coleman, L. E. Nitrogen-Containing Monomers. II. Reactivity Ratios of n-Vinyloxazolidone and N-Vinylpyrrolidone with Vinyl Monomers.

J. Polym. Sci. **1960**, *43* (142), 413–421.

(52) Congdon, T.; Shaw, P.; Gibson, M. I. Thermoresponsive, Well-Defined, Poly(Vinyl Alcohol) Co-Polymers. *Polym. Chem.* **2015**, *6* (26), 4749–4757.

(53) Budke, C.; Dreyer, A.; Jaeger, J.; Gimpel, K.; Berkemeier, T.; Bonin, A. S.; Nagel, L.; Plattner, C.; Devries, A. L.; Sewald, N.; Koop, T. Quantitative Efficacy Classification of Ice Recrystallization Inhibition Agents. *Cryst. Growth Des.* **2014**, *14* (9), 4285–4294.

(54) Mochizuki, K.; Molinero, V. Antifreeze Glycoproteins Bind Reversibly to Ice via Hydrophobic Groups. *J. Am. Chem. Soc.* **2018**, *140* (14), 4803–4811.

5.7 Appendix

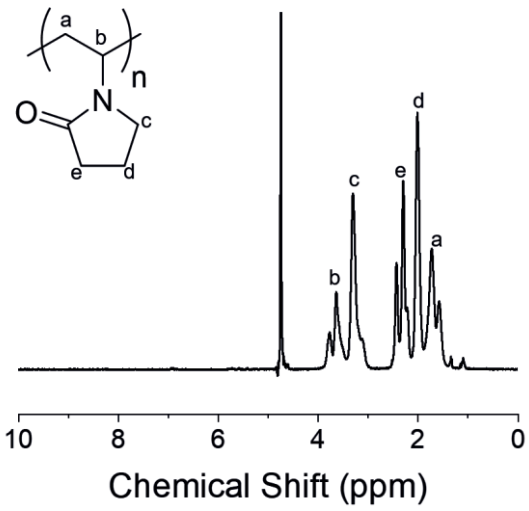

Figure 5.11: ^{1}H NMR of the VP Homopolymers synthesised as part of this work. NMR was carried out in D_2O.

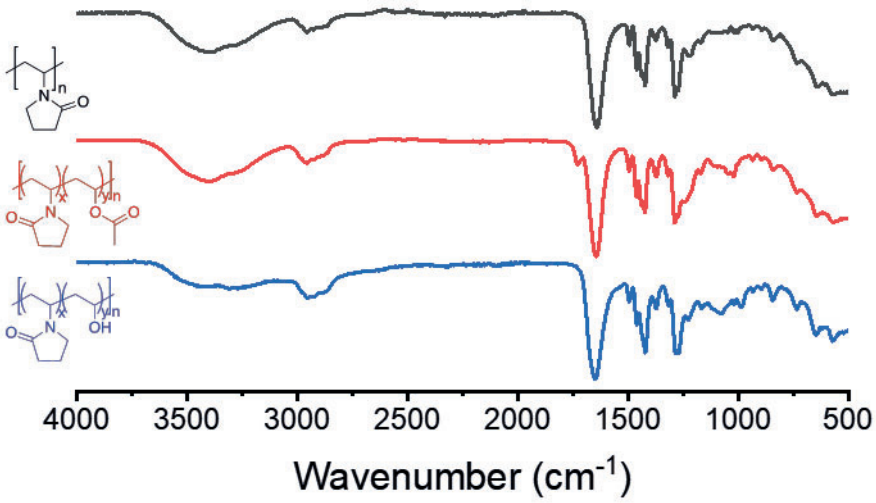

Figure 5.12: FTIR of the VP homopolymers, and PVP-VAc and PVP-VA polymers used in this study. The peak at 3300-3000 cm^{-1} is due to atmospheric water absorbed by the PVP homopolymer.

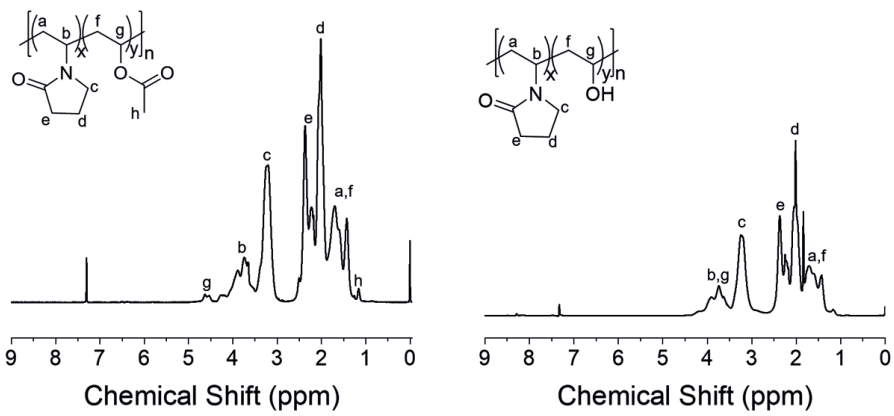

Figure 5.13: ^{1}H NMR of the PVP-VAc and PVP-VA polymers synthesised. NMRs were run in $CDCl_3$.

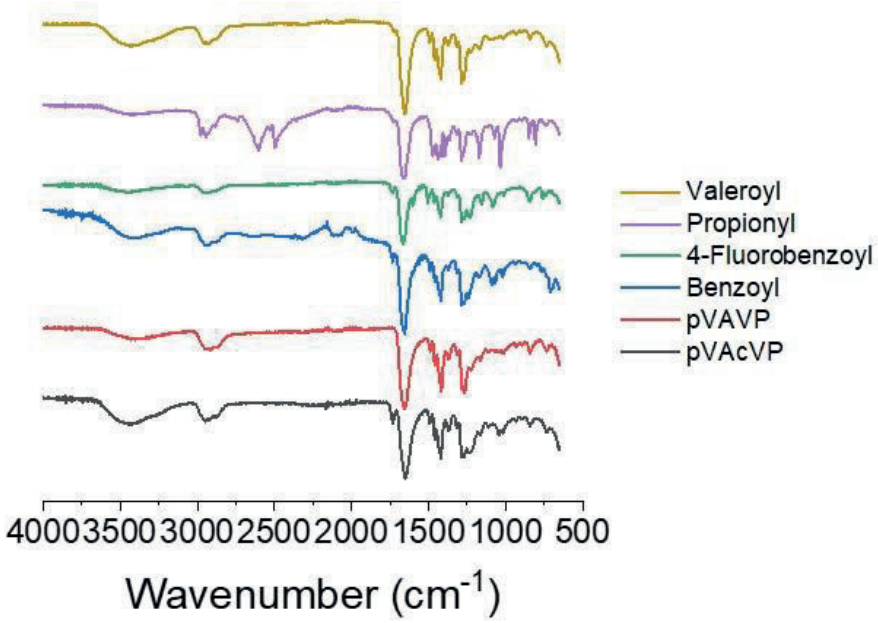

Figure 5.14: FTIR spectra for the functionalised polymers synthesised.

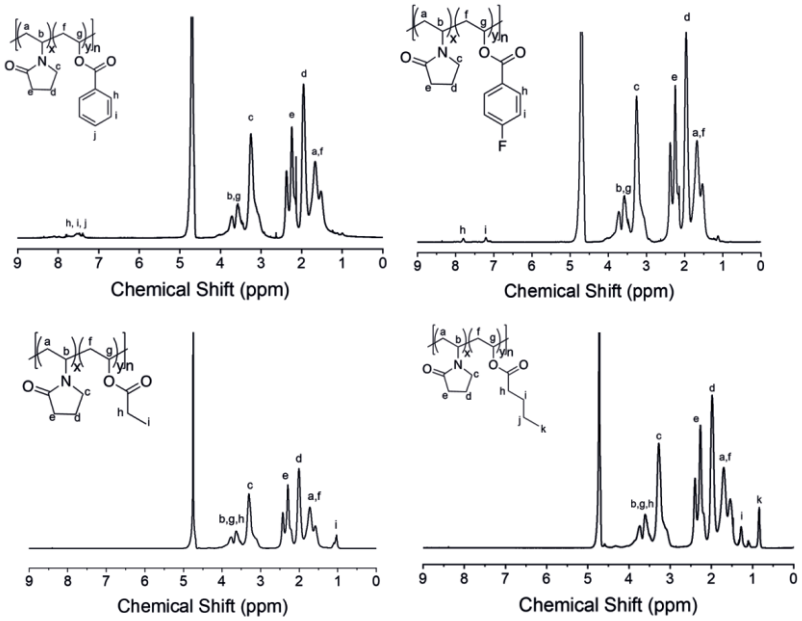

Figure 5.14: ^{1}H NMR for the functionalised polymers synthesised. NMR's were run in D_2O.

Chapter 6

6.1 Conclusion

Cryopreservation is an essential technique for prolonging the usability of biological materials, however current generation cryoprotectants are often toxic, expensive or fail to achieve 100% recovery. The aim of this thesis was to aid in the identification of design rules for polymeric materials that enable efficient cryopreservation whilst overcoming some of the issues with current generation materials.

Initially, poly(vinyl alcohol) a well-known and highly active ice recrystallisation inhibitor was investigated. Whilst this material has been studied previously, there are still a number of unanswered questions about its mechanism of action, and whether it can be enhanced, with almost all previous attempts to modify it reducing or removing its activity. Multivalent PVA coated nanoparticles were synthesised and compared to free PVA. It was found that on a PVA mass basis, free PVA is of equal activity to multivalent PVA coated particles. This is also interesting when compared with 3-arm star PVA, in which the third arm is observed to be redundant. It is hypothesised that due to the low grafting density, PVA chains are able to explore the surface of the particle until optimal PVA-Ice binding is achieved, enabling equivalent activity to free PVA. It is suggested that this technique could be used in the future to enable imaging or local rewarming of cryopreserved tissues, however this was not investigated. The specific structural features of PVA were also investigated using a number of structurally simple water soluble polymers. It was shown that any modification to the specific PVA structure will reduce all activity, with both the spacing and nature of the hydrophilic group being required for optimal inhibition. This therefore suggests that

designing a PVA-based IRI active material which has the required OH groups and spacing, that is not simply PVA, would be incredibly challenging. It was therefore decided that other classes of cryoprotectant materials be investigated.

Poly(ampholytes) have been shown to be an interesting class of cryoprotectant materials, whilst also not being widely investigated. Previous reports used random copolymers of anionic and cationic monomers, demonstrating that a 1:1 ratio is optimal, however the importance of regioregularity of the polymer chain had not been investigated. We therefore carried out a systematic investigation into the effect of regioregularity on IRI activity. By exploiting the alternating copolymerisation of maleic anhydride, a series of perfectly alternating poly(ampholytes) were synthesised by ring opening the anhydride, with backbones of varying hydrophobicity. Once the optimal backbone and chain length were determined, the nature of the hydrophobic group was investigated, with a balance between hydrophobicity and solubility being required. The most active of these materials displayed greater IRI activity at lower concentrations than those reported previously and acted as an effective cryoprotectant for the low temperature storage of red blood cells. These species, however, require relatively involved synthesis of the polymer precursor, and therefore commercially available alternatives were investigated. Poly(methyl vinyl ether-*alt*-maleic anhydride) is a low cost commercially available polymer which is available to GMP standards and in a number of different molecular weights. When reacted with the same amine found to give the highest IRI active previously, the resulting material was observed to be an incredibly active cryoprotectant, with activity greater than the $PIPAC_{92}$-NMe_2 tested previously. The IRI activity of this material was investigated, and it was shown to be very weakly active, suggesting that IRI activity is not necessarily the only mechanism by which materials can optimise cryopreservation

outcomes. These polymers however require relatively high concentrations, and therefore attempts were made to identify structures which resulted in similar recovery, however at lower concentrations.

In order to identify more active materials, a new method for synthesis and screening was developed, which enables large numbers of polymers to be synthesised with relative ease and little specialist equipment. By adapting a process used by Qiao, we developed a method which enables the synthesis of a large number of polymers in assay-ready plates with no degassing, and crucially for blood cryopreservation, no DMSO. This method was observed to reliably generate polymers in volatile solvents and with relatively easily removed deoxygenators, however with no control over the molecular weight or dispersity. Whilst this is potentially a major drawback for a lot of applications, for the investigation of poly(ampholyte) terpolymers, where composition is likely to be much more important than molecular weight, this technique massively reduced the required workflow. When paired with a modified high throughput SEC, and a modified blood cryopreservation assay carried out entirely in well plates, this method allowed the synthesis and testing of 120 different poly(ampholyte) terpolymers in less than 4 days. As the materials synthesised in plates are not fully characterised, the best, and worst, of these materials were then synthesised using standard RAFT polymerisation and their activity compared to a number of known cryoprotectant polymers. These materials displayed similar activity to the previously tested poly(ampholytes), suggesting that there may be a limit to the cryoprotectant activity displayed by this class of materials. As a result of these findings, our focus then returned to fully flexible, non-charged polymers. A number of previous reports have found that increasing the hydrophobicity of weakly IRI active polymers has the potential to greatly enhance their activity, therefore we were interested in the

possibility of inducing IRI activity in a non-active polymer through modulation of the hydrophobicity. Poly(*N*-vinylpyrrolidone) displays no IRI activity other than that which is expected on a colligative basis, and therefore was an ideal starting point for this research. PVP was hydrophobically modified *via* copolymerisation with vinyl acetate, followed by deprotection and installation of a number of pendant groups. This did not lead to any notable increase in IRI activity, and therefore suggests that hydrophobicity can only enhance activity in materials which are already able to interact with ice, even if this interaction is initially very weak.

In conclusion, these results demonstrate that there are a large number of incredibly complex factors which determine the IRI and cryoprotectant activity of a material. Whilst IRI is thought to be a good indicator of cryoprotectant activity for non-charged small molecules and polymeric cryopreservatives, there appears to be little correlation between IRI activity and cryoprotectant activity for poly(ampholytes). This suggests that when designing new cryoprotectants both interactions with ice and cells must be considered, presenting an incredibly complex system. The results presented here will help to direct the design of future cryopreservatives, hopefully one day enabling the cryopreservation of cells and tissues.

Chapter 7

7.1 List of Publications

[1] Stubbs, C., Lipecki, J., Gibson, M. I., Regioregular Alternating Polyampholytes Have Enhanced Biomimetic Ice Recrystallization Activity Compared to Random Copolymers and the Role of Side Chain versus Main Chain Hydrophobicity. *Biomacromolecules*. **2017**. 18(1), 295-302.

[2] Vail, N. S., Stubbs, C., Biggs, C. I., Gibson, M.I., Ultra-Low Dispersity Poly(vinyl alcohol) Reveals Significant Dispersity Effects on Ice Recrystallization Inhibition Activity. *ACS MacroLetters*, **2017**, 6, 101-104.

[3] Biggs, C. I., Bailey, T. L., Graham, B., Stubbs, C., Fayter, A., Gibson, M. I., Polymer Mimics of Biomacromolecular Antifreezes. *Nature Communications*, **2017**, 1546.

[4] Stubbs, C., Hedir, G., Aston, P. R., Dove A. P., Gibson., M. I., Synthesis of Degradable Poly(vinyl alcohol) by Radical Ring-Opening Copolymerization and Ice Recrystallization Inhibition Activity. *ACS MacroLetters* **2017**, 6, 1404 - 1408.

[5] Stubbs, C., Wilkins, L. E., Fayter, A. E. R., Walker, M., Gibson, M. I., Multivalent Presentation of Ice Recrystallization Inhibiting Polymers on Nanoparticles Retains Activity. *Langmuir*, **2018**, 35, 7347-7353.

[6] Stubbs, C., Congdon, T. R, Gibson, M. I., Photo-Polymerisation and Study of the Ice Recrystallisation Inhibition of Hydrophobically Modified Poly(vinyl pyrrolidone) Co-polymers. *European Polymer Journal*, **2019**, 110, 330-336.

[7] Biggs C. I., Stubbs. C., Graham, B., Fayter, A. E. R., Hasan, M., Gibson, M. I., Mimicking the Ice Recystallization Activity of Biological Macromolecules. When is a New Polymer 'Active'? *Macromolecular Bioscience*, 2019.